



HAL
open science

Development of hybrid clay/polymer materials with controlled selectivity applied to wastewater treatment

Abdallah Aoun

► **To cite this version:**

Abdallah Aoun. Development of hybrid clay/polymer materials with controlled selectivity applied to wastewater treatment. Material chemistry. Université Paris-Est; Université de Sfax. Faculté des sciences, 2021. English. NNT: 2021PESC0014 . tel-03855099

HAL Id: tel-03855099

<https://theses.hal.science/tel-03855099>

Submitted on 16 Nov 2022

HAL is a multi-disciplinary open access archive for the deposit and dissemination of scientific research documents, whether they are published or not. The documents may come from teaching and research institutions in France or abroad, or from public or private research centers.

L'archive ouverte pluridisciplinaire **HAL**, est destinée au dépôt et à la diffusion de documents scientifiques de niveau recherche, publiés ou non, émanant des établissements d'enseignement et de recherche français ou étrangers, des laboratoires publics ou privés.

THÈSE

Co-dirigée

pour le diplôme de docteur en

Chimie

DÉVELOPPEMENT DE MATÉRIAUX HYBRIDES ARGILE / POLYMÈRE À SÉLECTIVITÉ CONTRÔLÉE APPLIQUÉE AU TRAITEMENT DES EAUX USÉES

Proposé par

Abdallah AOUN

Défense publique : mercredi 27 janvier 2021

Devant le comité composé de

André DERATANI	<i>Directeur de recherche, IEM</i> Université de Montpellier	Rapporteur
Amine MNIF	<i>Lecturer-HDR,</i> Faculté des Sciences de Tunis Université de TunisEl Manar	Rapporteur
Mahmoud TRABELSI	<i>Professeur,</i> Faculté des Sciences de Sfax Université de Sfax	Examineur-Président
Samia MAHOUCHE-CHERGUI	<i>Lecturer, ICMPE</i> Université East-Paris Créteil	Examineur
Raja BEN AMAR	<i>Professeur,</i> Faculté des Sciences de Sfax Université de Sfax	Directrice de thèse
Benjamin CARBONNIER	<i>Professeur, ICMPE</i> Université East-Paris Créteil	Directeur de thèse

Dedications

I dedicate this work
To my beloved parents to whom I owe a lot,
To my family
To the soul of my big sister who I never saw
To my friends
and
To all those who are dear to me
As a token of my deep gratitude and my great affection

“ You can't have honey without a bee sting. ”

Arab proverb

Abdallah AOUN

Acknowledgment

This doctoral thesis was realized in the frame of a common supervision between the University of Sfax (US) in Tunisia and the University of Paris-Est Creteil Val de Marne (UPEC) in France under the scientific supervision of Professor Raja BEN AMAR from the Tunisian side and Professor Benjamin CARBONNIER and Samia MAHOUCHE-CHERGUI from the French side.

First of all, it is with a deep sense of gratitude I wish to record here my most sincere thanks to my three supervisors for having welcomed me within their teams and for having entrusted me with this fascinating research work. Thank you very much for your encouragement, your patience, your support and your personal guidance as well as the valuable suggestions that enabled me to steer my research works efficiently. I have learned a lot from you and your wide scientific knowledge that you shared with me. This opportunity was extremely useful to explore new approaches at the border between several scientific disciplines and provide an excellent basis for my thesis at the end.

I would like to sincerely thank the entire jury member for agreeing to participate and judge the content of this thesis.

I also thank all the staff of the Faculty of Sciences of Sfax (FSS) with whom I have interacted during these years, more particularly, my colleagues in the Laboratory of Materials and Environmental Sciences (MESLab).

My thanks and my feelings of friendship are addressed particularly to Housseem SAADAOU, Anoir Mabrouk BEN HAMDEN and Nouha TAHRI.

I express my deep gratitude to Mr Mohamed HBAIB, director of the Doctoral School of Fundamental Sciences (ED-SF) of Sfax, for his kindness and for providing me with financial support, which allows me to work in comfortable conditions.

I would also like to thank Mrs. Sadika FEKIH, for her advices, her help and her professionalism.

I also express my gratitude to the all ICMPE members, and more particularly the SPC team for welcoming me so warmly among them. I would like, herein, to thank Mr Daniel

GRANDE, Mrs Sabrina BELBEKHOUCHE, Mr Benjamin LE DROUMAGUET and Mr Mohamed GUERROUACHE for their kindness, their professionalism.

I associate also these warm thanks to the technical and administrative staff Mrs Marcelle AMMOUR, Mrs Séna HAMADI, Mr Laurent MICHELY, Mr Rémy PIRES BRAZUNA and Mr Benjamin VILLEROY for their support and their daily help.

My friends and colleagues are warmly thanked for the support in difficult times. A big thank you goes to Van Son VO, Vierajitha SRIKANTHAN, Aline-Sarah GLAIVE, Tina MODJINO and LE N'GUYEN Thi-Thanh-Tam. It was a pleasure to work and discuss together.

I will not forget to thank Christelle BEROL and Cecile BLANCHEMANCHE from the Doctoral School: Engineering and Environmental Sciences (ED-EES) of Paris-Est, for their kindness and sympathy.

This present research work constitutes also the result of scientific cooperation with the Central Glass and Ceramics Research Institute (CGCRI) in Kolkata - India.

A word of thanks here should be expressed to my collaborators, Dr. Ganesh C. SAHOO, Dr. Swachhha MAJUMDAR and Dr. Sandeep SARKAR for accepting to guide me during my RTF-DCS training program in the Ceramic Membrane division (CMD), Kolkata. Thanks for providing me such a good opportunity to work with you and your guidance and plentiful opinions on membrane technologies as well as your contributions in my first publications.

My gratitude also is extended to the Head Dr. Subrata DASGUPTA and all the CMD scientists; Dr. Sibdas BANDYOPADHYAY, Dr. Sourja GHOSH, Dr. Nandini DAS, Dr. Mahesh KUMAR GAGRAI and Dr. Somendra NATH ROY for providing help and fruitful discussions.

I would also like to thank the technical staff Mr. Subhendu SARKAR, Mr. Trilochan PRASAD SAHOO, Mr. Gouranga CHALAK and Mr. Nitai CHAND SINGH for helping me in my work with sample characterization and instrument training.

Special appreciation goes to Mr. Swapan SARKAR, for his kindness and the daily help with his incessant smile.

I am also grateful to my colleagues Mr. Marakkar Kutty P.V. MAILAM VEEDU, Mrs. Priyanka Mondal, Mr. Surajit DEY, Mr. Soumya DAS, Mrs. Priyanka ROY, Mr. Jugal DAS

and Mr. Biswajeet BERA as well as all members in the CGCRI for their collaborations. It is my deep pleasure and I'm very lucky to meet with them.

Special thanks to all my friends in SURPA building Mr. Safeer SALAHUDEEN, Mr. Niyas MOHAMED, Mr. Jijo V. ITTIARAH, Arun V.S. NAIR, and Abiodun Is-haq EGUNJOBI for their kind help, all the fun we shared and being remarkable friends.

In that regard, I cannot fail to express my appreciation to the Dr. Sirshendu DE and his student Mr. Sankha KARMAKAR for the warm welcome in Department of Chemical Engineering and the pleasant stay that I spent in Indian Institute of Technology (IIT), Kharagpur.

I am also grateful to all those have made my six months in India so enjoyable stay and enriching experience.

The achievement of this research thesis was subsidized by the following three doctoral level partner programs:

- Ministry of Higher Education and Scientific Research (MHESR), Tunisia
- Scholarship program of excellence for doctoral student's mobility from Campus France and the French Institute in Tunisia (FIT) affiliated with the Ministry of Higher Education, Research and Innovation (MHERI), France.
- Research Training Fellowship for Developing Country Scientists (RTF-DCS) – Award of Fellowship – from Council of Scientific and Industrial Research (CSIR), India and Centre for Science and Technology of the Non-Aligned and Other Developing Countries (NAM S&T Centre), New Delhi-India.

I would like to warmly thank the responsible in charge of the three scientific cooperation programs who allocated the necessary financial support to this research work that giving me chance to carrying out my thesis.

I was fortunate throughout my thesis period to meet such diverse and interesting people in every way. This experience was therefore enriching for me both scientifically and humanly.

I therefore thank the people with whom I shared the office and with whom I had a good time.

A big thanks to all my doctoral colleagues and my friends for their sympathy, their moral support and these memorable years that we have spent together.

Finally, I would especially like to thank my dear parents, my brother-in-law, my sister and all my family for supporting me.

To them I address my deep gratitude for their patience, their comfort in times of doubt and discouragement.

May they find in this work the testimony of my affection?

Publications List

- **Abdallah Oun**, Samia Mahouche Chergui, Mouna Khemakhem, Benjamin Carbonnier & Raja Ben Amar. **2018**. Chapter 4 - Preparation and Surface Modification of Porous Ceramic Membranes for Water Treatment. pp. 101-126. In: Stephen Gray, Toshinori Tsuru, Yoram Cohen, Woei-Jye Lau (Eds). *Advanced Materials for Membrane Fabrication and Modification*, 600. New York: CRC Press, Taylor & Francis Group.

- **Abdallah Oun**, Nouha Tahri, Samia Mahouche-Chergui, Benjamin Carbonnier, Swachchha Majumdar, Sandeep Sarkar, Ganesh C. Sahoo & Raja Ben Amar. **2017**. Tubular ultrafiltration ceramic membrane based on titania nanoparticles immobilized on macroporous clay-alumina support: Elaboration, characterization and application to dye removal. *Separation and Purification Technology*. 188, 126–133.

- **Abdallah Oun**, Van Son VO, Séna Hamadi, Raja Ben Amar, Benjamin Carbonnier, Samia Mahouche-Chergui. Gold nanospheres-decorated nanostructures as a recyclable heterogeneous catalyst for ultrafast conversion of endocrine disruptors. Submitted on *Journal of hazardous materials*.

Table of Contents

Table of Contents	vii
<i>List of Abbreviations</i>	<i>XIII</i>
<i>List of Figures</i>	<i>XVIII</i>
<i>List of Tables</i>	<i>XXII</i>
GENERAL INTRODUCTION	2
1. Background	3
2. Aims and Objectives	3
3. Thesis Outline.....	5
Chapter 1	8
LITERATURE REVIEW	8
Section 1	9
<i>Preparation and Surface Modification of Porous Ceramic Membranes for Water Treatment</i>	<i>9</i>
1. Introduction	9
2. Development of ceramic membranes derived from low cost raw materials	11
3. Surface modification of ceramic membrane via structuration.....	13
3.1. Ceramic Membrane from Slip-Casting Method	15
3.2. Ceramic Membrane from Atomic Layer Deposition.....	16
4. Surface modification of ceramic membranes via chemical grafting	18
4.1. Membrane hydrophobization.....	21
4.2. Grignard reagents	21
4.3. Organophosphonic acids	22
4.4. Organosilanes	24
4.5. Organic polymers	26
5. Application of chemically modified ceramic membranes	27
5.1. Water Desalination	28
5.2. Oil/Water Separation.....	30
6. Conclusion.....	31
References	32
Section 2	42
<i>Polymer-based nanocomposites: focus on heterogeneous catalysts for environmental remediation</i>	<i>42</i>
1. Introduction	42
2. Graphene-polymer nanocomposites	44
3. Nanoclay- polymer nanocomposites	45
4. Metal nanoparticles-polymer nanocomposites	45

4.1.	Synthesis of metal nanoparticles-polymer nanocomposites	45
4.2.	Application of metal nanoparticles-polymer nanocomposites in bulk heterogeneous catalysis 48	
5.	Characterization of polymer-based nanocomposites	49
6.	Conclusion.....	50
	References	51
	Section 3	65
	<i>Hybrid catalytic separation process for continuous and simultaneously water remediation in membrane reactor</i>	65
1.	Introduction	65
2.	Membrane reactor configurations.....	66
3.	Ceramic membrane function in membrane reactor	67
4.	Surface modification of ceramic membrane.....	68
4.1.	Surface pre-treatment	68
4.2.	Modification by (Nano)structuration and chemical grafting	69
4.3.	Catalytic and catalytically active ceramic membrane	70
5.	Membrane reactor study	71
6.	Applications in water pollution removal	78
7.	Success key factors of the Process	84
7.1.	Fouling control and membrane regeneration.....	84
7.2.	Catalyst retention and properties recovery	86
8.	Conclusion.....	87
	References	89
	Chapter 2	107
	NANOHYBRID MATERIALS FOR CATALYTIC REDUCTION OF DYES AND NITROAROMATIC ENDOCRINE DISRUPTORS	107
	Section 1	108
	<i>Gold nanospheres-decorated nanostructures as a recyclable heterogeneous catalyst for ultrafast conversion of endocrine disruptors</i>	108
1.	Introduction	108
2.	Experimental section	110
2.1.	Materials.....	110
2.2.	Synthesis of MMT-PGMA nanocomposite	110
2.3.	Amine-surface functionalization of MMT-PGMA.....	111
2.4.	In-situ generation of gold NPs on MMT-PGMA-NH ₂	111
2.5.	Characterization.....	111
2.6.	Conversion of nitroaromatic derivatives using AuNPs-decorated clay nanostructures as heterogeneous nanocatalysts	112
2.7.	Recovery of MMT-supported AuNPs nanocatalyst	114

3.	Results and discussion.....	114
3.1.	Characterization of MMT-PGMA-NH ₂ chelant platforms.....	114
3.2.	Gold NPs immobilization on MMT-PGMA-NH ₂ platforms.....	119
3.3.	Catalytic performances of the AuNPs-decorated clay nanostructures.....	123
3.4.	Effect of size and concentration of immobilized AuNPs nanocatalyst on the rate reduction of 4NP 124	
3.5.	Pendimethalin pesticide conversion.....	127
3.6.	Reusability test of the nanocatalysts.....	128
4.	Conclusion.....	130
	References.....	131
	Section 2	137
	<i>Palladium nanoparticles decorated dually functionalized green synthesized graphene/clay nanohybrid: A promising heterogeneous catalyst for water remediation</i>	137
1.	Introduction.....	137
2.	Experimental section.....	139
2.1.	Chemicals.....	139
2.2.	Preparation of GHN.....	140
2.3.	GPTMS surface functionalization of GHN (GHN-GPTMS).....	140
2.4.	TGE surface functionalization of GHN (GHN-TGE).....	141
2.5.	Post functionalization of GHN (GHN-GPTMS-TGE / GHN-TGE-GPTMS).....	141
2.6.	Ring opening of the epoxide modified GHN (GHN-COOH).....	141
2.7.	Immobilization of palladium nanoparticles (GHN-COOH@PdNPs).....	141
2.8.	Evaluation of catalytic activity of GHN-COOH@PdNPs.....	142
2.9.	Characterization.....	142
3.	Results and discussion.....	145
3.1.	Preparation and structural characterization of GHN.....	145
3.2.	Surface functionalization of GHN.....	148
3.3.	Palladium nanoparticles decorated GHN.....	151
3.4.	Catalytic properties of GHN-COOH@PdNPs.....	152
3.5.	GHN-COOH@PdNPs Catalyst regeneration.....	157
4.	Conclusion.....	158
	References.....	159
	Chapter 3	167
	NANOSTRUCTURED CERAMIC MEMBRANES FOR DISCOLORATION OF WATER LOADED WITH DYES	167
	<i>Tubular ultrafiltration ceramic membrane based on titania nanoparticles immobilized on macroporous clay-alumina support: Elaboration, characterization and application to dye removal</i>	168
1.	Introduction.....	168

2.	Experimental	169
2.1.	Materials	169
2.2.	Characterization and instruments	170
2.3.	Preparation of tubular clay-alumina supports.....	171
2.4.	Design of TiO ₂ -based tubular ceramic UF membrane	172
2.5.	Cross flow ultrafiltration (UF).....	173
3.	Results and discussion.....	174
3.1.	Design and characterization of macroporous tubular ceramic membranes	174
3.1.1.	Mechanical strength.....	174
3.1.2.	Thermal analysis.....	175
3.1.3.	Porosity and pore size distribution	176
3.1.4.	Morphology	177
3.2.	Characterization of TiO ₂ -coated C25A75M6 ultrafiltration membrane.....	178
3.2.1.	Morphology	178
3.2.2.	Water permeability and permeate flux	178
3.3.	Application of TiO ₂ -coated C25A75M6 ultrafiltration membrane to decolorization of alizarin dye aqueous solution	180
3.3.1.	Effect of pH of the feed dye solution	180
3.3.2.	Effect of the concentration of the feed dye solution.....	181
3.3.3.	Effect of transmembrane pressure	182
4.	Conclusion.....	183
	References	184
	Chapter 4	190
	HYBRID CERAMIC MEMBRANE REACTOR SYSTEM FOR WATER AND WASTEWATER TREATMENT INTENSIFICATION	190
	Introduction	191
	Section 1	193
	<i>Hybrid Treatment System Combining Heterogeneous Catalysis with Membrane Separation for Improved removal of 4-Nitrophenol and Textile Wastewater</i>	193
1.	Experimental	193
1.1.	Chemicals and materials.....	193
1.2.	Material design and membrane nanostructuration.....	193
1.3.	Membrane characterization	193
1.4.	Experimental procedure (CMR).....	194
1.5.	Analytical methods.....	194
2.	Results and discussion.....	195
2.1.	Permeation experiments and rejection performance	195
2.2.	Hybrid water treatment system in CMR.....	198

2.2.1.	Nanocatalyst integration for 4NP removal	198
2.2.2.	CMR for textile wastewater removal.....	200
2.2.2.1.	Permeation study: influence of VCF on permeate flux	201
2.2.2.2.	Enhancement of permeate flux quality	202
2.3.	Membrane regeneration.....	204
3.	Conclusion.....	205
	References	206
	Section 2	213
	<i>Novel Ceramic Membrane for Removal of Explosives and Pesticides Contaminants from Water: Combination of Monolithic Catalyst with Co-Sintered Tight UF Membrane</i>	213
1.	Experimental	213
1.1.	Materials.....	213
1.2.	Synthesis of P1-IDA@NiNPs and P1-EDA@AuNPs monolithic catalysts.....	213
1.2.1.	Preparation of poly(EGDMA-co-GMA) monoliths “P1”.....	213
1.2.2.	Nickel NPs decorated IDA functionalized polymeric monolith.....	214
1.2.3.	Gold NPs decorated EDA functionalized polymeric monolith	214
1.3.	Low cost membrane design	215
1.3.1.	Porous mud support elaboration.....	215
1.3.2.	Preparation of tight ultrafiltration titania layer.....	215
1.3.3.	Characterization and Analytical methods.....	215
1.4.	Experimental Procedures.....	216
2.	Results and discussion.....	217
2.1.	Monolithic nanocomposites characterization	217
2.2.	4NP removal using P1-IDA@Ni and P1-EDA@Au.....	220
2.3.	Reusability of monolithic catalysts	222
2.4.	Ceramic membrane characterization	222
2.4.1.	Raw mud powder characterization	222
2.4.2.	Scanning electron microscopy (SEM).....	223
2.4.3.	Pore size distribution and wettability properties	226
2.5.	Application to Chloramphenicol (CAP) drug and 2,6-Dinitroaniline (2,6-DNA) removal 228	
2.6.	Synergistic effect of catalysis reaction and membrane filtration in CMR system.....	229
2.7.	Reusability evaluation of the T-UF CMR	231
2.8.	Membrane filtration resistance	233
2.9.	Antifouling properties	234
3.	Conclusion.....	236
	References	237
	GENERAL CONCLUSION AND PERSPECTIVES	243

Abstract	248
Résumé	248

List of Abbreviations

μ	Permeate Viscosity
1-Dod	1-Dodecanol
2,6-DNA	2,6-Dinitroaniline
2NP	2-Nitrophenol
4AP	4-Aminophenol
4NP	4-Nitrophenol
AAPTS	N-(2-aminoethyl)-3-aminopropyltrimethoxysilane
ACN	Acetonitrile
AFM	Atomic Force Microscopy
Ag	Silver
AGMD	Air-gap membrane distillation
AIBN	2,2'-Azobisisobutyronitrile
Al₂O₃	Alumina
ALD	Atomic Layer Deposition
ALZ	Alizarin
ALZ-Red	Alizarin Red
AO7	Acid Orange 7
APTES	3-aminopropyl triethoxysilane
Au	Gold
BET	Brunauer, Emmett and Teller
BT	Bentonite clay
CA	Contact Angle
CAP	Chloramphenicol
CB	Cresyl Blue
CM	Ceramic Membrane
CMR	Ceramic Membrane Reactor
CNTs	Carbon Nanotubes
COD	The chemical Oxygen Demand
CPNCs	Clay-Polymer Nanocomposites
CPV	Cumulative Permeate Volume

CtCMR	Catalytic Ceramic Membrane Reactor
CtMR	Catalytic Membrane Reactor
CVD	Chemical Vapor Deposition
DCMD	Direct Contact Membrane Distillation
DETA	Diethylenetriamine
DLBS	Dynamic Laser Beam Scattering
DTA	Differential Thermal Analyses
DWP	Drinking Water Production
EDA	Ethylenediamine
EDX	Energy Dispersive X-ray
EGDMA	Ethylene Glycol Dimethacrylate
Eo-Y	Eosin Y
Et₃-N	Trimethylamine
EVD	Electrochemical Vapor Deposition
FCC	Face-Centered Cubic
FEG	Field Emission Gun
FESEM	Field Emission Scanning Electron Microscopy
FRCP	Free-radical Copolymerization
FRP	Free-radical Polymerization
FTIR	Fourier Transform Infrared Spectroscopy
GHN	Graphene Hybrid Nanomaterial
GMA	Glycidyl Methacrylate
GO	Graphene Oxide
GPNCs	Graphene-Polymer Nanocomposites
GPTMS	(3-glycidyloxypropyl) trimethoxysilane
HA	Humic acid
HAuCl₄	Chloroauric Acid
HDPA	Hexadecyl Phosphonic Acid
HFTCM	Hollow Fiber Tubular Ceramic Membrane
ICM	Inert Ceramic Membrane
IDA	Iminodiacetic Acid
IMs	Inorganic Membranes
IUPAC	International Union of Pure and Applied Chemistry

J₀	Initial Permeate Flux (L.m ⁻² .h ⁻¹)
J	Permeate Flux
J_N	Normalized Permeate Flux
J_w	Water Flux
LbL	Layer-by-Layer
J_c	Critical Flux
JCPDS	Joint Committee on Powder Diffraction Standards (New name: International Centre for Diffraction Data)
L_p	Water Permeability
MAPS or Y-MAPS	3-methacryloxypropyl trimethoxysilane
MB	Methylene Blue
MePCM	Mesoporous Ceramic Membrane
MiPCM	Microporous Ceramic Membrane
MD	Membrane Distillation
MGR	MGR Methyl Magnesium Bromide
MHLP	Mud of Hydrocyclone Laundries of Phosphates
MF	Microfiltration
MLD	Molecular Layer Deposition
MMT	Montmorillonite
MNPs	Metallic nanoparticles
MO	Metal Oxide
MR	Membrane Reactor
MRP	Membrane Reactor Process
MW	Molecular Weight
MWCO	Molecular Weight Cut-Off
NaBH₄	Sodium Borohydride
NCs	Nanocomposites
NF	Nanofiltration
Ni	Nickel
NiCl₂	Nickel(II) Chloride
NiO	Nickel Oxide
OWWT	Oily Wastewater Treatment
PAA	Polyacrylic Acid

PAC	Powder Activated Carbon
PAH	Polyallyl amine
PCM	Porous Ceramic Membrane
PCP	Plasma Chemical Process
Pd(OAc)₂	Palladium(II) Acetate
Pd	Palladium
PDA	Polydopamine
PdO	Palladium Oxide
PEG	Polyethylene Glycol
PGMA	PolyGlycidyl Methacrylate
PGR	Phenyl Magnesium Bromide
pH	Hydrogen Potential
PNCs	Polymer-based Nanocomposites
PPA	Phenyl Phosphonic Acid
PV	Permeate Volume (mL)
PVA	Polyvinyl Alcohol
PVP	Polyvinyl Pyrrolidone
R_{ir}	Irreversible Fouling Resistance (m ⁻¹)
R_m	Intrinsic Membrane Resistance / Self-Membrane Resistance (m ⁻¹)
RO	Reverse Osmosis
R_r	Total Reversible Resistance (m ⁻¹)
R_T	Total Membrane Resistance (m ⁻¹)
SFE	Surface Free Energy
SiO₂	Silica
SS	Suspended Solids
SSMR	Side-Stream Membrane Reactor
SWD	Sea water Desalination
T-UF	Tight Ultrafiltration
TDS	Total Dissolved Solids
TETA	Triethylenetetramine
TGA	Thermogravimetric Analysis
THF	Tetrahydrofuran
TiO₂	Titania

TMP	Transmembrane Pressure
UF	Ultrafiltration
UV-Vis	Ultraviolet-Visible
VCF	Volume Concentration Factor
WD	Water Desalination
WOS	Water-Oil Separation
WWT	Wastewater Treatment
XPS	X-Ray Photoelectron Spectroscopy
XRD	X-Ray Diffraction
XRF	X-Ray Fluorescence
ZrO₂	Zirconia
ZVMs	Zero-Valent Metals

List of Figures

Figure 1. FESEM images showing (a and b) top and (c and d) cross-sectional views (From Suresh and Pugazhenthii 2017).....	15
Figure 2. FESEM images showing (a) top-surface and (b) cross-sectional views of ceramic membrane support prepared from the composition clay/alumina/methocel 25/75/6 and coated with a titania layer. The inset in (a) shows a magnified image of the surface of the titania-based membrane (From Oun et al., 2017).....	16
Figure 3. Cross sectional SEM images together with EDS spectra of ceramic membranes subjected to 600 atomic layer deposition cycles with varied exposure time: (a, d, and g) 0 s; (b, e, and h) 10 s; (c, f, and i) 40 s. The EDS spectra were recorded at three different points (Points 1–3 marked in the corresponding locations in SEM images). Only the EDS profile for Point 2 of each sample is shown in the inset of the corresponding SEM image. (d–f) Plots of the relative atomic percentages of Al recorded at different positions (Points 1–3 in the SEM images). (g–i) High magnification SEM images showing the surface layer and transition layer (From Li et al., 2012).....	17
Figure 4. Schemes of the possible interactions of (a) Grignard reagents and (b) phosphonic acids with the surface of MOs (From Mustafa et al., 2014).	22
Figure 5. Schematic illustration of the grafting mechanism by (a) the non-self-assembling silylated PEG grafting agents versus (b) the self-assembling silylated ureido PEG grafting agents (From Tanardi et al., 2016a).....	27
Figure 6. Schematic illustration of air-gap membrane distillation in counter current flow configuration (From Khemakhem et al., 2013).....	29
Figure 7. Statistics showing the evolution of the number of publications related to nanocomposites: (a) pie chart describing the distribution of different types of nanocomposites and (b) the equivalent data as presented by <i>Kumar and co-workers</i> in a review article (Kumar et al., 2018).....	42
Figure 8. Some various epoxy-GMA grafting using realties ligands (From Gokmen and Du Prez 2012).....	47
Figure 9. Coupling of the membrane with catalysts: (a) pellet catalyst on an inert ceramic membrane, (b) inherently catalytic membrane and (c) catalyst integrated into the pores of the membrane (From Li 2007).....	66
Figure 10. Side-stream membrane reactor (SSMR) configuration (From Jiang et al. 2013).....	67
Figure 11. Schematic diagram of catalysis/separation system in SSMR (1) Reaction tank (2L), (2) Feed pump, (3) Membrane module, (4) Air compressor, (5) mechanical stirrer, (6) Feeding system, (7) Feed entry, (8) Retentate, (9) Permeate, (10) Permeate collecting system, (11) Catalysts, (12) Membrane sealing "Steel", P1–P2: Pressure gauges, V1–V6: Valves and T: Temperature indicator and controller.	75
Figure 12. Schematic diagram of membrane sides for (a) tubular configuration: cross-flow filtration and (b) planar configuration: dead-end filtration.	76
Figure 13. Membrane filtration processes displaying and representative water contaminants removed according to pore size range (From Meng et al., 2015).....	77
Figure 14. Reduction of 4-nitrophenol to 4-aminophenol, in presence of NaBH ₄ , over MNP-based catalyst immobilized on CM (From Liu et al., 2017).....	78

Figure 15. Schematic illustration of the different procedures for preparing MNPs-loaded ceramic membranes (a) into the membrane pores using nano-coating modification of ZnO and Pd nanoparticles or supported onto the membrane surface using (a) silane grafting, (b) polymer coating and (c) adsorption of polyelectrolytes (From Dotzauer et al., 2006; Jiang et al., 2014; Liu et al., 2017; Peng et al., 2016).....	81
Figure 16. MMT, MMT-OH, MMT-MAPS, MMT-PGMA, MMT-PGMA-NH ₂ (a) FTIR spectra, (b) XPS survey spectra, and C1s High resolution XPS scans of (c) MMT-MAPS, (d) MMT-PGMA, (e) MMT-PGMA-NH ₂	118
Figure 17. (a) XPS survey spectrum of MMT-PGMA-NH ₂ @AuNPs, (b) Au 4f high resolution XPS spectrum of MMT-PGMA-NH ₂ @AuNPs, (c) XRD patterns of MMT-PGMA-NH ₂ @AuNPs, and (d) TGA curves of MMT-PGMA-NH ₂ @AuNPs (R ₁), NH ₂ @AuNPs (R ₂), and NH ₂ @AuNPs (R ₃).	120
Figure 18. SEM images and AuNPs size distribution of (a, b) MMT-PGMA-NH ₃ ⁺ @Au (R ₁), (c, d) and MMT-PGMA-NH ₃ ⁺ @Au (R ₂), and (e, f) MMT-PGMA-NH ₃ ⁺ @Au (R ₃) and SEM image of MMT-PGMA@AuNPs.....	122
Figure 19. UV-vis absorption spectra of (black) pure p-nitrophenol, (red) p-nitrophenol directly after addition of NaBH ₄ , (grey) p-nitrophenol 72 h after addition of NaBH ₄ , (blue) p-nitrophenol 72 h after addition of MMT-PGMA-NH ₃ ⁺ @AuNPs . The insets show (1) the catalytic reduction of p-nitrophenol by MMT-PGMA-NH ₃ ⁺ @AuNP (R ₁) nanostructures and NaBH ₄ , (2) photographs of pure p-nitrophenol solution, p-nitrophenolate obtained by addition of NaBH ₄ to p-nitrophenol solution, and p-aminophenol solution as a result of reduction of p-nitrophenol by MMT-PGMA-NH ₃ ⁺ @AuNP (R ₁) and NaBH ₄	124
Figure 20. Time-dependent evolution of UV-vis absorption spectra showing the gradual reduction of p-nitrophenol and plots of ln(A/A ₀) versus reaction time for the catalytic reduction of p-nitrophenol by (a, b) MMT-PGMA-NH ₃ ⁺ @AuNPs (R ₁), (c, b) MMT-PGMA-NH ₃ ⁺ @AuNPs (R ₂), (e, b) MMT-PGMA-NH ₃ ⁺ @AuNPs (R ₃) and NaBH ₄ . Plot of k _{app} versus (d) AuNPs size (f) concentration of MMT-PGMA-NH ₃ ⁺ @AuNPs (R ₁) nanocatalyst for the catalytic reduction of p-nitrophenol.....	126
Figure 21. (a) UV-vis absorption spectra of (black) pure pendimetalin, (red) pendimetalin 72 h after addition of NaBH ₄ , (blue) pendimetalin 72 h after addition of MMT-PGMA-NH ₃ ⁺ @AuNPs, (grey) pendimetalin 72 h after addition of MMT-PGMA-NH ₃ ⁺ @AuNPs and NaBH ₄ and (b) time-dependent evolution of UV-vis absorption spectra showing the gradual reduction of pendimetalin by MMT-PGMA-NH ₃ ⁺ @AuNPs (R ₁) and NaBH ₄ . The insets show (a) the catalytic reduction of pendimetalin by MMT-PGMA-NH ₃ ⁺ @AuNP (R ₁) and NaBH ₄ and photographs of pure pendimetalin and the obtained reduced pendimetalin, and (b) plots of ln(A/A ₀) versus reaction time.....	127
Figure 22. Reusability of the MMT-PGMA-NH ₃ ⁺ @AuNPs nanostructure as heterogeneous catalyst for the reduction of 4NP using NaBH ₄	129
Figure 23. (a) Raman spectrum, (b) XPS survey scan, and (c) XPS C1s high-resolution region, (d) SEM images of GHN, and TGA curves of (e1) bentonite, (e2) sucrose, and (e3) GHN.	147
Figure 24. Atomic fraction and values of O1s/C1s ratios of pristine and all functionalized GHN samples.....	149
Figure 25. XPS survey and C1s high-resolution spectra of (a) GHN-GPTMS, (b) GHN-TGE, (c) GHN-GPTMS-TGE, (d) GHN-TGE-GPTMS, (e) GHN-COOH prepared by conversion of epoxy groups of GHN-GPTMS-TGE to carboxylic acid ones.....	150
Figure 26. (a) SEM image, (b) EDS spectrum, (c) Pd 3d high-resolution XPS spectrum, (d) XRD pattern of GHN-COOH@PdNPs.....	152
Figure 27. (a, b, c) UV-vis absorption spectra of pure (blue) ALZ, MB, and Eo-Y, and (red) 24h after addition of GHN-COOH@PdNPs nanocatalyst without NaBH ₄ , respectively. (b, d, f) UV-vis	

absorption spectra of pure (blue) ALZ, MB, and Eo-Y, and (green) 24h after addition of an excess NaBH ₄ without catalyst, respectively. Reaction conditions: [Dyes] = 0.1 mM, [NaBH ₄] = 25 mM, [GHN-COOH@PdNPs] = 0.25 g/L.....	153
Figure 28. Time-dependent of UV–Vis absorption spectra showing the gradual of the reduction of (a) Alz, (b) MB and (c) Eo-Y. (d) Plots of ln(A/A ₀) versus reaction time for pseudo-first-order reaction for the reduction of Alz, MB and Eo-Y at room temperature by using excess NaBH ₄ in the presence of GHN-COOH@PdNPs as catalysts. Reaction conditions: [Dyes] = 0.1 mM, [NaBH ₄] = 25 mM, [GHN-COOH@PdNPs] = 0.25 g/L.....	155
Figure 29. Reusability of GHN- GHN-COOH@PdNPs catalyst for the reduction of MB with NaBH ₄ for eight cycles.	158
Figure 30. (a) Schematic representation of the homemade cross flow UF membrane set up. (b) Firing schedule applied for the preparation of the porous tubular ceramic supports. (c) Photograph of extruded porous tubular ceramic supports sintered at a temperature of 1350 °C for 90 min.	171
Figure 31. Effect of (a) methocel and (b) clay contents on the mechanical strength of the porous tubular ceramic supports sintered at a temperature of 1350 °C for 90 min. In (a) the clay/alumina ratio is 50/50 while in (b) the methocel content was kept constant at 6 g.	175
Figure 32. TGA and DTA plots recorded for the porous tubular ceramic support C25A75M6 prepared from the composition clay/alumina/methocel 25/75/6 and sintered at a temperature of 1350 °C for 90 min.....	176
Figure 33. Pore size distribution measured for the porous tubular ceramic support C25A75M6 prepared from the composition clay/alumina/methocel 25/75/6 and sintered at a temperature of 1350 °C for 90 min.....	177
Figure 34. Field emission scanning electron microscopy images of (a) top surface and (b) cross section of the porous tubular ceramic support C25A75M6 prepared from the composition clay/alumina/methocel 25/75/6 and sintered at a temperature of 1350 °C for 90 min.	177
Figure 35. Field emission scanning electron microscopy images of (a) top-surface and (b) cross-section of ceramic membrane support C25A75M6 prepared from the composition clay/alumina/methocel 25/75/6 and coated with a TiO ₂ layer. The inset in part (a) shows a magnified image of the TiO ₂ -based membrane’s surface.....	178
Figure 36. Variation of the water permeability as a function of the transmembrane pressure for the ceramic membrane support C25A75M6 (square) before and (circle) after coating with TiO ₂ layer. .	179
Figure 37. Time-dependences of the flux of alizarin red solutions at different transmembrane pressures for the ceramic membrane support C25A75M6 coated with a TiO ₂ layer. UF conditions: [ALZ] = 150 ppm and pH = 9.	180
Figure 38. Variation of the retention rate (R, expressed in %) of Alizarin Red as a function of the pH of the dye solution as measured for the ceramic membrane support C25A75M6 coated with a TiO ₂ layer. UF conditions: [ALZ] = 150 ppm, TMP = 5 bar and t = 100 min.....	181
Figure 39. Time-dependences of the retention rate (R, expressed in %) for various initial concentrations of Alizarin Red as measured for the ceramic membrane support C25A75M6 coated with a TiO ₂ layer. UF conditions: TMP = 5 bar and pH = 9.	182
Figure 40. Variation of the retention rate of alizarin red dye from spiked water solution (150 ppm) as a function of the transmembrane pressure. The insets showing images of the feed dye solution (left) and the permeate solution (right) as obtained after ultrafiltration process during 100 min at 5 bar evidence the effectiveness of dye removal.	183

Figure 41. (a) Normalized flux ($J_N = J/J_0$), (b) CPV of 250ppm 4NP solution as function of UF operation time at different TMP, (c) critical permeation flux and (d) effect of 4NP concentration on the membrane rejection rate at 2 bar.	197
Figure 42. Effect of the catalyst dose on (a) Permeate flux stability with filtration time (b) Permeate flux and 4NP retention; (TMP = 2, initial 4NP concentration = 500ppm, working time= 3h).	199
Figure 43. Variation of the permeate flux with VCF for textile wastewater treatment (Conditions: $W_{\text{catalyst}} = 0.5 \text{ g/L}$; TMP= 2bar).....	202
Figure 44. Regeneration of UF membrane operating in hybrid system in the case of the use of 500mg/L of catalyst (case of textile effluent treatment).....	204
Figure 45. Physicochemical characterization of P1-IDA@Ni and P1-EDA@Au monolithic catalysts by FTIR (a and b), TGA (c and d) and XRD (e and f).	219
Figure 46. UV-vis spectra of 4NP during the reducing reaction using (a) P1-IDA@Ni, (b) P1-EDA@Au hybrid catalysts, (c) the corresponding pseudo-first order kinetics and (d) the reference catalytic reaction. Conditions: $[4\text{NP}] = 5 \cdot 10^{-4} \text{ M}$; $[\text{NaBH}_4] = 0,05 \text{ M}$; Dose of catalyst= 1mg/mL.....	221
Figure 47. Cycling performance plots of (a) P1-IDA@Ni and (b) P1-EDA@Au catalysts for 4NP reduction within 200s and 100s respectively.....	222
Figure 48. Particle size distribution of mud powder used for membrane elaboration.....	223
Figure 50. Pore size distribution of co-sintered bilayer membrane.....	226
Figure 51. Water contact angle measurement for (a) bare mud support and co-sintered TiO_2 membrane surface after (b) first and (c) second LbL coating.	227
Figure 52. Variation of the (a) rejection rate and (b) permeation flux with CAP and 2,6-DNA concentrations at 4 bar using nanostructured titania membrane.....	229
Figure 53. Effect of catalyst loading on the permeate flux during CAP and 2,6-DNA treatment by hybrid catalysis / T-UF process. Catalyst: (a) P1-IDA@Ni; (b) P1-EDA@Au. ($[2,6\text{-DNA}] = [\text{CAP}] = 200\text{ppm}$, TMP =4bar, t=2h).....	231
Figure 54. Reusability potential of the bilayer titania membrane in terms of (a) permeate flux and (b) rejection performances in the CMR system after each inter-cycle cleaning.	232
Figure 55. Membrane resistance distribution in the single filtration process and the hybrid treatment system.....	235
Figure 56. (a) TEM images, (b) line scan for Au, Ag, Si, Al, O and C elements and (c) pore size distribution of bimetallic $\text{MMT-PGMA-NH}_3^+@Au/Ag$ and UV-VIS absorption spectra of 4-NP reduction by using monometallic (d) $\text{MMT-PGMA-NH}_3^+@Ag$, (e) $\text{MMT-PGMA-NH}_3^+@Au$ and (f) bimetallic $\text{MMT-PGMA-NH}_3^+@Au/Ag$ and (g) reaction kinetics.....	247

List of Tables

Table 1. Examples of using ceramic membranes in major industrial applications.....	11
Table 2. Summary of the Mains Characteristic of Different Ceramic Membrane after Surface Modification and Their Applications.	19
Table 3. Chemical properties of 4-Nitrophenol and Pendimethalin.	113
Table 4. Comparison of literature results obtained with Pd PNs catalysts for the reduction of various dyes.....	156
Table 5. Composition of the ceramic supports and mixing conditions.....	172
Table 6. Alizarin red dye characteristics.	173
Table 7. Characterization of the raw effluent of SITEX textile industry.....	201
Table 8. Performance of the hybrid catalysis/UF process.	203
Table 9. Chemical composition of phosphate mud.....	222
Table 10. Membrane resistance analysis during the different treatment processes.	234

Les demandes éventuelles de corrections faites par le jury.

Comme il a été signalé hier à la fin de ta soutenance par le jury, il y a des corrections à apporter à ton MS et le délai est de 10 jours.

Tu trouveras ci-dessous les corrections demandées par le jury.

1. Dans l'introduction: ajouter une partie qui définit bien quels sont les verrous à lever dans ces la thèse.

2. Ajouter à la fin de la partie bibliographique une partie stratégie suivie (comme ce que nous avons ajouté dans ta présentation de soutenance) en expliquant bien pourquoi le choix des procédés membranes et catalyse mais aussi des matériaux (argile, argile-graphène, monolithes, polymères, nanoparticules métalliques...

3. Dans la partie nanocomposites:

* page 122 du MS: Tracer une courbe de $K_{app}=f(\text{surface des particules})$ et expliquer l'allure de la courbe.

* remplacer dans les courbes ATG du MS par celles où on montre la quantité de métal immobilisé.

D'ailleurs, à faire ça pour les différentes courbes que nous avons modifié mais aussi les schémas de synthèse.

* A mettre le mécanisme de catalyse à la surface des particules métalliques (un schéma et aussi deux lignes dans le texte de chaque article)

4. Dans le chapitre membranes :

* parler de perte de couleur au lieu de rétention.

* Réexpliquer (corriger) le mécanisme de rétention des différentes molécules: vérifier le type d'interactions (électrostatiques? ou plutôt hydrophobes?) les interactions électrostatiques sont-elles vraiment possibles ? ou c'est plus de l'accumulation de molécules à la surface.

➤ Pour répondre penser d'abord à définir le pH de la solution et la charge de surface des membranes et ensuite répondre à cette question.

* essayer d'expliquer pourquoi la rétention (perte de couleur) est-elle plus importante dans le cas de membranes avec des petits pores. et comment ça se fait que des petites molécules sont retenues par des membranes de pores de large diamètres.

Creuser un peu les résultats de cette partie!

* faire une comparaison entre les trois types de membranes et dire que celles à base de phosphates sont plus intéressantes et pourquoi?

5. Dans les perspectives, ajouter un paragraphe sur les procédés en continu (à volume constant).

GENERAL INTRODUCTION

1. Background

The protection of the environment has become a major concern for all countries especially the protection of water resources. Indeed, water is a vital resource for human health, with significant impact on sustainable development, including poverty eradication, gender equality, food security and the preservation of ecosystems. Water resource preservation is nowadays a social, economic and environmental issue and water resources are becoming weaker every day with huge inequalities over the planet. Sustainable management of water resources is needed including not only lower consumption but also lower pollution.

Industrialization that has been highly beneficial to improving everyday life is also responsible for pollution. Exemplarily, Industrial effluents in textile industries are weakly biodegradable and characterized by a strong coloration and significant pollution, of both mineral and organic nature. Thus, recycling wastewater with a high efficiency and limiting polluting discharges into the natural environment are currently among the most challenges that are facing manufacturers in all sectors.

Since decades, the introduction of nanotechnology in industry as well as in academic research has allowed for the development of a new class of functional materials. These advances have also benefited to environmental sciences and there is a growing interest in developing environmentally friendly materials meant to reducing public health risks. Nanosensors for pollutants detection, nanophotocatalysts for pollutant degradation and conversion in benign compounds, nanostructures membranes for water filtration, to name but a few are examples of such materials that can include a large family of ceramics, polymers, nanoparticles and nanocomposites.

Currently, the economic challenges for the development of these materials are multiple and concern varied constraints such as the availability of raw materials in significant amounts and at low cost, as well as their easy transformation to end use functional materials via green and cost-effective (energy consumption) methods without altering their performances. To address such an ambitious issue, the present PhD project focused on designing low cost UF ceramic membranes from clays or phosphate by-products (Mud) of the phosphate laundries industry and catalytic polymer hybrid materials incorporating natural resources nanoparticles such as clays and graphene-like and meant to polluted water treatment.

2. Aims and Challenges

Therefore, the experimental work performed during this PhD project aimed at (1) designing membrane supports with tubular geometries by a combination of extrusion (ceramic pastes) and calcination (at a temperature as low as possible) processes, (2) The synthesis of polymer-based nanocomposites incorporating nanometric fillers and further used as supports for highly immobilized catalytic metallic nanoparticles.

One of the aims of this experimental work was to establish correlations between the preparation processes and the characteristics of the materials (morphology, porosity, mechanical strength, physicochemical stability, dispersion and the interaction between catalytic nanoparticles and polymer-based materials) so as to obtain materials with optimized properties and best suited to the envisioned applications.

In addition, the wide choice with regard to the nature of the raw materials offers nearly unlimited possible combinations and is of great advantage to develop innovative nanocomposites and membranes whose properties are already exploited in the context of water remediation. Coupling membrane separation processes (based on UF ceramic membranes) together with heterogeneous catalytic reactions (based on the implementation of catalytic polymer hybrid materials) was also investigated.

This thesis project therefore aims, on the one hand, to employ natural materials to synthesize high-performance and low-cost filtration membranes, and on the other hand, to develop functional and robust hybrid materials for potential use as heterogeneous catalysts for applications in the treatment of polluted water through efficient processes.

In order to cover all these aspects, various challenges inherent in scientific, technical and economic sides must be removed in this work.

One of the significant challenges of this thesis will be to study the feasibility of preserving the quality of the water and protecting the environment by setting up effective processes for treating water before it is discharged into the receiving environment. At this level, the synthesis in large quantities and with low cost of hybrid powder catalyst still constitutes a technological barrier on an industrial scale. Another challenge to be removed in this thesis when investigating the chemistry of metallic nanoparticles complexes is to examine the nature of ligands to construct hybrid catalyst strongly coordinating having homogeneous distribution of MNPs which inhibit its aggregation by potential non-covalent interactions.

To overcome these challenges, it was also necessary, on the one hand, to prepare high-performance substrates from the exploitation of inexpensive natural materials such as phosphate, sugar graphene and clay, for example. On the other hand, we seek in this work to

develop simple design approaches that allow producing efficient catalyst even when used in low quantities.

3. Thesis Outline

This present manuscript of thesis consists of four chapters. The first chapter is devoted to a bibliographic study providing a "state-of-the-art" about the Preparation and surface modification of porous ceramic membranes for water treatment. The chapter is divided into three parts, which present the main subjects of literature reviews followed by three experimental chapters, each presenting a brief introduction and the main experimental results. The outlines and the specific objectives of each chapter are highlighted as follows.

The first chapter presents a comprehensive literature review of the works already carried out and related to our thesis aims. It is structured around three main subsections including: (i) Ceramic membrane for separation technology, (ii) Heterogeneous catalysis based on catalytic reduction reaction using nanohybrid catalyst for organics degradation and (iii) Intensification of water pollution remediation using membrane reactor, coupling membrane separation with heterogeneous catalysis for hybrid continuous treatment process. The first subsection is focused on the preparation, surface modification and specific properties of inorganic membrane based on ceramic mesoporous support and a particular attention is paid to low cost raw materials. The effectiveness of these membranes was then investigated in the water and wastewater treatments. The second subsection is summarizing different polymer-based supports for catalytic metallic nanoparticles stabilization. Finally, an overview and experimental evaluation of the membrane separation intensification by simultaneously integration of heterogeneous catalysis in ultrafiltration membrane reactors for organic pollution removal and the potential application in the raw wastewater treatment are presented in the third section.

The second chapter presents the preparation of catalytic hybrid nanostructures based on chelatatant-functionalized clay and graphene-like heterostructures immobilized gold (Au) and palladium (Pd) metallic nanoparticles, respectively. As initial robust platforms, single or mixed montmorillonite clay and graphene was firstly chemically modified by chelatatant functional groups which enable complexing high densities of homogeneously dispersed metallic nanoparticles in order to generate active catalytic sites. These nanoparticles were generated using in-situ reduction of gold and palladium nanoparticles from previously complexed their corresponding metal ions by using sodium borohydride (NaBH_4) reducing agent. Afterwards, monometallic hybrid catalysts ($\text{MMT-PGMA-NH}_2@AuNPs$ and GHN-

COOH@PdNPs) were used to degrade hazardous organic compounds such as nitroaromatics and dyes.

Chapter 3 is devoted to the experimental study of ceramic membranes fabrication, nano-structuration and characterization for membrane separation process. These experiments were performed on a home-made laboratory setup by using two different types of low-cost ceramic membranes. In this study, membrane nanostructuration was achieved by deposition of selective titania nanolayer on clay/alumina mesoporous tubular support. The evolution of the thermal, mechanical and physico-chemical properties of the membranes as well as ultrafiltration unit and the operating protocols are studied and presented in this chapter. The performances notably in term of flux and retention rate of the as-fabricated ultrafiltration membranes are investigated toward synthetic dyes treatment, which are widely used in dyeing industries (textile).

The Chapter 4 presents the last chapter of this manuscript, where feasibility tests in the use of Ceramic Membrane Reactors (CMR) operated in continuous mode to eliminate water contaminants have been performed. The used CMR is constituted of both titania UF and (tight-UF) T-UF membrane deposited on 100% mud support and hybrid catalysts based on gold (AuNPs) and Nickel (NiNPs) nanoparticles decorated monolithic composites and the gold immobilized on chelatant polymer nanostructures described above. Here, synthetic effluent solutions such as nitroaromatics (nitrophenol, pesticides, explosives and antibiotic drugs) as well as real industrial wastewater were treated through coupled hybrid process combining heterogeneous catalysis and membrane ultrafiltration in continuous flowreactor. The mechanism for the degradation of organic pollutants is a catalytic hydrogenation reaction induced by the metallic nanoparticles-containing composites that is rich in electrons. The coupling strategy for separation and catalysis aimed at highlighting the synergistic effects between both processes and yield intensification of each by other in the membrane reactor as well as the potential performances of this hybrid process toward industrial wastewater recycling and the reuse of the membrane (antifouling study).

Finally, this thesis manuscript ends with a general conclusion summarizing the entirety of the performed work including a synoptic presentation of the major obtained results and possible future work of research is also suggested as perspectives.

Chapter 1

LITERATURE REVIEW

Section 1

Preparation and Surface Modification of Porous Ceramic Membranes for Water Treatment

1. Introduction

Membrane separation is well-recognized as a mature technology well-suited to address issues of separation and treatment of complex mixtures and reject handling arising from the textile, chemical, food, and pharmaceutical industries, to name but a few. This large success can be rationalized by the intrinsic characteristics of membrane processes such as high stability and efficiency, low energy requirement, and ease of operation (Saufi et al., 2004; Tin et al., 2011). Membrane materials can be classified as function of their chemical nature, organic vs. inorganic or pore size and related separation mechanism. Organic membranes are made of polymers including polyamide, polysulfone, polyethersulfone, and polydimethylsiloxane and are typically prepared by casting methods (air, immersion, and melt casting), track etching techniques, or controlled film stretching. Polymer-based microporous membranes are commercially available for use in ultrafiltration (UF) and microfiltration (MF) in health care for sample preparation prior to, for instance, chromatographic analysis, virus removal, and diagnosis purposes. They are also widely applied in the area of energy, as in lithium-ion batteries and fuel cells as well as in the petrochemical industry to treat produced water. Although polymeric membranes can be cost-effectively designed with well-controlled characteristics such as pore size and hydrophilic/hydrophobic balance, these constructed membranes suffer from limited chemical, thermal, and mechanical stability compared to their inorganic counterparts.

Porous inorganic membranes (IMs) are mainly manufactured from metal oxides (MOs) such as alumina (Al_2O_3), silica (SiO_2), zirconia (ZrO_2), and titania (TiO_2) (Chowdhury et al., 2003; Lenza et al., 2000; Van Gestel et al., 2006), while metals such as palladium, nickel, silver, zirconium, and their alloys are used for the preparation of dense membranes (Biswas et al., 2018). It is reported also that zeolite-based (alumino silicate) membranes (Ghouil et al., 2015) showed the characteristic of dense membranes. IMs can resist harsh conditions making their use possible in wide pH (pH 1–14) and temperature (up to 500°C) ranges. These advantages also allow for regeneration of the membranes through washing with aggressive chemicals, organic solvents, or a hot water stream.

Ceramic membranes with a broad range of pores size can be elaborated through different preparation approaches, including slip casting, tape casting, pressing, extrusion, sol-gel

process, dip coating, and chemical vapor deposition. Most IMs are made of a combination of a thin separation layer and a porous support and are mainly employed in pressure-driven separation processes (Guizard et al., 1996).

Production of industrial ceramic membranes relies on the use of a limited choice of raw materials and generally involves a high temperature-sintering step to ensure strong bonding between membrane and support. The high sintering temperature used in the case of titania and alumina ceramic membranes may explain their relatively high price (Anderson et al., 1988). The presence of hydroxyl groups on the membrane surface governs the permeation properties of the membrane and allows for modification of surface properties such as surface roughness and hydrophilicity or hydrophobicity. Khemakhem et al. (2011a; 2011b), for instance, reported that chemical modification of a membrane surface with hydrophilic moieties may prevent membrane fouling.

To date, a number of methods have been proposed such as plasma-enhanced chemical vapor deposition (CVD) (Wu et al., 2002), plasma polymerization (Chen et al., 1999), and chemical grafting (Alami Younssi et al., 2003; Kujawa et al., 2013a; 2013b; 2014a). *The research group of Ben Amar* (Tunisia) described an elegant method for the chemical functionalization of ceramic materials through a grafting process of perfluoroalkylsilane (Khemakhem et al., 2013). The newly developed ceramic MF membranes that have 7 L/m².h bar as water permeability are very promising in the field of membrane distillation, exhibiting total salt rejection of 99% with permeate flux of 165 L/day.m² under ΔT of 85°C.

The use of aliphatic organosilanes such as trimethylsilyl chloride (Me₃SiCl) (Alami Younssi et al., 2003), triphenylsilyl chloride (Si(C₆H₅)₃Cl), tert-butyldimethylsilyl chloride (C₄H₉(CH₃)₂SiCl) (Caro et al., 1998; Sah et al., 2004), dichlorodimethylsilane ((CH₃)₂SiCl₂), and dichloromethyloctylsilane (C₈H₁₇CH₃SiCl₂) (Van Gestel et al., 2003) was reported for hydrophobization purposes. It was notably shown that the degree of hydrophilic or hydrophobic modification depends on both the extent of grafting and the length of the grafted segment. Indeed, steric hindrance may limit the grafting reaction of bulky silanes at the internal surface of the membrane.

The aim of this chapter is to conclusively highlight the synergy of inorganic materials and surface functionalization for the design of microporous ceramic membranes (MiPCMs) with controlled permeability and selectivity. In this chapter, particular attention is paid to the chemical modification of membrane surface with the aim to control the hydrophilic/hydrophobic balance and control the pore size. We discuss the application of the

so-chemically modified membranes for water treatment including membrane distillation (MD), oil/water separation (OWS), and wastewater treatment (WWT).

2. Development of ceramic membranes derived from low-cost raw materials

Ceramic membranes have been extensively applied in different industrial areas such as the food and beverage industry (Almandoz et al., 2015; Bogianchini et al., 2011; Cissé et al., 2011; Nandi et al., 2009; Zulewska et al., 2009), chemistry (Athanasekou et al., 2009; Padaki et al., 2015), water treatment and reuse (Van Der Bruggen et al., 2003), and biotechnology and pharmaceuticals (Díaz-Reinoso et al., 2009; Liu et al., 2017), as summarized in **Table 1**. In general, ceramic membranes have tubular and multi-tubular geometry.

Table 1. Examples of using ceramic membranes in major industrial applications.

Area	Process	Applications	References
Food and beverage industry	MF and UF	Concentration of milk, concentration of protein, clarification of fruit juice/wine, and microorganism separation from fermented juice.	Almandoz et al., (2015); Nandi et al., (2009); Zulewska et al., (2009)
Biotechnology and pharmaceutical industry	MF and UF	Microorganism separation, cell debris filtration and plasma separation.	Liu et al., (2017); Díaz-Reinoso et al., 2009
Chemical and industrial applications	MF and UF	Oil-water separation, purification of used oil and removal of precipitated heavy metals and solids.	Padaki et al., (2015); Athanasekou et al., (2009)
Recovery and Recycling	UF and NF	Drinking water and wastewater treatment.	Van Der Bruggen et al., (2003)

For instance, the commercial membranes from Orelis (KERASEP membrane), made of $\text{Al}_2\text{O}_3\text{-TiO}_2$ or $\text{Al}_2\text{O}_3\text{-ZrO}_2$, have a multi-tubular geometry with 7 or 19 channels with each channel having a diameter of 6 mm (Wallberg et al., 2003). KLEANSEP ceramic membranes are commercially available in a wide range of molecular weight cut-off (MWCO), providing industrial solutions in the filtration of suspensions, emulsions, and solutions.

Crucial requirements for using ceramic membranes are high permeability, long lifetime, and selectivity. Undoubtedly, the high mechanical resistance and chemical stability of ceramic membranes toward harsh operating conditions under continuous flow are key features of their success. Indeed, ceramic materials enable the use of high pressures and temperatures,

chemically aggressive cleaning methods, and back pulsing during processes (Ben Amar et al., 1990). MF and UF ceramic membranes have been used in a wide variety of filtration processes such as separation of microorganisms, proteins, and colloidal solutes. Although nanofiltration (NF) membranes have been applied to water treatment, including wastewater containing heavy metals and synthetic dyes, the ceramic membranes are not widely applied to NF compared to organic membranes (Arnell et al., 2014). The application of ceramic membranes has also been extended to non-aqueous solution separation especially in petrochemical processing. Al_2O_3 , SiO_2 , and ZrO_2 UF membranes have been applied to the separation of asphaltene from crude oil in the temperature range of 155–180°C (Guizard, 1996). The treated oils were considered clean oils owing to the effective removal of heavy metals such as copper, lead, iron, and chromium.

A quick overview of the literature dedicated to the field of ceramic membranes reveals that various inorganic materials have been considered precursors for membrane design. Asymmetric membranes are typically manufactured from MOs among which pure or mixed Al_2O_3 (Gaber et al., 2013; Garmsiri et al., 2017; Ren et al., 2015), ZrO_2 (Bouzerara et al., 2015; Guo et al., 2016), TiO_2 (Cai et al., 2015; Gaber et al., 2013; Garmsiri et al., 2017; Guo et al., 2016; Palacio et al., 2009; Yacou et al., 2015) and SiO_2 (Lim et al., 2009; Yoshino et al., 2008) have been primarily used. Although MO-based membranes have proved very efficient for a variety of separation processes associated with pollution treatment, they suffer from high preparation cost. The use of MO powders and the high sintering temperature would make the commercial-quality membranes costly. This drawback slows down the development of this type of membranes.

Today, the trend is toward using low-cost materials and, if possible, recycling by-products that arise from industrial activities with the aim to reduce cost and to develop green processes. Researchers and engineering firms are continuously working on the development of cost-effective processes, and one of the solutions relies on the use of low-cost materials of natural origin.

Natural clays (Bouazizi et al., 2016; Garmsiri et al., 2017; Khemakhem et al., 2009; 2011a; Oun et al., 2017; Vinoth Kumar et al., 2015), zeolites (Kosinov et al., 2016; Lafleur et al., 2017), sand (Aloulou et al., 2017; Kouras et al., 2017), quartz (Kouras et al., 2017), fly ash (Jedidi et al., 2009a; 2011; Suresh et al., 2016), calcite (Kouras et al., 2017), apatite (Masmoudi et al., 2007; Sahoo et al., 2016), phosphate (Bouazizi et al., 2017; Palacio et al., 2009) and phosphate sub-products (Khemakhem et al., 2011c; 2015) have proven to be very promising. This is because natural raw powders may provide high chemical and thermal

stability, enhanced mechanical resistance, long-term durability, and ease of cleaning between each application run to prevent surface fouling phenomena (Garmsiri et al., 2017). Moreover, formulations derived from low-cost materials may require low thermal treatment temperatures contributing significantly to cost reduction (Khemakhem et al., 2006a; 2009; 2011c; Sarkar et al., 2012; Tahri et al., 2013).

The research group of Ben Amar showed that the use of mud, a by-product of the mining industry in Tunisia, allows for a significant decrease of the sintering temperature to 700°C for the support and 650°C for the active layer (Khemakhem et al., 2015). This range of temperature is much lower than the one obtained with other raw materials (e.g., clay, apatite, sand, and fly ash), which have a sintering temperature higher than 1000°C (Khemakhem et al., 2015). Many researchers have discussed the potential use of natural Moroccan and Tunisian clays to produce membrane supports for MF and UF applications (Khemakhem et al., 2006b; 2007; 2011a; Saffaj et al., 2004). In addition, Masmoudi et al. (2007) studied the elaboration of UF membranes based on natural phosphates as well as synthetic apatite while Aloulou et al. (2017) reported on the design of MF membranes meant to be used for wastewater treatment (WWT) using Tunisian natural sand. Other authors also demonstrated the possibility of developing ceramic membranes from abundant industrial sub-products, such as fly ash arising from coal fired power stations (Jedidi et al., 2009a; 2009b; 2011) and muds obtained from the washing steps of phosphates rocks (Khemakhem et al., 2015). The so-designed ceramic membranes were applied in different areas of water treatment.

3. Surface modification of ceramic membrane via structuration

Tailoring the microstructure of ceramic membrane surface has been accomplished with a variety of oxide particles via depositing a thin layer on the membrane support. A broad range of membrane properties can be obtained through a judicious choice of both particle nature and size as well as thickness of the coating. Membrane structuration is a subject of much interest in the purification of oily wastewater because it yields small pores that favor efficient oil particles rejection. It is highly possible to provide anti-adhesive properties against oil to the membrane surface by increasing the membrane hydrophilicity.

Among the MOs that have been considered to date, TiO₂ nanoparticles emerged as promising candidates since their structural morphology and formed coating thickness can be easily adjusted by simply changing the experimental conditions. Chang et al. (2014) improved the hydrophilicity of 19-channel tubular ceramic MF membrane using a one-step nano-

TiO₂ synthesis-deposition procedure. The TiO₂ nanoparticles were synthesized directly inside the membrane channels by filling them with a solution containing a 1:2 molar ratio of Ti(SO₄)₂/urea. The titane-containing membrane support was treated twice at 85°C for 3 h followed by a calcination at 950°C for 2 h. This produced an inner surface alumina membrane with a uniform TiO₂ nanoparticles array (30 nm TiO₂ spheres), causing a decrease of the contact angle from 33° to 8°. Such an increase in wettability of the composite ceramic membrane led to an improvement of the membrane flux in separation of a stable oil-in-water emulsions compared to the unmodified ceramic membrane for the optimized cross-flow MF conditions (trans-membrane pressure of 0.16 MPa, feed cross-flow velocity of 5 m/s and temperature of 40°C). Under these conditions, the maximum flux was reported to be about 330 L/m².h.

A different route to prepare TiO₂ composite ceramic membrane was described by Suresh and Pugazhenth (2017). It was based first on the co-precipitation of the TiO₂ nanoparticles using TiCl₄ in the presence of a solution of NH₄OH. Subsequently, the as-prepared titania nanoparticles suspension was placed together with the low-cost clay-based porous ceramic membrane (PCM) support for hydrothermal treatment at 160°C for 12 h followed by a calcination step at 400°C for 3 h in a muffle furnace. The contact angle of a deposited water droplet on the surface of the as-designed TiO₂ ceramic membrane reached a value of about 15° revealing the significant surface hydrophilicity (see *Figure 1*). The average pore size as determined by N₂ adsorption-desorption decreased slightly from about 0.981 μm in the case of the unmodified membrane to 0.877 μm after TiO₂ coating. Remarkable improvement in both flux (648 L/m².h) and oil removal efficiency (>99%) was obtained for the elaborated TiO₂-ceramic membrane compared to the native ceramic support, which exhibited a permeate flux and oil removal efficiency of 313.2 L/m².h and 93–96%, respectively, when both membranes were tested using feed oil concentration of 200 mg/L and at 2.07 bar. This effect was due to the hydrophilic nature of titania membrane surface, which prevents access of the oil droplets into the pores and significantly reduces membrane fouling.

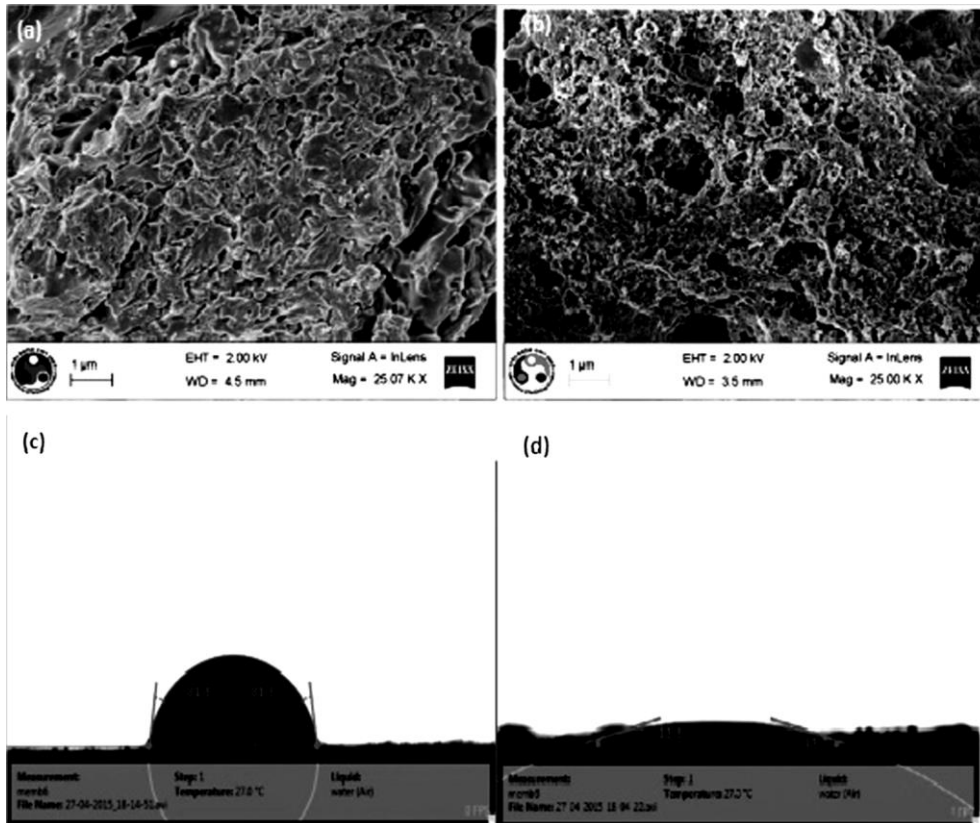


Figure 1. FESEM images showing (a and b) top and (c and d) cross-sectional views (From Suresh and Pugazhenthii 2017).

3.1. Ceramic Membrane from Slip-Casting Method

TiO₂-modified ceramic membranes have also been largely used in the domain of the separation of dyes from wastewater because of their ability to improve permeate flow and antifouling capacity. Oun et al. (2017) developed novel asymmetric UF ceramic membranes by the deposition of a single separation layer of TiO₂ particles on the inner surface of extruded tubular porous clay-alumina membranes (ID/OD = 7 mm/10 mm) by the slip casting method. The separation UF layer was prepared via a one-step slip casting at room temperature of an aqueous suspension of TiO₂ particles (4 g), containing 12 wt% of polyvinyl alcohol (PVA) used as binder and 0.2 wt% of Dolapix CE64 used as dispersant, directly inside the tubular supports.

SEM characterization indicated the presence of a dense and homogeneous 4.2 μm thin TiO₂ layer with a mean pore size of about 50 nm (see *Figure 2*). The UF TiO₂-coated tubular ceramic membranes showed high performance towards the removal of alizarin red dye (MW: 240.21 g/mol) at a transmembrane pressure of 5 bar and at pH of 9. In comparison to previous works on removal of dyes from wastewater, the membranes designed by Oun et al. (2016)

exhibited greater performance in terms of water flux ($117 \text{ L/m}^2\cdot\text{h}$) and alizarin red dye rejection rate (99%) than the ceramic tubular membranes made of $\text{TiO}_2\text{-ZnAl}_2\text{O}_4\text{-clay}$ (Saffaj et al., 2004), Kaolin-based membrane (Bouzerara et al., 2009), and $\text{TiO}_2\text{-ZrO}_2\text{-Al}_2\text{O}_3$ (Ma et al., 2017) that showed water flux of 9.42, 33 and $28.1 \text{ L/m}^2\cdot\text{h}$ with rejection rate of 90% ($P = 10 \text{ bar}$), 98% ($P = 3 \text{ bar}$), and 97% ($P = 3 \text{ bar}$), respectively. This finding can be attributed to the contribution of the TiO_2 nanoparticles that enhance the filtration performances. The color retention is mainly due to the adsorption onto the membrane surface (Ganesh et al., 2016).

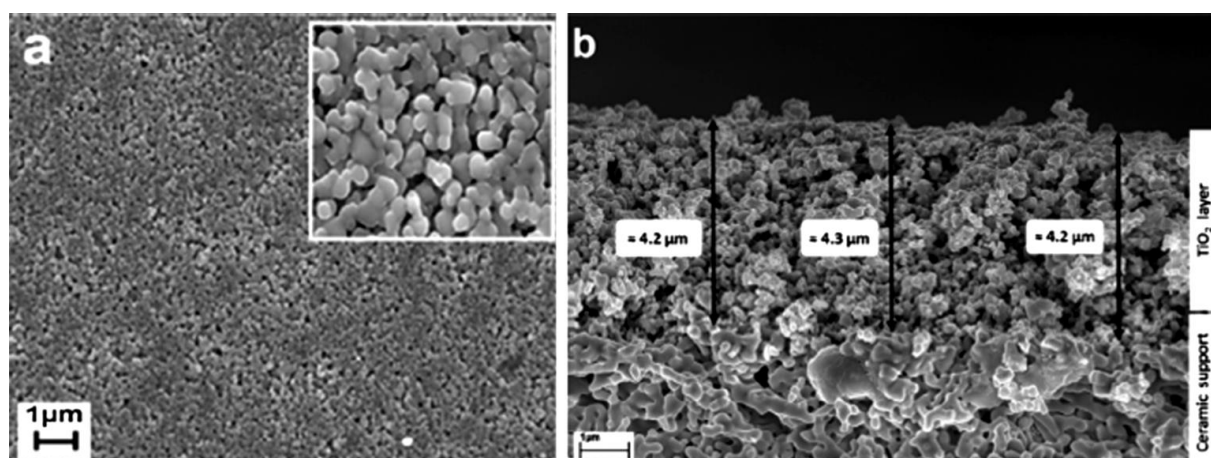


Figure 2. FESEM images showing (a) top-surface and (b) cross-sectional views of ceramic membrane support prepared from the composition clay/alumina/methocel 25/75/6 and coated with a titania layer. The inset in (a) shows a magnified image of the surface of the titania-based membrane (From Oun et al., 2017).

3.2. Ceramic Membrane from Atomic Layer Deposition

MO thin films with 3-D structures can also be deposited on ceramic membrane surface via the novel ALD method, which is a gas phase deposition technique. This one-step pathway enables the generation of a uniform atomic-scale thin layer of oxides that strongly attaches to the membrane surface as well as to the pore walls. Moreover, both thickness and pore size of the atomic layer can easily be tuned by varying the number of deposition cycles and adjusting the exposure time of the membrane support and metal precursors to the oxidant source. This method was described for the first time when Li et al. (2012) deposited a thin film of Al_2O_3 on tubular ceramic membranes based on a layer of ZrO_2 nanoparticles-coated Al_2O_3 supports. The coating process was carried out at 250°C using trimethylaluminum and deionized water as precursors. SEM analysis, as shown in *Figure 3*, indicated that consecutive deposition steps induced a continuous decrease of the membrane pore size from about 50 to 6.8 nm,

suggesting controllable conversion from MF to UF and NF and even dense membranes by increasing the number of ALD cycles. Furthermore, an increase of the number of ALD cycles from 0 to 800 led to a significant decrease in the membrane permeability from about 1698 to 118 L/m².h.bar. This result was attributed to the decrease of the pore size of the membranes after surface modification.

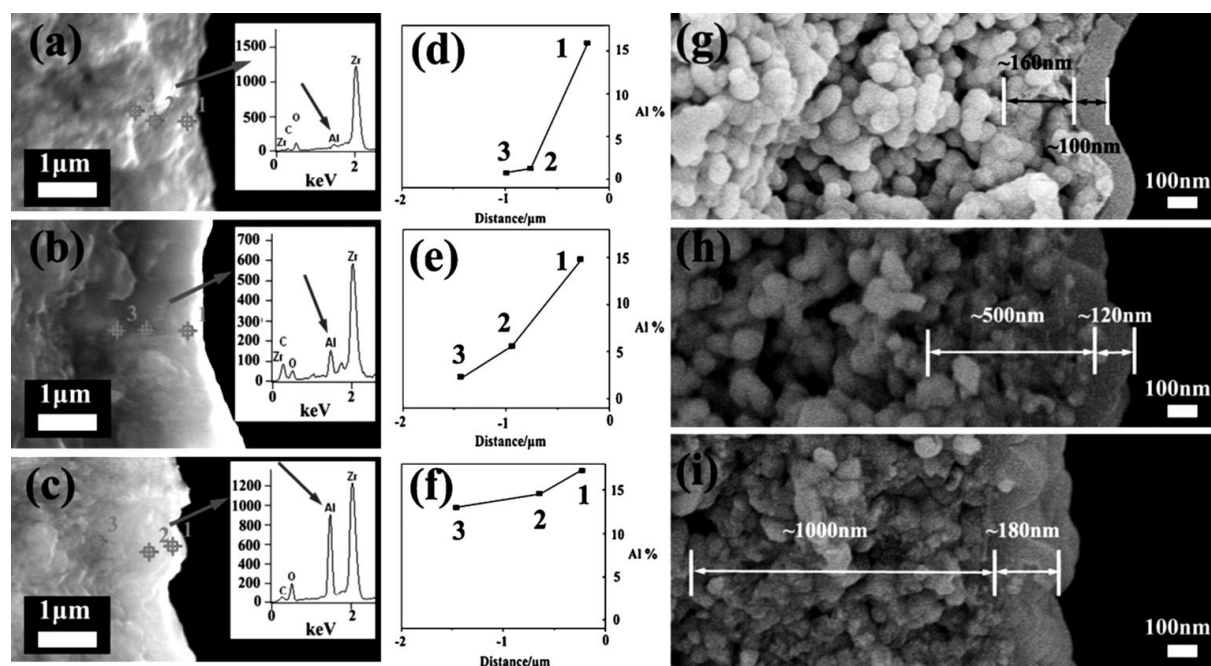


Figure 3. Cross sectional SEM images together with EDS spectra of ceramic membranes subjected to 600 atomic layer deposition cycles with varied exposure time: (a, d, and g) 0 s; (b, e, and h) 10 s; (c, f, and i) 40 s. The EDS spectra were recorded at three different points (Points 1–3 marked in the corresponding locations in SEM images). Only the EDS profile for Point 2 of each sample is shown in the inset of the corresponding SEM image. (d–f) Plots of the relative atomic percentages of Al recorded at different positions (Points 1–3 in the SEM images). (g–i) High magnification SEM images showing the surface layer and transition layer (From Li et al., 2012).

More recently, atmospheric pressure ALD has been explored for the fabrication of tight ceramic NF membranes (Shang et al., 2017). Compared to the work of Li et al. (2012), the deposition step could be successfully achieved without the need for an expensive vacuum system, and thus the atmospheric pressure ALD method is more cost-effective for the fabrication of modified membranes. The thickness of the TiO₂ coating was estimated to be 0.05 nm/cycle by AFM technique. It is worth noting that the increase of the number of cycles leads to the decrease of the pore size. This finding was fully evidenced by molecular weight cut-off (MWCO) characterization using polyethylene glycols (PEG: 200 to 1000 g/mol). The performances were evaluated by measuring the water permeability before and after treatment.

A slight improvement in water permeability was observed as the value increased from 11 to 16 L/m².h.bar.

4. Surface modification of ceramic membranes via chemical grafting

In this section, we will discuss different synthetic strategies that are employed for the surface modification of ceramic membranes. Surface modification is considered the key step in tuning the morphological structure, the chemical composition, and thus the separation properties of ceramic membranes for water and WWT applications. Furthermore, membrane surface post-modification is shown to be an efficient route to solve one of the most critical issues in membrane technology, namely, the fouling tendency. To be able to prevent fouling problems while maintaining a correct flux is of high economic and ecological importance because it both increases the productivity and lifetime of membranes and reduces cleaning steps.

Significant research efforts have been devoted to developing surface modification strategies compatible with ceramic materials in order to enhance filtration performance. To this aim, many surface modifying agents such as Grignard reagents (Hosseinabadi et al., 2015), organophosphonic acids (Mustafa et al., 2014), metal/MO particles (Chang et al., 2014; Li et al., 2012; Oun et al., 2017; Suresh and Pugazhenthii 2017), organosilanes (Gao et al., 2013; Khemakhem et al., 2014; Kujawa et al., 2013a; 2014b; Lee et al., 2016), and polyethylene glycols (Tanardi et al., 2016a) have been proposed. These materials can be divided into two categories: MO particles and hydrophobic modifiers. The first category is frequently used for developing nanostructured membranes while the second is employed to prepare hydrophobic hybrid membranes. **Table 2** summarizes the main characteristics of the different ceramic membranes made from natural and MO materials after surface modification and their applications.

Table 2. Summary of the Mains Characteristic of Different Ceramic Membrane after Surface Modification and Their Applications.

Modification Method	Modifying Agents	Membrane Materials	Water Permeability (Lp)	Contact Angle (CA)	Applications	References
Silanization	(3-aminopropyl)triethoxysilane; 3-(trihydroxysilyl)1-propanesulfonic acid and trimethoxy(propyl)silane	Al ₂ O ₃	848 – 1037 L/m ² h.bar	N/A	HA filtration	Lee et al., (2016)
	n-octyltrichlorosilane (C ₈ Cl ₃); n-octyltriethoxysilane (C ₈ OE ₃); and trichloro(octadecyl)-silane (C ₁₈ Cl ₃)	TiO ₂ and Al ₂ O ₃	0.7 – 4.8 kg/m ² h.bar	CA (TiO ₂ -C ₈)= 113° ±2° CA (Ti O ₂ -C ₈ Cl ₃)= 128° ± 2° CA (Ti O ₂ -C ₁₈ Cl ₃)= 132° ±2°	WD	Kujawa et al., (2017)
	1H,1H,2H,2H-perfluorooctyltriethoxysilane (C ₆); 1H,1H,2H,2H-perfluorotetradecyltriethoxy- silane (C ₁₂);	TiO ₂	Lp (Ti O ₂ -C ₆)= 3.74 L/m ² h.bar Lp (Ti O ₂ -C ₁₂)= 3.86 L/m ² h.bar	CA (TiO ₂ -C ₆) = 135° CA (TiO ₂ -C ₁₂) = 145°	WD	Kujawa et al., (2014b)
	Ethyltrimethoxysilane (C ₂); Hexyltrimethoxysilane (C ₆) ; Octyltrimethoxysilane (C ₈) and hexadecyltrimethoxy-silane (C ₁₂)	Al ₂ O ₃	N/A	CA (unmodified membrane) = 9.1° CA (Al ₂ O ₃ -C ₆)= 126° ± 1° CA (Al ₂ O ₃ -C ₈)= 131.4° ± 1° CA (Al ₂ O ₃ -C ₁₆)= 140° ± 1°	WOS	Gao et al., (2013)
	1H,1H,2H,2H-perfluorodecyltriethoxy- silane (C ₈);	MHLP	Lp= 720 L/m ² h.bar (unmodified membrane) Lp= 7 L/m ² h.bar (functionalized membrane)	CA ((unmodified membrane) = 25° CA (functionalized membrane) = 160°)	WOS	Khemakhem et al., (2013)
	1H,1H,2H,2H-perfluorodecyltriethoxy- silane (C ₈);	Tunisian clay	Lp=155 L/ m ² day (MF membrane) Lp=110 L/ m ² day (UF membrane)	CA (Clay-C ₈) = 180°	WD	Khemakhem et al., (2011b)

Phosphorylation	MPA; PPA and HDPA	TiO ₂	Lp (TiO ₂ -MPA) = 15 L/m ² h.bar Lp (TiO ₂ -MPA) = Low L/m ² h.bar Lp (TiO ₂ -MPA) = 0 L/m ² h.bar	CA (TiO ₂ -MPA) = 37° CA (TiO ₂ -PPA) = 80° CA (TiO ₂ -HDPA) = 124°	DWP	Mustafa et al., (2014)
	MGR; PGR and MPA	TiO ₂	Lp (unmodified UF membrane) = 170-200 L/m ² h.bar Lp (TiO ₂ -MGR) = 104 L/m ² h.bar Lp (TiO ₂ -MPA)= 118 L/m ² h.bar Lp (unmodified NF membrane) =10-30 L/m ² h.bar Lp (TiO ₂ -MGR) = 5-13 L/m ² h.bar Lp (TiO ₂ -PGR) = 5-14 L/m ² h.bar Lp (TiO ₂ -MPA) = 8-27 L/m ² h.bar	UF membrane: N/A NF membranes: CA (unmodified NF membrane) = 10-20 ° CA (TiO ₂ -MGR) = 50-60 ° CA (TiO ₂ -PGR)= 50-60° CA (TiO ₂ -MPA)= 35-45°	WWT (paper mill effluents, olive oil wastewater)	Mustafa et al., (2016)
Polymer grafting	Triglyceride	MHLP	Lp (unmodified membrane) = 90 L/m ² h.bar Lp (functionalized membrane) = 7 L/m ² h.bar	CA (unmodified membrane)= 16° CA (functionalized membrane)= 121°	SWD	Derbel et al., (2017)

4.1. Membrane hydrophobization

Although ceramic membranes have been successfully used in the industrial applications, fouling phenomena still remain highly challenging. To overcome this problem, the surface functionalization of ceramic membranes through efficient chemistry strategies and the use of different modifying agents have largely been considered. This has resulted in the production of tailor-made hybrid organo-modified ceramic membranes.

Native ceramic membranes prepared using unique or mixed MO(s) and clay are characterized by their high hydrophilic character due to the presence of abundant surface hydroxyl groups. This hydrophilicity may induce water adsorption and/or capillary condensation in the pores, reducing the number of pores. Numerous studies have been dedicated to the introduction of hydrophobic chemical moieties onto ceramic membrane surface through strong interfacial bonding involving the replacement of the -OH surface groups by organic moieties.

4.2. Grignard reagents

Grignard reagents are a class of coupling agents proposed as a new class of surface modifiers of MOs (Hosseinabadi et al., 2015; Mustafa et al., 2016). These organometallic molecules have the generic formula of RMgX , where X is a halogen and R is an alkyl or aryl group. They were used for the first time by Van Heetvelde et al. (2013) for the chemical modification of titanium alkoxides as an alternative to organosilane coupling agents. Grignard modification yields non-hydrolysable bonding between the surface of the MO and the functional group, since the Grignard organic groups are directly bonded through a Metal-C bond at room temperature, as schematically shown in *Figure 4* (Mustafa et al., 2014). These bonds in the submonolayer coating exhibit higher stability towards hydrolysis than the M-O-Si bonds obtained with silanes. The benefit of such hybrid membranes relies on the combination of both organic and inorganic materials, which induces new interesting properties. Interestingly, Grignard modification method makes membrane amphiphilic due to the partial surface replacement of the membrane surface -OH groups by the Grignard hydrophobic groups.

Hosseinabadi et al. (2014) have successfully attached different organometallic Grignard molecules (C_1 to C_{12} groups) to 1 nm TiO_2 membranes in dry diethyl ether solvent, producing a series of hydrophobic titania ceramic membranes. After functionalization, removal of any remaining by-product, namely MgBr salt, requires multiple successive washings of the membranes in Et_2O , HCl (0.1 or 1 M), and H_2O . Examination of the modified membranes by ATR/FTIR spectroscopy revealed the presence of organic moieties on the membrane surface,

leading to an increase in the contact angle from 19° (unmodified TiO_2 membrane) to 83° ($\text{TiO}_2\text{-C}_8$ membrane). This confirmed the partial hydrophobization of the ceramic membrane.

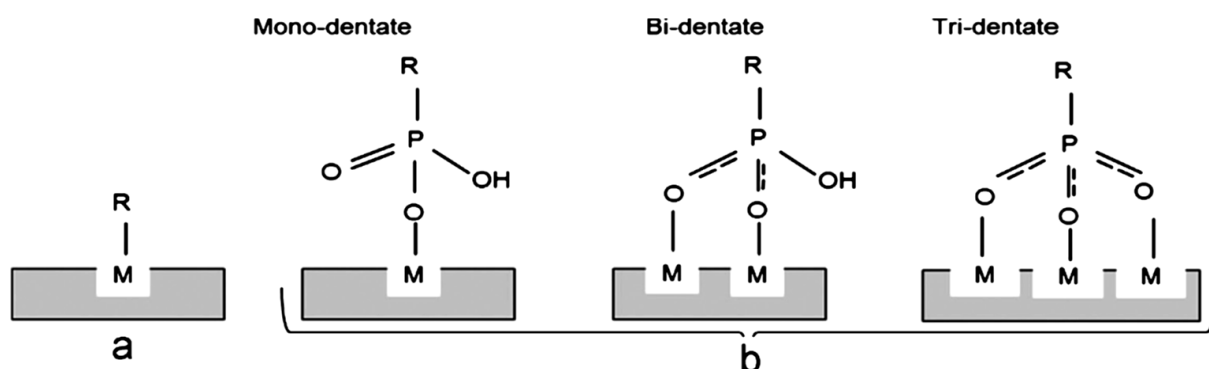


Figure 4. Schemes of the possible interactions of (a) Grignard reagents and (b) phosphonic acids with the surface of MOs (From Mustafa et al., 2014).

The as-prepared amphiphilic TiO_2 ceramic membranes were used to treat wastewater containing organic solvents, and they exhibited higher flux for tetrahydrofuran (THF), toluene, n-hexane, and polyethylene glycol retentions in water than unmodified membranes.

This Grignard grafting method has been found to be very promising in developing enhanced antifouling TiO_2 ceramic membranes applied in filtration of three challenging wastewater streams, namely pulp and paper mill effluent, olive oil wastewater, and oil/water emulsions (Mustafa et al., 2016). Mustafa et al. (2016) reported that the membranes grafted with methyl groups in particular showed an enhancement of filtration performances.

4.3. Organophosphonic acids

Phosphorylation using organophosphonic acids has been applied to derivatize ceramic membranes with organic moieties that act as surface hydrophobization agents. Moreover, the phosphorylation strategy is known to be fast, cheap, and can be successfully performed in water in contrast with the Grignard surface modification, which requires anhydrous organic media. This method involves generally three reactive groups (P-OH, P-OR, and PO) resulting in the formation of strong mono-, bi-, or tridentate bonds with the membrane surface. However, implementation of the phosphorylation approach in surface modification of ceramic membranes remains limited because of the low commercial availability of organophosphonic acid derivatives.

Randon et al. (1995) applied this strategy for the functionalization of TiO₂ and ZrO₂ mesoporous ceramic membranes (MCMs) phosphoric acid and alkyl (methyl, ethyl, and phenyl) phosphonic acids. The grafting reactions were performed in a 0.1 M toluene solution of phosphonic acid precursor at reflux during 4 h and were shown to proceed successfully by infrared analysis. The separation properties of the resulting hydrophobic membranes have been studied by UF process and demonstrated high efficiency in filtering bovine serum albumin (BSA).

Mustafa et al. (2014) have compared organophosphonic acids and Grignard reagents in the chemical modification of commercial TiO₂ membranes by using different functional groups. In the case of the Grignard method, alkyl and phenyl groups have been grafted onto the TiO₂ membranes under dry atmosphere using methyl and phenyl magnesium. The reaction was carried out in diethyl ether solvent for 48 h at room temperature. It should be noted that prior to the grafting reaction, the TiO₂ membranes were pre-treated in order to remove traces of adsorbed water. In the case of surface phosphorylation, methyl-, phenyl-, and hexadecyl phosphonic acid groups (HDPA) have been used. The authors showed an increase of the water contact angle and a decrease of the water permeability values after phosphorylation of the TiO₂ membranes with the different groups. These changes were attributed to the transformation of the surface characteristics of the membranes from hydrophilic to hydrophobic ones. Hydrophobization of the membranes induced a decrease in water flux. Interestingly, the fouling tendency of the functionalized tubular TiO₂ membranes, as determined using humic acid (HA) as model foulant, decreased obviously compared with the unmodified membrane. It has been shown that the effect of the surface functionalization on the membrane fouling depended strongly on both the grafting method and the chemical nature of the surface modifier. The most efficient antifouling effect was obtained with methyl Grignard reagent.

Caro et al. (1998) also compared silanization and phosphorylation of UF Al₂O₃ ceramic membranes by organic moieties. XPS analyses have shown that, in the case of silanization reaction, the surface modification was efficient when the Al₂O₃ membrane surface contained a Si-OH-rich thin layer. Phosphorylation was successful by reacting the phosphonic acid with the Al on the membrane surface. Investigation of the thermal stability of the phosphonic-modified membranes revealed that the silylated membranes were stable up to 230°C while the phosphonic-functionalized ones were stable up to 400°C. The effect of the surface modification on both single gases permeation and liquid mixtures pervaporation has been demonstrated.

4.4. Organosilanes

Organosilane agents have been shown to be useful for the functionalization of the surface of ceramic membranes with a high variety of both hydrophobic and hydrophilic moieties. These molecules with formula of either $X-CH_2CH_2CH_2Si(OR)_{3-n}$ or $X-CH_2CH_2CH_2SiCl_3$, where $n = 0, 1, 2$, OR is a hydrolysable alkoxy group, and X is an organo-functional group, bear two different reactive groups (OR or Cl and X) on their silicon atom and permit their coupling with a large variety of materials surface. The chemical grafting of an organosilane layer onto ceramic membranes is achieved through a silanization reaction in polar aprotic solvents between the surface hydroxyl groups arising from the ceramic membrane and the chloro or alkoxy groups coming from organosilane agents. The silanization reaction consists of two main steps involving (1) hydrolysis of the trialkoxy or chloro groups of silane that generates silanol (Si-OH) moieties and (2) reaction of the silanols with hydroxyl groups on the membrane surface that results in the chemical bonding of a silane layer onto the ceramic membrane. In order to avoid the polycondensation of organosilane molecules in the presence of traces of air or solvent moisture, the silanization reaction requires anhydrous solvent and an inert atmosphere.

The preparation of ceramic membranes meant to be used for desalination and oilwater separation requires a hydrophobic membrane surface. Generally, this modification leads to an increase of the membrane roughness and a decrease of membrane pore size. This can be explained by the condensation of silane moieties at the membrane surface, which may increase to a large extent the degree of densification.

Various examples of silanized ceramic membranes with hydrophobic surfaces have been reported in literature. Perfluoroalkyltriethoxysilanes and/or perfluoroalkyltrichlorosilanes are the most widely used hydrophobic agents to this aim. Khemakhem et al. (2011b) grafted triethoxy-1H,1H,2H,2H perfluorodecylsilane onto the MF (dpore = 0.18 μm) and NF (dpore = 15 nm) planar and tubular membranes made of Tunisian clay. The surface functionalization was performed under mild conditions (room temperature and 15 min of grafting time in silane solution) using 0.01 M silane solution. Water contact angle measurements and infrared characterization showed that all the membranes have been effectively grafted with superhydrophobic moieties. After surface modification, the membranes exhibited non-wettable surfaces as ascertained by the contact angle value of approximately 180°. The chemical attachment of fluoroalkyl moieties onto the membrane surface has been demonstrated by the presence of the stretching vibrations of C-C, Si-C, and C-F at 1540 cm^{-1} , 1270 cm^{-1} , and 1240

cm⁻¹, respectively. The success of seawater desalination (SWD) using air gap membrane distillation further suggested the great potential of these hydrophobic membranes.

The same research group, in pursuit of their investigations on developing hydrophobized ceramic membranes, has described the surface modification of ceramic microfiltration membrane made of zirconium/mud of hydrocyclone laundries of phosphates (MHLP) (Khemakhem et al., 2014). In the presence of triethoxy-1H,1H,2H,2H perfluorodecylsilane as a grafting agent, they reported a significant increase in the contact angle from 25° to values higher than 150°, as well as a sharp decrease in the pore size of the membrane as shown by SEM analysis. Similarly, Das et al. (2016) reported the hydrophobization of capillary clay-alumina-based ceramic membranes prepared using 55 wt% of clay with a pore size of 1.43 µm in diameter. Both the water contact angle (145°) and liquid entry pressure (1 bar) revealed the hydrophobic character of the clay-alumina functionalized membrane.

As an alternative to this type of organosilanes, the use of alkylsilanes with different length as hydrophobic surface modifiers has been proposed by Gao et al. (2013). The authors studied the influence of ceramic alumina membranes hydrophobicity on the filtration performance of water-in-oil emulsions. Ethyltrimethoxysilane, hexyltrimethoxysilane, octyltrimethoxysilane, and hexadecyltrimethoxysilane were used as organic modifiers. The chemical composition as well as the morphological surface of the as-prepared membranes were studied using X-ray photoelectron spectroscopy (XPS), infrared characterization, thermogravimetric analysis (TGA), and SEM. Although no significant changes in surface morphology have been highlighted, a decrease in the pore size together with an increase of the surface hydrophobicity and change in the chemical composition were observed. Despite the small changes in the membrane surface morphology, the modified membranes exhibited greater hydrophobic character than the pristine membrane. Moreover, the membrane hydrophobicity increased with increasing the length of the silane alkyl chains.

To study the effect of the surface charge on antifouling properties of ceramic membranes, Lee et al., (2016) described a similar strategy. The authors used three different functional alkylsilanes, namely trimethoxy(propyl)silane, (3-aminopropyl) triethoxysilane, and 3-(trihydroxysilyl)-1-propanesulfonic acid that possessed neutral (-CH₃), positive (-NH₂), and negative (-SO₃) charge, respectively, to plane alumina ceramic membranes. The alumina membranes were first washed with ethanol and subsequently introduced separately in a 0.1 M silane solution prepared in anhydrous ethanol for 5 h at room temperature. SEM, mercury intrusion porosimetry, and TGA have shown no change in the membrane surface morphology, and only a slight decrease in the average pore size of the alumina membranes was observed

after surface silanization. The authors explained these negligible surface modifications by the ultrathin organosilane grafts (thickness of approximately 0.1 μm). When tested using HA feed solution, the negatively charged (SO_3 -functionalized) membranes exhibited the lowest fouling (flux recovery rate of 80–85%), and a noticeable resistance to flux decline. As a comparison, the amine-grafted membrane and the unmodified membrane exhibited a higher degree of flux decline and a lower flux recovery rate (52%), which could be explained by their electrostatic interactions with the negatively charged HA (isoelectric point = 4.7).

4.5. Organic polymers

The surface functionalization of ceramic membranes through the deposition or grafting of macromolecules holds huge potential in water treatment processes. Indeed, ceramic-polymer composite membranes are a very interesting class of membranes as they combine the high chemical, thermal, and mechanical stability of ceramic membranes with the ease of surface modification and the low cost of organic polymers. As an important result, this combination imparts high selectivity and thus provides efficient water purification.

Mittal et al. (2011) prepared membranes by dip-coating hydrophilic UF ceramic membranes using hydrophilic cellulose acetate (10% w/v in acetone). The effective pore size of the deposited polymer top-layer, calculated by a novel theoretical approach based on the mass of the polymer film and the hydraulic permeability of the composite membrane, was found to be in the UF range (28 nm). The authors indicated that the chemical resistance of the prepared composite membrane was highly dependent on pH, as a slight change was detected in the polymer film after acid treatment contrary to basic treatment, which induced approximately 19.6% change in porosity. It has been shown that the acetate cellulose-ceramic membranes are suitable for separation of oil molecules from low concentrated oily wastewater (<250 mg/L).

Taking advantage of the strong adhesion between organosilanes and ceramic membranes, organosilanes were used as coupling agents in the preparation of polymerbased ceramic membranes. More precisely, the reactive functionality of silane-grafted ceramic membranes enabled the chemical attachment of polymer chains onto the ceramic support. Two strategies consisting of two successive steps can be envisioned to graft polymer films on ceramic membranes, i.e., (1) modification of the ceramic membrane surface by organosilane moieties followed by the coupling of the polymer and (2) functionalization of the polymer chains by organosilane agents prior to their grafting onto ceramic membranes. The latter strategy has been used by Tanardi et al. (2016a) for the grafting of various hydrophilic silylated PEG agents on mesoporous γ -alumina membranes. PEGs were initially chemically modified by the

reaction between amines and isocyanate groups. The silane terminated PEGs solution (3 mM in toluene) were then considered to accomplish the silylation reaction between the silane terminated PEGs and the mesoporous membrane for 24 h at 110°C, as schematically illustrated in **Figure 5**.

The effective grafting of PEG moieties to the alumina surface was proven by FTIR and ^{29}Si -NMR. The degree of self-condensation is about the same for most of the grafting agents. The grafting density decreased for PEG with long chain length.

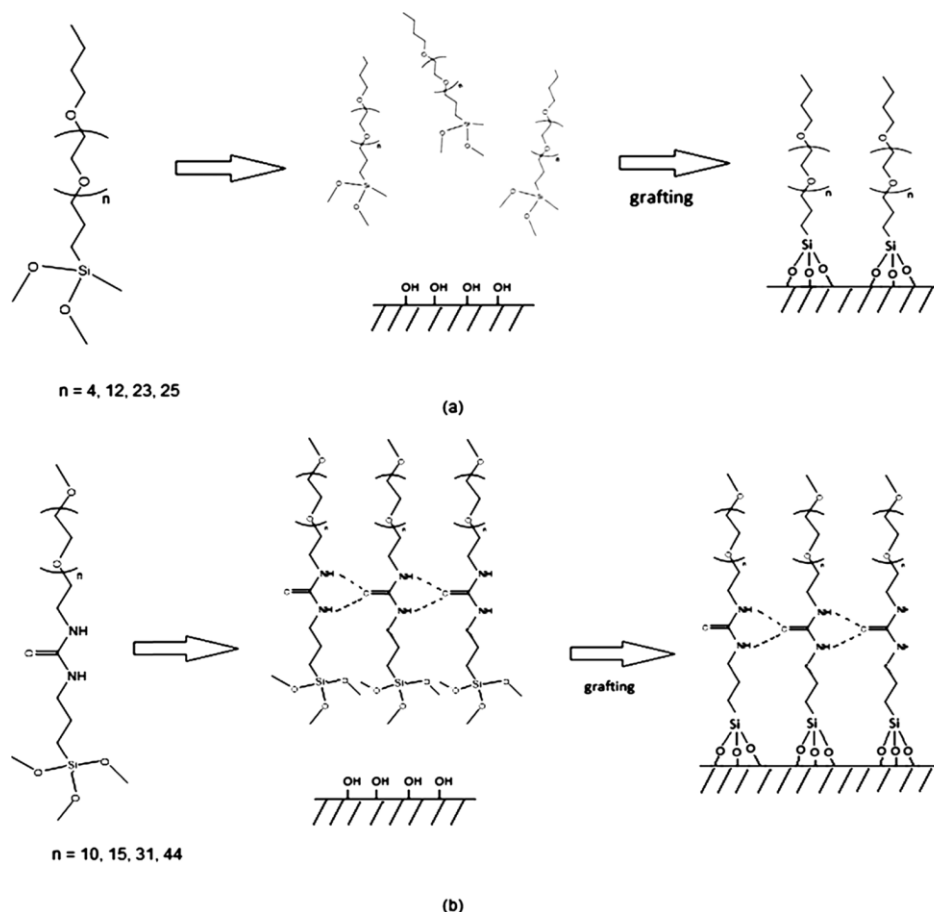


Figure 5. Schematic illustration of the grafting mechanism by (a) the non-self-assembling silylated PEG grafting agents versus (b) the self-assembling silylated ureido PEG grafting agents (From Tanardi et al., 2016a).

5. Application of chemically modified ceramic membranes

Functionalized ceramic membranes have gained increasing interest for separation and purification issues, especially in the context of water purification. The surface of ceramic membranes can be easily modified with a plethora of chemical modifiers that provide highly flexible and robust solutions for the separation of solutes from complex mixtures with enhanced selectivity, permeate water recycling and reuse, as well as improved antifouling

properties. Two domains of application of chemically modified ceramic membranes are presented in the following subsections. They are (1) desalination using membrane distillation method and (2) water/oil separation.

5.1. Water Desalination

Membrane distillation (MD) is a very useful strategy for water desalination. The method consists in a thermally driven separation process of two solutions. The difference of temperature between the feed and the permeate generates a water vapor pressure gradient that acts as the driving force for the water transfer in the MD process. A three-step mechanism has been suggested for the mass transfer based on (1) evaporation of the feed solution and vapor formation at the membrane pores entrance, (2) transport of the vapor through the membrane pores, and (3) condensation of the vapor at the permeate side. In order to prevent the undesirable phenomenon of penetration of the aqueous solutions into the MD pores, non-wetted hydrophobic porous membranes are required.

Khemakhem et al. (2013) proposed an air-gap membrane distillation (AGMD) process using grafted MF tubular mud/zirconia membrane with 1H,1H,2H,2Hperfluorodecyltriethoxysilane (C₈) for water desalination as shown in *Figure 6*. The authors indicated that the modified membrane was able to reject salt from oily wastewater with a rejection rate higher than 99% and a membrane permeability of 7 L/m².h.bar. They also found that the change in the salt concentration in the feed solution did not alter the retention of salts in the AGMD process. Using the same experimental setup, Khemakhem et al. (2011b) found that the C₈-grafted MF and UF tubular clay membranes were suitable for seawater desalination. They reported that the membranes could achieve a permeate flux of 155 and 110 L/m².day, respectively, with a complete removal of salts.

Similarly, Kujawa et al. (2014b) prepared hydrophobic hybrid titania ceramic membranes (300 kD) by chemical grafting of C₆F₁₃C₂H₄Si(OC₂H₅)₃ and C₁₂F₂₅C₂H₄Si(OC₂H₅)₃ perfluorinated agents and used the resultant membranes for NaCl removal. The effects of operating conditions, namely feed temperature, salt feed concentration, and MD mode (AGMD or direct contact MD (DCMD)) on the membrane performance were investigated. They showed that a higher permeate flux could be obtained using the membrane grafted with a smaller alkyl group (C₆) regardless of MD mode, achieving >99% NaCl retention. Under the feed temperature of 90°C and salt feed concentration of 2 M, the membrane grafted with C₆ exhibited water flux of 2300 g/m².h and 2100 g/m².h for AGMD and DCMD mode, respectively.

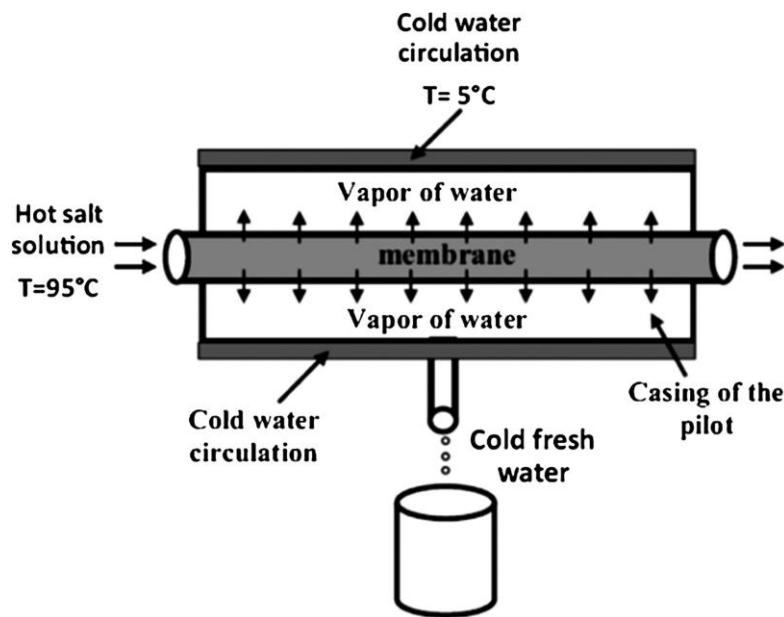


Figure 6. Schematic illustration of air-gap membrane distillation in counter current flow configuration (From Khemakhem et al., 2013).

More recently, Kujawa et al. (2017) grafted three various non-fluorinated hydrophobic coupling agents to TiO_2 and Al_2O_3 ceramic membranes for the AGMD of desalination. They observed that the permeate fluxes were in the range of $0.7\text{--}4.8 \text{ kg/m}^2\cdot\text{h}$ for tests with pure water whereas the fluxes were in the range of $0.4\text{--}2.8 \text{ kg/m}^2\cdot\text{h}$ in contact with salt solution. Interestingly, all the hydrophobic prepared membranes showed a NaCl retention coefficient higher than 98%.

Derbel et al. (2017) used Tunisian olive oil to chemically modify ceramic UF membranes made of MHLF from hydrophilic to hydrophobic. Increasing the contact angle values from 16° before modification to 121° after olive oil grafting revealed highly hydrophobic membranes. This membrane hydrophobization led to a significant decreasing of the water permeability from $90 \text{ L/m}^2\cdot\text{h}$ before modification to $7 \text{ L/m}^2\cdot\text{h}$ after modification. Upon grafting the olive oil on the UF membrane, 99% salt rejection was achieved using feed solution containing 30 g/L NaCl .

Ren et al. (2015) grafted $0.76 \mu\text{m}$ alumina planar membranes with fluoroalkyl silane using phase-inversion tape casting method for DCMD of water desalination. They tested the water desalination performance by exposing the hydrophobic separation layer to different concentrations of NaCl aqueous solution (2–6 wt%). They observed that the hydrophobic membranes could be operated up to 2 bar. When tested using a salt solution of 2 wt%, the

permeate flux was 19.1 L/m².h under a feed temperature of 80 °C. The hydrophobic membrane achieved >99.5% salt rejection. It is interesting to note that the MD flux exhibited a slight decrease when the concentration increased.

5.2. Oil/Water Separation

Separation of oil and water from stable oil/water emulsions is very challenging because of the sub-micrometer size of the oil droplets. Conventional oily wastewater treatment (OWWT) processes such as gravity separation, coagulation, thermal de-emulsification, free-floating oil, flocculation, and biological treatments show very poor removal of low oil concentrations (Zhu et al., 2014). Among the existing oil/water separation membranes, hydrophilic membranes exhibited the most effective fouling resistance behavior. As such, chemically-modified ceramic UF membranes are appealing candidates for oil/water separation.

Mittal et al. (2011) prepared cellulose acetate-grafted clay ceramic membranes using the dip-coating method for the treatment of oil-in-water emulsion with concentration of 50–200 mg/mL. The maximum rejection of 93% was obtained at a pressure of 138 kPa after 41 min of filtration using a feed solution with 200 mg/L oil concentration. The membrane water flux meanwhile was recorded at 6.66 L/m².h.bar.

Gao et al. (2013) grafted four non-fluorinated alkylsilanes (C₂, C₆, C₈, and C₁₆) to Al₂O₃ membranes and employed the resultant membranes for OWWT at 0.1 MPa. The separation tests of kerosene from water revealed that the hydrophobic coated membranes showed improved permeate flux compared to the unmodified membranes (214.9 L/m².h) and that the highest oil flux could be obtained using the C₁₆-modified alumina membrane (668.7 L/m².h). The separation efficiency for the unmodified and the four grafted membranes were 75.4%, 77.8%, 85.2%, 84.2%, and 84.3%, respectively, which clearly indicates the increase of the retention of the modified membrane.

Hydrophilized ceramic membranes are also found to be useful for the separation of oil and water. Chen et al. (2016) designed superhydrophilic ceramic membranes for the treatment of oil-contaminated wastewater using in-situ surface membrane modification via the deposition of Stöber silica inorganic nanoparticles. The silica nanoparticles top separation layer has been obtained by immersion of ceramic membrane supports previously fabricated from a mixture of kaolin, quartz, alumina oxide, and corn starch raw materials in a homogeneous silica sol in aqueous media in the presence of ammonia as a catalyst. The resultant hierarchical-structured silica membrane has been reported to offer excellent separation efficiency for 658 ppm oil-in-

water emulsion with oil droplet mean diameter of 1.54 μm , achieving >99.95% oil rejection under mild pressure-driven conditions (0.1 MPa).

6. Conclusion

For several decades, ceramic membrane materials have been synthesized using a plethora of raw materials and synthetic routes enabling the fine control of both membrane support properties and the surface chemistry of the active membrane layer with respect to pore size and size distribution, chemical nature, roughness, and hydrophilicity or hydrophobicity. The ceramic membrane support affords mechanical resistance for applications under pressure-driven conditions while the membrane selective layer provides specific separation mechanism and wettability properties. However, significant research is still needed related to the reduction of the production cost of ceramic membranes, reduction and prevention of membrane fouling and pores clogging during cake formation, enhancement of membrane life time through efficient cleaning, and regeneration processes. The wide range of potential applications of ceramic membranes in the water treatment area will continue to drive research in this field forward. Recent studies on surface modification of ceramic supports through either structuration with MO nanoparticles or chemical grafting are very promising. The former approach allows for the design of asymmetric membranes with finely controlled pore size that depends on both the size of the MO nanoparticles and the thickness of the membrane layer. A decrease in pore size down to some tens of nanometers gives access to NF process that is highly relevant for water and wastewater treatment. In the future, it is expected that MO-coated ceramic membranes will be widely applied to the filtration process in combination with photocatalysis, preferably under visible light, for the treatment of effluents. We also summarized the recent grafting strategies involving Grignard reagents, organophosphonic acids, organosilanes, and polymers applied to the robust chemical modification of ceramic membrane surface. The covalent attachment of organic moieties on ceramic membrane surface ensures the robustness of the coating and enables a change in the intrinsic hydrophilic nature of ceramic membranes to make the membrane hydrophobic or in contrast, to enhance the membrane's hydrophilicity. Grafting time and density, together with the type (fluorinated versus aliphatic) of the grafting molecules as well as the grafting conditions (in water versus organic solvent), and hydrolytic and thermal stability of the bonds are key parameters to be considered. Considering membrane hydrophilization, the grafting of PEG derivatives proved highly efficient to minimize membrane fouling while hydrophobic modified membranes are very promising for MD of water desalination and the separation of oil and water.

References

A

- Alami Younssi, S., Iraqi, A., Rafiq, M., Persin, M., Larbot, A., Sarrazin, J., 2003. Alumina membranes grafting by organosilanes and its application to the separation of solvent mixtures by pervaporation. *Separation Science Technology*. 32, 175–179.
- Almandoz, M.C., Pagliero, C.L., Ochoa, N.A., Marchese, J., 2015. Composite ceramic membranes from natural aluminosilicates for microfiltration applications. *Ceramics International*. 41, 5621–5633.
- Aloulou, H., Bouhamed, H., Ben Amar, R., Khemakhem, S., 2017. New ceramic microfiltration membrane from Tunisian natural sand: Application for tangential wastewater treatment. *Desalination and Water Treatment*. 78, 41–48.
- Anderson, M.A., Gieselmann, M.J., Xu, Q., 1988. Titania and alumina ceramic membranes. *Journal of Membrane Science*. 39, 243–258.
- Arkell, A., Olsson, J., Wallberg, O., 2014. Process performance in lignin separation from softwood black liquor by membrane filtration. *Chemical Engineering Research and Design*. 92, 1792–1800.
- Athanasekou, C.P., Papageorgiou, S.K., Kaselouri, V., Katsaros, F.K., Kakizis, N.K., Sapalidis, A.A., Kanellopoulos, N.K., 2009. Development of hybrid alginate/ceramic membranes for Cd²⁺ removal. *Microporous and Mesoporous Materials*. 120, 154–164.

B

- Ben Amar, R., Gupta B.B., Jaffrin M.Y., 1990. Clarification of apple juice using crossflow microfiltration with mineral membranes: Membrane fouling control by backpulsing and pulsatile flow. *Journal of Food Science*. 55, 1620–1620.
- Biswas, D.P., O'Brien-Simpson, N.M., Reynolds, E.C., O'Connor, A.J., Tran, P.A., 2018. Comparative study of novel in situ decorated porous chitosan-selenium scaffolds and porous chitosan-silver scaffolds towards antimicrobial wound dressing application. *Journal of Colloid and Interface Science*. 515, 78–91.
- Bogianchini, M., Cerezo, A.B., Gomis, A., López, F., García-Parrilla, M.C., 2011. Stability, antioxidant activity and phenolic composition of commercial and reverse osmosis obtained dealcoholised wines. *LWT - Food Science and Technology*. 44, 1369–1375.
- Bouazizi, A., Saja, S., Achiou, B., Ouammou, M., Calvo, J.I., Aaddane, A., Alami Younssi, S., 2016. Elaboration and characterization of a new flat ceramic MF membrane made

from natural Moroccan bentonite. Application to treatment of industrial wastewater. *Applied Clay Science*. 132–133, 33–40.

Bouazizi, A., Breida, M., Karima, A., Achiou, B., Ouammou, M., Calvo, J.I., Aaddane, A., Khiat, K., Alami Younssi, S., 2017. Development of a new TiO₂ ultrafiltration membrane on flat ceramic support made from natural bentonite and micronized phosphate and applied for dye removal. *Ceramics International*. 43, 1479–1487.

Bouzerara, F., Harabi, A., Condom, S., 2009. Porous ceramic membranes prepared from kaolin. *Desalination and Water Treatment*. 12, 415–419.

Bouzerara, F., Boulanacer, S., Harabi, A., 2015. Shaping of microfiltration (MF) ZrO₂ membranes using a centrifugal casting method. *Ceramics International*. 41, 5159–5163.

C

Cai, Y., Wang, Y., Chen, X., Qiu, M., Fan, Y., 2015. Modified colloidal sol–gel process for fabrication of titania nanofiltration membranes with organic additives. *Journal of Membrane Science*. 476, 432–441.

Caro, J., Noack, M., Kolsch, P., 1998. Chemically modified ceramic membranes. *Microporous and Mesoporous Materials*. 22, 321–332.

Chang, Q., Wang, Y., Cerneaux, S., Zhou, J-E., Zhang, X., Wang, X., Dong, Y., 2014. Preparation of microfiltration membrane supports using coarse alumina grains coated by nano TiO₂ as raw materials. *Journal of the European Ceramic Society*. 34, 4355–4361.

Chen, T., Duan, M., Fang, S., 2016. Fabrication of novel superhydrophilic and underwater superoleophobic hierarchically structured ceramic membrane and its separation performance of oily wastewater. *Ceramics International*. 42, 8604–8612.

Chen, W., Fadeev, A.Y., Hsieh, M.C., Oner, D., Youngblood, J., McCarthy, T.J., 1999. Ultrahydrophobic and ultralyophobic surfaces: Some comments and examples. *Langmuir*. 15, 3395–3399.

Chowdhury, S., Schmuhl, R., Keizer, K., Ten Elshof, J., Blank, D., 2003. Pore size and surface chemistry effects on the transport of hydrophobic and hydrophilic solvents through mesoporous γ -alumina and silica MCM-48. *Journal of Membrane Science*. 225, 177–186.

Cissé, M., Vaillant, F., Pallet D., Dornier, M., 2011. Selecting ultrafiltration and nanofiltration membranes to concentrate anthocyanins from roselle extract (*Hibiscus sabdariffa* L.). *Food Research International*. 44, 2607–2614.

D

- Das, R., Sondhi, K., Majumdar, S., Sarkar, S., 2016. Development of hydrophobic clay-alumina based capillary membrane for desalination of brine by membrane distillation. 4, 243–251.
- Derbel, I., Khemakhem, M., Cerneaux, S., Cretin, M., Ben Amar, R., 2017. Grafting of low cost ultrafiltration ceramic membrane by Tunisian olive oil molecules and application to air gap membrane distillation. *Desalination and Water Treatment*. 82, 20–25.
- Díaz-Reinoso, B., Moure, A., Domínguez H., Parajó, J.C., 2009. Ultra- and nanofiltration of aqueous extracts from distilled fermented grape pomace. *Journal of Food Engineering*. 91, 587–593.

G

- Gaber, A.A.A., Ibrahim, D.M., Fawzia Fahm Abd-Elmohsen, F.F., El-Zanati E.M., 2013. Synthesis of alumina, titania, and alumina-titania hydrophobic membranes via sol-gel polymeric route. *Journal of Analytical Science and Technology*. 4, 1–20.
- Gao, N., Ke, W., Fan, Y., Xu, N., 2013. Evaluation of the oleophilicity of different alkoxy silane modified ceramic membranes through wetting dynamic measurements. *Applied Surface Science*. 283, 863–870.
- Garmsiri, E., Rasouli, Y., Abbasi, M., Izadpanah, A.A., 2017. Chemical cleaning of mullite ceramic microfiltration membranes which are fouled during oily wastewater treatment. *Journal of Water Process Engineering*. 19, 81–95.
- Ghouil, B., Harabi, A., Bouzerara, F., Boudaira, B., Figoli, A., 2015. Development and characterization of tubular composite ceramic membranes using natural aluminosilicates for microfiltration applications. *Materials Characterization*. 103, 18–27.
- Guizard, C., 1996. Sol-Gel Chemistry and its Application to Porous Membrane Processing. In Burggraaf A.J., Cot, L. (Eds.), *Fundamentals of Inorganic Membrane Science and Technology*, 689. The Netherlands: Elsevier Science.
- Guo, H., Zhao, S., Wu, X., Qi, H., 2016. Fabrication and characterization of TiO₂/ZrO₂ ceramic membranes for nanofiltration. *Microporous and Mesoporous Materials*. 260, 125–131.

H

- Hosseinabadi, S.R., Wyns, K., Meynen, V., Carleer, R., Adriaensens, P., Buekenhoudt, A., Vander Bruggen, B., 2014. Organic solvent nanofiltration with Grignard functionalised ceramic nanofiltration membranes. *Journal of Membrane Science*. 454, 496–504.
- Hosseinabadi, S.R., Wyns, K., Buekenhoudt, A., Van der Bruggen, B., Ormerod, D., 2015. Performance of Grignard functionalized ceramic nanofiltration membranes. *Separation and Purification Technology*. 147, 320–328.

J

- Jedidi, I., Saïdi, S., Khemakhem, S., Larbot, A., Elloumi-Ammar, N., Fourati, A., Charfi, A., Ben Salah, A., Ben Amar, R., 2009a. Elaboration of new ceramic microfiltration membranes from mineral coal fly ash applied to waste water treatment. *Journal of Hazardous Materials*. 172, 152–158.
- Jedidi, I., Khemakhem, S., Larbot, A., Ben Amar, R., 2009b. Elaboration and characterisation of fly ash based mineral supports for microfiltration and ultrafiltration membrane. *Ceramics International*. 35, 2747–2753.
- Jedidi, I., Khemakhem, S., Saïdi, S., Larbot, A., Elloumi-Ammar, N., Fourati, A., Charfi, A., Ben Salah, A., Ben Amar, R., 2011. Preparation of a new ceramic microfiltration membrane from mineral coal fly ash: Application to the treatment of the textile dyeing effluents. *Powder Technology*. 208, 427–432.

K

- Khemakhem, M., Khemakhem, S., Ben Amar, R., 2013. Emulsion separation using hydrophobic grafted ceramic membranes by Air Gap Membrane Distillation process. *Colloids and Surfaces A: Physicochemical and Engineering Aspects*. 436, 402–407.
- Khemakhem, M., Khemakhem, S., Ben Amar, R., 2014. Surface modification of microfiltration ceramic membrane by fluoroalkylsilane. *Desalination and Water Treatment*. 52, 1786–1791.
- Khemakhem, M., Khemakhem, S., Ayedi, S., Cretin, M., Ben Amar, R., 2015. Development of an asymmetric ultrafiltration membrane based on phosphates industry sub-products. *Ceramics International*. 41, 10343–10348.
- Khemakhem, S., Ben Amar, R., Ben Hassen, R., Larbot, A., Ben Salah, A., Cot, L., 2006a. Fabrication of mineral supports of membranes for microfiltration/ultrafiltration from Tunisian clay. *Annales de Chimie Science des Matériaux*. 31, 169–181.

- Khemakhem, S., Larbot, A., Ben Amar, R., 2006b. Study of performances of ceramic microfiltration membrane from Tunisian clay applied to cuttlefish effluents treatment. *Desalination*. 200, 307–309.
- Khemakhem, S., Ben Amar, R., Larbot, A., 2007. Synthesis and characterization of a new inorganic ultrafiltration membrane composed entirely of Tunisian natural illite clay. *Desalination*. 206, 210–214.
- Khemakhem, S., Larbot, A., Ben Amar, R., 2009. New ceramic microfiltration membranes from Tunisian natural materials: Application for the cuttlefish effluents treatment. *Ceramics International*. 35, 55–61.
- Khemakhem, S., Ben Amar, R., 2011a. Grafting of fluoroalkylsilanes on microfiltration Tunisian clay membrane. *Ceramics International*. 37, 3323–3328.
- Khemakhem, S., Ben Amar, R., 2011b. Modification of Tunisian clay membrane surface by silane grafting: Application for desalination with air process. *Colloids and Surfaces A: Physicochemical and Engineering Aspects*. 387, 79–85.
- Khemakhem, M., Khemakhem, S., Ayedi, S., Ben Amar, R., 2011c. Study of ceramic ultrafiltration membrane support based on phosphate industry subproduct: Application for the cuttlefish conditioning effluents treatment. *Ceramics International*. 37, 3617–3625.
- Kosinov, N., Gascon, J., Kapteijn, F., Hensen, E.J.M., 2016. Recent developments in zeolite membranes for gas separation. *Journal of Membrane Science*. 499, 65–79.
- Kouras, N., Harabia, A., Bouzerara, F., Foughali, L., Policicchio, A., Stelitano, S., Galiano, F., Figoli, A., 2017. Macro-porous ceramic supports for membranes prepared from quartz sand and calcite mixtures. *Journal of the European Ceramic Society*. 37, 3159–3165.
- Kujawa, J., Kujawski, W., Koter, S., Jarzynka, K., Rozicka, A., Bajda, K., Cerneaux, S., Persin, M., Larbot, A., 2013a. Membrane distillation properties of TiO₂ ceramic membranes modified by perfluoroalkylsilanes. *Desalination and Water Treatment*. 51, 1352–1361.
- Kujawa, J., Kujawski, W., Koter, S., Rozicka, A., Cerneaux, S., Persin, M., Larbot, A., 2013b. Efficiency of grafting of Al₂O₃, TiO₂ and ZrO₂ powders by perfluoroalkylsilanes. *Colloids and Surfaces A: Physicochemical and Engineering Aspects*. 420, 64–73.
- Kujawa, J., Cerneaux, S., Kujawski, W., 2014a. Investigation of the stability of metal oxide powders and ceramic membranes grafted by perfluoroalkylsilanes. *Colloids and Surfaces A: Physicochemical and Engineering Aspects*. 443, 109–117.

Kujawa, J., Cerneaux, S., Koter, S., Kujawski, W., 2014b. Highly Efficient Hydrophobic Titania Ceramic Membranes for Water Desalination. *ACS Applied Materials and Interfaces*. 6, 14223–14230.

Kujawa, J., Cerneaux, S., Kujawski, W., Knozowska, K., 2017. Hydrophobic ceramic membranes for water desalination. *Applied Sciences*. 7, 402–412.

L

Lafleur, M., Bougie, F., Guilhaume, N., Larachi, F., Fongarland, P., Iliuta, M.C., 2017. Development of a water-selective zeolite composite membrane by a new pore-plugging technique. *Microporous and Mesoporous Materials*. 237, 49–59.

Lee, J., Ha, J.H., Song, I.H., 2016. Improving the antifouling properties of ceramic membranes via chemical grafting of organosilanes. *Separation Science and Technology*. 51, 2420–2428.

Lenza, R.F.S., Vasconcelos, W.L., 2000. Synthesis and properties of microporous sol-gel silica membranes. *Journal of Non-Crystalline Solids*. 273, 164–169.

Li, F., Yang, Y., Fana, Y., Xinga, W., Wang, Y., 2012. Modification of ceramic membranes for pore structure tailoring: The atomic layer deposition route. *Journal of Membrane Science*. 397–398, 17–23.

Lim, G.L., Jeong, H.G., Hwang, I.S., Kim, D.H., Park, N., Cho, J., 2009. Fabrication of a silica ceramic membrane using the aerosol flame deposition method for pretreatment focusing on particle control during desalination. *Desalination*. 238, 53–59.

Liu, B., Qu, F., Liang, H., Gan, Z., Yu, H., Li, G., Van der Bruggen, B., 2017. Algae-laden water treatment using ultrafiltration: Individual and combined fouling effects of cells, debris, extracellular and intracellular organic matter. *Journal of Membrane Science*. 528, 178–186.

M

Ma, X., Chen, P., Zhou, M., Zhong, Z., Zhang, F., Xing, W. 2017. Tight ultrafiltration ceramic membrane for separation of dyes and mixed salts (both NaCl/Na₂SO₄) in textile wastewater treatment. *Industrial & Engineering Chemistry Research*. 56, 7070–7079.

Masmoudi, S., Larbot, A., El Feki, H., Ben Amar, R., 2007. Elaboration and characterisation of apatite based mineral supports for microfiltration and ultrafiltration membranes. *Ceramics International*. 33, 337–344.

Mittal, P., Jana, S., Mohanty, K., 2011. Synthesis of low-cost hydrophilic ceramic–polymeric composite membrane for treatment of oily wastewater. *Desalination*. 282, 54–62.

Mustafa, G., Wyns, K., Vandezande, P., Buekenhoudt, A., Meynen, V., 2014. Novel grafting method efficiently decreases irreversible fouling of ceramic nanofiltration membranes. *Journal of Membrane Science*. 470, 369–377.

Mustafa, G., Wyns, K., Buekenhoudt, A., Meynen, V., 2016. Antifouling grafting of ceramic membranes validated in a variety of challenging wastewaters. *Water Research*. 104, 242–253.

N

Nandi, B.K., Das, B., Uppaluri, R., Purkait, M.K., 2009. Microfiltration of mosambi juice using low cost ceramic membrane. *Journal of Food Engineering*. 95, 597–605.

O

Oun, A., Tahri, N., Mahouche-Chergui, S., Carbonnier, B., Majumdar, S., Sarkar, S., Sahoo, G.C., Ben Amar, R., 2017. Tubular ultrafiltration ceramic membrane based on titania nanoparticles immobilized on macroporous clay-alumina support: Elaboration, characterization and application to dye removal. *Separation and Purification Technology*. 188, 126–133.

P

Padaki, M., Surya Murali, R., Abdullah, M.S., Misdan, N., Moslehyani, A., Kassim, M.A., Hilal, N., Ismail, A.F., 2015. Membrane technology enhancement in oil-water separation. A review. *Desalination*. 357, 197–207.

Palacio, L., Bouzerdib, Y., Ouammoub, M., Albizaneb, A., Bennazhab, J., Hernández, A., Calvo, J.I., 2009. Ceramic membranes from Moroccan natural clay and phosphate for industrial water treatment. *Desalination*. 245, 501–507.

R

Randon, J., Blanc, P., Paterson, R., 1995. Modification of ceramic membrane surfaces using phosphoric acid and alkyl phosphonic acids and its effects on ultrafiltration of BSA protein. *Journal of Membrane Science*. 98, 119–129.

Ren, C., Fang, H., Gu, J., Winnubst, L., Chen, C., 2015. Preparation and characterization of hydrophobic alumina planar membranes for water desalination. *Journal of the European Ceramic Society*. 35, 723–730.

S

- Saffaj, N., Loukili, H., Alami Younssi, S., Albizane, A., Bouhria, M., Persin, M., Larbot A., 2004. Filtration of solution containing heavy metals and dyes by means of ultrafiltration membranes deposited on support made of Moroccan clay. *Desalination*. 168, 301–306.
- Sah, A., Castricum, H.L., Bliet, A., Blank, D.H.A., ten Elshof, J.E., 2004. Hydrophobic modification of γ -alumina membranes with organochlorosilanes. *Journal of Membrane Science*. 243, 125–132.
- Sahoo, G.C., Halder, R., Jedidi, I., Oun, A., Nasri, H., Roychoudhury, P., 2016. Preparation and characterization of microfiltration apatite membrane over low cost clay-alumina support for decolorization of dye solution. *Desalination and Water Treatment*. 57, 27700–27709.
- Sarkar, S., Bandyopadhyay, S., Larbot, A., Cerneaux, S., 2012. New clay–alumina porous capillary supports for filtration application. *Journal of Membrane Science*. 392–393, 130–136.
- Saufi, S.M., Ismail, A.F., 2004. Fabrication of carbon membranes for gas separation - A review. *Carbon*. 42, 241–259.
- Shang, R., Goulas, A., Tang, C.Y., de Frias Serra, X., Rietveld, L.C., Heijman, S.G.J., 2017. Atmospheric pressure atomic layer deposition for tight ceramic nanofiltration membranes: Synthesis and application in water purification. *Journal of Membrane Science*. 528, 163–170.
- Suresh, K., Pugazhenti, G., Uppaluri, R., 2016. Fly ash based ceramic microfiltration membranes for oil-water emulsion treatment: Parametric optimization using response surface methodology. *Journal of Water Process Engineering*. 13, 27–43.
- Suresh, K., Pugazhenti, G., 2017. Cross flow microfiltration of oil-water emulsions using clay based ceramic membrane support and TiO_2 composite membrane. *Egyptian Journal of Petroleum*. 26, 679–694.

T

- Tahri, N., Jedidi, I., Cerneaux, S., Cretin, M., Ben Amar, R., 2013. Development of an asymmetric carbon microfiltration membrane: Application to the treatment of industrial textile wastewater. *Separation and Purification Technology*. 118, 179–187.

- Tanardi, C.R., Catana, R., Barboiu, M., Ayrat, A., Vankelecom, I.F.J., Nijmeijer, A., Winnubst L., 2016a. Polyethyleneglycol grafting of γ -alumina membranes for solvent resistant nanofiltration. *Microporous and Mesoporous Materials*. 229, 106–116.
- Tin, P.S., Lin, H.Y., Ong, R.C., Chung, T.S., 2011. Carbon molecular sieve membranes for biofuel separation. *Carbon*. 49, 369–375.

V

- Van Der Bruggen, B., Vandecasteele, C., Van Gestel, T., Doyen, W., Leysen, R., 2003. A review of pressure-driven membrane processes in wastewater treatment and drinking water production. *Environmental Progress*. 22, 46–56.
- Van Gestel, T., Van der Bruggen, B., Buekenhoudt, A., Dotremont, C., Luyten, J., Vandecasteele, C., Maes, G., 2003. Surface modification of γ - $\text{Al}_2\text{O}_3/\text{TiO}_2$ multilayer membranes for applications in non-polar organic solvents. *Journal of Membrane Science*. 224, 3–10.
- Van Gestel, T., Kruidhof, H., Blank, D.H.A., Bouwmeester, H.J.M., 2006. ZrO_2 and TiO_2 membranes for nanofiltration and pervaporation Part1. Preparation and characterization of a corrosion resistant ZrO_2 nanofiltration membrane with a MWCO<300. *Journal of Membrane Science*. 284, 128–136.
- Van Heetvelde, P., Beyers, E., Wyns, K., Adriaenssens, P., Maes, B.U.W., Mullens, S., Buekenhoudt, A., Meynen, V., 2013. A new method to graft titania using Grignard reagents. *Chemical Communications*. 49, 6998–7000.
- Vinoth Kumar, R., Kumar Ghoshal, A., Pugazhenti, G., 2015. Elaboration of novel tubular ceramic membrane from inexpensive raw materials by extrusion method and its performance in microfiltration of synthetic oily wastewater treatment. *Journal of Membrane Science*. 490, 92–102.

W

- Wallberg, O., Jarwon, A.S., Wimmerstedt, R., 2003. Ultrafiltration of kraft black liquor with a ceramic membrane. *Desalination*. 156, 145–153.
- Wu, Y., Sugimura, H., Inoue, Y., Takai, O., 2002. Thin films with nanotextures for transparent and ultra water-repellent coatings produced from trimethylmethoxysilane by microwave plasma CVD. *Chemical Vapor Deposition*. 8, 47–50.

Y

Yacou, C., Smart, S., Diniz da Costa, J.C., 2015. Mesoporous TiO₂ based membranes for water desalination and brine processing. *Separation and Purification Technology*. 147, 166–171.

Yoshino, Y., Suzuki, T., Taguchi, H., Nomura, M., Nakao, S.-I., Itoh, N., 2008. Development of an all-ceramic module with silica membrane tubes for high temperature hydrogen separation. *Separation Science and Technology*. 43, 3432–3447.

Z

Zhu, Y., Wang, D., Jiang, L., Jin, J., 2014. Recent progress in developing advanced membranes for emulsified oil/water separation. *NPG Asia Materials*. 6, 1–11.

Zulewska, J., Newbold, M., Barbano, D.M., 2009. Efficiency of serum protein removal from skim milk with ceramic and polymeric membranes at 50 °C. *Journal of Dairy Science*. 92, 1361–1377.

Section 2

Polymer-based nanocomposites: focus on heterogeneous catalysts for environmental remediation

1. Introduction

For decades, the development of innovative polymer-based hybrid materials has gone through the design of composites made of a polymer matrix reinforced with micrometric particles named filler. More recently, growing interest has been focused on the development of a new class of composite materials reinforced by sub-micrometric fillers, nanocomposites (NCs) (Kojima et al., 1993). The specificity of these nanocomposite materials lies in the specific dimensions of at least one of the phases which has one, two or three dimensions in the nanometer range that is less than 100 nanometers. The introduction of nanofillers (eg. clay, carbon nanotube, NPs, silica nanoparticles, etc.) makes it possible to improve significantly the physicochemical properties of the matrix at a moderate cost.

Since the pioneering report by *Theng* in 1970 (Theng 1970), development of novel polymer-based nanocomposites (PNCs) has been attracting growing research effort worldwide, taking advantage of the introduction of both components, polymer as performing matrix and nanostructures as reinforcing agent, fire retardant providing new promising prospects for modern technology (Loos 2015). According to the literature, PNCs are nowadays among the most investigated nanomaterials (*Figure 7*).

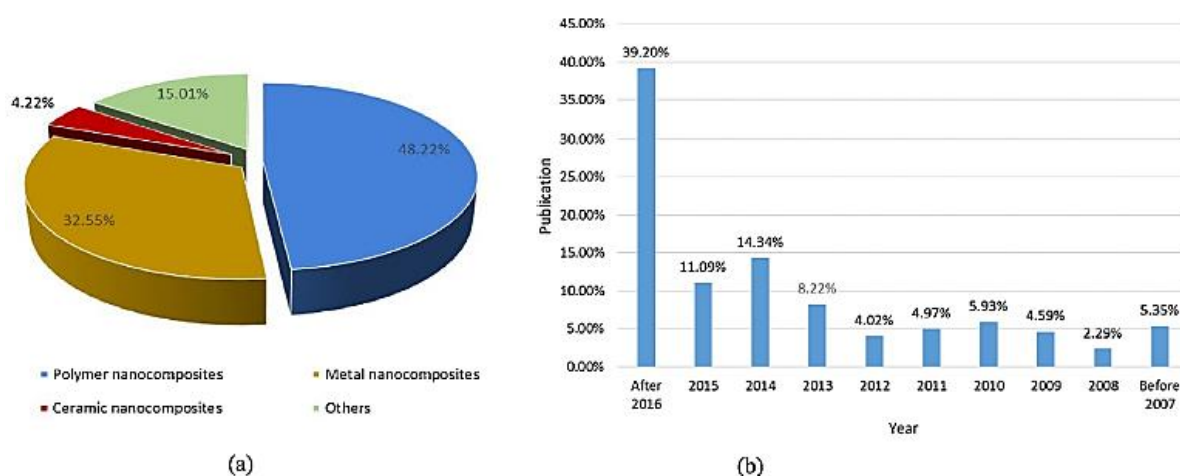


Figure 7. Statistics showing the evolution of the number of publications related to nanocomposites: (a) pie chart describing the distribution of different types of nanocomposites and (b) the equivalent data as presented by *Kumar and co-workers* in a review article (Kumar et al., 2018).

The main benefit of using PNCs is rationalized by the value-added properties provided by incorporation of nanofillers as compared to the pristine polymer without sacrificing its inherent properties such as processability (Vaia and Wagner 2004; Verdejo et al., 2011). The key features influencing the synthesis of PNCs are the size and property of nanofiller as well as the nature of the interactions and the interface between nanofiller and the polymer matrix (Terrones et al., 2011).

The most investigated PNCs consist of a polymeric matrix in the form of a homopolymer, copolymer, polymer blend, porous polymer combined with nanosized components in the form of particles, whiskers, fibres, nanotubes (Miguel-García et al., 2012; Najafinejad et al., 2019; Ostovar et al., 2020; Pavlidou and Paspaspyrides 2008; Qiu et al., 2019; Snoussi et al., 2018; Wassel et al., 2020; Zaferani 2018).

The large variety of organic and inorganic materials used as nanoscale fillers includes layered clay such as montmorillonite (MMT), carbon nanotubes (CNTs), graphene (G) and its derivatives (graphene oxide “GO” and reduced graphene “Gr”), metal oxides (MOs), silica and zero-valent metals (ZVMs) (Gam-Derouich et al., 2011; Hu et al., 2014; Mahouche-Chergui et al., 2010 and 2013; Mangeon et al., 2015; Mukhopadhyay et al., 2019; Saleh et al., 2019; Sun et al., 2013; Vo et al., 2017a and 2018; Yadav et al., 2019) that proved efficient for tuning the properties of the polymer matrices allowing for a wide range of applications. Indeed, besides enhancement of thermal and mechanical properties, the use of PNCs has been extended to varied applications including drug delivery, packaging, sensors, membranes, medical devices, catalysis, pollutants removal.

One of the major environmental issues that the modern world is experiencing today is water contamination. Pesticide residues (pendimethalin, trifluralin and nitrophenols), nitro-arenes, organic dyes, as well as textile and pharmaceutical wastewater (Draper and Crosby 1984; Gatermann et al., 1995; Joseph and Mathew 2015a; Kavitha and Palanivelu 2005; Mao et al., 2014; Wu et al., 2015) are the main sources of water pollution.

Many of these organic compounds are toxic, carcinogenic, and biologically resistant (Kusic et al., 2006; Moussavi and Mahmoudi 2009). Studies have shown that the repeated exposure to these pollutants induces organs damage and its discharges in river water and water systems causes serious aquatic perturbation, and substantial environmental pollution even at low concentration (Khalil et al., 2015; Zollinger 1987). Indeed, effluent treatment by using conventional methods (biological and physical–chemical treatments) were ineffective especially, at high hazardous chemicals concentration (Ghoreishi and Haghghi 2003; Joseph

and Mathew 2015a; Vidhu and Philip 2014). Presently, more efficient and cost-effective approaches to treat contaminated water are strongly needed.

In recent years, the beneficial impact of nanotechnology has undergone significant expansion in the field of water remediation (Shih et al., 2010). As a representative example, polymer composites with metallic nanoparticles have been developed as innovative nanocatalytic materials for novel applications in heterogeneous catalysis (Khalil et al., 2015). Heterogeneous catalysis processes based on supported metallic nanoparticles have emerged as very appealing methods for large-scale treatment process. These methods exhibit favorable features such as high efficiency in dye removal, eco-friendly process, modest energy requirement, etc (Turner et al., 2008; Vidhu and Philip 2014). This is largely due to the physicochemical properties (surface area and size) and the unique catalytic activities of metallic nanoparticles.

2. Graphene-polymer nanocomposites

In recent years, graphene has emerged as one of the most promising class of nanofiller materials to create new PNCs. Moreover, the incorporation of extremely low content of graphene has shown efficient to provide significant enhancement in the final electrical, physical, mechanical, thermal, absorptive and barrier properties of PNCs (Dai et al., 2016; Tan and Thomas 2016).

Graphene has a very high surface-to-volume ratio, which makes it more advantageous compared to other nanofillers (eg. CNTs). In addition, graphene use cost is much less than CNTs due to its readily availability, in important quantity, from a graphite precursor (Kuilla et al., 2010). However, due to the layered structure, an appropriate surface functionalization of graphene sheets is often needed to generate more available surface area and then providing additionally physicochemical properties (Kuilla et al., 2010; Tan and Thomas 2016). Due to the all above reasons, graphene and graphene derivatives have been broadly investigated in the literature (Al-Attabi et al., 2017; Mahouche-Chergui et al., 2013; Sen et al., 2017). Consequently, the use of polymer/graphene NCs (GPNCs) has been reported in water remediation applications (Alghunaimi et al., 2019; Khan et al., 2017; Mahmoodi et al., 2019; Zhao et al., 2011) and also for catalysis purposes (Ameen et al., 2012; Chen et al., 2015; Nasrollahzadeh et al., 2020; Saleh et al., 2019; Singh et al., 2018; Zhao et al., 2011).

3. Nanoclay- polymer nanocomposites

As it is well-known, when the mineral clay undergoes a chemical modification with organic molecules, the resulting products are called organo-clay. In the science dealing with NCs, mixing clay nanopowders with organic polymer phase has emerged as one of the most widespread combination to produce nanostructured organoclays. Clay-polymer nanocomposites (CPNCs) can be viewed as hybrid materials made from a dispersion of lamellar nanoclay such as MMT in a polymer matrix. To the best of our knowledge, there is no impediment to modify all mineral clays varieties to improve compatibility with the polymeric matrix. Nevertheless, lamellar or layered clays such as MMT are the most commonly used clay

loads for the production of CPNCs (Mohammed 2014; Mukhopadhyay et al., 2019; Passador et al., 2017). The incorporation of MMT in polymer was initially reported in the early 1990s, by the *Toyota research group*. In order to synthesize nylon-6 polymer with improved thermal and mechanical properties, the potential use of MMT clay as nanoloads has been explored during the in-situ polymerization of ϵ -caprolactam (Usuki et al., 1993). Other advantages of MMT clay including high specific surface area, cationic exchange capacity and aspect ratio of more than 1000 as well as the relatively inexpensive cost contributed to the success of MMT for the synthesis of NCs (Mohammed 2014). This has been well illustrated in many research works (Kumar et al., 2018; Mahmoodi et al., 2019; Odom 1984; Zhao et al., 2011). In recent years, CPNCs have also attracted an important interest because they were applied to the synthesis of new sustainable materials for several applications namely WWT such as catalysis (Nasir et al., 2019; Unuabonah and Taubert 2014). However, the number of studies dealing with the use of clay-polymer nanocomposites for water treatment applications remains limited (Sadjadi et al., 2020, Saleh et al., 2019).

4. Metal nanoparticles-polymer nanocomposites

4.1. Synthesis of metal nanoparticles-polymer nanocomposites

Synthesis method, nanocatalyst stability and size of NPs are the main characteristics to be considered for enhanced catalytic activity in the degradation of organic pollutant (Snoussi et al., 2018; Vidhu and Philip 2014). In this respect, metal NPs-containing polymeric nanocomposites have also received much consideration in recent years due to favorable role of polymer matrices to provide high catalyst stabilization and control over the size of metal NPs (Li and Cooper-White 2013; Snoussi et al., 2018; Zhao et al., 2011).

Synthetic approaches can be categorized into physical, chemical, photochemical and biological methods for the preparation of metallic nanocatalysts (Dhand et al., 2015; Joseph and Mathew 2015b; Khanna et al., 2019; Mao et al., 2014). All these methods have been successfully reported for the synthesis of a wide range of shapes and morphology of metal nanocrystals including, spherical (Vidhu and Philip 2014), nanowires (Pei et al., 2004) nanoplates (Sadeghi et al., 2009), core-shell (Snoussi et al., 2018), nanoflower (Mao et al., 2014) and other architectures (Chen and Liu 2011). Also, *in-situ* (Mahouche-Chergui et al., 2013) or *ex-situ* (Iwan et al., 2015) synthesis strategies can be implemented for the incorporation of the NPs into the host polymer matrices. In typical experiments, NPs immobilization within the bulk or at the surface of the polymer matrix occurred through the presence of sensitive complexing groups (ionic, electrophile or nucleophile sites) (Khalil et al., 2015; Mahouche-Chergui et al., 2013) providing a robust anchoring of the metal NPs.

Furthermore, the main benefits of the *in situ* synthesis method are the short reaction time, lower energy consumption and mostly the potential influence of the host polymer matrices on the properties of the final nanocomposite (nanosized and uniform dispersion of NPs tightly bonded onto the sorbents) (Ghosh et al., 2003; Khalil et al., 2015; Li and Cooper-White 2013; Zhao et al., 2011). Accordingly, impregnation of the polymer with metal nanoparticles precursor ions followed by chemical reduction of the said metal ions (in presence of a reducing agent and stabilizing agents) are the main two steps of nanoparticle *in situ* synthesis (Nasrollahzadeh et al., 2019; Poupart et al., 2017; Snoussi et al., 2018). Hither, initial chemical modification of the polymer is usually performed to provide functional groups with high affinity that act as anchors for the *in situ* synthesized NPs (Ghosh et al., 2003; Mahouche-Chergui et al., 2013).

Functionalized polymers having functional groups are suitable materials for immobilizing metal nanoparticles. (Basheer et al., 2020; Li et al., 2007; Mahouche-Chergui et al., 2013).

Epoxy-containing monomers, such as glycidyl methacrylate (GMA) have attracted a lot of attention as functional monomers (Gokmen and Du Prez 2012; Marković et al., 2017; Stefanović et al., 2015). According to Grochowicz et al. (2018) and Hwang et al. (2013), the exceptional interest on such monomer is originated not only from its lower cost compared to other monomers but also due to its dual functionality, allowing for the synthesis of crosslinked and functional materials (Rahman et al., 2012).

Interestingly, the presence of the reactive epoxy groups permits several modification opportunities on the initial polymer (Gokmen and Du Prez 2012). Additionally, the easy

functionalization by epoxide cycle opening allows the possibility of unlimited ligands grafting ways with: e.g., imine, thiol, pyrazole and amino group (see **Figure 8**).

The use of the appropriate organic ligands allows creating polymer reactive functions such as amines (R_3-N , R_2-NH , $R-NH_2$), thiol ($-SH$) carboxylate ($O=C-O^-$) capable of serving as chelating groups to immobilize MNPs (Pd, Au, Ag, Ni, etc). Importantly, many investigators have proved the high capacity and selectivity of ethylenediamine (EDA), diethylenetriamine (DETA), triethylenetetramine (TETA) and iminodiacetic acid (IDA) as promising organic modifiers towards grafting complexing groups on polymers (Hwang et al., 2013; Maksin et al., 2012; Malović et al., 2007; Nastasović et al., 2004a and 2004b). The so-designed functional polymers exhibited high selectivity toward heavy metal sorption.

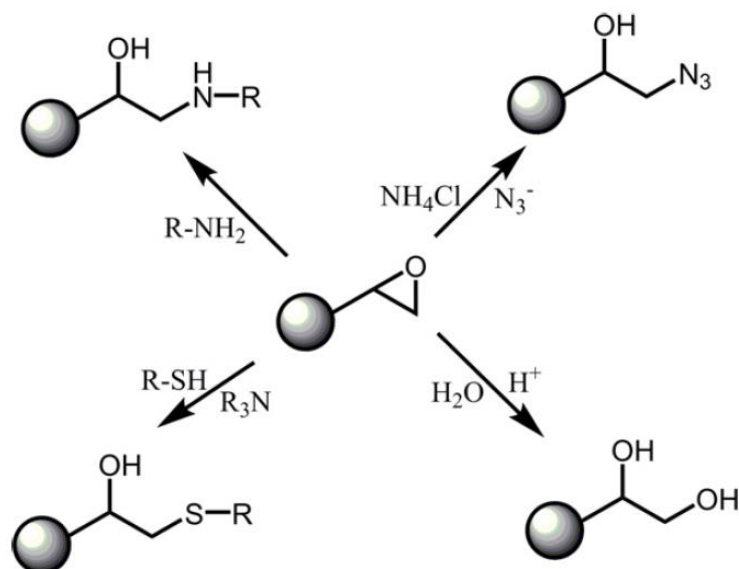


Figure 8. Some various epoxy-GMA grafting using realties ligands (From Gokmen and Du Prez 2012).

The development of supported and recyclable catalysts is still considered as a significant challenge in catalysis chemistry. Many specific approaches are commonly documented in literature to prepare MNPs for the development of robust heterogeneous catalyst. Most commonly in heterogeneous catalysts, noble and transition metals are immobilized onto the matrix surface by the chemical colloidal method. This method presents the advantage of being inexpensive and handier than other NPs synthesis procedures. It can be simply carried out in aqueous or/and organic phase and consist of two easy impregnation and reduction steps.

However, two main ways have been reported to date in the literature, referred to as ex-situ and in-situ ways. Regarding the in-situ approach, MNPs catalysts are synthesized by impregnation of metal salt precursor on the polymer surface and the subsequent reduction (NaBH_4 being the most used reducing agent) onto the polymer matrix utilizing the reduction process. As previously mentioned, reactive polymers with accessible functional groups (amines, thiols, cyanos, and carboxylic groups) may easily be designed to ensure specific interactions with the metal in its ionic or reduced form. The morphology as well as the size distribution of NPs can be controlled by the reduction kinetics (processing and concentration of both reducer and precursor) and the stabilizer nature (chelating ligand).

4.2. Application of metal nanoparticles-polymer nanocomposites in bulk heterogeneous catalysis

Today, the actual ever-growing challenges for the water resources protection are multiple and already touch many areas such as the treatment processes of polluted water. Interestingly, metal nanoparticle-polymer nanocomposites provide innovative and appealing solutions in the field of organic pollutant degradation for water and wastewater remediation (Najafinejad et al., 2019; Snoussi et al., 2018; Wassel et al., 2020). Of particular importance, one may cite the implementation of PNCs with high catalytic activities based on the incorporation of catalytically active monometallic and bimetallic NPs (Au, Pd, Ni, Au/Ag, Pd/Cu, etc.) (Zhao et al., 2011).

Snoussi and colleagues have developed catalytic core/double shell NCs based noble MNPs immobilized on polypyrrole functionalized mesoporous silica to catalyze the degradation of hazardous nitroaromatics and dyes (Snoussi et al., 2018).

Throughout the recent years, porous monolithic polymers have been used as versatile platform for MNPs immobilization. Such composite materials appeared as an appealing material for the quick catalytic removal of Eosin Y dye in aqueous solution (Poupart et al., 2017). In addition, *Khalil et al.* have reported recently the catalytic reduction of various nitrophenols molecules using monolith-supported Au catalysts (Khalil et al., 2015). Heterogeneous supported catalysis prepared through immobilization of MNPs on monoliths have been widely reported in the literature (Lee and Chang 2020; Liu et al., 2017; Poupart et al., 2016 and 2019; Tripathy et al., 2017).

5. Characterization of polymer-based nanocomposites

To establish correlated conclusions about structure-property relationships, thorough characterization of morphological, structural and physic-chemical properties of PNCs materials is strongly requested. Then, a large variety of instrumentations and characterization methods have been reported in literature in order to identify pristine materials and the produced NCs as well as to control the different stages of synthesis or chemical modification. This include, X ray diffractometry (XRD), atomic force microscopy (AFM), Fourier transformed infrared spectroscopy (FTIR), X ray photoelectron spectroscopy (XPS), nuclear magnetic resonance (NMR), thermogravimetric analysis (TGA)/differential thermal analysis (DTA), scanning and transmission electron microscopy (SEM/TEM), etc.

To examine the level of dispersion of the filler and the overall morphology, SEM and TEM are usual strongly suggested. The SEM provides images of the materials at the micro- and nano-metric scale. This technique can provide insight and information on the state of dispersion, the size range of the nanoparticles and their distribution into the polymer phase. It is very informative to check the interaction between the filler and matrix by studying fractured samples.

TEM allows understanding of the internal structure and the view of structural defects through direct visualization. TEM is also very helpful to determine size and distribution of nanoparticles in the polymer matrix and the number of nanofillers layers (thickness) at low nanometric scale. However, TEM only gives qualitative information about the entire sample, while the wide-angle peaks obtained by DRX allow quantification of changes in nanostructures such as for instance the d-spacing between filler layers. The complete exfoliation of layered fillers inside the polymer matrix and the arrangement of atoms in networks can be traced by XRD. On the other hand, XRD studies have been used in the field of hybrid nanostructured materials for the distinction of the crystallite from amorphous phases in some PNCs.

FTIR spectra are very informative to understand the oxidation, reduction, polymerization and functionalization processes. It is very convenient for identifying characteristic functional groups and then to exhibit a great control of different modification stages.

The coupled TGA/DTA analysis is a thermal analysis technique for proving thermal effects studied throughout a temperature range or time cycle at controlled atmosphere on the mass loss and thermal transitions of a material. Thus, this technique makes it possible to study the thermal stability of a material and to determine the load extent and organic grafting rates.

6. Conclusion

In this section, we briefly discussed recent advances in nanocomposite materials made from a combination of polymers and nanoparticles such as clay graphene and metal nanoparticles. Polymers-clay nanocomposites have been mainly developed for the production of materials with enhanced mechanical and thermal properties while graphene-based polymer composites are promising with regard to their electrical properties. Metal nanoparticles- polymer nanocomposites have been the most widely investigated for catalysis applications thanks to the unique catalytic activity of nanometals. The design of robust polymer-supported metal nanoparticles heterogeneous catalysts can be obtained through the specific chemical modification of the polymer with chelating groups enabling the robust anchoring of the metal nanoparticles. It can also be mentioned that MNPs have also been supported on other substrates than polymer for applications in catalysis for the reduction of organic effluents (Feng et al., 2019; Louisia et al., 2018; Yu et al., 2019; Corma et al., 2005; Zhang et al., 2010; Alshehri et al., 2016; Fu et al., 2018; Li and Cooper-White 2013; Wang et al., 2013).

References

A

- Abedi, S., & Abdouss, M., 2014. A review of clay-supported Ziegler–Natta catalysts for production of polyolefin/clay nanocomposites through in situ polymerization. *Applied Catalysis A: General*. 475, 386–409. doi:10.1016/j.apcata.2014.01.028.
- Al-Attabi, N. Y., Kaur, G., Adhikari, R., Cass, P., Bown, M., Evans, M., Gunatillake, P., Malherbe, F., Yu, A., 2017. Preparation and characterization of highly conductive polyurethane composites containing graphene and gold nanoparticles. *Journal of Materials Science*. 52, 11774–11784. doi:10.1007/s10853-017-1335-8.
- Alexandre, M., & Dubois, P., 2000. Polymer-layered silicate nanocomposites: preparation, properties and uses of a new class of materials. *Materials Science and Engineering: R: Reports*. 28, 1–63. doi:10.1016/s0927-796x(00)00012-7.
- Alghunaimi, F.I., Alsaeed, D.J., Harith, A.M., Saleh, T.A., 2019. Synthesis of 9-octadecenoic acid grafted graphene modified with polystyrene for efficient light oil removal from water. *Journal of Cleaner Production*. doi:10.1016/j.jclepro.2019.05.239.
- Alshehri, S.M., Almuqati, T., Almuqati, N., Al-Farraj, E., Alhokbany, N., Ahamad, T., 2016. Chitosan based polymer matrix with silver nanoparticles decorated multiwalled carbon nanotubes for catalytic reduction of 4-nitrophenol. *Carbohydrate Polymers*. 151, 135–143. doi:10.1016/j.carbpol.2016.05.018.
- Ameen, S., Seo, H.-K., Shaheer Akhtar, M., Shin, H.S., 2012. Novel graphene/polyaniline nanocomposites and its photocatalytic activity toward the degradation of rose Bengal dye. *Chemical Engineering Journal*. 210, 220–228. doi:10.1016/j.cej.2012.08.035.
- An, X., Simmons, T., Shah, R., Wolfe, C., Lewis, K.M., Washington, M., Nayak, S.K., Talapatra, S., Kar, S., 2010. Stable Aqueous Dispersions of Noncovalently Functionalized Graphene from Graphite and their Multifunctional High-Performance Applications, *Nano Lett.* 10, 4295-4301.

B

- Basheer, B. V., George, J. J., Siengchin, S., Parameswaranpillai, J., 2020. Polymer grafted carbon nanotubes—Synthesis, properties, and applications: A review. *Nano-Structures & Nano-Objects*. 22, 100429. doi:10.1016/j.nanoso.2020.100429.
- Bikiaris, D., 2010. Microstructure and Properties of Polypropylene/Carbon Nanotube Nanocomposites. *Materials*. 3, 2884–2946. doi:10.3390/ma3042884.

C

- Camargo, P.H.C., Satyanarayana, K.G., Wypych, F., 2009. Nanocomposites: Synthesis, Structure, Properties and New Application Opportunities. *Materials Research*. 12, 1-39. doi:10.1590/S1516-14392009000100002.
- Chen, F., Chen, Q., Zhang, Y., Wang, P., Zheng, X., Chen, Z., Fang, S., 2015. Multifunctional composite of rGO/Fe₃O₄/Ag@AgCl for the repeated use in simultaneous adsorption, in-situ SERS monitoring and photocatalytic degradation of rhodamine B under visible light irradiation. *Materials Letters*. 139, 451–454. doi:10.1016/j.matlet.2014.10.124.
- Chen, H.M., Liu, R.S., 2011. Architecture of Metallic Nanostructures: Synthesis Strategy and Specific Applications. *J. Phys. Chem. C*. 115, 3513–3527.
- Corma, A., Garcia, H., Leyva, A., 2005. Catalytic activity of palladium supported on single wall carbon nanotubes compared to palladium supported on activated carbon. *Journal of Molecular Catalysis A: Chemical*. 230, 97–105. doi:10.1016/j.molcata.2004.11.030.

D

- Dai, Z., Wang, G., Liu, L., Hou, Y., Wei, Y., Zhang, Z., 2016. Mechanical behavior and properties of hydrogen bonded graphene/polymer nano-interfaces. *Composites Science and Technology*. 136, 1–9. doi:10.1016/j.compscitech.2016.09.005.
- Dhand, C., Dwivedi, N., Loh, X.J., Ying, A.N.J., Verma, N.K., Beuerman, R.W., Lakshminarayanan, R., Ramakrishna, S., 2015. Methods and strategies for the synthesis of diverse nanoparticles and their applications: a comprehensive overview, *Rsc Adv*. 5, 105003–105037.
- Draper, W.M., & Crosby, D.G., 1984. Solar photooxidation of pesticides in dilute hydrogen peroxide. *J. Agric. Food Chem*. 32, 231–237.
- Du, X.S., Xiao, M., Meng, Y.Z., 2004. Facile synthesis of highly conductive polyaniline/graphite nanocomposites. *Eur Polym J*. 40,1489–1493.

F

- Feng, Y., Jiao, T., Yin, J., Zhang, L., Zhang, L., Zhou, J., Peng, Q., 2019. Facile Preparation of Carbon Nanotube-Cu₂O Nanocomposites as New Catalyst Materials for Reduction of P-Nitrophenol. *Nanoscale Research Letters*. 14. doi:10.1186/s11671-019-2914-1.

- Fim, F. de C., Guterres, J.M., Basso, N.R.S., Galland, G.B., 2010. Polyethylene/graphite nanocomposites obtained by in situ polymerization. *Journal of Polymer Science Part A: Polymer Chemistry*. 48, 692–698. doi:10.1002/pola.23822.
- Fu, P., Xiao, Z., Liu, Y., Wang, L., Zhang, X., Li, G., 2018. Support-Independent Surface Functionalization for Efficient Pd Loading in Catalytic Hydrogenation. *Chemistry Select*. 3, 3351–3361. doi:10.1002/slct.201800106.

G

- Gam-Derouich, S., Mahouche-Chergui, S., Truong, S., Ben Hassen-Chehimi, D., Chehimi, M.M., 2011. Design of molecularly imprinted polymer grafts with embedded gold nanoparticles through the interfacial chemistry of aryl diazonium salts. *Polymer*. 52, 4463–4470. doi:10.1016/j.polymer.2011.08.007.
- Gatermann, R., Hühnerfuss, H., Rimkus, G., Wolf, M., Franke, S., 1995. The distribution of nitrobenzene and other nitroaromatic compounds in the North Sea. *Mar. Pollut. Bull.* 30, 221–227.
- Ghoreishi, S.M., & Haghghi, R., 2003. Chemical catalytic reaction and biological oxidation for treatment of non-biodegradable textile effluent. *Chemical Engineering Journal*. 95, 163–169. doi:10.1016/s1385-8947(03)00100-1.
- Ghosh, A., Ranjan Patra, C., Mukherjee, P., Sastry, M., Kumar, R., 2003. Preparation and stabilization of gold nanoparticles formed by in situ reduction of aqueous chloroaurate ions within surface-modified mesoporous silica. *Microporous and Mesoporous Materials*. 58, 201–211. doi:10.1016/s1387-1811(02)00626-1.
- Ginzburg, V.V., Singh, C., Balazs, A.C., 2000. Theoretical Phase Diagrams of Polymer/Clay Composites: The Role of Grafted Organic Modifiers. *Macromolecules*. 33, 1089–1099. doi:10.1021/ma991324e.
- Gokmen, M.T., & Du Prez, F.E., 2012. Porous polymer particles—A comprehensive guide to synthesis, characterization, functionalization and applications. *Progress in Polymer Scienc*. 37, 365–405. doi:10.1016/j.progpolymsci.2011.07.006.
- Grochowicz, M., Pączkowski, P., Gawdzik, B., 2018. Investigation of the thermal properties of glycidyl methacrylate–ethylene glycol dimethacrylate copolymeric microspheres modified by Diels–Alder reaction. *Journal of Thermal Analysis and Calorimetry*. 133, 499–508. doi:10.1007/s10973-017-6785-3.

Gu, Z., Zhang, L., Li, C., 2009. Preparation of Highly Conductive Polypyrrole/Graphite Oxide Composites via in situ Polymerization. *Journal of Macromolecular Science, Part B*. 48, 1093–1102. doi:10.1080/00222340903035576.

H

Ha, S.R., & Rhee, K.Y., 2008. Effect of surface-modification of clay using 3-aminopropyltriethoxysilane on the wear behavior of clay/epoxy nanocomposites. *Colloids and Surfaces A: Physicochemical and Engineering Aspects*. 322, 1–5. doi:10.1016/j.colsurfa.2008.03.007.

Hu, K., Kulkarni, D.D., Choi, I., Tsukruk, V.V., 2014. Graphene-polymer nanocomposites for structural and functional applications. *Progress in Polymer Science*. 39, 1934–1972. doi:10.1016/j.progpolymsci.2014.03.001.

Hwang, C.W., Kwak, N.-S., Hwang, T.S., 2013. Preparation of poly(GMA-co-PEGDA) microbeads modified with iminodiacetic acid and their indium adsorption properties. *Chemical Engineering Journal*. 226, 79–86. doi:10.1016/j.cej.2013.04.041.

I

Iwan, M., Andryszewski, T., Wydryszek, M., Fialkowski, M., 2015. Fabrication of nanocomposites by covalent bonding between noble metal nanoparticles and polymer matrix. *RSC Advances*. 5, 70127–70138. doi:10.1039/c5ra12474c.

J

Jang, J.Y., Kim, M.S., Jeong, H.M., Shin, C.M., 2009. Graphite oxide/poly(methyl methacrylate) nanocomposites prepared by a novel method utilizing macroazoinitiator. *Composites Science and Technology*. 69, 186–191. doi:10.1016/j.compscitech.2008.09.039.

Joseph, S., & Mathew, B., 2015a. Facile synthesis of silver nanoparticles and their application in dye degradation. *Materials Science and Engineering: B*. 195, 90–97. doi:10.1016/j.mseb.2015.02.007.

Joseph, S., & Mathew, B., 2015b. Microwave assisted facile green synthesis of silver and gold nanocatalysts using the leaf extract of *Aerva lanata*. *Spectrochimica Acta Part A: Molecular and Biomolecular Spectroscopy*. 136, 1371–1379. doi:10.1016/j.saa.2014.10.023.

K

- Kalaitzidou, K., Fukushima, H., Drzal, L.T., 2007. Multifunctional polypropylene composites produced by incorporation of exfoliated graphite nanoplatelets. *Carbon*. 45, 1446–1452.
- Kavitha, V., & Palanivelu, K., 2005. Degradation of nitrophenols by Fenton and photo-Fenton processes. *J. Photochem. Photobiol. A*. 170, 83–95.
- Keteklahijani, Y.Z., Zeraati, A.S., Sharif, F., Roberts, E.P. L., Sundararaj, U., 2020. In situ chemical polymerization of conducting polymer nanocomposites: Effect of DNA-functionalized carbon nanotubes and nitrogen-doped graphene as catalytic molecular templates. *Chemical Engineering Journal*. 389, 124500. doi:10.1016/j.cej.2020.124500.
- Khalil, A. M., Georgiadou, V., Guerrouache, M., Mahouche-Chergui, S., Dendrinou-Samara, C., Chehimi, M.M., Carbonnier, B., 2015. Gold-decorated polymeric monoliths: In-situ vs ex-situ immobilization strategies and flow through catalytic applications towards nitrophenols reduction. *Polymer*. 77, 218–226. doi:10.1016/j.polymer.2015.09.040.
- Khan, A., Wang, J., Li, J., Wang, X., Chen, Z., Alsaedi, A., Hayat, T., Chen, Y., Wang, X., 2017. The role of graphene oxide and graphene oxide-based nanomaterials in the removal of pharmaceuticals from aqueous media: a review. *Environmental Science and Pollution Research*. 24, 7938–7958. doi:10.1007/s11356-017-8388-8.
- Khanna, P., Kaur, A., Goyal, D., 2019. Algae-based metallic nanoparticles: Synthesis, characterization and applications. *Journal of Microbiological Methods*. 105656. doi:10.1016/j.mimet.2019.105656.
- Kojima, Y., Usuki, A., Kawasumi, M., Okada, A., Fukushima, A, Y., 1993. Mechanical properties of nylon 6 - clay hybrid. *J. Mater. Res*. 8, 1185–1189.
- Kranbuehl, D.E., Cai, M., Glover, A.J., Schniepp, H.C., 2011. Measurement of the interfacial attraction between graphene oxide sheets and the polymer in a nanocomposite. *J. Appl. Polym. Sci*. 122, 3739-3743.
- Kuilla, T., Bhadra, S., Yao, D., Kim, N.H., Bose, S., Lee, J.H., 2010. Recent advances in graphene based polymer composites. *Progress in Polymer Science*. 35, 1350–1375. doi:10.1016/j.progpolymsci.2010.07.005.
- Kumar, S., Sarita, Nehra, M., Dilbaghi, N., Tankeshwar, K., Kim, K.-H., 2018. Recent advances and remaining challenges for polymeric nanocomposites in healthcare applications. *Progress in Polymer Science*. 80, 1–38. doi:10.1016/j.progpolymsci.2018.03.001.

Kusic, H., Koprivanac, N., Srsan, L., 2006. Azo dye degradation using fenton type processes assisted by UV irradiation: a kinetic study. *J. Photochem. Photobiol.* A181, 195–202.

L

Lee, J., & Chang, J.Y., 2020. A hierarchically porous catalytic monolith prepared from a Pickering high internal phase emulsion stabilized by microporous organic polymer particles. *Chemical Engineering Journal.* 381, 122767. doi:10.1016/j.cej.2019.122767.

Li, H., & Cooper-White, J.J., 2013. Hyperbranched polymer mediated fabrication of water soluble carbon nanotube–metal nanoparticle hybrids. *Nanoscale.* 5, 2915. doi:10.1039/c3nr00407d.

Li, S., Chen, H., Bi, W., Zhou, J., Wang, Y., Li, J., Cheng, W., Li, M., Li, L., Tang, T., 2007. Synthesis and characterization of polyethylene chains grafted onto the sidewalls of single-walled carbon nanotubes via copolymerization. *Journal of Polymer Science Part A: Polymer Chemistry.* 45, 5459–5469. doi:10.1002/pola.22290.

Liang, J, Wang, Y., Huang, Y., Ma, Y., Liu, Z., Cai, J., Zhang, C., Gao, H., Chen, Y., 2009. Electromagnetic interference shielding of graphene/epoxy composites. *Carbon.* 47, 922–925. doi:10.1016/j.carbon.2008.12.038.

Liu, Y., Guerrouache, M., Kebe, S. I., Carbonnier, B., Le Droumaguet, B., 2017. Gold nanoparticles-supported histamine-grafted monolithic capillaries as efficient microreactors for flow-through reduction of nitro-containing compounds. *Journal of Materials Chemistry A.* 5, 11805–11814. doi:10.1039/c7ta00410a.

Loos, M., 2015. Chapter 2 - Composites. In Loos, M., (Ed)., *Carbon Nanotube Reinforced Composites.* 289. Oxford: Elsevier Science, William Andrew. doi:10.1016/b978-1-4557-3195-4.00002-3.

Louisia, S., Contreras, R.C., Heitzmann, M., Rosa Axet, M., Jacques, P.-A., Serp, P., 2018. Sequential catalytic growth of sulfur-doped carbon nanotubes and their use as catalyst support. *Catalysis Communications,* 109, 65–70. doi:10.1016/j.catcom.2018.02.024.

M

Mahmoodi, N.M., Oveisi, M., Bakhtiari, M., Hayati, B., Shekarchi, A.A., Bagheri, A., Rahimi, S., 2019. Environmentally friendly ultrasound-assisted synthesis of magnetic zeolitic imidazolate framework - Graphene oxide nanocomposites and pollutant removal from water. *Journal of Molecular Liquids.* 282, 115–130. doi:10.1016/j.molliq.2019.02.139.

- Mahouche Chergui, S., Abbas, N., Matrab, T., Turmine, M., Bon Nguyen, E., Losno, R., Pinson, J., Chehimi, M.M., 2010. Uptake of copper ions by carbon fiber/polymer hybrids prepared by tandem diazonium salt chemistry and in situ atom transfer radical polymerization. *Carbon*. 48, 2106–2111. doi:10.1016/j.carbon.2010.01.050.
- Mahouche-Chergui, S., Guerrouache, M., Carbonnier, B., Chehimi, M.M., 2013. Polymer-immobilized nanoparticles. *Colloids and Surfaces A: Physicochemical and Engineering Aspects*. 439, 43–68. doi:10.1016/j.colsurfa.2013.04.013.
- Maksin, D.D., Nastasović, A.B., Milutinović-Nikolić, A.D., Suručić, L.T., Sandić, Z.P., Hercigonja, R.V., Onjia, A.E., 2012. Equilibrium and kinetics study on hexavalent chromium adsorption onto diethylene triamine grafted glycidyl methacrylate based copolymers. *Journal of Hazardous Materials*. 209-210, 99–110. doi:10.1016/j.jhazmat.2011.12.079.
- Malović, L., Nastasović, A., Sandić, Z., Marković, J., Đorđević, D., Vuković, Z., 2007. Surface modification of macroporous glycidyl methacrylate based copolymers for selective sorption of heavy metals. *Journal of Materials Science*. 42, 3326–3337. doi:10.1007/s10853-006-0958-y.
- Mangeon, C., Mahouche-Chergui, S., Versace, D.L., Guerrouache, M., Carbonnier, B., Langlois, V., Renard, E., 2015. Poly(3-hydroxyalkanoate)-grafted carbon nanotube nanofillers as reinforcing agent for PHAs-based electrospun mats. *Reactive and Functional Polymers*. 89, 18–23. doi:10.1016/j.reactfunctpolym.2015.03.001.
- Mao, K., Chen, Y., Wu, Z., Zhou, X., Shen, A., Hu, J., 2014. Catalytic Strategy for Efficient Degradation of Nitroaromatic Pesticides by Using Gold Nanoflower. *Journal of Agricultural and Food Chemistry*. 62, 10638–10645. doi:10.1021/jf5034015.
- Marković, B.M., Vuković, Z.M., Spasojević, V.V., Kusigerski, V.B., Pavlović, V.B., Onjia, A.E., Nastasović, A.B., 2017. Selective magnetic GMA based potential sorbents for molybdenum and rhenium sorption. *Journal of Alloys and Compounds*. 705, 38–50. doi:10.1016/j.jallcom.2017.02.108.
- Mealey, S.K., & Thomas, B., 2005. Past, present and future of organosilane treatments for fillers. *Rubber World*. 233, 32–35.
- Miguel-García, I., Berenguer-Murcia, Á., García, T., Cazorla-Amorós, D., 2012. Effect of the aging time of PVP coated palladium nanoparticles colloidal suspensions on their catalytic activity in the preferential oxidation of CO. *Catalysis Today*. 187, 2–9. doi:10.1016/j.cattod.2012.02.015.
- Mohammed, N.A., 2014. Rheology, processing and properties of polymer nanocomposites

based on poss and boehmite. PhD Thesis. Technische Universität, Berlin. doi:10.14279/depositonce-3981.

- Moussavi, G., and Mahmoudi, M., 2009. Degradation and biodegradability improvement of the reactive red 198 azo dye using catalytic ozonation with MgO nanocrystals. *Chem. Eng. J.* 152, 1–7.
- Mukhopadhyay, R., Bhaduri, D., Sarkar, B., Rusmin, R., Hou, D., Khanam, R., Sarkar, S., Biswas, J.K., Vithanage, M., Bhatnagar, A., Ok, Y.S., 2019. Clay–polymer nanocomposites: Progress and challenges for use in sustainable water treatment. *Journal of Hazardous Materials.* 383, 121125. doi:10.1016/j.jhazmat.2019.121125.

N

- Najafinejad, M. S., Mohammadi, P., Mehdi Afsahi, M., Sheibani, H., 2019. Biosynthesis of Au nanoparticles supported on Fe₃O₄@polyaniline as a heterogeneous and reusable magnetic nanocatalyst for reduction of the azo dyes at ambient temperature. *Materials Science and Engineering: C.* 28, 19-29. doi:10.1016/j.msec.2018.12.098.
- Nasir, A., Masood, F., Yasin, T., Hameed, A., 2019. Progress in polymeric nanocomposite membranes for wastewater treatment: Preparation, properties and applications. *Journal of Industrial and Engineering Chemistry.* 79, 29–40. doi:10.1016/j.jiec.2019.06.052.
- Nasrollahzadeh, M., Nezafat, Z., Gorab, M.G., Sajjadi, M., 2020. Recent progresses in graphene-based (photo)catalysts for reduction of nitro compounds. *Molecular Catalysis.* 484, 110758. doi:10.1016/j.mcat.2019.110758.
- Nasrollahzadeh, M., Sajjadi, M., Shokouhimehr, M., Varma, R.S., 2019. Recent developments in palladium (nano)catalysts supported on polymers for selective and sustainable oxidation processes. *Coordination Chemistry Reviews.* 397, 54–75. doi:10.1016/j.ccr.2019.06.010.
- Nastasović, A.B., Jovanović, S.M., Đorđević, D., Onjia, A.E., Jakovljević, D., Novaković, T., 2004a. Metal sorption on macroporous poly(GMA-co-EGDMA) modified with ethylene diamine. *Reactive and Functional Polymers.* 58, 139–147. doi:10.1016/j.reactfunctpolym.2003.11.015.
- Nastasović A.B., Jovanović S.M., Jakovljević, D., Stanković S., Onjia A.E., 2004b. Noble metal binding on macroporous poly(GMA-co-EGDMA) modified with ethylenediamine. *Journal of the Serbian Chemical Society.* 69, 455–460. doi:10.2298/JSC0406455N.

O

- Odom, I.E., 1984. Smectite clay Minerals: Properties and Uses. *Philosophical Transactions of the Royal Society A: Mathematical, Physical and Engineering Sciences*. 311, 391–409. doi:10.1098/rsta.1984.0036.
- Ostovar, S., Rezvani, A., Luque, R., Carrillo-Carrión, C., 2020. Core-shell iron oxide@cathecol-polymer@palladium/copper nanocomposites as efficient and sustainable catalysts in cross-coupling reactions. *Molecular Catalysis*. 493, 111042. doi:10.1016/j.mcat.2020.111042.

P

- Parida, D., Simonetti, P., Frison, R., Bülbül, E., Altenried, S., Arroyo, Y., Balogh-Michels, Z., Caseri, W., Ren, Q., Hufenus, R., Gaan, S., 2019. Polymer-assisted in-situ thermal reduction of silver precursors: a solventless route for silver nanoparticles-polymer composites. *Chemical Engineering Journal*. 123983. doi:10.1016/j.cej.2019.123983.
- Passador, F.R., Ruvolo-Filho, A., Pessan, L.A., 2017. Chapter 7: Nanocomposites of Polymer Matrices and Lamellar Clays. In Da Róz, A.L., Ferreira, M., de Lima Leite, F., Oliveira, Jr. O.N., (Eds.), *Nanostructures* (pp187–207). 272. London: Elsevier. doi:10.1016/b978-0-323-49782-4.00007-3.
- Pavlidou, S., & Papaspyrides, C.D., 2008. A review on polymer-layered silicate nanocomposites. *Progress in Polymer Science*. 33. 1119–1198. doi:10.1016/j.progpolymsci.2008.07.008.
- Pei, L., Mori, K., Adachi, M., 2004. Formation process of twodimensional networked gold nanowires by citrate reduction of AuCl_4^- and the shape stabilization. *Langmuir*. 20, 7837–7843.
- Pomogailo, A.D., 2000. Hybrid polymer-inorganic nanocomposites. *Russian Chemical Reviews*. 69, 53–80. doi:10.1070/rc2000v069n01abeh000506.
- Potts, J.R., Dreyer, D.R., Bielawski, C.W., Ruoff, R.S., 2011. Graphene-based polymer nanocomposites. *Polymer*. 52, 5–25. doi:10.1016/j.polymer.2010.11.042.
- Poupart, R., Grande, D., Carbonnier, B., Le Droumaguet, B., 2019. Porous polymers and metallic nanoparticles: A hybrid wedding as a robust method toward efficient supported catalytic systems. *Progress in Polymer Science*. 96, 21–42. doi:10.1016/j.progpolymsci.2019.05.003.
- Poupart, R., Le Droumaguet, B., Guerrouache, M., Grande, D., Carbonnier, B., 2017. Gold nanoparticles immobilized on porous monoliths obtained from disulfide-based

dimethacrylate: Application to supported catalysis. *Polymer*, 126, 455–462. doi:10.1016/j.polymer.2017.04.034.

Poupart, R., Nour El Houda, D., Chellapermal, D., Guerrouache, M., Carbonnier, B., Le Droumaguet, B., 2016. Novel in-capillary polymeric monoliths arising from glycerol carbonate methacrylate for flow-through catalytic and chromatographic applications. *RSC Advances*. 6, 13614–13617. doi:10.1039/c5ra27248c.

Q

Qiu, J., Zhang, X., Xie, K., Zhang, X-F., Feng, Y., Jia, M., Yao, J., 2019. Noble metal nanoparticle-functionalized Zr-metal organic frameworks with excellent photocatalytic performance. *Journal of Colloid and Interface Science*. 538, 569–577. doi:10.1016/j.jcis.2018.12.024.

R

Rahman, A., Iqbal, M., Rahman, F. ur, Fu, D., Yaseen, M., Lv, Y., Omer, M., Garver, M., Yang, L., Tan, T., 2012. Synthesis and characterization of reactive macroporous poly(glycidyl methacrylate-triallyl isocyanurate-ethylene glycol dimethacrylate) microspheres by suspension polymerization: Effect of synthesis variables on surface area and porosity. *Journal of Applied Polymer Science*. 124, 915–926. doi:10.1002/app.35026.

Ray, S.S., & Okamoto, M., 2003. Polymer/layered silicate nanocomposites: a review from preparation to processing. *Progress in Polymer Science*. 28, 1539–1641. doi:10.1016/j.progpolymsci.2003.08.002.

S

Sadeghi, B., Sadjadi, M., Vahdati, R., 2009. Nanoplates controlled synthesis and catalytic activities of silver nanocrystals. *Superlattice Microst.* 46, 858–863.

Sadjadi, S., Akbari, M., Kahangi, F.G., Heravi, M.M., 2020. Acidic polymer containing sulfonic acid and carboxylic acid groups heterogenized with natural clay: A novel metal free and heterogeneous catalyst for acid-catalyzed reactions. *POLYHEDRON* 179, 114375

Saleh, T.A., Parthasarathy, P., Irfan, M., 2019. Advanced Functional polymer nanocomposites and their use in water ultra-purification. *Trends in Environmental Analytical Chemistry*. 24, e00067. doi:10.1016/j.teac.2019.e00067.

- Sen, B., Kuzu, S., Demir, E., Akocak, S., Sen, F., 2017. Polymer-graphene hybride decorated Pt nanoparticles as highly efficient and reusable catalyst for the dehydrogenation of dimethylamine–borane at room temperature. *International Journal of Hydrogen Energy*. 42, 23284–23291. doi:10.1016/j.ijhydene.2017.05.112.
- Shih, Y.H., Tso, C.P., Tung, L.Y., 2010. Rapid degradation of methyl orange with nanoscale zerovalent iron particles. *Journal of Environmental Engineering and Management*. 20, 137–143.
- Singh, P., Shandilya, P., Raizada, P., Sudhaik, A., Rahmani-Sani, A., Hosseini-Bandegharaei, A., 2018. Review on various strategies for enhancing photocatalytic activity of graphene based nanocomposites for water purification. *Arabian Journal of Chemistry*. doi:10.1016/j.arabjc.2018.12.001.
- Snoussi, Y., Bastide, S., Abderrabba, M., Chehimi, M.M., 2018. Sonochemical synthesis of Fe₃O₄@NH₂-mesoporous silica@Polypyrrole/Pd: A core/double shell nanocomposite for catalytic applications. *Ultrasonics Sonochemistry*. 41, 551–561. doi:10.1016/j.ultsonch.2017.10.021.
- Srivastava, I., Mehta, R.J., Yu, Z.-Z., Schadler, L., Koratkar, N., 2011. Raman study of interfacial load transfer in graphene nanocomposites. *Applied Physics Letters*. 98, 063102. doi:10.1063/1.3552685.
- Stefanović, I.S., Ekmešćić, B.M., Maksin, D.D., Nastasović, A.B., Miladinović, Z.P., Vuković, Z.M., Micic, D.M., Pergal, M.V., 2015. Structure, Thermal, and Morphological Properties of Novel Macroporous Amino-Functionalized Glycidyl Methacrylate Based Copolymers. *Industrial & Engineering Chemistry Research*. 54, 6902–6911. doi:10.1021/acs.iecr.5b01285.
- Sun, X., Sun, H., Li, H., Peng, H., 2013. Developing Polymer Composite Materials: Carbon Nanotubes or Graphene?. *Advanced Materials*. 25, 5153–5176. doi:10.1002/adma.201301926.

T

- Tan, B., & Thomas, N.L., 2016. A review of the water barrier properties of polymer/clay and polymer/graphene nanocomposites. *Journal of Membrane Science*. 514, 595–612. doi:10.1016/j.memsci.2016.05.026.
- Terrones, M., Martín, O., González, M., Pozuelo, J., Serrano, B., Cabanelas, J.C., Vega-Díaz, S.M., Baselga, J., 2011. Interphases in Graphene Polymer-based Nanocomposites: Achievements and Challenges. *Adv. Mater*. 23, 5302-5310.

- Theng, B.K.G., 1970. Interactions of clay minerals with organic polymers. Some practical applications. *Clays and Clay Minerals*. 18, 357–362. doi:10.1346/ccmn.1970.0180608.
- Tripathy, T., Kolya, H., Jana, S., Senapati, M., 2017. Green synthesis of Ag-Au bimetallic nanocomposites using a biodegradable synthetic graft copolymer; hydroxyethyl starch-g-poly (acrylamide- co -acrylic acid) and evaluation of their catalytic activities. *European Polymer Journal*. 87, 113–123. doi:10.1016/j.eurpolymj.2016.12.019.
- Turner, M., Golovko, V.B., Vaughan, O.P., Abdulkin, P., Berenguer-Murcia, A., Tikhov, M.S., Johnson, B.F., Lambert, R.M., 2008. Selective oxidation with dioxygen by gold nanoparticle catalysts derived from 55-atom clusters. *Nature*. 454, 981–983.

U

- Unuabonah, E.I., & Taubert, A., 2014. Clay–polymer nanocomposites (CPNs): Adsorbents of the future for water treatment. *Applied Clay Science*. 99, 83-92. doi:10.1016/j.clay.2014.06.016.
- Urbano, B.F., Villenas, I., Rivas, B.L., Campos, C.H., 2015. Cationic polymer–TiO₂ nanocomposite sorbent for arsenate removal. *Chemical Engineering Journal*. 268, 362–370. doi:10.1016/j.cej.2015.01.068.
- Usuki, A., Yoshitsugu, K., Masaya, K., Akane, O., Yoshiaki, F., Toshio, K., Osami, K., 1993. Synthesis of Nylon 6-clay hybrid. *Journal of Materials Research*. 8, 1179–1184. doi:10.1557/JMR.1993.1179.

V

- Vaia, R.A., Wagner, H.D., 2004. Framework for nanocomposites. *Materials Today*. 7, 32-37.
- Verdejo, R., Bernal, M.M., Romasanta, L.J., Lopez-Manchado, M.A., 2011. Graphene filled polymer nanocomposites. *J. Mater. Chem.*, 21, 3301-3310.
- Vidhu, V.K., & Philip, D., 2014. Catalytic degradation of organic dyes using biosynthesized silver nanoparticles. *Micron*. 56, 54–62. doi:10.1016/j.micron.2013.10.006.
- Vo, V.S., Mahouche-Chergui, S., Nguyen, V.-H., Naili, S., Carbonnier, B., 2019. Crucial role of covalent surface functionalization of clay nanofillers on improvement of the mechanical properties of bio-epoxy resin. *ACS Sustainable Chemistry & Engineering*. doi:10.1021/acssuschemeng.9b02088.
- Vo, V.S., Mahouche-Chergui, S., Nguyen, V.-H., Naili, S., Singha, N.K., Carbonnier, B., 2017a. Chemical and Photochemical Routes Toward Tailor-Made Polymer–Clay Nanocomposites. In Jlassi K., Chehimi, MM., Sabu T., (Eds.), *Clay-Polymer*

Nanocomposites (pp145–197). 546. Netherlands: Elsevier. doi:10.1016/b978-0-323-46153-5.00005-7.

- Vo, V.S., Nguyen, V.-H., Mahouche-Chergui, S., Carbonnier, B., Di Tommaso, D., Naili, S., 2017b. From atomistic structure to thermodynamics and mechanical properties of epoxy/clay nanocomposites: Investigation by molecular dynamics simulations. *Computational Materials Science*. 139, 191–201. doi:10.1016/j.commatsci.2017.07.024.
- Vo, V.S., Nguyen, V.-H., Mahouche-Chergui, S., Carbonnier, B., Naili, S., 2018. Estimation of effective elastic properties of polymer/clay nanocomposites: A parametric study. *Composites Part B: Engineering*. 152, 139–150. doi:10.1016/j.compositesb.2018.06.018.

W

- Wang, H., Dong, Z., Na, C., 2013. Hierarchical Carbon Nanotube Membrane-Supported Gold Nanoparticles for Rapid Catalytic Reduction of p-Nitrophenol. *ACS Sustainable Chemistry & Engineering*. 1, 746–752. doi:10.1021/sc400048m.
- Wassel, A.R., El-Naggar, M.E., Shoueir, K., 2020. Recent advances in polymer/metal/metal oxide hybrid nanostructures for catalytic applications. *Journal of Environmental Chemical Engineering*. 8, 104175. doi:10.1016/j.jece.2020.104175.
- Wu, J., Gao, H., Yao, S., Chen, L., Gao, Y., Zhang, H., 2015. Degradation of Crystal Violet by catalytic ozonation using Fe/activated carbon catalyst, *Sep. Purif. Technol.* 147, 179–185.

X

- Xiao, M., Sun, L., Liu, J., Li, Y., Gong, K., 2002. Synthesis and properties of polystyrene/graphite nanocomposites. *Polymer*. 43, 2245–2248.

Y

- Yadav, V.B., Gadi, R., Kalra, S., 2019. Clay based nanocomposites for removal of heavy metals from water: A review. *Journal of Environmental Management*. 232, 803–817. doi:10.1016/j.jenvman.2018.11.120.
- Yu, J., Tian, X., Liu, M., Jia, Z., Fang, H., Liu, Y., Yu, C., 2019. Catalytic activity of $Cu_xMn_xFe_{3-2x}O_4$ /multi-walled carbon nanotubes ($0 \leq x \leq 0.1$) nanocomposites for p-

nitrophenol degradation in catalyst/H₂O₂ system. *Water Science and Technology*. doi:10.2166/wst.2019.236.

Z

- Zabihi, O., Ahmadi, M., Nikafshar, S., Chandrakumar Preyeswary, K., Naebe, M., 2018. A technical review on epoxy-clay nanocomposites: Structure, properties, and their applications in fiber reinforced composites. *Composites Part B: Engineering*. 135, 1–24. doi:10.1016/j.compositesb.2017.09.066.
- Zaferani, S.H., 2018. Introduction of polymer-based nanocomposites. In Jawaid, M., Mansoob Khan, M.M., (Eds)., *Polymer-Based Nanocomposites for Energy and Environmental Applications*. 700. Duxford-united kingdom: Elsevier. doi:10.1016/b978-0-08-102262-7.00001-5.
- Zhang, Y., Chu, W., Xie, L., Sun, W., 2010. Preparation and Catalytic Performance of Carbon Nanotube Supported Palladium Catalyst. *Chinese Journal of Chemistry*. 28, 879–883. doi:10.1002/cjoc.201090165.
- Zhao, X., Lv, L., Pan, B., Zhang, W., Zhang, S., Zhang, Q., 2011. Polymer-supported nanocomposites for environmental application: A review. *Chemical Engineering Journal*. 170, 381–394. doi:10.1016/j.cej.2011.02.071.
- Zheng, W., Lu, X., Wong, S.C., 2004. Electrical and mechanical properties of expanded graphite-reinforced high-density polyethylene. *Journal of Applied Polymer Science*. 91, 2781–2788. doi:10.1002/app.13460.
- Zollinger, H., 1987. *Color Chemistry: Syntheses, Properties and Applications of Organic and Pigments*. New York: Wiley-VCH.

Section 3

Hybrid catalytic separation process for continuous and simultaneously water remediation in membrane reactor

1. Introduction

Since 1960s, Membrane Reactor (MR) has been introduced as a concept for the membrane technology intensification (Cassano et al. 2013; He et al. 2018; Szegner et al. 1997)

Generally, different attempts have been made in the literature to specify a definition to the membrane reactor. The main definition, according to the IUPAC (International Union of Pure and Applied Chemistry), presents the MR as a device for simultaneously combination of both membrane separation and a chemical reaction in a single apparatus (Koros et al. 1996). Therefore, the MR is classified as a multidisciplinary subject, at the frontier of several research area that mainly requires the connection between membrane separation, materials sciences, catalysis and chemical engineering (Dalmon et al. 2007; Das and Bose 2017; Jiang et al. 2013; Julbe et al. 2001; Koros et al. 1996; Szegner et al. 1997).

The interest on membrane reactors (MRs) has been hugely studied not only at the laboratory scale (Oxidation reactions, hydrogenation, purification and decomposition), but also adopted for several industrial activities (Das et al. 2012; Hai et al. 2013; Kemmere et al. 2001; Molinari et al. 2013; Palo et al. 2018; Takht Ravanchi et al. 2009).

The catalytic reaction integration in the MR provides the improvement of the conventional membrane processes. In such hybrid system, the CMs and catalysts are considered the basis of this enhancement of process efficiency in terms of selectivity, kinetic and total conversion yield (Das and Bose 2017; Dittmeyer et al. 2008). Nowadays, for the evident need to avoid the high cost and maintain the benefic properties, low-cost materials (clay, mud, zeolite and others) were strongly suggested in membrane fabrication, especially used in CMs systems (Guesmi et al., 2020; Oun et al., 2017; Sahoo et al., 2016; Tan and Li 2015).

It is highlighted in literature that coupling membrane filtration with heterogeneous catalysis reaction in single device for the polluted water treatment may intensificate the process performance (Dotzauer et al., 2006). Currently, hybrid process is strongly progressed and widely proposed as promising technology for wastewater remediation and water recycling (Adham et al., 1991; Hammami et al., 2017; Tomaszewska and Mozia 2002).

In this work, the efficient method for water and wastewater treatment by using hybrid treatment system in ceramic membrane reactor has been revealed. Further, amplified filtration

performance by the ceramic membrane was due to the integration with the catalytic reduction reaction that provided by nano-sized catalyst.

2. Membrane reactor configurations

Several research works have classified the membrane natures according to the combination way between membrane and catalysts (Coronas et al. 1999; Julbe et al. 2001; Li 2007). Generally, the relative placement of the catalyst with respect to the membrane includes three possible combinations as shown in *Figure 9*. Here, the catalyst is physically separated from the membrane (*Figure 9a*), the membrane itself is catalytically active (*Figure 9b*) and the membrane is loaded with catalyst (*Figure 9c*).

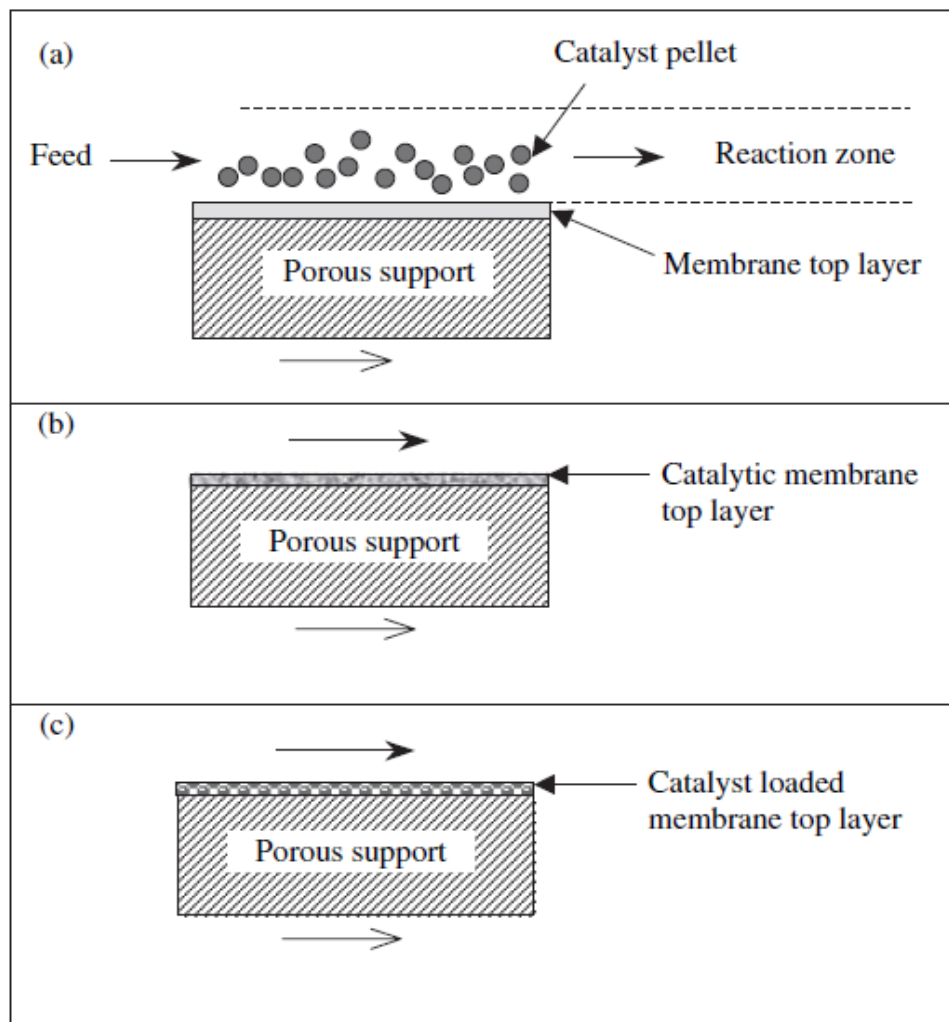


Figure 9. Coupling of the membrane with catalysts: (a) pellet catalyst on an inert ceramic membrane, (b) inherently catalytic membrane and (c) catalyst integrated into the pores of the membrane (From Li 2007).

Few years ago, *Jiang and co-workers* developed a new concept of integrating of separation and heterogeneous catalysis processes in a simple design (Jiang et al. 2013). Quite often, side-stream membrane reactor is the most widespread used configuration. Additionally, the presence of the suspended catalysts in the reaction tank avoid considering whether the materials of such membrane is inert or exhibit a catalytic activity. In such way, the ceramic membrane (CM) and the reactor are connected in series (*Figure 10*). Then, an operational approach of coupling membrane separation with heterogeneous catalysis can easily achieved by circulating the catalysts loaded feed into the system.

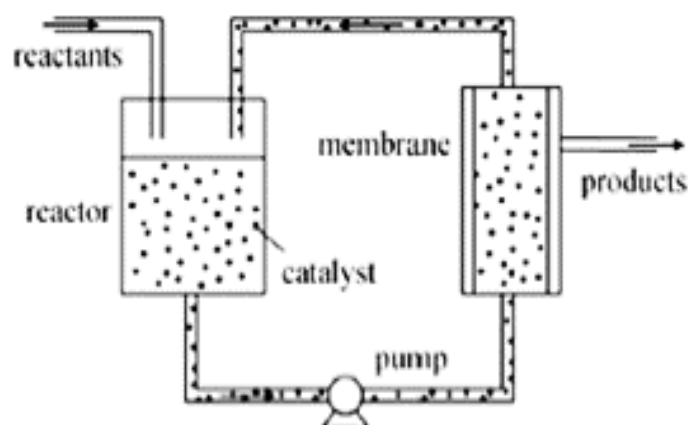


Figure 10. Side-stream membrane reactor (SSMR) configuration (From Jiang et al. 2013).

3. Ceramic membrane function in membrane reactor

The implementation of the SSMR involves the use of uniform (Wang et al., 2008) or composite (Choudhury et al., 2018) ceramic membrane with symmetric (Saja et al., 2018) or asymmetric structure (mono, bi or multilayered) (Alem et al. 2009; Ebrahimi et al., 2010; Fard et al., 2018; Oun et al., 2017). Moreover, several ceramic membrane configurations are widely famous for possible applications in SSMR particularly tubular mono or multichannel (Choudhury et al., 2019 and 2020; Oun et al., 2017), planar discs (Saja et al., 2018), hollow fibers and monolithic multi-channel geometries (Hsieh 1996; Nath et al. 2012). As it is known, selectivity and permeability are considered as the main interesting characteristics of the membrane separation technology (Das and Bose 2017; Osegueda Chicas 2013). Hence, efficient catalytic-separation treatment into the SSMR is strongly dependent to various parameters such as membrane porosity, mean pores size and filtration layer(s) thickness as well as the membrane materials (Osegueda Chicas 2013; Szegner et al. 1997). Furthermore, these parameters define the transport mechanisms through the membrane and the nature of

interactions between the membrane materials and the feeding compounds. On one hand, the better performances (permselectivity and reaction rate) implies a higher and stable permeability and controllable selectivity. On the other hand, lower cost and longer lifespan (reuse cycle number) could be very much appreciated. All these key factors are considered as the highlights of this hybrid process that appear as attractive for the heterogeneous catalysis in CMRs (Das and Bose 2017; Ertl et al., 2008; Hsieh 1996; Jiang et al., 2011; Julbe et al., 2001; Lu et al., 2008; Mozia 2010; Chen et al., 2009a) and especially in organic pollutants removal from water as well as WWT (Ahmad et al., 2018 and 2019; Chang et al., 2019; Dumée et al., 2017; Lan et al., 2020).

4. Surface modification of ceramic membrane

For further effective applications of CMs, particular attention should be focused on membrane adhesion, selectivity, hydrophobicity, mechanical property, thermal and chemical stability (Takagi et al., 2000; Tsuru et al., 2001).

In order to satisfy these required conditions, ceramic membrane surface may be modified with the intention of enhancing separation performances (Zaman et al., 1994). Generally, for CMs that did not presents catalytic activity a possible surface modification suitable for more demanding separation applications can be realized with several materials and methods. In fact, the modification processes encompass two main ways: (Nano)structuration by thin layer deposition and chemical surface grafting.

4.1. Surface pre-treatment

In most cases, surface modification can only be employed when the membrane undergoes a surface pre-treatment (Chen et al. 2013; Kujawa et al. 2020; Liu et al. 2017; Menne et al., 2016; Tanardi et al., 2016). There are four main considerations for ceramic membrane surface pre-treatment process. Firstly, it is judicious to clean and degrease surface from dust and any other contamination, which can limit deposition of the active layer (inert or catalytic coating). Secondly, surface cleaning allows removing impurities to increase the available specific and top surface area for better contact with the pollutant to be treated. Furthermore, this procedure aims to provide a sufficient number of active sites (e.g., hydroxyl group) capable to ensure chemical modification and enhance grafting rate. Finally, the pre-treatment step leads to improve the adhesion of coatings in order to achieve the full potential for immobilization of the catalyst (Tanimu et al., 2017).

Various methods have been used for pre-treatment involves oxidation by using plasma, ozonation, anodic and chemical oxidation such as piranha solution (Da Silva et al., 2020) as well as chemical treatment by acetone, alcohol and in an alkaline medium (Kujawa et al. 2020; Zhang et al., 2017). UV radiation (Tanimu et al., 2017) and ultrasonic cleaning (Zhang et al., 2017) can be also used for ceramic surface treatment. Da Silva et al. (2020) used Piranha solution (3:1, v/v, 99.99% H₂SO₄/ 99.99% H₂O₂) for chemically modification of tape casted-zirconia membranes with 3-aminopropyl triethoxysilane (APTES). Similarly, *Lv and co-workers* showed that before modification porous ceramic surface were activated with gently boiling Piranha solution (3:1, v/v, 98% H₂SO₄/30% H₂O₂) for 20 min. Then the sample was amino-grafted with APTES silane after being washed with ultrapure water (Lv et al., 2009). In other research work, Zhang et al. (2017) suggested for the preparation of TiO₂-loaded CM, an ultrasonic cleaning of ceramic Al₂O₃-substrate for 30 min in an equal volume ratio of mixing solution of deionized water, acetone, and 2-propanol.

Efficiency of surface pre-treatment processes has been sufficiently presented in literature reviews. Several authors evaluated and justified enhanced adhesion after pre-treatment methods. To the best of our knowledge, anodic oxidation is particularly useful on titanium and aluminium surfaces to generate hydrophilic titania and alumina surface (Haas-Santo et al., 2001). In the same context, Glazneva et al. (2007) have proven that 2 h of UV radiation of a titanium substrate permit to produce a super hydrophilic titania layer which provide a better adhesion with a deposited silica film. Gu and al. (2019)suggested an improved adhesion of the Graphene Oxide (GO) modified ceramic Al₂O₃-membrane layers. Alumina layer surface has been activated by ultrasonic treatment in water followed by cleaning in 30% hydrogen peroxide for 10 min. Thus, the hydroxyl groups onto the alumina surface have been increased. Consequently, stable interfacial adhesion between GO and coated ceramic surface via a chemical-grafting has been achieved.

4.2. Modification by (Nano)structuration and chemical grafting

The membrane modification by(Nano)structuration mechanism aims to active layer deposition. This involve various coating technics including centrifugal casting (Bouzerara et al., 2015), slip-casting (Oun et al., 2017), dip-coating (Mittal et al., 2011), spin-coating (Bouazizi et al., 2017), sol-gel (Gaber et al., 2013), atomic layer deposition (ALD) (Li et al., 2012), molecular layer deposition (MLD) (Song et al., 2016), chemical vapor deposition (CVD) (Chi et al., 2020; De Haart et al., 1991; Han et al., 2013), electrochemical vapor deposition (EVD) (De Haart et al., 1991) and plasma chemical process (PCP) (Ida et al.,

2000). This large variety of established coating technics for the ceramic membrane modification may occurred on gas, vapor or liquid phase. However, the deposited layers may be made of single or mixed materials. The coating process can be done once or repeatedly. In addition, surface coating of the same membrane is possible by several coating methods (De Haart et al., 1991).

The chemical grafting strategy includes the integration of a very large number of organic compounds capable of being covalently bound to the ceramic surface due to the surface functions initially existing on the membrane. For example, chemical modification can include ceramic membrane surface grafting by Grignard Reagents, Organophosphonic Acids, Organosilanes and Organic Polymers (Hosseinabadi et al., 2011; Kim, et al., 2010; Kujawa et al., 2015 and 2020; Kumar et al., 2016; Mittal et al., 2011; Mustafa et al., 2014 and 2016; Oun et al. 2019; Randon et al., 1995).

The main membrane nanostructuring processes and chemical grafting ways that received attention is the ceramic membrane surface modification was enough elaborated in *section 2* of this chapter.

4.3. Catalytic and catalytically active ceramic membrane

Ceramic membrane can be surface modified for strengthening the catalytic function. For such reason, many approaches have been strongly suggested to be suitable. Firstly, an appropriate approach aims to synthesize an inherently catalytic membrane (Das and Bose 2017). Here, the selective membranes are made from (LaOCl) (Chanaud et al. 1995) or mixed oxides (such as VMgO and VPO) (Cot et al. 2000; Farrusseng et al. 2000).

Secondly, the catalytic activity can be achieved by deposition of a membrane layer doped with catalytically active materials or the catalysts are dispersed into the membrane matrix (Reif et al., 2003; Tereshchenko et al., 2009; Zaman 1994; Zhang et al., 2016; Zou et al., 2020). From another side, a great deal of progress in the catalytically active membranes has been tightly mentioned in the MR manufacturing. To realize this approach, Raman et al. (1993) have suggested two wet ways for rhodium metal particles dispersing onto a composite silica membrane. The first way allows the impregnation of the inert membrane in a metal-organic precursor solution. Then, the impregnated CM was brought to calcination, to remove organic matter, followed by reduction reaction to reduce the catalysts to the metallic nanoparticles state (Bottino et al. 2002; Champagnie et al. 1992; Cini et al. 1991; Harold et al. 1989; Perez et al. 2001; Tsotsis et al. 1992; Uzio et al. 1991; Ziaka et al. 1993). The second way permits to produce catalysts organo-bounded with the CM. Thus, the ceramic membrane

surface was chemically treated with grafting process by using, commonly, silane-coupling agents (Chen et al. 2013; Du et al. 2015; Jiang et al. 2014; Li et al. 2013; Miao et al. 2019) as well as polymers (Dotzauer et al. 2006; Liu et al. 2017; Wales et al. 2016). After that, modified membrane was impregnated in precursor solution of metallic catalyst before reduced under hydrogen flux (Perez et al. 2001; Uzio et al. 1991) or in an alkaline solution such as hydrazine hydrate (Li et al. 2013; Peng et al. 2016).

In general, no matter which process is selected for modification of the ceramic membrane surfaces, the modified membranes exhibit a very much benefits in comparison with that unmodified, in terms of performances and lifetime. The clear advantages improved and generated by modification processes that exist in the resulting membranes are numerous and concerns the: i) increase of membrane stability, ii) promote the preferred permeation, iii) control both of hydrophilicity and hydrophobicity, iv) reinforcement of the selectivity versus specific components, v) ensure antifouling properties and vi) increase degradation rate by catalysis reaction integration.

As a result, there is currently a considerable level of applications of these membranes, in the CtCMR for an efficient treatment of polluted water including industrial wastewater (Ahmad et al., 2018; Chang et al., 2019; Dumée et al., 2017; Meng et al., 2013; Yan et al., 2015).

For a better comprehensive explanation, the evolution of membrane performance with and without modification should compared. Therefore, the influence, of pore size and membrane porosity to achieve optimal permeation, as well as the membrane thickness and manufacturing materials on the permeate transport mechanism and fouling behavior have been studied. The statistically interpretations of the modified characteristic parameters with improving the efficiency of catalytic separation will largely developed in the following section.

5. The Synthesis strategy adapted in this work

In front of the diversity of wastewater purification and treatment processes and techniques, the selection and set up of a good choice of the treatment strategy remains a critical step.

This depends on the one hand, on the compliance of discharge regulatory standards in force, and on the other hand, on the economic aspect which corresponds to reducing as much as possible the quantities of discharged water and the toxicity of subproducts generated and its impact on the environment.

Currently, membrane processes and heterogeneous catalysis are presented as suitable solutions to solve this problem due to their efficiency, low energy consumption and simplicity of operation.

Within the framework of this work, we envisage the development of an original approach combining heterogeneous catalysis with membrane filtration to achieve a new hybrid treatment process of catalytic filtration of wastewater.

This concept allows to expand the field of application of membranes to improve the quality of treated effluents, which simultaneously satisfy environmental, legislative and economic requirements.

One of the expected consequences of this strategy is to obtain multitasking materials with improved properties compared to individual components which, for example, are able to separate and degrade pollutants, resist to fouling and harsh effluent conditions, at the same time, having good stability to be reused in the long term.

In this context, catalytic hybrid materials based on metallic NPs immobilized on hybrid platforms functionalized by chelating groups and tubular ceramic membranes based on local materials at low cost have been synthesized.

Therefore, various synthesis strategies of asymmetric ceramic membranes and catalytic hybrid materials have been adapted in the present work.

5.1. Synthesis of powdered nano hybrid catalytic materials

Regarding the catalytic hybrid materials, two synthesis methodologies have been developed:

- The first consists to prepare purely synthetic organic monoliths with microspheres.

The synthesis of the monoliths was carried out by radical photopolymerization of a reactive monomer (Glycidyl methacrylate, GMA) copolymerized with a crosslinking agent (ethylene glycol dimethacrylate, EGDMA) in a porogenic solvent mixture consisting of 1-decanol and cyclohexanol and in the presence of 2,2'-azobisisobutyronitrile (AIBN) as photoinitiator.

Then, this approach consists in the functionalization of chemical groups of the monolith obtained by covalent grafting of molecules of iminodiacetic acid (IDA) and ethylenediamine (EDA) having complexing groups of -COOH and -NH₂, on which metallic NPs of Au and Ni were immobilized.

- As for the second strategy, two types of nanostructured catalysts based on natural materials have been developed, such as the clay-based nanocomposites grafted with PGMA polymer chains and the graphene of sugar/clay nanomaterials organo-modified through (3-glycidyloxypropyl) trimethoxysilane (GPTMS) and tris(4-hydroxyphenyl)methane triglycidyl ether.

Regarding these hybrid catalysts materials, the synthesis strategy is as follows:

Initially, the pristine materials undergo a surface activation step in order to generate reactive groups and then chemically modified by coupling agents, before being grafted by photopolymerization of the polymer chains of GMA via covalent bonds.

In order to confer to the obtained nanocomposites complexing properties of metals, the epoxy functions were functionalized by cycle openings to generate complexing functions of primary amine and carboxylic acids able to immobilize the NPs after the reduction of the ions of precursor metal salt under the effect of NaBH₄ solution.

5.2. Fabrication of nanostructured ceramic ultrafiltration membranes

Regarding ceramic membranes, we proposed two manufacturing strategies which resulted in three families of asymmetric ultrafiltration membranes.

- The first strategy constitutes a realization in two stages:

First, a robust macroporous support from natural clay and phosphate which ensures the mechanical strength of the final material was developed.

Initially, the mineral powders with determined particle size are dry mixed with organic additives and then rigorously mixed with the gradual addition of water for better formulation of the ceramic paste. Later, this plastic paste has been shaped by the extrusion process. Afterwards, the green tubes undergo a slowly drying in ambient air and finally, calcined at high temperatures which allow the consolidation of the support.

In a second step, a thin separating layer is synthesized by using slip casting and dip coating techniques.

These techniques consist of the nanostructuring of the membrane by deposition, on the internal face of the support, of a homogeneous suspension of titanium dioxide nanopowders stabilized in an aqueous solution of polyvinyl alcohol in the presence of dolapix CE64 as deflocculant.

Finally, a second sintering process high temperature allows the cohesion of the membrane layer and its adherence with the support and then obviously defines the final membrane porosity.

- In a second approach, we have developed an original strategy for synthesizing new low-cost asymmetric membrane through the layer-by-layer coating coupled to co-sintering method.

According to this strategy, tight ultrafiltration bilayer ceramic membrane was developed by deposition of two separation layers on the inner surface of the dry substrate in phosphate using the dip-coating technique twice in a stable suspension of titanium dioxide for 60s each.

Finally, a co-sintering process consists of a single heat treatment at 800 °C, the densification and consolidation of the matrix (from phosphate mud) and membrane structures as well as ensuring adhesion between the different layers.

6. Membrane reactor study

Use of membrane reactors, which combine reaction and separation in one unit operation, has been recognized to control the integration of the permeation process into chemical reaction. To enhance the reaction yield and selective permeation through a membrane, *Coronas and co-workers* have comprehensively investigate this integration in such hybrid process (Coronas et al. 1999). In that work, the authors presented the main developments on the inert and catalytic ceramic membrane (ICM and CtCM) for membrane reactor process (MRP).

Nowadays, the functional integration (catalyst-membrane) presents a promising and innovative solution in environment remediation. Hence, a great success having been proven particularly in the control of water pollution (Bassyouni et al., 2019; Buruga et al., 2019; Fard et al., 2018; Kumar et al., 2017; Lu and Ballauff 2016; Nasir et al., 2019; Poupart et al., 2017). Unfortunately, there is few researches works related to the use of both catalysts and porous ceramic membranes (PCMs) for simultaneously water purification.

In this work, the attention has been focused on the feasibility of using SSMR as a hybrid system for continuous catalysis-separation process by using ceramic membrane and nanosized powdered catalyst. *Figure 11* depicts the diagrammatical representation of the experimental setup according to the side-stream mode.

This device mainly consisted of a reaction tank, a ceramic membrane module, feeding and permeate collecting system as well as pressure and temperature control systems. The reaction tank was made of stainless steel with a working volume of 2 L, which was equipped with an internal thermocouple and an external heater for temperature control. The ceramic membrane placed into a membrane module and sealed with stainless steel and connected to the permeation outlet valve. Working pressure in the both extremities of the membrane (feed and retentate sides) was monitored by equipped the system with an air compressor and pressure gauges.

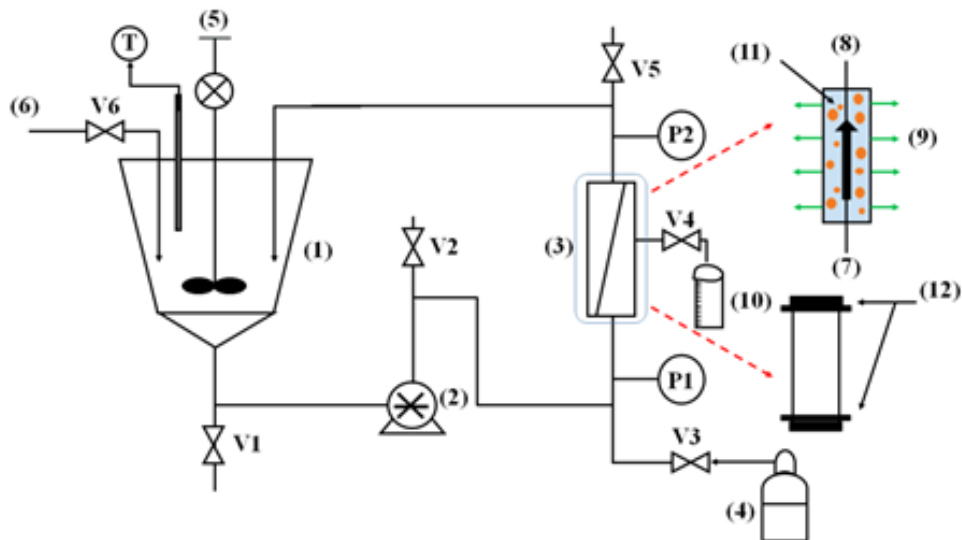


Figure 11. Schematic diagram of catalysis/separation system in SSMR (1) Reaction tank (2L), (2) Feed pump, (3) Membrane module, (4) Air compressor, (5) mechanical stirrer, (6) Feeding system, (7) Feed entry, (8) Retentate, (9) Permeate, (10) Permeate collecting system, (11) Catalysts, (12) Membrane sealing "Steel", P1–P2: Pressure gauges, V1–V6: Valves and T: Temperature indicator and controller.

The effluent solution and suspended catalysts from the feed tank were violently stirred then, driven into the ceramic membrane using a circulation pump. In this hybrid experimental process, catalysis takes place initially in the feed tank. Subsequently, equal pressure, at both extremities of the membrane, was applied in the attempt to remove pollutants through continuously separation and catalysis reaction and push out permeation (Zhong et al., 2007).

Thereby, as shown in *Figure 12*, when applied SSMR for wastewater treatment, the membrane side brought directly into contact with the initial effluent introduced by feed tank is the “*feed side*”. However, the side from where the treated feed penetrates through membrane structure then collected is referred the “*permeate side*” (outer side/surface of membrane). Otherwise, in the cross-flow filtration, the opposite of feed side, from where the concentrate feed return to the reaction tank is the “*retentate side*”.

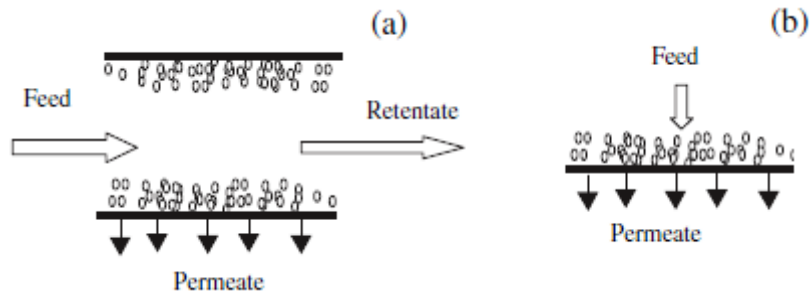


Figure 12. Schematic diagram of membrane sides for (a) tubular configuration: cross-flow filtration and (b) planar configuration: dead-end filtration.

To make membranes suitable for more demanding variety of applications, the different classes of membrane filtration can be integrated. In general, microfiltration (MF), ultrafiltration (UF), nanofiltration (NF) and reverse osmosis (RO) are largely used for emerging contaminations removal from water (*Figure 13*).

Many large-aspects give rise to the applicable membrane filtration class that determine the contaminant type that can be retained (Schäfer et al., 2011; Simmons et al., 2011). Very often, the aspect that received attention involves the membranes features such as pore size, surface charge and hydrophobicity (Rodriguez-Narvaez et al., 2017). Moreover, to increase the transport rate of permeate and inhibit a possible fouling behaviors, a pre-treatment process can be undertaken. In that case, MF is widely used because it can be taking place at low pressure (Lu and Liu 2010). In addition, a pre-treatment by MF leads to remove suspended solids (SS) and high molecular weight solutes. Then, an accurate measurement of emerging contaminants in water will be easily considered (Rodriguez-Narvaez et al., 2017).

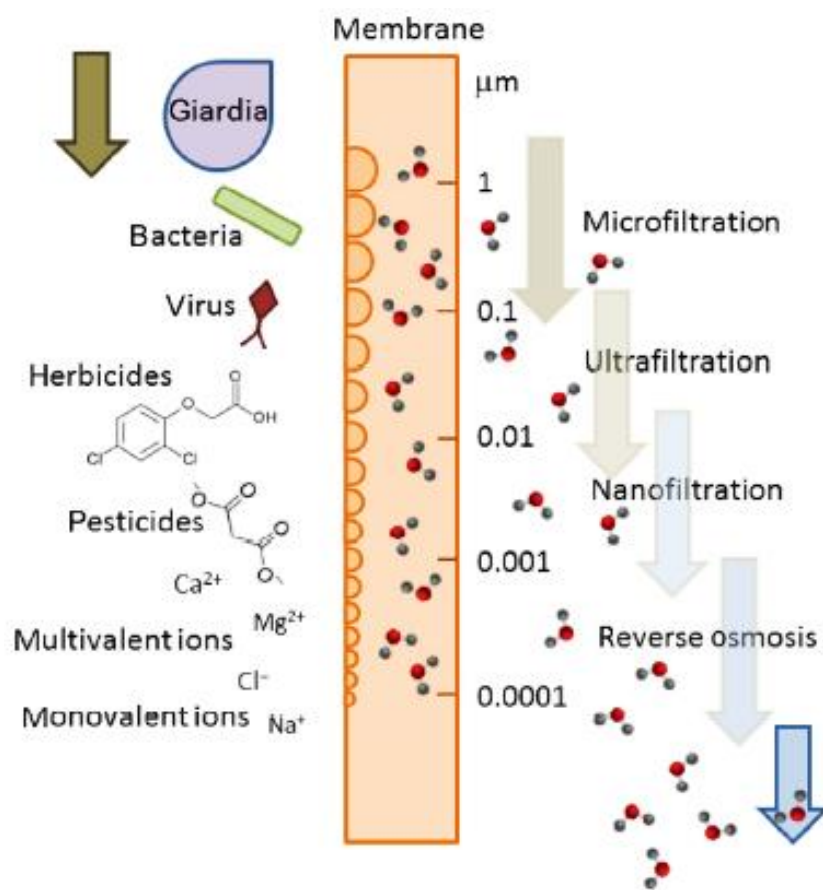


Figure 13. Membrane filtration processes displaying and representative water contaminants removed according to pore size range (From Meng et al., 2015).

Likewise than for the membrane, nanocatalysts is of especial importance in the development of stable and efficient operations of membrane reactor. As long as the nanocatalyst exhibit a long-term stability and high catalytic activity, a significant progress can be achieved for water purification in the membrane reactor. For that, *Zhang and coworkers* have investigated the leaching properties of the catalyst with a durability tests during the organic pollutants removal from water in MR by continuous catalysis-separation (Zhang et al., 2011). Hence, one of the main functions of the membrane may also be the retention of the heterogeneous catalysts from the residual reaction mixture. This concept may be realized either by immobilizing the catalyst on the membrane surface or by a membrane filtration for the suspended heterogeneous catalyst (Westermann and Melin 2009). Consequently, the synergistic effect between reaction and separation have been well manifested which prove the significant benefit of using heterogeneous catalysis in CMR.

7. Applications in water pollution removal

Use of membrane reactors concept for polluted water purification can typically be applied for hydrogenation (Chen et al., 2016; Liu et al., 2017; Liu et al., 2018; Liu et al., 2020) or oxidation processes (Ahmad et al., 2017; Alpatova et al., 2013; He et al., 2018; Kang et al., 2019; Luo et al., 2018; Pedrosa et al., 2019; Trinh and Samhaber 2016; Wang et al., 2018; Zhao 2013; Zhang et al., 2011; Zhang et al., 2016; Zhu 2013). Thereby, coupling of membrane technology with various catalytic reactions have proven promising results in view of the progress in the development of ultrafine and nanosized hybrid catalysts.

In the present work, the applications of hydrogenation processes are taken as main reaction model to investigate catalysis enhanced-filtration in continuous system. In order to discuss the significant effectiveness of the hybrid process, hydrogenation reaction in membrane reactor like catalytic reduction of nitrate existing in water (Aran et al., 2011 and 2012; Reif and Dittmeyer 2003) and organic water pollutants such as nitroarenes (Xu et al., 2019; Dotzauer et al., 2006) and dyes (Jia et al., 2014) has been reviewed here.

Generally, it is difficult to specify the exact contribution of catalyst and membrane in the resulting coupling process. Alternatively, the aim behind this concept is to attain full conversion of the pollutant and to avoid its slippage out through the membrane. Therefore, the effectiveness is measured by the evaluation of the analysis on the quality of the treated water and then total coupling capacity will be considered.

In most of the existing studies that made use of this concept, 4NP reduction to 4AP over immobilized hybrid catalyst with presence of NaBH_4 as reducing agent has been adopted like model reaction, as depicted in *Figure 14*.

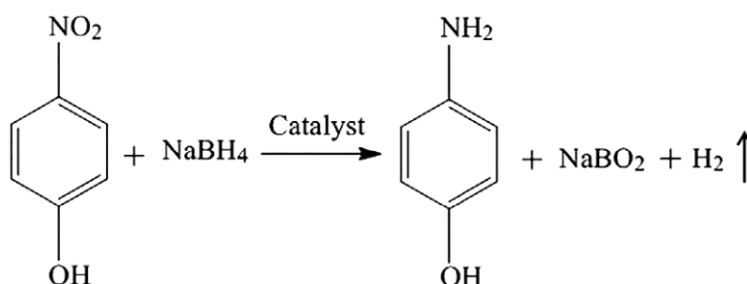


Figure 14. Reduction of 4-nitrophenol to 4-aminophenol, in presence of NaBH_4 , over MNP-based catalyst immobilized on CM (From Liu et al., 2017).

Zhong et al. (2007) and Chen et al. (2009b) studied the hydrogenation of 4NP to 4AP over nickel nanocatalyst, in membrane reactor coupling heterogeneous nanocatalysis with membrane UF and MF respectively. Note that in the submerged configuration a conversion rate less than 100% of 4NP was occurred Chen et al. (2009b). Trapped 4NP molecules by membrane was the origin of this incomplete conversion. While, a totally reduction reaction of 4NP was achieved in side-stream membrane reactor Zhong et al. (2007). On the other hand, the hydrogenation rate suffers 48% decline throughout four continuous catalysis-separation cycles. This may be due to the mass loss of catalysts during membrane separation.

Few years later, *Zhong and co-workers* designed tubular ceramic membrane for nanosized nickel catalysts separation from suspension in hydrogenation reaction of 4NP to 4AP. Experimental results have revealed totally retention (100%) of nickel catalysts and preserving of catalytic performance with almost the same hydrogenation rate. However, water flux has been found to be dramatically decreased and filtration resistance of around $R_t=20\%$, originated from Ni particles aggregation, was obtained (Zhong et al., 2011).

However, it has been demonstrated that is majorly difficult to simultaneously control of the catalytic performances, loss of nanosized catalyst and membrane fouling arises from the membrane pores blocking by the adhesion of the too fine catalysts particles (Zhang et al., 2018; Jiang et al., 2013). To overcome this problematic limitation, supported metal nanoparticles onto membrane surfaces or into membrane pores was strongly suggested as promising approach for solving the abovementioned drawbacks as shown in **Figure 15** (Chen et al., 2011 and 2013; Dotzauer et al., 2006 and 2009; Du and Chen 2015; Jiang et al., 2014; Li et al., 2013; Liu et al., 2017; Ouyang et al., 2010; Peng et al., 2016; Xu and Bhattacharyya 2008).

To fabricate ceramic membrane catalysts, *Peng and co-workers* adopted the flow-through method by impregnation of uncoated (CM) and ZnO nano-coated (ZnO-CM) membrane in $\text{Pd}(\text{OAc})_2$ precursor solution (**Figure 15a**). Then, Pd NPs were deposited into membrane pores under 600 °C calcination temperature (Peng et al., 2016). For comparison, they evaluated the catalytic activities of both fabricated Pd/CM and Pd/ZnO–CM membranes catalysts with the 4NP reducing reaction test. However, after a treatment time of 60 min, similar 4NP conversion rates of only 60% and 65 were reached and considerable decreases of 35% and 20% in catalytic properties were also observed respectively for Pd/CM and Pd/ZnO–CM.

Many investigations have demonstrated that membrane catalysts based MNPs immobilization on chemically modified CM may exhibit better catalytic properties and enhanced catalyst

stabilities. In this context, supported Pd NPs on polydopamine (PDA) functionalized tubular alumina membranes (*Figure 15b*) was tested for 4NP reducing reaction in membrane reactor setup (Liu et al., 2017). Hydrogenation reactions were carried out on both Pd-loaded unmodified membrane (Pd/CM) and Pd-loaded PDA modified membrane (Pd/PDA-CM). According to the experimental results, a conversion rate of 100% was achieved for Pd/PDA-CM after 30min, whereas only about 87% of 4NP conversion reaction occurred when using Pd/-CM after a twice-longer treatment period. On the other hand, both Pd/CM and Pd/DAP-CM exhibit a modest catalytic stability despite the obviously different in favor of Pd-loaded PDA functionalized CM. Otherwise, *Chen and co-workers* propose Pd-loaded APTES-modified membrane (Pd-CMS) for catalytic hydrogenation reaction in membrane reactor. Meanwhile, Pd-loaded unmodified membrane (Pd-CM) was also tested on 4NP reduction (Chen et al., 2011).

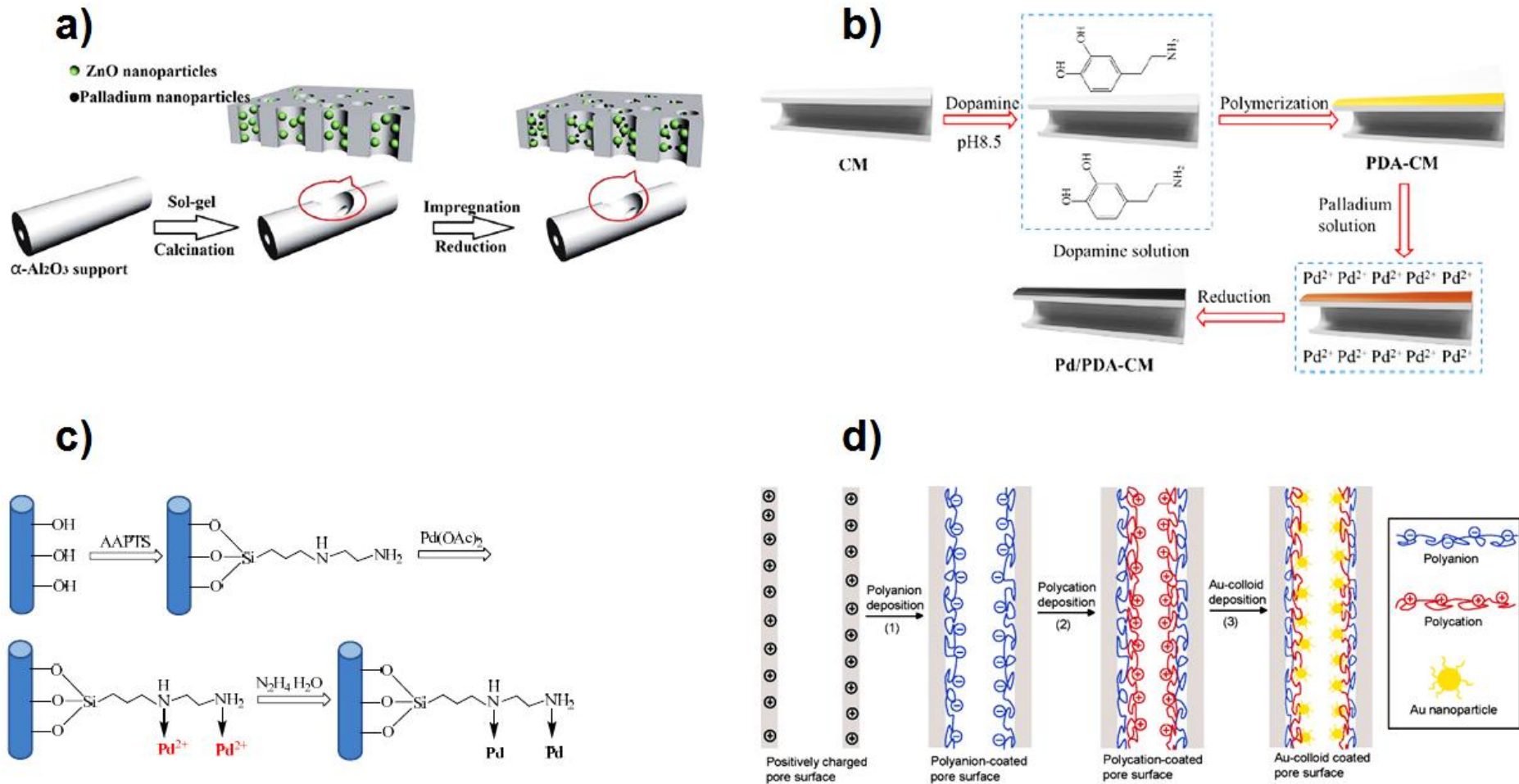


Figure 15. Schematic illustration of the different procedures for preparing MNPs-loaded ceramic membranes (a) into the membrane pores using nano-coating modification of ZnO and Pd nanoparticles or supported onto the membrane surface using (a) silane grafting, (b) polymer coating and (c) adsorption of polyelectrolytes (From Dotzauer et al., 2006; Jiang et al., 2014; Liu et al., 2017; Peng et al., 2016).

For comparison, the APTES indicate a beneficial effect on the enhancement of loading metal particles on the membrane surface and then on the catalytic stability of Pd NPs despite the deactivation trends at long-term. Besides, *the research group* proposed in another research paper a flow-through method to design catalytic membrane with improved loading amount of Pd NPs. The synthesis solution has been forced to flow through the membrane (Li et al., 2013). Thus, Pd NPs are deposited not only on the membrane surface, but also in the membrane pores. They found that AAPTSS-silane grafted surface (**Figure 15c**) assisted with flow-through method provide a superior 4NP conversion and better catalytic stability compared with the traditional impregnation method (Li et al., 2013).

Nevertheless, *Chen and co-workers* have recommended hollow fiber tubular ceramic membrane (HFTCM) as beneficiary for higher Pd catalyst loading and easily diffusion of molecules onto the catalyst surface (Chen et al., 2013). Inspired from the experimental results, authors suggested that Pd-loaded HFTCM support provide higher catalytic activity than Pd-loaded TCM due to its higher surface area at the same volume of membrane module. Unfortunately, they mentioned that the HFCM was not satisfying as a robust support for Pd NPs immobilization. Therefore, to improve catalytic stability authors suggested the optimization of the preparation conditions and the operation mode of the membrane reactor.

Dotzauer and co-workers proposed new bilayer polymer modified alumina membrane for Au-loaded alumina membrane elaboration (Dotzauer et al., 2006). The layer-by-layer deposition of polyacrylic acid (PAA) and polyallyl amine (PAH) was used to immobilize Au NPs to alumina membrane (**Figure 15d**). In order to evaluate the catalytic power of Au-loaded alumina membrane, 4NP reducing reaction in a continuous membrane filtration was examined. The experimental results shows that nearly 100% conversion rate has been achieved by the resulting Au-loaded membranes at permeate flux of 0.3 mL/(cm²s). Furthermore, constant reduction rate of >99% has been maintained during the compilation of five sequential permeate volume (PV) of 500 mL. Moreover, the high gold loading made it difficult to determine rate constants for PAA/PAH/Au modified ceramic membranes. However, since higher flux are occurred the conversion rate declines from 100% to 92% at 0.2 and 0.55 mL/cm²s respectively. Subsequently, reduction reaction becomes more difficult to be performed at further flux enhancement (Dotzauer et al., 2006).

Although ceramic membranes provide an attractive support for catalytic NPs immobilization applied to organic pollution degradation in water. It is well known that TCM cannot compete powder matrix in terms of the surface area to volume ratio (Zhang et al., 2018). However, powdered nanocomposite catalyst based on hybrid polymer matrix immobilized MNPs may

be the subject of an alternative catalyst. Importantly, suggested powdered nanocomposite polymer-MNPs catalysts were supported in order to improve catalytic processing in ceramic membrane reactor. In particular, such hybrid catalysts, in comparison with almost of their powdered counterparts, provide the catalytic performance enhancement, membrane fouling inhibition, the long-term stability and avoid catalyst deactivation/loss by mass transfer through membrane pores.

As it is obviously known, TCM are intensely reported as an effective technology applied for the WWT (Aloulou et al., 2017; Barredo-Damas et al., 2012; Hubadillah et al., 2017; Khemakhem et al., 2015; Ma et al., 2017). *The research group of Ben Amar* have largely exploited low-cost TCM based on abandoned natural inorganic materials for successful textile WWT (Aloulou et al., 2018; Ellouze et al., 2012; Hammami et al., 2017; Jedidi et al., 2009 and 2011; Khemakhem et al., 2015).

To date, the dyeing processes are, in particular, rated as the most polluting among the industrial activities (Koyuncu and Topacik 2003). It is susceptible to generate dirty raw effluent. Usually, the untreated wastewater is high turbid and characterized by a heavy color and high conductivity as well as substantial load of organic matter, heavy metals and high salt (mainly NaCl and Na₂SO₄) and COD content. In addition, these effluents often are of harsh alkaline pH (9–12) as well as bad smell nature (Allègre et al., 2006; Sostarturk et al., 2005). Particularly, some dye groups, mainly azo dyes and their by-products, have been mentioned as carcinogenic and/or mutagenic (Capar et al., 2006). In order to solve these problems, membrane technology (single or combined MF, UF, NF, RO) has been widely recommended as the most efficient way in the textile effluents treatment for water reclamation (Barredo-Damas et al., 2012). Thus, a possible water recycling was also mentioned (Allègre et al., 2006; Tahri et al., 2012). In relation to the membrane separation assess, *Hammami and co-workers* have coupled single channel TCM with powder activated carbon (PAC) in a hybrid PAC/UF process for real textile effluent treatment (Hammami et al., 2017). They found that such combination led to a total retention of toxic acid orange 7 (AO7). Thus, water remediation was considerably enhanced and the highest permeate fluxes was occurred by applying hybrid treatment. Moreover, the experimental results show a removal efficiency of 97% for color, 70% for COD and 30% for conductivity after 180 min of processing time. *Tomaszewska and Mozia* and *Adham and co-workers* explained the significant performances by the synergetic effect between membrane retention and PAC. They concluded that the PAC/UF system would play an excellent role in pollution removal yield as well as minimizing the flux decline (Adham et al., 1991; Tomaszewska and Mozia 2002). *Hammami et co-*

workers mentioned that a stabilized permeate flux (near to water permeability) was occurred at 3 bar due to the limitation of UF membrane fouling by adding PAC. By operating of hybrid treatment, the permeate flux is almost stable (from 460 L/h.m² to 400 L/h.m²) whereas a dramatic flux decline from 520 L/h.m² to 90 L/h.m² was observed when used classic UF. They have highlighted that further porous layer on the membrane surface can be occurred and acting as dynamic membrane for additional reactive AO7 dye and substances retention and membrane fouling deactivation (Hammami et al., 2017).

As discussed previously, it is well known that such properties are very interesting for some applications in the industrial scale to obtain highest performance. In order to achieve this goal, it is always necessary to use integrated membrane process synergistically coupling membrane separation and heterogeneous catalysis, that is to say MR. This is to improve the reduction rate efficiency of organic matters and reserve membrane separation for the removal of the remaining inorganic matters (suspended solids, microorganism, and salts) that can not be removed by simple catalytic reduction reaction.

To resume, coupling TCM and polymer-based nanocomposite catalyst, with enhanced structural, morphologic and physic-chemicals properties, in a single MR device presents the most interesting hybrid process for polluted water treatment. The CM with a tubular configuration, a porous morphology, a selective separation layers, lower fabrication cost, an appropriate thickness and controlled hydrophobicity constitute an excellent candidate for industrial membrane separation process. However, hybrid nano-sized catalyst based on immobilized MNPs over polymer mixing graphene, clay, MOs and monolith as a robust support with higher specific surface area and strong catalytic activity may benefit the better interest in heterogeneous catalysis. A much higher contact surface area and appropriate permeation, antifouling characters and active surface as well as long-term materials stability, a higher catalyst loading and catalytic power are preferable conditions for better synergistically treatment. Importantly, all these beneficial characteristics as well as the operations conditions (like pressure, temperature, additive and flow velocity) make successful of several industrial applications in the water remediation in side-stream catalytic ceramic membrane reactor.

8. Success key factors of the Process

8.1. Fouling control and membrane regeneration

Permeability constitutes the one of the most important parameters in membrane filtration. The permeate flux may be affected by membrane fouling during pollutants interception by

membranes. Then, flux decline occurred as retained species accumulate over time. Therefore, reduces fouling and maintain membrane performances are the major concerns in the last decencies in order to avoid as much as possible the operating costs increase and shortening of the membrane lifetime (Alvarado et al., 2016).

Coupling the membranes with catalysts may exhibit an antifouling capacity of the membrane. Chen et al. (2015) shown that the coating of commercial tubular ceramic α -Al₂O₃-membranes by Ti–Mn catalyst enhance fouling inhibition. On the other hand, potential catalyst loss or attrition are still challenges faced now for nanocatalyst incorporated in ceramic membranes. According to Liu et al. (2017), the leaching and agglomeration of NPs still represents the mainly limitation of recovered NPs-impregnated CM. In that research work, authors concludued that Pd-loaded CM may especially suffer from the catalytic activity deactivation. Based on the literature discussion, hybrid membranes, such as nanocomposite ceramic, exhibit a long-time stability. In addition, chemical modified ceramic membrane could control especially by monitoring hydrophobicity pore size and surface charge. Then, fouling-resistant properties are highly reported (Kujawa et al., 2014). Chemical modification of ceramic membrane promotes flux stability, this what was justified by *Kujawa and co-workers* (Kujawa et al., 2014). Indeed, marginal decrease of 21% and 32% in permeate flux of grafted titania ceramic membranes was observed, successively, after 1.5 and 4 years of use. *Faibish and Cohen* have justified that irreversible permeability loss did not occur with the modification of membrane by polyvinyl pyrrolidone (PVP). Compared with the uncoated membrane, PVP-modified zirconia membrane promotes irreversible fouling prohibition during UF treatment of oily wastewater (Faibish and Cohen 2001).

Usually, membrane fouling is scarcely to be fully prevented during the different membrane filtration processes. Thus, periodical cleaning is highly requested. So far, there is no standardized cleaning approach. Hence, various approaches have been operated (Alvarado et al., 2016; Gan et al. 1999; Zhang et al., 2016). For better fouling removal, many operations follows chemical cleaning in the cases of 10% decrease in normalized permeate flux is occurred (Brunetti et al., 2018). However, partial recovery of lost permeation is every now and then someway tolerated (Rautenbach and Melin 2004). On the other hand, *Brunetti and co-workers* suggested that improved module design and operation through more effective hydrodynamics are considered as mitigation approaches to reduce fouling (Brunetti et al., 2018).

Hybrid nanocomposite catalysts loaded into MRs are an important strategy that is increasingly becoming a valuable alternative to minimize or eliminate fouling. Such concept promotes

controlling the fluid dynamics of the feed and permeate streams contrast to the conventional membrane separation processes.

8.2. Catalyst retention and properties recovery

Usually, the membrane interacts as a selective barrier for the separation process in the MR system. Thereby, the concept of coupling MF and UF with catalysis reaction was used also for enhancing the reaction conversion as well as to retain the heterogeneous catalyst (Brunetti et al., 2018). For the retention of dispersed catalyst from residual reaction mixture in catalytic membrane reactor with flow-through mode, *Westermann and Melin* suggested NF process as a reasonable alternative of immobilization concept of a catalyst (Westermann and Melin 2009). In addition, intercept tests on the MF to ultrafine nickel catalyst were performed by Zhong et al. (2011) after used for catalytic hydrogenation of 4-nitrophenol to 4-aminophenol in the membrane reactor. In such research work, the researchers studied the ability of 100% recovery of the catalysts (30nm-8 μ m) by using 800nm pore size ceramic membrane. Similarly, Jiang et al. (2013) found that nanosized particles of hybrid TS-1 catalysts were completely retained inside the reactor by a porous 0.2, 0.5, and 0.8 μ m pore size α -Al₂O₃ membrane. The retained catalysts are rinsed, dried and then recycled back to the reactor and reused for the next batch of reaction. Zhong et al. (2011) proven a similar catalytic activity of fresh Ni catalyst compared to a recovered one after used for 4NP reduction in MR system. In addition, authors demonstrated no evident change in the used catalyst characteristics. Therefore, authors finished by concluded that cross-flow filtration have not pejorative effect on the performance and high stability of the catalysts. Thus, long-time stability of recovering catalysts is considered as attractive feature of the membrane reactor to make the reaction process continuous.

Unfortunately, a major difficulty of used inorganic nanosized catalyst has been arisen by the adhesion of catalyst nanoparticles on the membrane surface during filtration process. Experimental researches have demonstrated a quick decline in the conversion rate of 4NP and membrane flux in the coupled nanocatalysis/UF system the catalysts due to the adhesion problem of nickel particles onto the membrane surface (Zhong et al., 2007). This suggests that Ni nanoparticles increase the filtration resistance (Zhong et al., 2011). To decrease the adhesion and avoid cake layer formation, *Zhong and co-workers* suggested increasing cross-flow velocity and the addition of microsized particles during membrane surface modification (Zhong et al., 2007). Jiang et al. (2011) proposed the feasibility of continuous catalytic reaction as efficient way to leveled off membrane resistance.

Several researcheswork suggest the use of the nanocomposite catalyst-based polymer supported MNPs for reduction reactions of hazardous organics molecules such as nitro-aromatic compounds and dyes (Amari et al., 2017 and 2019; Dong et al., 2015; Wang et al., 2015). *Haider and co-workers* noted that same Cu/CS-CMM strip of hybrid nanocomposite Cu catalyst may be used for several consecutive catalytic reaction of 2-nitrophenol (2NP) and 4-nitrophenol as well as an organic cresyl blue (CB) dye with effectively conserving of catalytic activity (Haider et al., 2016). As a new kind of catalyst, strongly chelated AuNPs onto thiazole-grafted triazinebased ligands for catalytic reduction tests of 4NP and nitro-containing pesticide has been recently proposed (Amari et al., 2017). It should be noted here that *Amari and co-workers* have consolidate the assumption which exclude MNPs leaching. Moreover, to verify the above assumption, recorded characterizations on the hybrid Au-modified PS-AT catalyst by using SEM coupled energy dispersive X-ray were demonstrate an homogenous distribution of AuNPs on PS matrix. Besides, the authors proposed such nanocomposite polystyrene/Au as potential catalyst for extended applications (e.g. catalytic oxidation).

Consequently, polymer supported nanocatalyst is well known as an efficient way for maintaining continuous reaction and overcome the particles adhesion limitation. So far, the facile synthesis route, the long-term stability and the perfect performances of the robust hybrid nanocomposite catalyst based on polymer immobilized MNPs allows, along side to the further advantages to the PCM, to the membrane reactor as an eco-friendly, cost-effective and highly efficient technology.

9. Conclusion

Ceramic membranes separation and heterogeneous catalysis are gaining more and more attention in assisted filtration processes. Membrane reactors are able to combine various advantages by avoiding membrane fouling, improving separation selectivity and the catalytic reaction yield. Several investigations have demonstrated that ceramic membrane based membrane reactors show great potential in a wide range of laboratory scale and industrial applications. This is was due to the possible catalytic reactions and separations under harsh conditions.

The aim of this chapter was to review current research, mostly, on the side-stream reactor configuration based on the porous ceramic membrane separation and heterogeneous catalytic reduction for polluted water remediation. This work mainly focused on the innovative developments of the membrane reactor from the perspective of materials (membrane and

catalyst) design and optimization. Membrane reactor do not only integrate membrane operations simply into one unit but also intensify the process by operating in a synergistic fashion. Currently, various membrane reactor types, configurations and applications may be involved in the coupled membrane separation and heterogeneous catalysis. The membrane reactor performance towards water remediation is depending on three main factors. Firstly, on their configurations (bestly the side-stream categories) and the processing conditions on term on pressure, flow velocity and the effluents pre-treatment if necessary. Moreover, membrane properties are very interesting in such coupling system.

This reviewed study evidences that hybrid catalysis-separation in ceramic catalytic membrane reactor represent a very promising technology of great research and industrial interest. Clearly, the investigation will provide guidance for the water and raw wastewater remediation by continuous catalytic separation in ceramic membrane reactor on account of its outstanding performance.

References

A

- Adham, S.S., Snoeyink, V.L., Clark, M.M., Bersillon, J.L., 1991. Predicting and verifying organics removal by PAC in an ultrafiltration system. *Journal / American Water Works Association*. 83, 81-91. doi:10.1002/j.1551-8833.1991.tb07269.x.
- Ahmad, R., Aslam, M., Park, E., Chang, S., Kwon, D., Kim, J., 2018. Submerged low-cost pyrophyllite ceramic membrane filtration combined with GAC as fluidized particles for industrial wastewater treatment. *Chemosphere*. 206, 784–792. doi:10.1016/j.chemosphere.2018.05.045.
- Ahmad, R., Guo, J., Kim, J., 2019. Structural characteristics of hazardous organic dyes and relationship between membrane fouling and organic removal efficiency in fluidized ceramic membrane reactor. *Journal of Cleaner Production*. 232, 608-616.
- Ahmad, R., Kim, J. K., Kim, J.H., Kim, J., 2017. Well-organized, mesoporous nanocrystalline TiO₂ on alumina membranes with hierarchical architecture: Antifouling and photocatalytic activities. *Catalysis Today*. 282, 2–12. doi:10.1016/j.cattod.2016.03.051.
- Alem, A., Sarpoolaky, H., Keshmiri, M., 2009. Sol–gel preparation of titania multilayer membrane for photocatalytic applications. *Ceramics International*. 35, 1837–1843.
- Allègre, C., Moulin, P., Maisseu, M., Charbit, F., 2006. Treatment and reuse of reactive dyeing effluents. *Journal of Membrane Science*. 269, 15–34. doi:10.1016/j.memsci.2005.06.014.
- Aloulou, H., Bouhamed, H., Ghorbel, A., Ben Amar, R., Khemakhem, S., 2017. Elaboration and characterization of ceramic microfiltration membranes from natural zeolite: application to the treatment of cuttlefish effluents. *Desalination and Water Treatment*. 95, 9–17. doi: 10.5004/dwt.2017.21348.
- Aloulou, W., Hamza, W., Aloulou, H., Oun, A., Khemakhem, S., Jada, A., Chakraborty, S., Curcio, S., Ben Amar, R., 2018. Developing of titania-smectite nanocomposites UF membrane over zeolite based ceramic support. *Applied Clay Science*, 155, 20–29. doi:10.1016/j.clay.2017.12.035.
- Alpatova, A.L., Davies, S.H., Masten, S.J., 2013. Hybrid ozonation-ceramic membrane filtration of surface waters: The effect of water characteristics on permeate flux and the removal of DBP precursors, dicloxacillin and ceftazidime. *Separation and Purification Technology*. 107, 179–186. doi:10.1016/j.seppur.2013.01.013.

- Alvarado, C., Farris, K., Kilduff, J., 2016. Membrane fouling, modelling and recent developments for mitigation (pp. 433–462). In Hankins, N.P., Singh, R., (Eds.), *Emerging Membrane Technology for Sustainable Water Treatment*. 480. Amsterdam: Elsevier B.V.
- Amari, H., Guerrouache, M., Mahouche-Chergui, S., Abderrahim, R., Carbonnier, B., 2017. 2-Aminothiazole-functionalized triazine-modified polystyrene decorated with gold nanoparticles as composite catalyst for the reduction of 4-nitrophenol. *Reactive and Functional Polymers*. 121, 58–66. doi:10.1016/j.reactfunctpolym.2017.10.018.
- Amari, H., Guerrouache, M., Mahouche-Chergui, S., Abderrahim, R., Carbonnier, B., 2019. In situ synthesis of silver nanoparticles on densely amine-functionalized polystyrene: Highly active nanocomposite catalyst for the reduction of methylene blue. *Polymers for Advanced Technologies*. 30, 320–328. doi:10.1002/pat.4468.
- Aran, H.C., Chinthaginjala, J.K., Groote, R., Roelofs, T., Lefferts, L., Wessling, M., Lammertink, R.G.H., 2011. Porous ceramic mesoreactors: A new approach for gas–liquid contacting in multiphase microreaction technology. *Chemical Engineering Journal*. 169, 239–246. doi:10.1016/j.cej.2010.11.005.
- Aran, H.C., Klooster, H., Jani, J.M., Wessling, M., Lefferts, L., Lammertink, R.G.H., 2012. Influence of geometrical and operational parameters on the performance of porous catalytic membrane reactors. *Chemical Engineering Journal*. 207–208, 814–821. doi:10.1016/j.cej.2012.07.080.

B

- Barredo-Damas, S., Alcaina-Miranda, M.I., Iborra-Clar, M.I., Mendoza-Roca, J.A., M.I., 2012. Application of tubular ceramic ultrafiltration membranes for the treatment of integrated textile wastewaters. *Chemical Engineering Journal*. 192, 211–218. doi:10.1016/j.cej.2012.03.079.
- Bassouini, M., Abdel-Aziz, M.H., Zoromba, M.Sh., Abdel-Hamid, S.M.S., Drioli, E., 2019. A review of polymeric nanocomposite membranes for water purification. *Journal of Industrial and Engineering Chemistry*. 73, 19–46. doi.org/10.1016/j.jiec.2019.01.045.
- Bhattacharya, P., Mukherjee, D., Deb, N., Swarnakar, S., Banerjee, S., 2020. Application of green synthesized ZnO nanoparticle coated ceramic ultrafiltration membrane for remediation of pharmaceutical components from synthetic water: reusability assay of treated water on seed germination. *Journal of Environmental Chemical Engineering*. 8, 103803.

- Bottino, A., Capannelli, G., Comite, A., Di Felice, R., 2002. Polymeric and ceramic membranes in three-phase catalytic membrane reactors for the hydrogenation of methylenecyclohexane. *Desalination*. 144, 411-416.
- Bouazizi, A., Breida, M., Karim, A., Achiou, B., Ouammou, M., Calvo, J.I., Aaddane, A., Khiata, K., Younssi, S.A., 2017. Development of a new TiO₂ ultrafiltration membrane on flat ceramic support made from natural bentonite and micronized phosphate and applied for dye removal. *Ceramics International*. 43, 1479–1487.
- Bouzerara, F., Boulanacer, S., Harabi, A., 2015. Shaping of microfiltration (MF) ZrO₂ membranes using a centrifugal casting method. *Ceramics International*. 41, 5159–5163.
- Brunetti, A., Zito, P.F., Giorno, L., Drioli, E., Barbieri, G., 2018. Membrane reactors for low temperature applications: An overview. *Chemical Engineering and Processing - Process Intensification*. 124, 282–307. doi:10.1016/j.cep.2017.05.002.
- Buruga, K., Song, H., Shang, J., Bolan, N., Kalathi, J.T., Kim, K-H., 2019. A review on functional polymer-clay based nanocomposite membranes for treatment of water. *Journal of Hazardous Materials*. 379, 120584. doi.org/10.1016/j.jhazmat.2019.04.067.

C

- Capar, G., Yetis, U., Yilmaz, L., 2006. Membrane based strategies for the pre-treatment of acid dye bath wastewaters. *Journal of Hazardous Materials*. 135, 423–430. doi:10.1016/j.jhazmat.2005.12.008.
- Cassano, A., & Basile, A., 2013. Integrating different membrane operations and combining membranes with conventional separation techniques in industrial processes. In Basile, A., (Ed.), *Handbook of Membrane Reactors* (Vol. 2, pp. 296-343). 968. USA: Woodhead Publishing.
- Champagnie, A.M., Tsotsis, T.T., Minet, R.G., Wagner, E., 1992. The study of ethane dehydrogenation in a catalytic membrane reactor. *J. Catal.* 134, 7-13.
- Chanaud, P., Julbe, A., Larbot, A., Guizard, C., Cot, L., Mirodatos, C., Giroir-Fendler, A., Borges, H., 1995. Catalytic membrane reactor for oxidative coupling of methane. Part 1: preparation and characterisation of LaOCl membranes. *Catal Today*. 25, 225–230.
- Chang, S., Ahmad, R., Kwon, D., Kim, J., 2019. Hybrid ceramic membrane reactor combined with fluidized adsorbents and scouring agents for hazardous metal-plating wastewater treatment. *Journal of Hazardous Materials*. 388, 121777. doi:10.1016/j.jhazmat.2019.121777.

- Chen, R., Du, Y., Wang, Q., Xing, W., Jin, W., Xu, N., 2009b. Effect of Catalyst Morphology on the Performance of Submerged Nanocatalysis/Membrane Filtration System. *Industrial & Engineering Chemistry Research*. 48, 6600–6607. doi:10.1021/ie900033m.
- Chen, R., Jiang, H., Jin, W., Xu, N., 2009a. Model Study on a Submerged Catalysis/Membrane Filtration System for Phenol Hydroxylation Catalyzed by TS-1. *Chinese Journal of Chemical Engineering*. 17, 648-653.
- Chen, R., Jiang, Y., Xing, W., Jin, W., 2011. Fabrication and Catalytic Properties of Palladium Nanoparticles Deposited on a Silanized Asymmetric Ceramic Support. *Industrial & Engineering Chemistry Research*. 50, 4405–4411. doi:10.1021/ie1022578.
- Chen, R., Jiang, Y., Xing, W., Jin, W., 2013. Preparation of Palladium Nanoparticles Deposited on a Silanized Hollow Fiber Ceramic Membrane Support and Their Catalytic Properties. *Industrial & Engineering Chemistry Research*. 52, 5002–5008. doi:10.1021/ie303104m.
- Chen, S., Yu, J., Wang, H., Yu, H., Quan, X., 2015. A pilot-scale coupling catalytic ozonation–membrane filtration system for recirculating aquaculture wastewater treatment. *Desalination*. 363, 37–43. doi:10.1016/j.desal.2014.09.006.
- Chen, X., Wang, Z., Bi, S., Li, K., Du, R., Wu, C., Chen, L., 2016. Combining catalysis and separation on a PVDF/Ag composite membrane allows timely separation of products during reaction process. *Chemical Engineering Journal*. 295, 518–529. doi:10.1016/j.cej.2016.03.043.
- Chi, Y., Chong, J.Y., Wang, B., Li, K., 2020. Pristine graphene membranes supported on ceramic hollow fibre prepared via a sacrificial layer assisted CVD approach. *Journal of Membrane Science*. 595, 117479.
- Choudhury, P.R., Majumdar, S., Sahoo, G.C., Saha, S., Mondal, P., 2018. High pressure ultrafiltration CuO/hydroxyethyl cellulose composite ceramic membrane for separation of Cr (VI) and Pb (II) from contaminated water. *Chemical Engineering Journal*. 336, 570-578.
- Choudhury, P.R., Majumdar, S., Sarkar, S., Kundu, B., Sahoo, G.C., 2019. Performance investigation of Pb(II) removal by synthesized hydroxyapatite based ceramic ultrafiltration membrane: Bench scale study. *Chemical Engineering Journal*. 355, 510-519.
- Cini, P., Harold, P.H., 1991. Experimental study of the tubular multiphase catalyst. *American Institute of Chemical Engineers Journal*. 37, 997.

Coronas, J., Santamaria, J., 1999. Catalytic reactors based on porous membrane. *Catalysis Today*. 51, 377- 389.

Cot, L., Ayral, A., Durand, J., Guizard, C., Hovnanian, N., Julbe, A., Larbot, A., 2000. Inorganic membranes and solid state sciences. *Solid State Sci.* 2, 313–334.

D

Dalmon, J.A., 1997. Catalytic membrane reactors (Chapter 9.3). In Ertl, G., Knözinger, H., Weitkamp, J., (Eds.), *Handbook of Heterogeneous Catalysis*, Weinheim :VCH Publishers.

Dalmon, J.A., Cruz-Lopez, A., Farrusseng, D., Guilhaume, N., Iojoiu, E., Jalibert, J.C., Miachon, S., Mirodatos, C., Pantazidis, A., Rebeilleau-Dassonneville, M., Schuurman, Y., Van Veen, A.C., 2007. Oxidation in catalytic membrane reactors. *Applied Catalysis A: General*. 325, 198–204.

Das, C., Bose, S., 2017. *Advanced Ceramic Membranes and Applications*, p. 250, New York: CRC Press NY, USA.

Das, R., Ghosh, S., Bhattacharjee, C., 2012. Enzyme membrane reactor in isolation of antioxidative peptides from oil industry waste: A comparison with non-peptidic antioxidants. *LWT - Food Science and Technology*. 47, 238–245.

Da Silva, B. A., de Souza Godim de Oliveira, V., Di Luccio, M., Hotza, D., Rezwan, K., Wilhelm, M., 2020. Characterization of functionalized zirconia membranes manufactured by aqueous tape casting. *Ceramics International*. doi:10.1016/j.ceramint.2020.03.162.

De Haart, L.G.J., Lin, Y.S., de Vries, K.J., Burggraaf, A.J., 1991. Modified CVD of nanoscale structures in and EVD of thin layers on porous ceramic membranes. *Journal of the European Ceramic Society*. 8, 59-70.

Dittmeyer, R., Caro, J., 2008. Catalytic Membrane Reactors. In Ertl, G., Knoezinger, H., Schueth, F., Weitkamp, J., (Eds.), *Handbook of Heterogeneous Catalysis*, 3865. Weinheim, Germany: Wiley-VCH. doi.10.1002/9783527610044.hetcat0117.

Dong, X.L., Jin, W.Q., Xu, N.P., Li, K., 2011. Dense ceramic catalytic membranes and membrane reactors for energy and environmental applications. *Chem. Commun.* 47, 10886-10902.

Dong, Z., Le, X., Dong, C., Zhang, W., Li, X., Ma, J., 2015. Ni@Pd core–shell nanoparticles modified fibrous silica nanospheres as highly efficient and recoverable catalyst for

- reduction of 4-nitrophenol and hydrodechlorination of 4-chlorophenol. *Applied Catalysis B: Environmental*. 162, 372–380. doi:10.1016/j.apcatb.2014.07.009.
- Dotzauer, D.M., Abusaloua, A., Miachon, S., Dalmon, J.A., Bruening, M.L., 2009. Wet air oxidation with tubular ceramic membranes modified with polyelectrolyte/Pt nanoparticle films. *Applied Catalysis B: Environmental*. 91, 180–188. doi:10.1016/j.apcatb.2009.05.022.
- Dotzauer, D.M., Dai, J., Sun, L., Bruening, M.L., 2006. Catalytic Membranes Prepared Using Layer-by-Layer Adsorption of Polyelectrolyte/Metal Nanoparticle Films in Porous Supports. *Nano Letters*. 6, 2268–2272. doi:10.1021/nl061700q.
- Du, Y., & Chen, R., 2015. Fabrication of palladium nanoparticles immobilized on an amine-functionalized ceramic membrane support using a nanoparticulate colloidal impregnation method with enhanced catalytic properties. *Korean Journal of Chemical Engineering*. 32, 1759–1765. doi:10.1007/s11814-015-0030-1.
- Dumée, L.F., Maina, J.W., Merenda, A., Reis, R., He, L., Kong, L., 2017. Hybrid thin film nano-composite membrane reactors for simultaneous separation and degradation of pesticides. *Journal of Membrane Science*. 528, 217–224. doi:10.1016/j.memsci.2017.01.041.

E

- Ebrahimi, M., Willershausen, D., Ashaghi, K.S., Engel, L., Placido, L., Mund, P., Bolduan, P., Czermak, P., 2010. Investigations on the use of different ceramic membranes for efficient oil-field produced water treatment. *Desalination*. 250, 991–996.
- Ellouze, E., Tahri, N., Ben Amar, R., 2012. Enhancement of textile wastewater treatment process using Nanofiltration. *Desalination*. 286, 16–23. doi:10.1016/j.desal.2011.09.025.
- Ertl, G., Knözinger, H., Schüth, F., Weitkamp, J., 2008. *Handbook of heterogeneous catalysis*. 3865, Weinheim, Germany: Wiley-VCH Verlag GmbH & Co. KGaA.

F

- Faibish, R.S., & Cohen, Y., 2001. Fouling and rejection behavior of ceramic and polymer-modified ceramic membranes for ultrafiltration of oil-in-water emulsions and microemulsions. *Colloids and Surfaces A: Physicochemical and Engineering Aspects*. 191(1-2), 27–40. doi:10.1016/s0927-7757(01)00761-0.

Fard, A.K., McKay, G., Buekenhoudt, A., Al-Sulaiti, H., Motmans, F., Khraisheh, M., Atieh, M., 2018. Inorganic Membranes: Preparation and Application for Water Treatment and Desalination. *Materials*. 11, 74-120.

Farrusseng, D., Julbe, A., Lopez, M., Guizard, C., 2000. Investigation of sol–gel methods for the synthesis of VPO membrane materials adapted to the partial oxidation of n-butane. *Catal Today*. 56, 211–220.

G

Gaber, A.A.A., Ibrahim, D.M., Abd-Elmohsen, F.F., El-Zanati, E.M., 2013. Synthesis of alumina, titania, and alumina-titania hydrophobic membranes via sol–gel polymeric route. *Journal of Analytical Science and Technology*. 4, 18.

Gan, Q., Howell, J.A., Field, R.W., England, R., Bird, M.R., McKechnie, M.T., 1999. Synergetic cleaning procedure for a ceramic membrane fouled by beer microfiltration. *Journal of Membrane Science*. 155, 277-289. doi:10.1016/s0376-7388(98)00320-2.

Glazneva, T., Rebrov, E., Schouten, J., Paukshtis, E., Ismagilov, Z.R., 2007. Synthesis and characterization of mesoporous silica thin films as a catalyst support on a titanium substrate, *Thin Solid Films*. 515, 6391–6394.

Gu, Q., Ng, T.C.A., Zain, I., Liu, X., Zhang, L., Zhang, Z., Lyu, Z., He, Z., Ng, H.Y., Wang, J., Wang, J., 2019. Chemical-grafting of Graphene Oxide Quantum Dots (GOQDs) onto Ceramic Microfiltration Membranes for Enhanced Water Permeability and Anti-organic Fouling Potential. *Applied Surface Science*. 144128. doi:10.1016/j.apsusc.2019.144128.

Guesmi, Y., Lafi, R., Agougui, H., Jabli, M., Oun, A., Majumdar, S., Hafiane, A., 2020. Synthesis and characterization of alpha alumina-natural apatite based porous ceramic support for filtration application. *Materials Chemistry and Physics*. 239, 122067. doi.org/10.1016/j.matchemphys.2019.122067.

H

Haas-Santo, K., Fichtner, M., Schubert, K., 2001. Preparation of microstructure compatible porous supports by sol-gel synthesis for catalyst coatings. *Applied Catalysis A: General*. 220, 79–92.

Hai, F.I., Nghiem, L.D., Modin, O., 2013. Biocatalytic membrane reactors for the removal of recalcitrant and emerging pollutants from wastewater. In Basile, A., (Eds.), *Handbook of Membrane Reactors*, (Vol. 2, pp. 763–807). 968. USA: Woodhead Publishing.

- Haider, S., Kamal, T., Khan, S.B., Omer, M., Haider, A., Khan, F. U., Asiri, A.M., 2016. Natural polymers supported copper nanoparticles for pollutants degradation. *Applied Surface Science*. 387, 1154–1161. doi:10.1016/j.apsusc.2016.06.133.
- Hammami, A., Charcosset, C., Ben Amar, R., 2017. Performances of Continuous Adsorption-Ultrafiltration Hybrid Process for AO7 Dye Removal from Aqueous Solution and Real Textile Wastewater Treatment. *Journal of Membrane Science & Technology*. 07. doi:10.4172/2155-9589.1000171.
- Han, H.H., Ryu, S.H., Nakao S-I., Lee, Y.T., 2013. Gas permeation properties and preparation of porous ceramic membrane by CVD method using siloxane compounds. *Journal of Membrane Science*. 431, 72-78.
- Harold, M.P., Cini, P., Patenaude, B., 1989. The catalytically impregnated ceramic tube: an alternative multiphase reactor. *AIChE Symp. Ser.* 268, 26.
- He, Z., Xia, D., Huang, Y., Tan, X., He, C., Hu, L., He, H., Zeng, J., Xu, W., Shu, D., 2018. 3D MnO₂ hollow microspheres ozone-catalysis coupled with flat-plate membrane filtration for continuous removal of organic pollutants: Efficient heterogeneous catalytic system and membrane fouling control. *Journal of Hazardous Materials*. 344, 1198-1208. Doi:10.1016/j.jhazmat.2017.11.024.
- Hosseinabadi, S.R., Wyns, K., Buekenhoudt, A., Van der Bruggen, B., Ormerod, D., 2015. Performance of Grignard functionalized ceramic nanofiltration membranes. *Separation and Purification Technology*. 147, 320–328.
- Hsieh, H.P., 1996. *Inorganic membranes for separation and reaction*. 1st edition, 590. Amsterdam. Elsevier Science.
- Hubadillah, S.K., Othman, M.H.D., Harun, Z., Ismail, A.F., Rahman, M. A., Jaafar, J., Jamil, S.M., Mohtor, N.H., 2017. Superhydrophilic, low cost kaolin-based hollow fibre membranes for efficient oily-wastewater separation. *Materials Letters*. 191, 119–122. doi:10.1016/j.matlet.2016.12.099.

I

- Ida, J-I., Matsuyama, T., Yamamoto, H., 2000. Surface corona discharge-induced plasma chemical process-chemical vapor deposition (SPCP-CVD) as a novel method for surface modification of ceramic membranes. *Advanced Powder Technology*. 11, 343-351.

J

- Jedidi, I., Khemakhem, S., Saïdi, S., Larbot, A., Elloumi-Ammar, N., Fourati, A., Charfi, A., Ben Salah, A., Ben Amar, R., 2011. Preparation of a new ceramic microfiltration membrane from mineral coal fly ash: Application to the treatment of the textile dyeing effluents. *Powder Technology*. 208, 427–432. doi:10.1016/j.powtec.2010.08.039.
- Jedidi, I., Saïdi, S., Khemakhem, S., Larbot, A., Elloumi-Ammar, N., Fourati, A., Charfi, A., Ben Salah, A., Ben Amar, R., 2009. Elaboration of new ceramic microfiltration membranes from mineral coal fly ash applied to waste water treatment. *Journal of Hazardous Materials*. 172, 152–158. doi:10.1016/j.jhazmat.2009.06.151.
- Jia, Z., Sun, H., Du, Z., Lei, Z., 2014. Catalytic bubble-free hydrogenation reduction of azo dye by porous membranes loaded with palladium nanoparticles. *Journal of Environmental Sciences*. 26, 478–482. doi:10.1016/s1001-0742(13)60416-7.
- Jiang, H., Meng, L., Chen, R., Jin, W., Xing, W., Xu, N., 2011. A Novel Dual-Membrane Reactor for Continuous Heterogeneous Oxidation Catalysis. *Industrial & Engineering Chemistry Research*. 50, 10458–10464. doi:10.1021/ie200398g.
- Jiang, H., Meng, L., Chen, R., Jin, W., Xing, W., Xu, N., 2013. Progress on Porous Ceramic Membrane Reactors for Heterogeneous Catalysis over Ultrafine and Nano-sized Catalysts. *Chinese Journal of Chemical Engineering*. 21, 205-215. doi: 10.1016/S1004-9541(13)60460-7.
- Jiang H., Sun, X., Du, Y., Chen, R., Xing, W., 2014. Catalytic activity of palladium nanoparticles immobilized on an amino-functionalized ceramic membrane support. *Chinese Journal of Catalysis*. 35, 1990–1996. Doi: 10.1016/S1872-2067(14)60190-x.
- Julbe, A., Farrusseng, D., Guizard, C., 2001. Porous ceramic membranes for catalytic reactors-overview and new ideas. *Journal of Membrane Science*. 181, 3–20.

K

- Kang, J., Zhang, H., Duan, X., Sun, H., Tan, X., Liu, S., Wang, S., 2019. Magnetic Ni-Co alloy encapsulated N-doped carbon nanotubes for catalytic membrane degradation of emerging contaminants. *Chemical Engineering Journal*. doi:10.1016/j.cej.2019.01.035.
- Kemmere, M.F., Keurentjes, J.T.F., 2001. Industrial Membrane Reactors. In Nunes, S.P., & Peinemann, K.V., (Eds.), *Membrane Technology in the Chemical Industry*, 295. Weinheim: Wiley-VCH.

- Khemakhem, M., Khemakhem, S., Ayedi, S., Cretin, M., Ben Amar, R., 2015. Development of an asymmetric ultrafiltration membrane based on phosphates industry sub-products. *Ceramics International*. 41, 10343–10348. doi:10.1016/j.ceramint.2015.05.101.
- Kim, J., Vander Bruggen, B., 2010. The use of nanoparticles in polymeric and ceramic membranes structures: Review of manufacturing procedures and performance improvement for water treatment. *Environmental Pollution*. 158, 2335-2349.
- Koros, W.J., Ma, Y.H., Shimidzu, T., 1996. Terminology for membrane and membrane process (IUPAC recommendation from 1996). *Journal of Membrane Science*. 120, 149-159. <http://www.che.utexas.edu/nams/IUPAC/iupac.html>.
- Koyuncu, I., & Topacik, D., 2003. Effects of operating conditions on the salt rejection of nanofiltration membranes in reactive dye/salt mixtures. *Separation and Purification Technology*. 33, 283–294. doi:10.1016/s1383-5866(03)00088-1.
- Kujawa, J., Cerneaux, S., Koter, S., Kujawski, W., 2014. Highly Efficient Hydrophobic Titania Ceramic Membranes for Water Desalination. *ACS Applied Materials & Interfaces*. 6, 14223–14230. doi:10.1021/am5035297.
- Kujawa, J., Cerneaux, S., Kujawski, W., 2015. Highly hydrophobic ceramic membranes applied to the removal of volatile organic compounds in pervaporation. *Chemical Engineering Journal*. 260, 43–54.
- Kujawa, J., Kujawski, W., Cerneaux, S., Li, G., Al-Gharabli, S., 2020. Zirconium dioxide membranes decorated by silanes based-modifiers for membrane distillation – Material chemistry approach. *Journal of Membrane Science*. 596, 117597.
- Kumar, S., Mandal, A., Guria, C., 2016. Synthesis, characterization and performance studies of polysulfone and polysulfone/polymer-grafted bentonite based ultrafiltration membranes for the efficient separation of oil field oily wastewater. *Process Safety and Environmental Protection*. 102, 214–228.
- Kumar, V., Kim, K.-H., Park, J.-W., Hong, J., Kumar, S., 2017. Graphene and its nanocomposites as a platform for environmental applications. *Chemical Engineering Journal*. 315, 210–232. doi:10.1016/j.cej.2017.01.008.

L

- Lan, Y., Barthe, L., Antonin, A., Causserand, C., 2020. Feasibility of a heterogeneous Fenton membrane reactor containing a Fe-ZSM5 catalyst for pharmaceuticals degradation: Membrane fouling control and long-term stability. *Separation and Purification Technology*. 231, 115920-115929.

- Li, F., Yangb, Y., Fana, Y., Xinga, W., Wang, Y., 2012. Modification of ceramic membranes for pore structure tailoring: The atomic layer deposition route. *Journal of Membrane Science*. 397– 398, 17– 23.
- Li, H., Jiang, H., Chen, R., Wang, Y., Xing, W., 2013. Enhanced Catalytic Properties of Palladium Nanoparticles Deposited on a Silanized Ceramic Membrane Support with a Flow-Through Method. *Industrial & Engineering Chemistry Research*. 52, 14099–14106. doi:10.1021/ie401903v.
- Li, K., 2007. *Ceramic Membranes for Separation and Reaction*, 316, Chichester: John Wiley & Sons Ltd.
- Liu, H., Zhang, J., Lu, M., Liang, L., Zhang, H., Wei, J., 2020. Biosynthesis Based Membrane Filtration Coupled with Iron Nanoparticles Reduction Process in Removal of Dyes. *Chemical Engineering Journal*. 387, 124202. doi:10.1016/j.cej.2020.124202.
- Liu, M., Zhu, X., Chen, R., Liao, Q., Ye, D., Zhang, B., Liu, J., Chen, G., Wang, K., 2018. Tube-in-tube hollow fiber catalytic membrane microreactor for the hydrogenation of nitrobenzene. *Chemical Engineering Journal*. 354, 35–41. doi:10.1016/j.cej.2018.07.203.
- Liu, Y., Peng, M., Jiang, H., Xing, W., Wang, Y., Chen, R., 2017. Fabrication of ceramic membrane supported palladium catalyst and its catalytic performance in liquid-phase hydrogenation reaction. *Chemical Engineering Journal*. 313, 1556–1566. doi.org/10.1016/j.cej.2016.11.037.
- Lu, C.J., Chen, R.Z., Xing, W.H., Jin, W.Q., Xu, N.P., 2008. A submerged membrane reactor for continuous phenol hydroxylation over TS-1. *American Institute of Chemical EngineersJournal*. 54, 1842-1849.
- Lu, N.C., Liu, J.C., 2010. Removal of phosphate and fluoride from wastewater by a hybrid precipitation–microfiltration process. *Separation and Purification Technology*. 74, 329–335. doi:10.1016/j.seppur.2010.06.023.
- Lu, Y., Ballauff, M., 2016. Spherical polyelectrolyte brushes as nanoreactors for the generation of metallic and oxidic nanoparticles: Synthesis and application in catalysis. *Progress in Polymer Science*. 59, 86–104. doi:10.1016/j.progpolymsci.2016.03.002.
- Luo, X., Liang, H., Qu, F., Ding, A., Cheng, X., Tang, C. Y., Li, G., 2018. Free-standing hierarchical α -MnO₂@CuO membrane for catalytic filtration degradation of organic pollutants. *Chemosphere*. 200, 237–247. doi:10.1016/j.chemosphere.2018.02.113.

Lv, Y., Liu, H., Wang, Z., Liu, S., Hao, L., Sang, Y., Liu, D., Wang, J., Boughton, R.I., 2009. Silver nanoparticle-decorated porous ceramic composite for water treatment. *Journal of Membrane Science*. 331, 50–56. doi:10.1016/j.memsci.2009.01.007.

M

Ma, X., Chen, P., Zhou, M., Zhong, Z., Zhang, F., Xing, W., 2017. Tight ultrafiltration ceramic membrane for separation of dyes and mixed salts (both NaCl/Na₂SO₄) in textile wastewater treatment. *Industrial & Engineering Chemistry Research*. 56, 7070–7079. doi:10.1021/acs.iecr.7b01440.

Meng, L., Guo, H., Dong, Z., Jiang, H., Xing, W., Jin, W., 2013. Ceramic hollow fiber membrane distributor for heterogeneous catalysis: Effects of membrane structure and operating conditions. *Chemical Engineering Journal*. 223, 356–363. doi:10.1016/j.cej.2013.03.049.

Meng, S., Greenlee, L. F., Shen, Y. R., & Wang, E., 2015. Basic science of water: Challenges and current status towards a molecular picture. *Nano Research*. 8, 3085–3110. doi:10.1007/s12274-015-0822-y.

Menne, D., Üzümc, C., Koppelman, A., Wong, J.E., Foeken, C., Borre, F., Dähne, L., Laakso, T., Pihlajamäki, A., Wessling, M., 2016. Regenerable polymer/ceramic hybrid nanofiltration membrane based on polyelectrolyte assembly by layer-by-layer technique. *Journal of Membrane Science*. 520, 924–932.

Miao, J., Lu, J., Jiang, H., Liu, Y., Xing, W., Ke, X., Chen, R., 2019. Continuous and complete conversion of high concentration p-nitrophenol in a flow-through membrane reactor. *American Institute of Chemical Engineers Journal*. 65, e16692.

Mittal, P., Jana, S., Mohanty, K., 2011. Synthesis of low-cost hydrophilic ceramic–polymeric composite membrane for treatment of oily wastewater. *Desalination*. 282, 54–62.

Molinari, R., Palmisano, L., Loddo, V., Mozia, S., Morawski, A.W., 2013. Photocatalytic membrane reactors: configurations, performance and applications in water treatment and chemical production. In Basile, A., (Eds.), *Handbook of Membrane Reactors*, (Vol. 2, pp. 808-845). 968. USA: Woodhead Publishing.

Mozia, S., 2010. Photocatalytic membrane reactors (PMRs) in water and wastewater treatment. A review. *Separation and Purification Technology*. 73, 71-91.

Mustafa, G., Wyns, K., Buekenhoudt, A., Meynen, V., 2016. Antifouling grafting of ceramic membranes validated in a variety of challenging wastewaters. *Water Research*. 104, 242–253.

Mustafa, G., Wyns, K., Vandezande, P., Buekenhoudt, A., Meynen, V., 2014. Novel grafting method efficiently decreases irreversible fouling of ceramic nanofiltration membranes. *Journal of Membrane Science*. 470, 369–377.

N

Nasir, A., Masood, F., Yasin, T., Hameed, A., 2019. Progress in polymeric nanocomposite membranes for wastewater treatment: Preparation, properties and applications. *Journal of Industrial and Engineering Chemistry*. 79, 29–40. doi:10.1016/j.jiec.2019.06.052.

Nath, K., Bhakhar, M.S., 2012. Membrane Reactor Concept, Applications, and Prospects. In Mohanty, K., Purkait, M.K., (Eds), *Membrane Technologies and Applications*, 499. London: CRC Press.

O

Osegueda Chicas, O.A., 2013. Development of a novel catalytic membrane reactor: Application in wastewater treatment. Doctoral Thesis, 152p, Tarragona, 2013.

Oun, A., Mahouche-Chergui, S., Khemakhem, M., Carbonnier, B., Ben Amar, R., 2019. Preparation and Surface Modification of Porous Ceramic Membranes for Water Treatment. In Gray, S., Tsuru, T., Cohen, Y., Lau, W-J., (Ed), *Advanced Materials for Membrane Fabrication and Modification*, 600. New York: CRC Press.

Oun, A., Tahri, N., Mahouche-Chergui, S., Carbonnier, B., Majumdar, S., Sarkar, S., Sahoo, G.C., Ben Amar, R., 2017. Tubular ultrafiltration ceramic membrane based on titania nanoparticles immobilized on macroporous clay-alumina support: Elaboration, characterization and application to dye removal. *Separation and Purification Technology*. 188, 126–133.

Ouyang, L., Dotzauer, D.M., Hogg, S.R., Macanás, J., Lahitte, J.-F., Bruening, M.L., 2010. Catalytic hollow fiber membranes prepared using layer-by-layer adsorption of polyelectrolytes and metal nanoparticles. *Catalysis Today*. 156, 100–106. doi:10.1016/j.cattod.2010.02.040.

P

Palo, E., Salladini, A., Morico, B., Palma, V., Ricca A., Iaquaniello, G., 2018. Application of Pd-Based Membrane Reactors: An Industrial Perspective. *Membranes*. 8, 101-115.

Pedrosa, M., Drazic, G., Tavares, P.B., Figueiredo, J.L., Silva, A.M.T., 2019. Metal-free graphene-based catalytic membrane for degradation of organic contaminants by

persulfate activation. *Chemical Engineering Journal*. 369, 223–232. doi:10.1016/j.cej.2019.02.211.

Peng, M., Liu, Y., Jiang, H., Chen, R., Xing, W., 2016. Enhanced catalytic properties of Pd nanoparticles by their deposition on ZnO-coated ceramic membranes. *RSC Advances*. 6, 2087–2095. doi:10.1039/c5ra24150b.

Perez, V., Miachon, S., Dalmon, J-A., Bredesen, R., Pettersen, G., Ræder, H., Simon, C., 2001. Preparation and characterisation of a Pt/ceramic catalytic membrane. *Separation and Purification Technology*. 25, 33–38.

Poupart, R., Le Droumaguet, B., Guerrouache, M., Grande, D., Carbonnier, B., 2017. Gold nanoparticles immobilized on porous monoliths obtained from disulfide-based dimethacrylate: Application to supported catalysis. *Polymer*. 126, 455-462. doi:10.1016/j.polymer.2017.04.034.

R

Raman, N.K., Ward, T.L., Brinker, C.J., Sehgal, R., Smith, D.M., Duan, Z., Hampden-Smith, M., Bailey, J.K., Headle, T.J., 1993. Catalyst dispersion on supported ultramicroporous inorganic membranes using derivatized silylation agents. *Appl. Catal. A*. 96, 65.

Randon, J., Blanc, P., Paterson, R., 1995. Modification of ceramic membrane surfaces using phosphoric acid and alkyl phosphonic acids and its effects on ultrafiltration of BSA protein. *Journal of Membrane Science*. 98, 119–129.

Rautenbach, R., Melin, T., 2004. *Membranverfahren: Grundlagen der Modul- und Anlagenauslegung* - 2nd edition. 555. New York: Springer-Verlag Berlin Heidelberg GmbH. doi:10.1007 / 978-3-662-08653-7.

Reif, M., & Dittmeyer, R., 2003. Porous, catalytically active ceramic membranes for gas–liquid reactions: a comparison between catalytic diffuser and forced through flow concept. *Catalysis Today*. 82, 3–14. doi:10.1016/s0920-5861(03)00197-4.

Rodriguez-Narvaez, O.M., Peralta-Hernandez, J.M., Goonetilleke, A., Bandala, E.R., 2017. Treatment technologies for emerging contaminants in water: A review. *Chemical Engineering Journal*. 323, 361–380. doi:10.1016/j.cej.2017.04.106.

S

Sahoo, G.C., Halder, R., Jedidi, I., Oun, A., Nasri, H., Roychoudhury, P., Majumdar, S., Bandyopadhyay S., Ben Amar R., 2016. Preparation and characterization of microfiltration apatite membrane over low cost clay-alumina support for decolorization

- of dye solution. *Desalination and Water Treatment*. 57, 27700-27709. doi: 10.1080/19443994.2016.1186565.
- Saja, S., Bouazizi, A., Achiou, B., Ouammou, M., Albizane, A., Bennazha, J., Younssi, S.A., 2018. Elaboration and characterization of low-cost ceramic membrane made from natural Moroccan perlite for treatment of industrial wastewater. *Journal of Environmental Chemical Engineering*. 6, 451–458.
- Schäfer, A.I., Akanyeti, I., Semião, A.J.C., 2011. Micropollutant sorption to membrane polymers: a review of mechanisms for estrogens; *Adv. Colloid Interface Sci.* 164, 100–117. doi:10.1016/j.cis.2010.09.006.
- Simmons, F.J., Kuo, D.H.W., Xagorarakis, I., 2011. Removal of human enteric viruses by a full-scale membrane bioreactor during municipal wastewater processing. *Water Res.* 45, 2739–2750. doi:10.1016/j.watres.2011.02.001.
- Song, Z., Fathizadeh, M., Huang, Y., Chu, K.H., Yoon, Y., Wang, L., Xu, W.L., Yu, M., 2016. TiO₂ nanofiltration membranes prepared by molecular layer deposition for water purification. *Journal of Membrane Science*. 510, 72–78.
- Sostarturk, S., Simonic, M., Petrinic, I., 2005. Wastewater treatment after reactive printing. *Dyes and Pigments*. 64, 147–152. doi:10.1016/j.dyepig.2004.04.001.
- Szegner, J., Yeung, K. L., Varma, A., 1997. Effect of catalyst distribution in a membrane reactor: Experiments and model. *American Institute of Chemical Engineers Journal*. 43, 2059–2072.

T

- Tahri, N., Masmoudi, G., Ellouze, E., Jrad, A., Drogui, P., Ben Amar, R., 2012. Coupling microfiltration and nanofiltration processes for the treatment at source of dyeing-containing effluent. *Journal of Cleaner Production*. 33, 226–235. doi:10.1016/j.jclepro.2012.03.025.
- Takagi, R., Larbot, A., Cotb, L., Nakagaki, M., 2000. Effect of Al₂O₃ support on electrical properties of TiO₂/Al₂O₃ membrane formed by sol–gel method. *Journal of Membrane Science*. 177, 33–40.
- Takht Ravanchi, M., Kaghazchi, T., & Kargari, A., 2009. Application of membrane separation processes in petrochemical industry: a review. *Desalination*. 235, 199-244.
- Tan, X., Li, K., 2015. *Inorganic Membrane Reactors: Fundamentals and Applications*. 290. United Kingdom: John Wiley & Sons, Ltd.

- Tanardi, C.R., Nijmeijer, A., Winnubst, L., 2016. Coupled-PDMS grafted mesoporous γ -alumina membranes for solvent nanofiltration. *Separation and Purification Technology*. 169, 223–229.
- Tanimu, A., Jaenicke, S., Alhooshani, K., 2017. Heterogeneous catalysis in continuous flow microreactors: A review of methods and applications. *Chemical Engineering Journal*. 327, 792-821.
- Tereshchenko, G.F., Malygin, A.A., Ermilova, M.M., Orekhova, N.V., Volkov, V.V., Lebedeva, V.I., Petrova, I.V., Tsodikov, M.V., Teplyakov, V.V., Trusov, L.I., Moiseev, I.I., 2009. Nanostructured Catalytic Membrane Reactors of the New Generation. *Catalysis in Industry*. 1, 29–37.
- Tomaszewska, M., & Mozia, S., 2002. Removal of organic matter from water by PAC/UF system. *Water Research*. 36, 4137–4143. doi:10.1016/s0043-1354(02)00122-7.
- Trinh, T-H-T., Samhaber, W.M., 2016. The Coupling of Catalysis with Submerged Ceramic MF Membrane for Hybrid Water Treatment Process. *Chemical Engineering Transactions*. 47, 247-252. Doi: 10.3303/CET1647042.
- Tsotsis, T.T., Champagnie, A.M., Vasileiadis, S.P., Zaika, Z.D., Minet, R.G., 1992. Packed bed catalytic membrane reactors. *Chem. Eng. Sci.* 47, 2903.
- Tsuru, T., Hironaka, D., Yoshioka, T., Asaeda, M., 2001. Titania membranes for liquidphase separation: effect of surface charge on flux. *Separation and Purification Technology*. 25, 307–314.

U

- Uzio, D., Peureux, J., Fendler, A.G., 1993. Platinum/ γ -alumina catalytic membrane: preparation, morphological and catalytic characterization. *Appl. Catal. A*. 96, 83.

W

- Wales, M.D., Joos, L.B., Traylor, W.A., Pfromm, P., Rezac, M., 2016. Composite catalytic tubular membranes for selective hydrogenation in three-phase systems. *Catalysis Today*. 268, 12–18.
- Wang, J., Wu, Z., Li, T., Ye, J., Shen, L., She, Z., Liu, F., 2018. Catalytic PVDF membrane for continuous reduction and separation of p-nitrophenol and methylene blue in emulsified oil solution. *Chemical Engineering Journal*. 334, 579–586. doi:10.1016/j.cej.2017.10.055.

Wang, Q., Wang, J., Wang, D., Turhong, M., Zhang, M., 2015. Recyclable and effective Pd/poly(N-isopropylacrylamide) catalyst for hydrodechlorination of 4-chlorophenol in aqueous solution. *Chemical Engineering Journal*. 280, 158–164. doi:10.1016/j.cej.2015.05.106.

Wang, Y.H., Liu, X.Q., Meng, G.Y., 2008. Preparation and properties of supported 100% titania ceramic membranes. *Materials Research Bulletin*. 43, 1480–1491.

Westermann, T., Melin, T., 2009. Flow-through catalytic membrane reactors—Principles and applications. *Chemical Engineering and Processing: Process Intensification*. 48, 17–28. doi:10.1016/j.cep.2008.07.001.

X

Xu, C., Pan, X., Fang, L., Li, J., Li, F., 2019. Enhanced reduction of organic pollutants by Fe/Cu@Pd ternary metallic nanoparticles under aerobic conditions: Batch and membrane reactor studies. *Chemical Engineering Journal*. 360, 180–189. doi:10.1016/j.cej.2018.11.212.

Xu, J., & Bhattacharyya, D., 2008. Modeling of Fe/Pd Nanoparticle-Based Functionalized Membrane Reactor for PCB Dechlorination at Room Temperature. *The Journal of Physical Chemistry C*. 112, 9133–9144. doi:10.1021/jp7097262.

Y

Yan, Y., Jiang, S., Zhang, H., Zhang, X., 2015. Preparation of novel Fe-ZSM-5 zeolite membrane catalysts for catalytic wet peroxide oxidation of phenol in a membrane reactor. *Chemical Engineering Journal*. 259, 243–251. doi:10.1016/j.cej.2014.08.018.

Z

Zaman, J., Chakma, A., 1994. Inorganic membrane reactors. *Journal of Membrane Science*. 92, 1–28.

Zhang, G., Jin, W., Xu, N., 2018. Design and Fabrication of Ceramic Catalytic Membrane Reactors for Green Chemical Engineering Applications. *Engineering*. 4, 848–860. doi:10.1016/j.eng.2017.05.001.

Zhang, J., Yu, H., Quan, X., Chen, S., Zhang, Y., 2016. Ceramic membrane separation coupled with catalytic ozonation for tertiary treatment of dyestuff wastewater in a pilot-scale study. *Chemical Engineering Journal*. 301, 19–26. Doi: 10.1016/j.cej.2016.04.148.

- Zhang, S., Du, Y., Jiang, H., Liu, Y., Chen, R., 2017. Controlled synthesis of TiO₂ nanorod arrays immobilized on ceramic membranes with enhanced photocatalytic performance. *Ceramics International*. 43, 7261–7270. Doi:10.1016/j.ceramint.2017.03.019.
- Zhang, Y.Y., He, C., Sharma, V.K., Li, X.-Z., Tian, S.H., Xiong, Y., 2011. A new reactor coupling heterogeneous Fenton-like catalytic oxidation with membrane separation for degradation of organic pollutants. *Journal of Chemical Technology & Biotechnology*. 86, 1488–1494. Doi:10.1002/jctb.2656.
- Zhao, H., Li, H., Yu, H., Chang, H., Quan, X., Chen, S., 2013. CNTs–TiO₂/Al₂O₃ composite membrane with a photocatalytic function: Fabrication and energetic performance in water treatment. *Separation and Purification Technology*. 116, 360–365. doi:10.1016/j.seppur.2013.06.007.
- Zhong, Z., Li, W., Xing, W., Xu, N., 2011. Crossflow filtration of nanosized catalysts suspension using ceramic membranes. *Separation and Purification Technology*. 76, 223–230. doi:10.1016/j.seppur.2010.08.005.
- Zhong, Z., Xing, W., Jin, W., Xu, N., 2007. Adhesion of nanosized nickel catalysts in the nanocatalysis/UF system. *American Institute of Chemical Engineers Journal*. 53, 1204–1210. Doi:10.1002/aic.11143.
- Zhu, Y., Chen, S., Quan, X., Zhang, Y., Gao, C., Feng, Y., 2013. Hierarchical porous ceramic membrane with energetic ozonation capability for enhancing water treatment. *Journal of Membrane Science*. 431, 197–204. doi:10.1016/j.memsci.2012.12.048.
- Ziaka, Z.D., Minet, R.G., Tsotsis, T.T., 1993. Propane dehydrogenation in a packed bed membrane reactor. *American Institute of Chemical Engineers Journal*. 39, 526.
- Zou, D., Chen, X., Drioli, E., Ke, X., Qiu, M., Fan, Y., 2020. Facile co-sintering process to fabricate sustainable antifouling silver nanoparticles (AgNPs)-enhanced tight ceramic ultrafiltration membranes for protein separation. *Journal of Membrane Science*. 593, 117402.

Chapter 2

NANOHYBRID MATERIALS FOR CATALYTIC REDUCTION OF DYES AND NITROAROMATIC ENDOCRINE DISRUPTORS

Section 1

Gold nanospheres-decorated nanostructures as a recyclable heterogeneous catalyst for ultrafast conversion of endocrine disruptors

1. Introduction

The ever-growing global industrialization has shaped the past century, and related environmental pollution has become a ubiquitous and crucial issue. Hazardous pollutants generated by industrial activities, are released into the environment and affect our water, land and air (Keith and Telliard 1979). Water is an essential resource for life and thus, one of the most threatened. Aromatic compounds including pesticides, industrial wastes, pharmaceuticals and personal care products are well-known water pollutants that present considerable hazard to living organisms. Azo dyes are mutagenic and are assumed to contribute to increasing incidences of cancer amongst textile workers (de Lima et al., 2007). The relationship between aromatic amines and cancer risks has been established based on epidemiological evidences particularly in the case of exposure to aromatic amines from occupational sources and tobacco smoking in human cancer development (De Roos et al., 2005; Vineis and Pirastu 1997; Woo and Lai 2001). Nitroaromatic compounds are also important recalcitrant contaminants; they are registered on the U.S. Environmental Protection Agency's list of priority pollutants for environmental remediation. Although they are relatively rare in nature, they have an anthropogenic origin as they are produced as intermediates and end products in the industrial manufacturing of dyes, explosives, pesticides, to name but a few. The combination of the electron-withdrawing character of the nitro group and the enhanced stability of the benzene ring, makes nitro-aromatics resistant to both chemical and biological oxidative degradation, and hydrolysis (Trempe et al., 1993). 4-Nitrophenol (4NP) is one of the most common organic pollutants found in industrial and agricultural waste waters. Its reduced counterpart, 4-aminophenol (4AP), is less toxic, and also it is in demand on the market in many industrial fields (Mirafzal and Summer 2000). 4AP is a key intermediate in the industrial synthesis of acetaminophen, and the global acetaminophen market was valued at around USD 801.3 million in 2014 and is expected to reach USD 999.4 million in 2020, growing at a compound annual growth rate of around 3.8% between 2015 and 2020. In terms of volume, the global acetaminophen market stood at above 149.3 kilo tons in 2014.

There is to date a plethora of protocols described in the literature including both research articles (Tafesh and Weiguny 1996) and patents (Benaglia and Bonsignore 2016) related to the reduction of nitro groups. The reactions are typically carried out in presence of catalysts, precious and transition metals (Zhao et al., 2015), metal oxide (Shivhare et al., 2013; Esumi et al., 2004) and alloyed bimetallic NPs have been successfully and widely applied. As it is well-established, in homogeneous processes, catalysts are dissolved in the reaction medium providing that all catalytic sites are available for reaction allowing for high efficiency, activity and selectivity. However, such processes suffer from major drawbacks arising from the difficulty to separate the catalysts from the reaction mixture, contamination of the products and the difficult reusability for consecutive cycle runs. An alternative to address the issue of catalysts separation and recovery relies on the use of heterogeneous catalysts where the catalytic species are supported on an insoluble material enabling efficient process development as well as easy handling, recovery and recycling (Corma and Garcia, 2008). Catalytically active metal NPs finely dispersed over supports such as graphene oxide (Zhang et al., 2016), chitosan-based membrane (Bibi et al., 2016), cellulose fibers (Islam et al., 2016), fibrous silica (Chen et al., 2018), carbon nanofibers (Zhang et al., 2011), titanium dioxide (Corma and Garcia 2008), to name but a few, hold great promise in heterogeneous catalysis for chemical manufacturing, energy harvesting, conversion and storage, and environmental remediation. The robust attachment and fine dispersion of nanocatalysts over the support surface is a key step in order to prevent leaching phenomena and optimize the catalyst's performances.

Herein, we report an efficient and straightforward synthetic route to design novel hybrid nanostructures based on gold nanoparticles-decorated on chelatant-functionalized clay-polymer nanocomposite. Montmorillonite (MMT) clay was successively surface-grafted with 3-(trimethoxysilyl)propyl methacrylate (γ -MAPS) and poly(glycidyl methacrylate) (PGMA) chains. The polymerization was conducted under UV-irradiation to ensure the fast growth of PGMA. The epoxy groups of MMT@PGMA have been readily converted into amino groups using ethylene diamine. Finally, these chelatant nanocomposites have been used as platforms for stabilizing monodisperse gold nanospheres in-situ generated through hydride-assisted reduction of gold ions previously chelated on the amino groups.

The hybrid nanostructures have been characterized after each synthesis step using a combination of complementary methods (TGA, TEM, XRD, FT-IR, XPS) providing information about their chemical composition, structure, and morphology. The effect of the NaBH_4 to HAuCl_4 molar ratio on the size of the AuNPs have been investigated in detail. The

as-prepared hybrid nanostructures served as efficient heterogeneous nanocatalysts for reduction of nitroaromatic endocrine disruptors, namely para-nitrophenol and pendimethalin. Efficient conversion of these compounds as well as stability/recyclability of the as-prepared nanocatalyst related to the high concentration of grafted chelant amino groups on the surface of these nanostructures, demonstrating the great potential of these AuNPs-decorated nanostructures in the selective removal of nitroaromatic harmful pollutants from wastewater. Moreover, immobilization of other metal nanoparticles (e.g. Ag, Pd, Ni, Fe...) could extend the use of these hybrid nanostructures for remediation of various hazardous pollutants in the environment.

2. Experimental section

2.1. Materials

Natural sodium montmorillonite (MMT-Na) was supplied by Southern Clay Products (ion-exchange capacity = 92 mequiv/100g, surface area = 750 m²/g).

The other chemicals used in this work, including (trimethoxysilyl) propyl methacrylate, MAPS), glycidyl methacrylate (GMA), 2,2-dimethoxy-2-phenylacetophenone (DMPA), ethylenediamine (EDA), chloroauric acid (HAuCl₄), sodium borohydride (NaBH₄), 4-nitrophenol (4NP) and pesticide (PDM) were purchased from Sigma–Aldrich Chemical Company, France. Ethanol (EtOH), acetonitrile (ACN), chloroform, and hydrochloric acid (HCl) were used as solvents and were purchased from Alfa-Aesar. All chemical reagents used in this work were of analytical grade and were used without any further purification. A Millipore Milli-Q system was used to generate deionized water (DI water).

2.2. Synthesis of MMT-PGMA nanocomposite

The poly(glycidyl methacrylate) grafted MMT-Na was synthesized using the procedure established in our previous work (Vo et al ., 2019). Briefly, a 2 wt.% of MMT-Na was activated in a solution of chlorohydric acid and after separation by centrifugation and an abundant rinsing with water, the dried activated powder (MMT-OH) was silanized with 3-(trimethoxysilyl)propyl methacrylate (γ -MAPS). The obtained MMT-MAPS was then dispersed with stirring in a mixture containing GMA, DMPA photoinitiator and ACN and then irradiated under UV light at 365 nm. The MMT-PGMA nanocomposite was obtained after 3h of photopolymerization followed by three cycles of centrifugation/rinsing in acetonitrile, ethanol, and chloroform, respectively. Finally, the MMT-PGMA powder was dried at 60°C under vacuum.

2.3. Amine-surface functionalization of MMT-PGMA

Amine-functionalized MMT-PGMA was obtained by mixing 100 mg of MMT-PGMA and 2 mL of EDA in 20 mL of ACN under continuous stirring at 60°C for 6 h. Subsequently, the resulting MMT-PGMA-NH₂ powder was recovered by centrifugation and rinsed with ACN and ethanol and then dried at 60°C under vacuum.

2.4. In-situ generation of gold NPs on MMT-PGMA-NH₂

Immobilized gold nanoparticles were synthesized through reduction of gold ionic precursor (i.e. AuCl₄⁻) chelated on MMT PGMA-NH₃⁺ using sodium borohydride as reducing agent. So, prior to adsorption of gold ions (AuCl₄⁻), the nitrogen atoms of MMT-PGMA-NH₂ were protonated via acid treatment. Typically, 100 mg of MMT-PGMA-NH₂ were dispersed in 20 mL of 0.1 M HCl under continuous stirring at room temperature for 1 h. After recovering by centrifugation and drying under vacuum, the MMT-PGMA-NH₃⁺ was dispersed in 10 mL of 10⁻³ M aqueous HAuCl₄ solution under continuous stirring at room temperature for 5 h. After water washing and vacuum drying, the nanomaterial showed a light pink color indicating the adsorption of gold ions. A control of gold nanoparticles size was obtained by variation of NaBH₄ to HAuCl₄ molar ratios (R₁=100:1, R₂=50:1 and R₃=10:1). For this, an aqueous solution of NaBH₄ was added under stirring to an aqueous dispersion of MMT-PGMA-NH₃⁺-AuCl₄⁻, and the powder color changed again from light pink to dark purple which is an evidence of the formation of gold nanoparticles. The reaction mixture was kept for 30 min under vigorous stirring at room temperature. Afterwards, the as-designed hybrid nanomaterials, abbreviated AuNPs-decorated clay nanostructures, was collected by centrifugation and thoroughly rinsed with DI water and then dried at 60°C under vacuum.

2.5. Characterization

X-ray photoelectron spectroscopy (XPS) analysis was recorded to determine the surface chemical compositions and the structures of the clay-based nanostructures samples using a Thermo Scientific K-Alpha spectrometer equipped with a monochromatic Al-K α X-ray source ($h\nu = 1486$ eV, spot size = 400 μ m, pass energy of surveys = 200 eV and of narrow regions = 50 eV), and magnetic lens enables analysis of small areas with increased sensitivity. The charge compensation was provided by a combination of an electron flood gun with an argon ion gun. The collected spectra were analyzed by using avantage software.

Fourier transform infrared (FTIR) analysis was conducted on a Bruker TENSOR 27 FTIR spectrometer equipped with a diamond attenuated total reflectance (ATR) module. The

measurements were performed in the wavenumber range of 400-4000 cm^{-1} at 4 cm^{-1} resolution. For comparison of the intensity of the different samples, the spectra are normalized with respect to the bands of Si-O-Si at $\sim 1115\text{-}1150 \text{ cm}^{-1}$.

Thermal gravimetric (TGA) measurements were performed in argon flow using a Setaram Setsys Evolution 16 apparatus in the temperature range of 20-800°C with a heating rate of 10°C/min. TGA was applied to evaluate the weight percentage of gold in the heterogeneous nanocatalysts.

Powder X-ray diffraction (XRD) measurements were performed to study the crystalline structure of the designed gold nanoparticles using a Bruker D8 Advance diffractometer using Cu $K\alpha$ source ($\lambda=1.54 \text{ \AA}$) in the 2θ range of 20-80°.

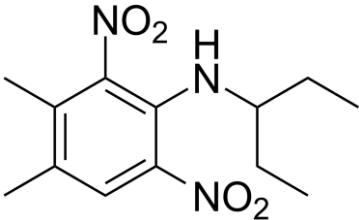
Transmission electron microscopy (TEM) micrographs was used to study the immobilized gold nanoparticles morphology and dispersion on the surface of MMT-PGMA-NH₂ chelant platforms. Before TEM analysis, the samples were first dispersed in ethanol, then small drop of the dispersion was deposited on the carbon coated copper grid of the microscope, finally the solvent was evaporated at room temperature under air. TEM analysis were then carried out on a FEI Tecnai F20 ST microscope, equipped with a Field Emission Gun (FEG), super twin objective lens, and an electron energy loss filter GIF and operating at 200 keV.

UV-Vis absorption spectra were recorded at room temperature on an Agilent Cary 60 UV-Vis spectrophotometer, where the measurements were performed directly in 3 mL quartz cuvettes between 200-800 nm at 25°C. This technique was used to monitor the conversion progress versus time of the nitroaromatic compounds to their corresponding aminoaromatic derivatives.

2.6. Conversion of nitroaromatic derivatives using AuNPs-decorated clay nanostructures as heterogeneous nanocatalysts

To examine catalytic efficiency of the as-prepared AuNPs-decorated clay nanostructures, hydrogenation para-nitrophenol was chosen as model reaction in the presence of excess of NaBH₄ as 4NP is converted to 4AP without the formation of by-products. In addition, the reaction monitoring is very convenient (Chenouf et al., 2019; Xiao et al., 2018). This catalyst was then tested in the conversion of a nitroaromatic herbicide with two nitro groups, namely pendimethalin (PDM), one of the commonly used pesticide. The structures and some chemical properties of these nitroaromatics are given in *Table 3*.

Table 3. Chemical properties of 4-Nitrophenol and Pendimethalin.

Characteristic	4-Nitrophenol	Pendimethalin
Molecular formula	C ₆ H ₅ NO ₃	C ₁₃ H ₁₉ N ₃ O ₄
Chemical name	4-Hydroxynitrobenzène	N-(1-ethylpro-pyl)-2,6-dinitro-3,4-xylydine
Molecular weight (g.mol ⁻¹)	139.10	281.31
λ _{max} (nm)	317	450
pka	7,15	2.8
Use	Drugs, pesticides, and dyes	Pesticides
Chemical structure		
References	ATSDR 1992	Mao et al., 2014

In a typical procedure for the hydrogenation experiments, to 3.3 mL of Milli-Q water placed in a 10 mL glass vial were added under stirring, 100 μL of 4 mM 4NP or pendimethalin solution and 100 μL of 0.05 M aqueous NaBH₄ freshly prepared. Subsequently, 500 μL of an aqueous suspension of AuNPs-decorated clay nanostructures at 2 mg/mL were injected to the above suspension, after a quick mixing, 2 mL of this reaction mixture was put in a 1 cm path length quartz cuvette equipped with a magnetic stirring bar. The reaction evolution was in-situ monitored using Cary 60 UV-vis spectrophotometer in a scanning range of 200 to 800 nm. It is worth to mention that no plasmon band has been observed in this wavelength range, for MMT-supported AuNPs nanocatalyst amount used here. Indeed, the gold NPs are strongly anchored to the rich-amine platforms preventing leaching of gold NPs, which in solution displays strong absorbance band in the visible region in the range of 500 nm and 600 nm.

The kinetic of the hydrogenation reactions was studied by following the evolution of the maximum optical absorption peaks of 4NP at 400 nm and PDM at 450 nm, and this every 30 second. Attention was also focused on the effect of different experimental conditions such as concentration of catalyst and 4NP as-well-as gold nanoparticles size on the rate of the

catalytic reduction of 4NP. Then the optimized conditions were selected to the conversion of PDM. The value of the catalysis apparent rate constant (k_{app}) was calculated from kinetic data following a pseudo-first-order reaction and its assumed to be independent of the concentration of NaBH_4 due to its large excess compared to those of 4NP ($[\text{NaBH}_4] = 12.5 [4\text{NP}]$) (Wunder et al., 2011).

k_{app} value was determined from plot of $\ln(A_t/A_0)$ versus time (t), using the kinetic equation:

$$\ln(A_t/A_0) = k_{app}.t \quad (1)$$

Herein, A_t are the values of absorbance of 4NP at 400 nm and PDM at 450 nm at any time and A_0 are the values of absorbance of 4NP at 400 nm and PDM at 450 nm at 0 min.

2.7. Recovery of MMT-supported AuNPs nanocatalyst

To validate the reusability of the heterogeneous nanocatalyst, we performed seven cycles of 4NP conversion under the optimized conditions using AuNPs-decorated clay nanostructures obtained with R_1 ratio. After each reaction cycle, the nanocatalyst powder was removed from the reaction medium by centrifugation for 10 min, rinsed thoroughly with ethanol and water to remove any adsorbed 4NP and then dried under vacuum at 60°C. Thereby, the recovered nanocatalyst is used for another reaction cycle.

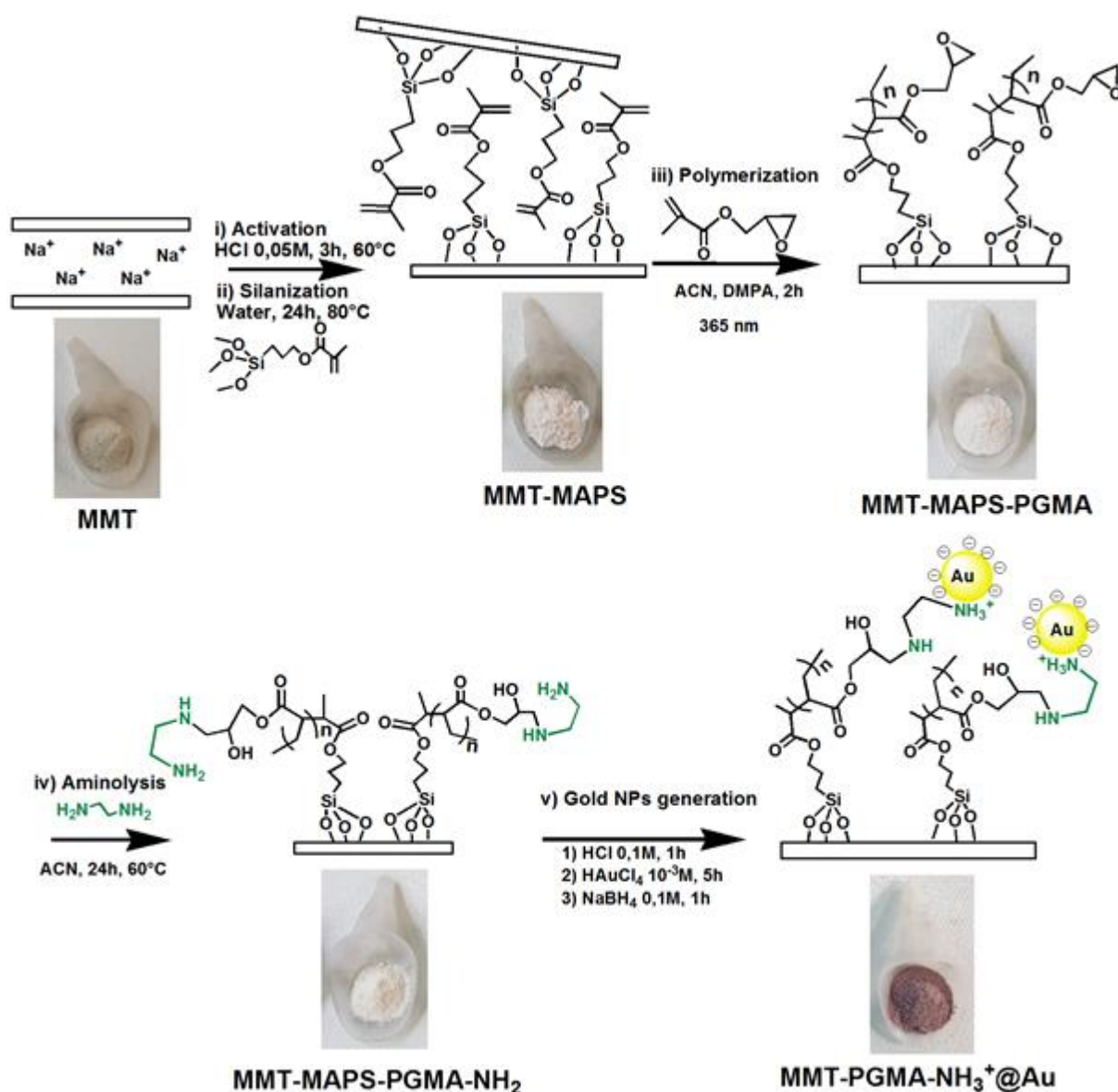
3. Results and discussion

3.1. Characterization of MMT-PGMA-NH₂ chelant platforms

For the present study, robust and reactive poly(glycidyl methacrylate)-montmorillonite clay nanocomposite (MMT-PGMA), previously reported in our earlier published work (Vo et al., 2019) has been selected as reactive nanomaterial for the design of an amine-functionalized platforms (MMT-PGMA-NH₂) as powerful chelant platforms for the stabilization of a high density of size-controlled gold nanoparticles (AuNPs). As well-dispersed supported fine gold particles are widely used as efficient heterogeneous catalysts for several important chemical transformation reactions under relatively mild conditions due to their outstanding activity, the designed hybrid nanomaterials AuNPs-decorated clay nanostructures served as catalysts support for reducing endocrine disruptors (4NP and pendimethalin) in the presence of NaBH_4 . *Scheme 1* depicts the different steps for the synthesis approach used for the preparation of the AuNPs-decorated clay nanostructures with photographs of the various samples.

The MMT clay was firstly acid treated in 0.5 M HCl at 60°C during 3 h in order to activate the clay surface groups ensuring covalent grafting of the internal surface of the layers with organosilane coupling agent (MMT-OH). In addition, this acid activation ensures swelling of

clay, which facilitate the penetration of these organosilane molecules in between the layers. In the absence of acid treatment, the covalent grafting takes place only on the edges of the clay layers leading to a low grafting density. Subsequently, a polymerizable coupling agent (3-(trimethoxysilyl)propyl methacrylate, MAPS) was grafted on the activated internal surface of the clay layers at room temperature using water as solvent. Indeed, it is well known that MAPS molecules bind to the clay surfaces through the formation of Si-O-Si bonds and this via covalent interaction between OH clay surface groups and ethoxy groups of MAPS. Then, exfoliated MMT-PGMA nanocomposite was fabricated by in-situ surface UV-initiated free-radical polymerization of glycidyl methacrylate (GMA) on the MMT-MAPS at 365 nm using 1wt.% DMPA photoinitiator to GMA in the presence of ACN. This polymerization reaction yields high density of pendent epoxide reactive groups on the surface of clay. The resulting MMT-PGMA was then covalently decorated with large amount of amine chelant groups through ring-opening nucleophilic addition of the epoxide groups involving ethylenediamine (MMT-PGMA-NH₂) in ACN solvent, providing suitable platforms for strong anchoring of uniformly dispersed and stable gold nanoparticles onto clay nanostructures. It can be observed from *Scheme 1* an evident color change of the clay-based nanomaterials powders after each synthesis step which may reveal chemical's physical properties have been occurred successfully. The whole synthetic process was confirmed by various characterization techniques as described below.



Scheme 1. Schematic illustration of the step-by-step synthetic procedure of supported gold nanoparticles nanocatalysts and photographs of pristine and functionalized MMT at different synthesis steps.

The chemical attachment of the methacrylate silane coupling agent on the surface of the clay layers was ascertained by IRTF and XPS analyses (*Figure 16*). As shown in *Figure 16a*, the FTIR spectrum of the MMT-MAPS reveals characteristic absorption bands at 2945 and 2890 cm^{-1} attributed to the stretching vibrations of CH_2 in the structure of the MAPS; the peaks at 1726, 1636 cm^{-1} are ascribed to the stretching vibration of $\text{C}=\text{O}$, $\text{C}=\text{C}$ groups, respectively, which exist in the MAPS structure. It clearly demonstrates the grafting of MAPS coupling agent on the clay surface. The presence of MAPS linkers on MMT surface allows for the formation of strong immobilization of PGMA onto MMT. The grafting of poly(glycidyl

methacrylate) on clay was first characterized by IRTF and the comparison to the MMT-MAPS spectrum reveals various differences. As shown in **Figure 16a**, the appearance of new peaks at 904, 845, and 757 cm^{-1} correspond to the stretching vibrations of the epoxide groups (Mahouche Chergui et al., 2010); the disappearance of the characteristic peak at 1634 cm^{-1} assigned to C=C functions together with the strong increase in the intensity of the band at 1726 cm^{-1} due to the stretching vibration of ester carbonyl (C=O) bond, confirm that the binding of poly(glycidyl methacrylate) chains on the MMT is performed successfully. After the reaction between MMT-PGMA and ethylene diamine, it can be obviously seen that all the peaks corresponding to the epoxide reactive groups has been disappeared owing to their complete conversion by nucleophilic addition. Moreover, new peaks were appeared in the IRTF spectrum of MMT-PGMA-NH₂ at 3330, 1630 and 1485 cm^{-1} , originating from N-H/O-H stretching vibrations, O-H and C-N vibrations, respectively. This provides additional evidence of successful grafting of the ethylene diamine chelant agent on the MMT-PGMA nanocomposite. So, these IRTF results reveal a high grafting density of tetheredPGMA to clay layers and hence led to a high content of amine functional groups which show great promise for adsorption of gold ions/gold nanoparticles.

XPS characterization was taken to provide additional detailed information on the surface chemical composition of the MMT samples. The XPS spectra of MMT, MMT-MAPS, MMT-MMT-PGMA, and MMT-PGMA-NH₂ chelant platforms are shown in **Figure 16b**. It can be observed from the survey XPS spectrum that the characteristic signals for Al2p, Si2p, Ca2p, O1s and Na1s of pristine MMT are clearly detected at 75, 103, 352.5, 532 and 1072.5 eV, respectively. Additionally, an unexpected weak peak is detected at 285 eV attributed to C1s, originating from organic contamination of the MMT surface coming from environmental air, which has been observed commonly in previous reports on MMT. The peak of Na1s disappears from the XPS spectrum of the activated MMT (MMT-OH) explained by the removal of sodium cations by acid treatment, which greatly enhance reaction ability of MMT with MAPS coupling agent. The survey spectrum of MMT-MAPS (**Figure 16b**) clearly indicates a significant increase in the relative C1s peaks intensity. Additionally, the high resolution C1s peak (**Figure 16c**) is fitted with four components centered at 284.2, 285, 286.6, 289 eV, corresponding to carbons in C-Si, C-C/C-H, C-O, O-C=O groups, respectively. This proves the successful functionalization of the MMT with MAPS which also supports the findings in the IRTF measurements of the MMT-MAPS. Next, the intensities of C1s and O1s peaks greatly increased after linking of the PGMA chains to the MMT-MAPS. The measured C1s/O1s atomic ratio (C1s/O1s=2.26) of MMT-PGMA; calculated from the

intensity of C1s and O1s peaks, multiplied by sensitivity factors (C1s = 1 and s O1s = 2.75), is very close to the theoretical ratio determined for GMA unit C_7O_3 (C1s/O1s = 2.33), which indicates the presence of a densely tethered PGMA polymer chains at the MMT surface. Moreover, the C1s peak is deconvoluted to three main peaks centered at 285 eV, corresponding to aliphatic backbone of PGMA (C-C and C-H); 286.6 eV, representing carbon atoms of C-O-C and C-O groups, and 289 eV, assigned to carbon atoms in ester groups (O-C=O) of PGMA (*Figure 16d*).

The chemical grafting of ethylene diamine was confirmed by the appearance of a new peak at 400 eV, which is ascribed to the N1s owing to the amino groups of ethylene diamine molecules. Moreover, the presence of an additional component centered at 285.9 eV (C-N bonds) as well as the disappearance of epoxide contribution (C-O-C) at 286.6 eV, and thus broadening of the main of the C1s deconvoluted peak, undoubtedly give a proof for the ring-opening reaction happen with amine functional groups (*Figure 16e*).

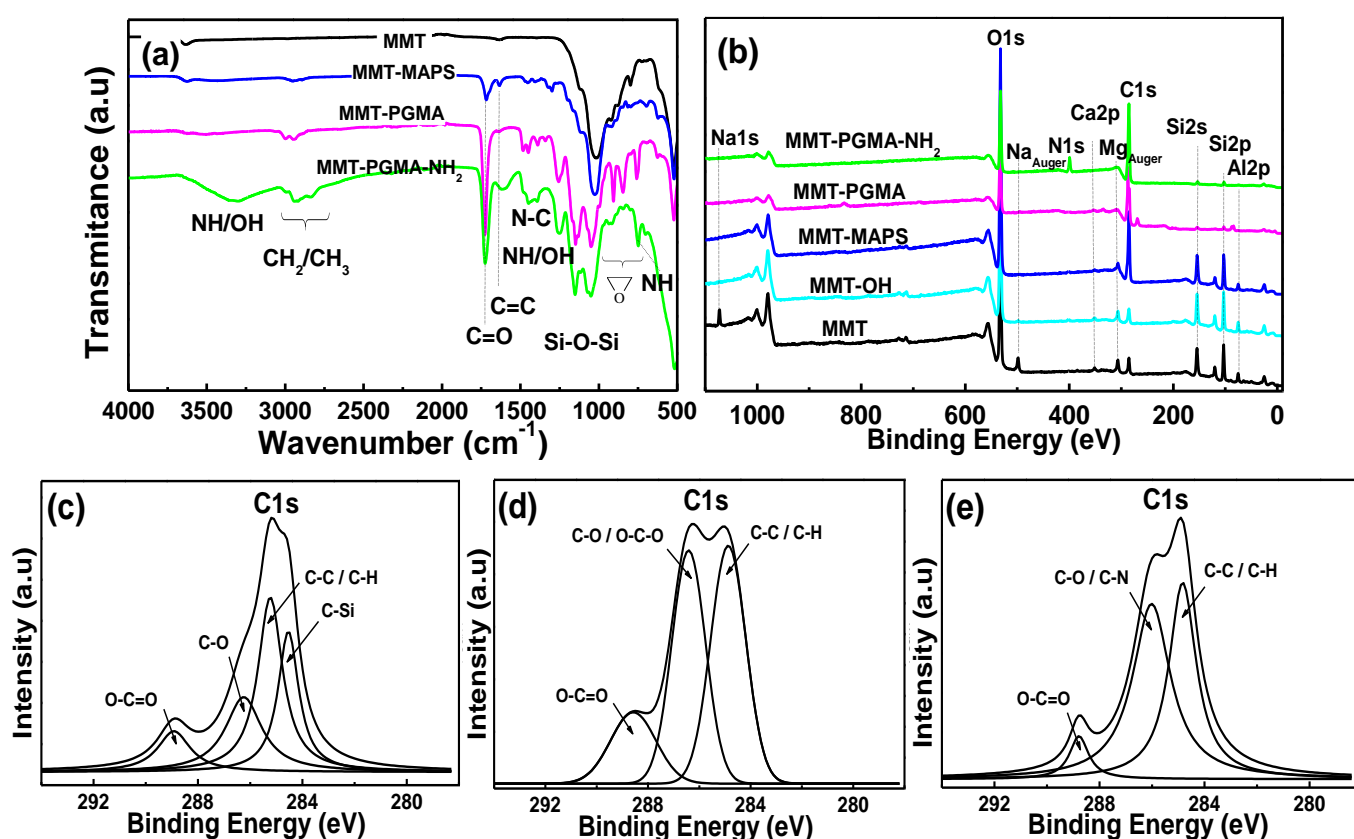


Figure 16. MMT, MMT-OH, MMT-MAPS, MMT-PGMA, MMT-PGMA-NH₂ (a) FTIR spectra, (b) XPS survey spectra, and C1s High resolution XPS scans of (c) MMT-MAPS, (d) MMT-PGMA, (e) MMT-PGMA-NH₂.

3.2. Gold NPs immobilization on MMT-PGMA-NH₂ platforms

Tetrachloroaurate (III) ions (AuCl₄⁻) were strongly adsorbed on the abundant protonated amine groups of amine-containing nanocomposite dispersed in water through electrostatic attraction, and then Au³⁺ ions were in-situ reduced to colloidal gold by adding aqueous NaBH₄ chemical reducing agent at room temperature. The adsorption of gold ions and their in-situ reduction to gold nanoparticles can be easily observed with the naked eye via the remarkable successive color change of the MMT samples from blank to light pink associated with the formation of amine-AuCl₄⁻ complexes on the surface of the amino-chelating platforms, then to dark purple indicating the formation of AuNPs (see *Scheme 1*). In order to tune the nanoparticles size, the NaBH₄/HAuCl₄ molar ratios fixed to 0.1, 0.5, and 1. These ratios were noted R₁, R₂, and R₃ for 0.1, 0.5, and 1, respectively.

To confirm the successful formation of gold nanocrystals on the amine-functionalized clay platforms, the as-designed AuNPs-decorated clay nanostructures were characterized by XPS, XRD, TGA, and SEM (*Figure 17 and 18*). *Figure 17a* displays a representative XPS spectra of AuNPs-decorated clay nanostructures obtained from R₁. As depicted in the XPS survey spectrum, several characteristic peaks are obviously observed at 84, 335/353 eV, which can be attributed to the Au4f and Au4d signals. The Au4f high-resolution scan (*Figure 17b*) shows a peak doublet centred at 83.5 and 87.5 eV, corresponding to the Au4f_{5/2} and Au4f_{7/2}, typical of metallic gold (Au⁰) (Rocha et al., 2018).

The crystalline structure of the same sample was monitored by powder X-ray diffraction (XRD) and its pattern is shown in *Figure 17c*. The five well-defined characteristic diffraction peaks with 2θ values of 38.1°, 44.4°, 64.7°, 77.84 and 81.4°, can be related to the (111), (200), (220), (311) and (222) crystalline planes corresponding to the face-centred cubic (fcc) structure of AuNPs, respectively, consistent with the zero valent gold data known in the literature (Borah et al., 2010). This result further proves the crystalline nature of the gold confirming XPS analysis. The hump around 2θ = 30° can be attributed to the amorphous framework of the PGMA.

TGA measurements aim to determine the content of gold on the surface of clay nanostructures.

It can be seen from the curves in *Figure 17d* that the different AuNPs-decorated clay nanostructures obtained from the three NaBH₄/HAuCl₄ molar ratios show very similar thermal properties with only a very slight difference in terms of gold content. From the comparison between the mass losses for the gold-free clay nanostructures and the three gold-containing one at 800°C, one can estimate the gold content to 22, 21, and 19 wt.% for R₁, R₂, and R₃,

respectively. This difference could be explained by the small difference observed in size of the AuNPs as shown by the SEM results in the following section.

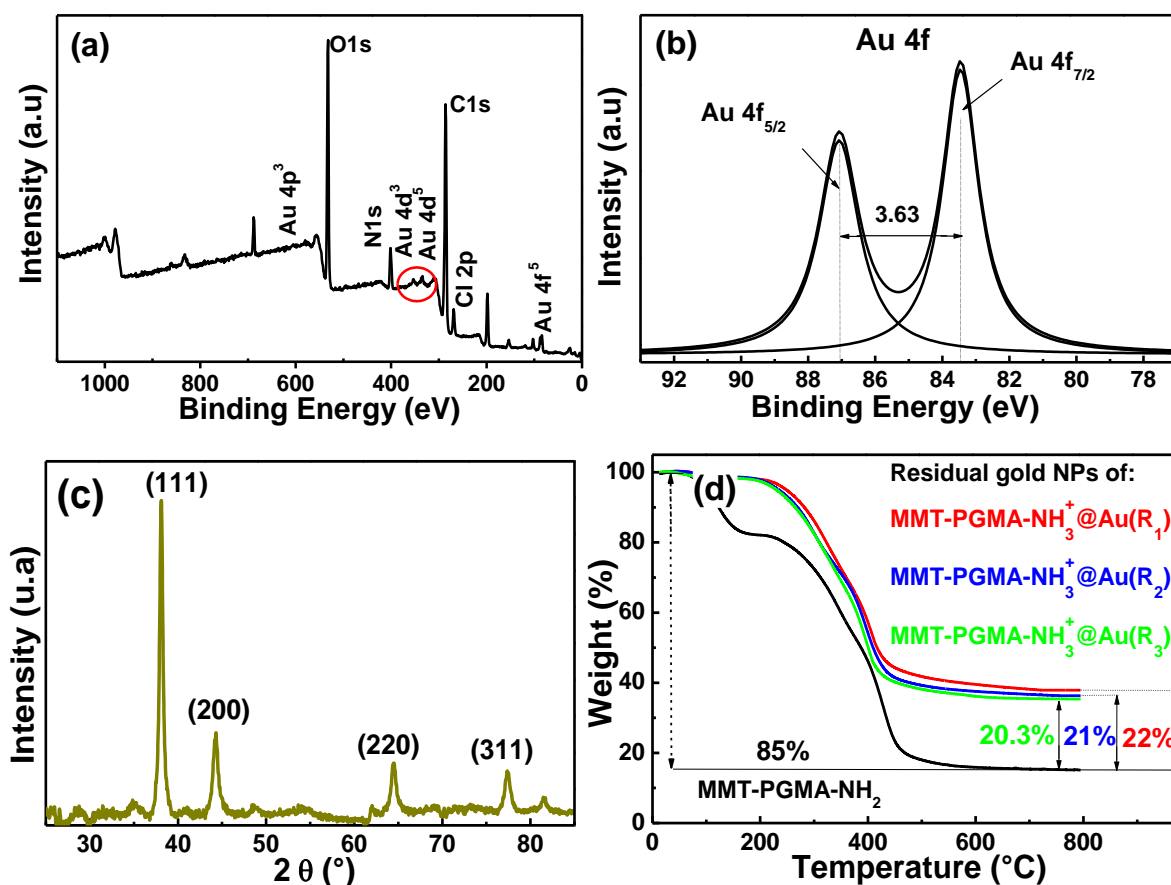


Figure 17. (a) XPS survey spectrum of MMT-PGMA-NH₂@AuNPs, (b) Au 4f high resolution XPS spectrum of MMT-PGMA-NH₂@AuNPs, (c) XRD patterns of MMT-PGMA-NH₂@AuNPs, and (d) TGA curves of MMT-PGMA-NH₂@AuNPs (R₁), NH₂@AuNPs (R₂) and NH₂@AuNPs (R₃).

Next, to study the morphological properties and the dispersion state of the AuNPs immobilized on the amine-functionalized MMT-PGMA platforms, scanning electron microscopy (SEM) analyses were conducted. As expected, the SEM images (**Figure 18**) show a uniform dispersion of stable spherical gold colloids (AuNPs) on the surface of amine-functionalized clay platforms for the three NaBH₄/HAuCl₄ molar ratios without detectable aggregation. The histogram analyses results obtained on more than 100 nanoparticles analysed using Image J software, shown in **Figure 18b**, d and f revealed that the AuNPs detected on the surface of the amino-chelant platforms are ultra-small and exhibited a relatively narrow size distribution (for 23.33, 30 and 33.33 % NPs) with an average size centred at 5, 8, and 9 nm for R₁, R₂ and R₃, respectively. Interestingly, it was observed that

the sizes of the AuNPs were sensitive to the $\text{NaBH}_4/\text{HAuCl}_4$ molar ratios, since the larger one was more favourable as it gives smaller average size and thus slightly greater amount of immobilized AuNPs on the surface of clay nanostructures. These results demonstrate that we were able to produce AuNPs with controlled size varying simply the concentrations of Au precursors.

Further evidence for the successful in-situ generation and stabilization of gold nanoparticles on amine-functionalized clay platforms.

To demonstrate the crucial role of amino-chelant groups in the adsorption and stabilization of AuCl_4^- ions converted to gold crystals by chemical reduction using NaBH_4 , a control experiment under the conditions of R_1 was carried out using MMT-PGMA before its functionalization with ethylene diamine. As could be seen in **Figure 18g**, AuNPs are poorly adsorbed and strongly aggregated on the surface of MMT-PGMA nanocomposite. As expected, the incorporation of the amine groups derived from ethylene diamine molecules into the MMT-PGMA brings about remarkable enhancement to the AuNPs stabilization as a result of binding of Au to amine groups.

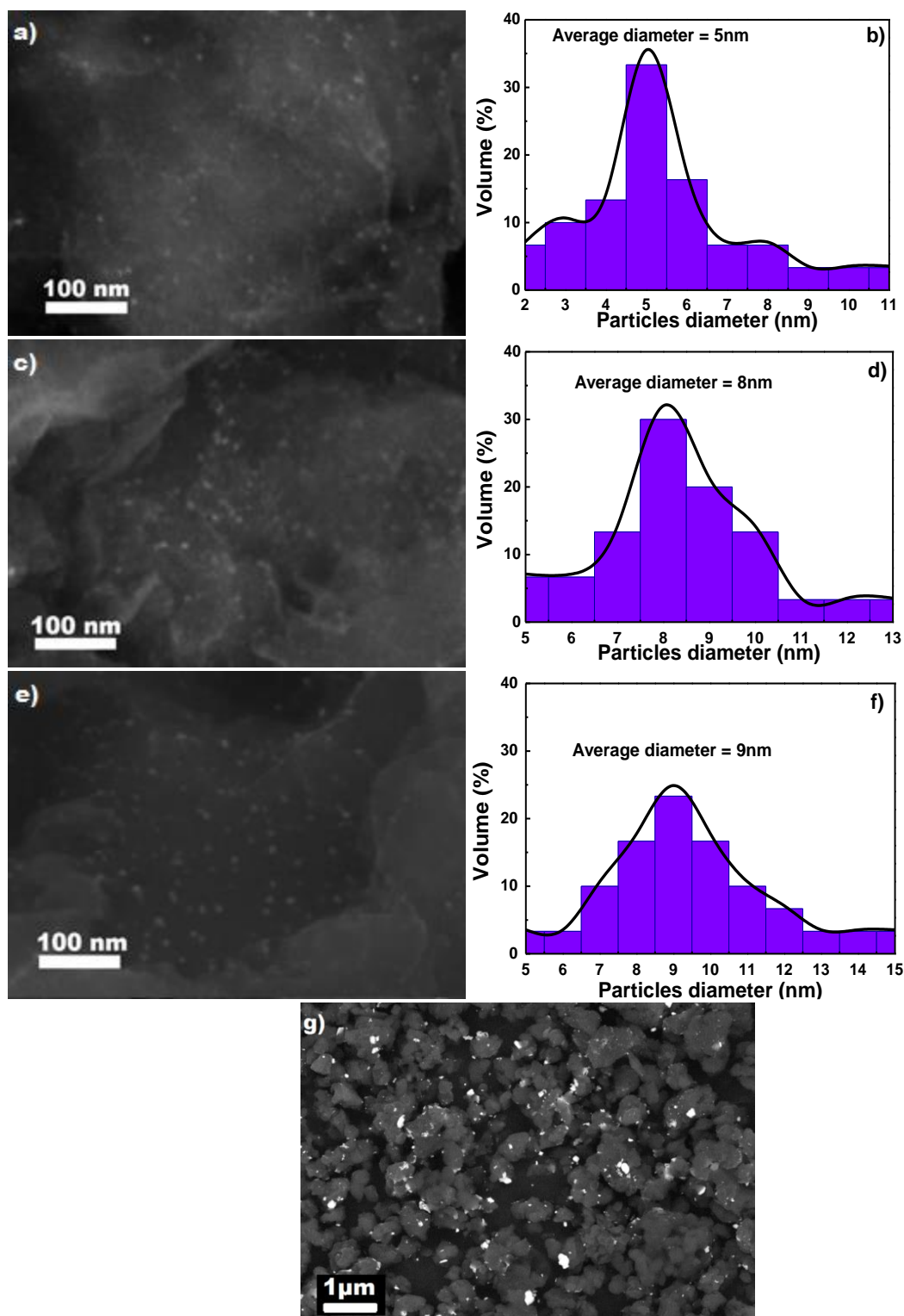


Figure 18. SEM images and AuNPs size distribution of (a, b) MMT-PGMA-NH₃⁺@Au (R₁), (c, d) and MMT-PGMA-NH₃⁺@Au (R₂), and (e, f) MMT-PGMA-NH₃⁺@Au (R₃) and SEM image of MMT-PGMA@AuNPs.

3.3. Catalytic performances of the AuNPs-decorated clay nanostructures

To evaluate the catalytic activity of the newly designed AuNPs-decorated nanostructures, they were employed as heterogeneous nanocatalyst for sodium borohydride-assisted catalytic hydrogenation of two nitroaromatic herbicides at room temperature (Mao et al., 2014).

As can be observed in **Figure 19**, the absorbance band of p-nitrophenol is shifted from 317 nm to 400 nm after addition of NaBH₄ solution accompanied with color change from light yellow to dark yellow, indicating the formation of p-nitrophenolate ions as a result of the deprotonation OH groups of 4NP under alkaline conditions (Esumi et al., 2004). It is worth to note that in the absence of MMT-PGMA-NH₃⁺@AuNPs nanocatalyst, the intensity of the absorption band of these phenolate ions remained almost unchanged even after a long period of time (72 h), demonstrating that the conversion of 4NP to 4AP does not occur. A same result was also observed in the case of presence of the nanocatalyst without NaBH₄. These observations evidence that the presence of BH₄⁻ or nanocatalyst alone is not enough for reduction of 4NP. While, after the addition of MMT-PGMA-NH₃⁺@AuNPs to a solution of 4NP containing NaBH₄ prepared in the same conditions as before, the 400 nm band absorption of p-nitrophenolate ions completely disappeared within only 3 min, while at the same time a new band was appeared at 296 nm as a result of the formation of p-aminophenol. This is revealed that gold nanoparticles stabilized on MMT-PGMA-NH₂ nanostructures act as a very efficient heterogeneous nanocatalyst for the reduction of p-nitrophenol to p-aminophenol in the presence of sodium borohydride in an aqueous medium. This catalytic ability is due to the interesting property of AuNPs which can act as an electron relay system when their potential redox is situated between a nucleophile (here BH₄⁻, E^o_{H₃BO₃/BH₄⁻ = -1.33V vs ENH) and an electrophile (here 4NP, E^o_{4NP/4AP} = -0.76V vs ENH). In fact, the reduction reaction takes place at the surface of the gold NPs where NaBH₄ gives electrons to AuNPs which in turn transfer these electrons to 4NP, making its reduction more favourable kinetically and thermodynamically. Thereby, in the absence of the nanocatalyst, the high difference between the two redox couples (ΔE^o = -0.57 V) originated a kinetic barrier and thus extremely low reduction rate.}

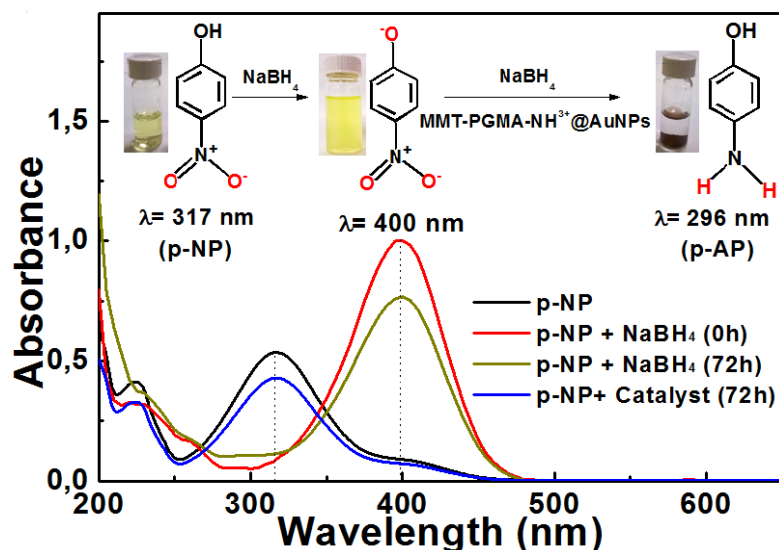


Figure 19. UV-vis absorption spectra of (black) pure p-nitrophenol, (red) p-nitrophenol directly after addition of NaBH_4 , (grey) p-nitrophenol 72 h after addition of NaBH_4 , (blue) p-nitrophenol 72 h after addition of $\text{MMT-PGMA-NH}_3^+@AuNPs$. The insets show (1) the catalytic reduction of p-nitrophenol by $\text{MMT-PGMA-NH}_3^+@AuNP$ (R_1) nanostructures and NaBH_4 , (2) photographs of pure p-nitrophenol solution, p-nitrophenolate obtained by addition of NaBH_4 to p-nitrophenol solution, and p-aminophenol solution as a result of reduction of p-nitrophenol by $\text{MMT-PGMA-NH}_3^+@AuNP$ (R_1) and NaBH_4 .

3.4. Effect of size and concentration of immobilized AuNPs nanocatalyst on the rate reduction of 4NP

To investigate the dependence of apparent rate constant (k_{app}) on the operating conditions, the influence of various parameters such as the size of the immobilized gold nanoparticles, the nanocatalyst dosage, and the 4NP initial concentration was studied in the catalytic conversion of 4NP to 4-aminophenol (4AP). This conversion was easily detected by UV_{vis} spectroscopy as well as with the naked eye as the color of the solution mixture changes gradually from dark yellow to light yellow before becoming finally colorless. Thus, the obtained absorption spectra were used to plot the curve of $\ln(A/A_0)$ versus time (min) from which k_{app} were determined from the slope of curves. As seen from these plots, all gave straight lines with negative slopes.

First, we conducted a comparative catalytic activity of the three sizes of AuNPs. The results of UV-vis spectra of **Figure 20 a, c, and e** show that the intensities of the 400 nm absorption bands related to p-nitrophenolate ions decreased gradually over time to give 100 % conversion. The correlation between the k_{app} and the AuNP size is shown in **Figure 20d**. As expected, a faster reduction reaction of 4NP was revealed using smaller AuNPs (~average

diameter of 5 nm) with respect to the other prepared nanostructures, and this to achieve a total conversion within 3 min. Hence, the order of efficiency is MMT-PGMA-NH₃⁺@AuNPs (R₁) > MMT-PGMA-NH₃⁺@AuNPs (R₂) > MMT-PGMA-NH₃⁺@AuNPs (R₃), with k_{app} values of 1.00 x 10⁻² s⁻¹, 5.29 x 10⁻³ s⁻¹, and 6.14 x 10⁻³ s⁻¹, respectively (**Figure 20b**). The obvious size-dependent catalytic activity of supported AuNPs can be explained by the increases of their active surface area with decreasing of their size resulting in the enhancement of the concentration of 4NP on the immobilized AuNPs, which accelerates the catalytic conversion of 4NP. We can see in **Figure 20d** that there is a linear relationship between the determined k_{app} and the size of AuNPs.

With the aim to study the effect of the concentration of catalyst on the conversion kinetic, experiments were conducted using the more active nanocatalyst (AuNPs of 5 nm diameter) at varying its dosage from 0.5 to 2 mg.mL⁻¹, and keeping other parameters constant ([BH₄⁻] = 12.5 10⁻⁴ M and [4NP] = 10⁻⁴ M, T = 22°C). **Figure 20f** shows the dependence of k_{app} on the amount of nanocatalyst in the conversion of 4NP to 4AP. It can be observed that k_{app} increased with an increase in the nanocatalyst concentration. Undoubtedly, a high concentration of the nanocatalyst would provide larger number of available active sites that can enhance the adsorption of 4NP and BH₄⁻, thus, leading to an obvious increase of reduction reaction rate.

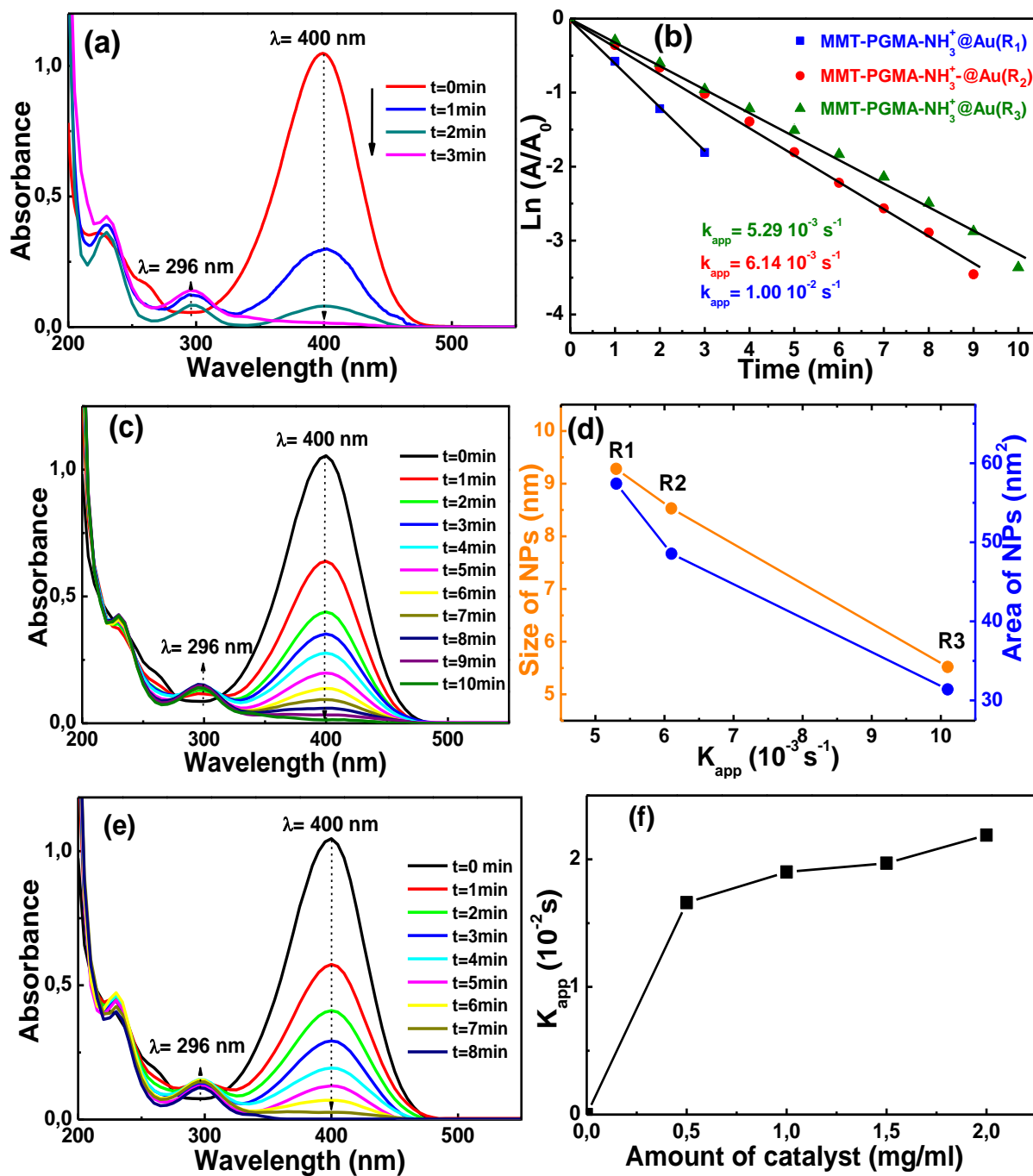


Figure 20. Time-dependent evolution of UV-vis absorption spectra showing the gradual reduction of p-nitrophenol and plots of $\ln(A/A_0)$ versus reaction time for the catalytic reduction of p-nitrophenol by (a, b) MMT-PGMA-NH₃⁺@AuNPs (R₁), (c, b) MMT-PGMA-NH₃⁺@AuNPs (R₂), (e, b) MMT-PGMA-NH₃⁺@AuNPs (R₃) and NaBH₄. Plot of k_{app} versus (d) size and area of AuNPs (f) concentration of MMT-PGMA-NH₃⁺@AuNPs (R₁) nanocatalyst for the catalytic reduction of p-nitrophenol.

3.5. Pendimethalin pesticide conversion

To demonstrate the catalytic performances of the as-designed AuNPs-decorated nanostructures, their application has been extended to the conversion of dinitroaromatic compounds such as pendimethalin herbicide, and this in the presence of an excess of NaBH_4 . For this, we used the prepared nanostructures containing the smaller gold nanoparticles, i.e., MMT-PGMA- NH_3^+ @AuNPs (R_1). This choice is justified by their high catalytic activity with respect to MMT-PGMA- NH_3^+ @AuNPs (R_2) and MMT-PGMA- NH_3^+ @AuNPs (R_3) nanocatalysts as demonstrated before. **Figure 21** shows that compared with the case where NaBH_4 was introduced to an aqueous solution of PDM, adding AuNPs-decorated nanostructures enhanced remarkably the reduction kinetic of PDM to its corresponding diaminoaromatic derivative under atmospheric conditions. As can be observed from **Figure 21b**, the characteristic absorption bands of PDM at 450 and 290 nm gradually decreased indicating that the complete reduction process required 10 min, and this with a rate value of $2.00 \times 10^{-3} \text{ s}^{-1}$. This confirms that the immobilized AuNPs play efficiently the role of mediator as they ensure a high transfer rate of electrons from NaBH_4 to PDM.

These results prove that the as-prepared AuNPs-decorated nanostructures are promising heterogeneous nanocatalysts towards the reduction of both mono- and dinitroaromatic compounds.

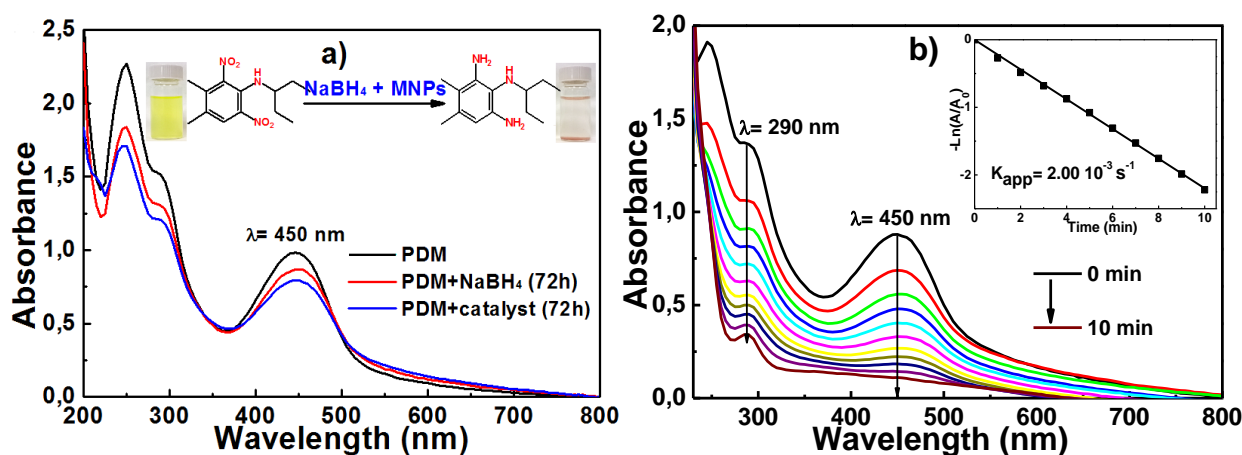


Figure 21. (a) UV-vis absorption spectra of (black) pure pendimethalin, (red) pendimethalin 72 h after addition of NaBH_4 , (blue) pendimethalin 72 h after addition of MMT-PGMA- NH_3^+ @AuNPs, (grey) pendimethalin 72 h after addition of MMT-PGMA- NH_3^+ @AuNPs and NaBH_4 and (b) time-dependent evolution of UV-vis absorption spectra showing the gradual reduction of pendimethalin by MMT-PGMA- NH_3^+ @AuNPs (R_1) and NaBH_4 . The insets show (a) the catalytic reduction of pendimethalin by MMT-PGMA- NH_3^+ @AuNP (R_1) and NaBH_4 and photographs of pure pendimethalin and the obtained reduced pendimethalin, and (b) plots of $\ln(A/A_0)$ versus reaction time.

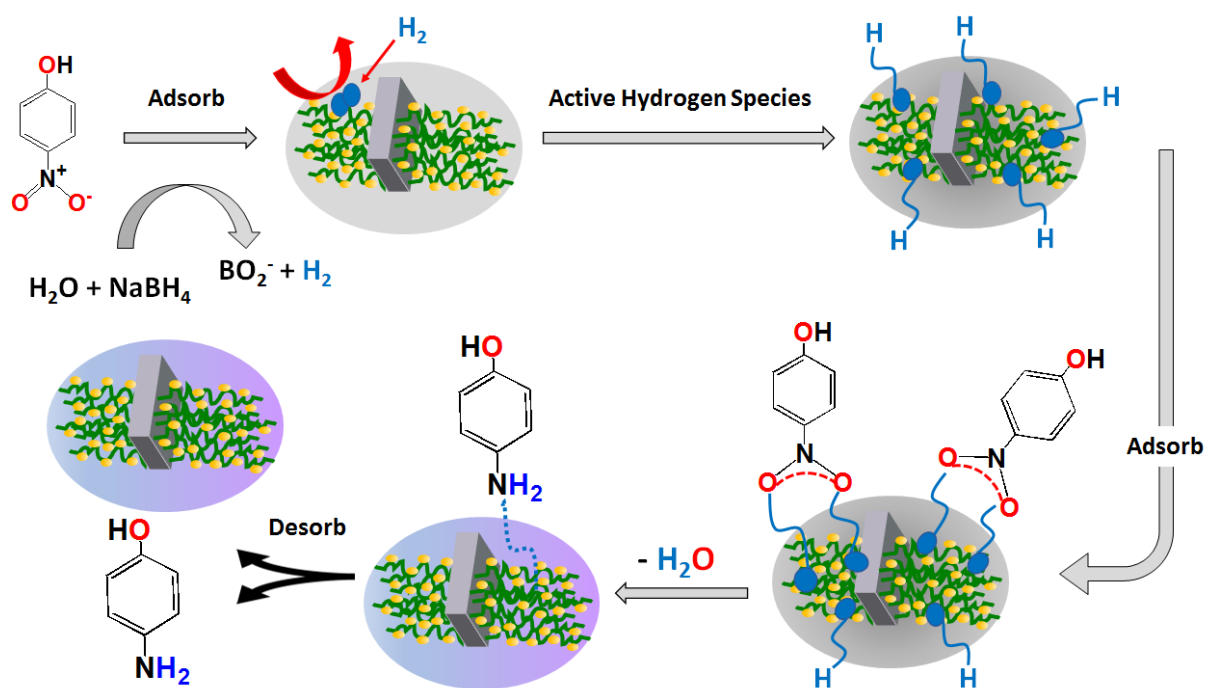
3.6. Mechanism of 4-NP Reduction Reaction by MMT-PGMA-NH₃⁺@AuNPs

In order to explain the reaction mechanism of the catalytic reduction of 4-NP onto metallic nanoparticle surfaces by using borohydride solution various studies have been reported in the literature (Fedorczyk et al., 2015; Gu et al., 2014; Tang et al., 2009)

Previous mechanistic investigations demonstrated that gold nanoparticles can act as electron donors in reactions under the effect of NaBH₄ as a good source for hydrogen generation (Wunder et al., 2011).

Since the reduction of 4-NP occurs on the surface of the catalyst, Langmuir-Hinshelwood mechanism was proposed by Wunder and co-workers as a mechanistic model to explain the reduction reaction of 4-NP by NaBH₄ in the presence of metallic nanoparticles.

Thereby, a detailed catalysis mechanism was proposed by Gu et al. (2014) and Kohantorabi and Gholami (2017) as shown in *Scheme 2*.



Scheme 2. Proposed mechanism of the catalytic reduction of 4-NP by NaBH₄ over the MMT-PGMA-NH₃⁺@Au nanocomposites.

According to their proposed model, the surface of metallic nanoparticles serves as the location where the catalytic reduction process occurs.

Firstly, 4-NP adsorbs on the surface of the metallic nanoparticles, and concomitantly, borohydride ions bind to the surface and would give electrons to the catalyst and quickly reach an adsorption/desorption equilibrium.

Subsequently, hydrogen is liberated due to reduction of water to H₂. Finally, active hydrogen species are formed on the surface of NPs and 4-NP is reduced.

3.7. Reusability test of the nanocatalysts

The recyclability is one of the most important properties of metal nanoparticles-based heterogeneous catalysts for their application. As well-known, regeneration is directly related to the ability of the catalyst to maintain the stability of the dispersion of the metal nanoparticles on the support while avoiding AuNPs leaching. Indeed, the high dispersion of metal nanoparticles facilitates the access of the nitroaromatics to the active sites of these heterogeneous nanocatalysts. To evaluate the recyclability of MMT-PGMA-NH₃⁺@AuNPs (R₁) nanocatalyst, the 4NP reduction reaction was tested for seven cycles under the optimum conditions employing the same catalyst sample after washing with ethanol, water, and drying under vacuum at 60°C. The percentage of reduction was calculated using the area under the p-nitrophenolate ion absorption band at 400 nm in the UV-vis. *Figure 22* revealed that this nanocatalyst was stable and could be used for several runs without significant loss of its activity as the conversion of 4NP kept 92.5% of the initial capacity even after 7 regeneration cycles. This very low alteration of the catalytic properties of the supported AuNPs could be explained by their non-aggregation during the reactions processes demonstrating the key role of the chemical surface functionalization of MMT support with amino chelant groups in the strong interactions with AuNPs.

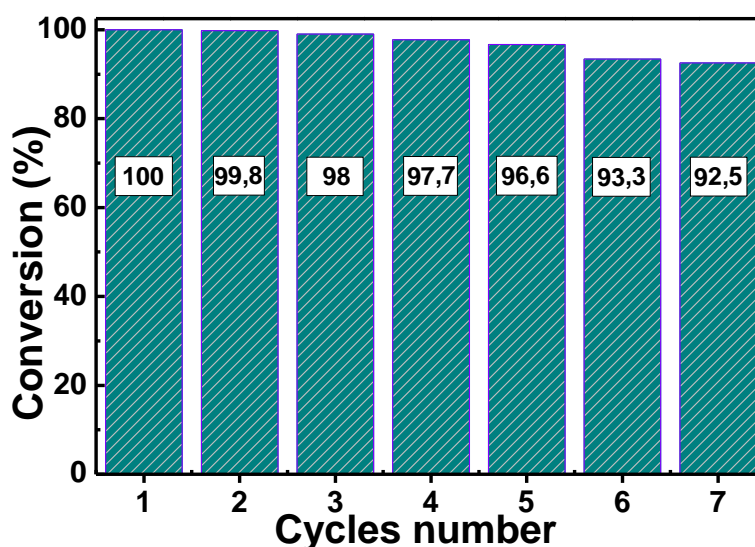


Figure 22. Reusability of the MMT-PGMA-NH₃⁺@AuNPs nanostructure as heterogeneous catalyst for the reduction of 4NP using NaBH₄.

4. Conclusion

In summary, size-controlled and stable AuNPs were in-situ generated and stabilized on amine-functionalized MMT-PGMA chelant platforms through a simple and fast reducing process using sodium borohydride.

The as-obtained AuNPs-decorated nanostructures served as highly active and reusable heterogeneous nanocatalysts for the complete reduction of nitroaromatic endocrine compounds, namely p-nitrophenol and pendimethalin. These chelant platforms could be used as promising supports for dispersing and stabilizing various catalytic metal or metal oxide nanoparticles with desired size, shape, and composition active in reduction, oxidation, or cross-coupling reactions.

References

A

- Amari, H., Guerrouache, M., Mahouche-Chergui, S., Abderrahim, R., Carbonnier, B., 2017. 2-Aminothiazole-functionalized triazine-modified polystyrene decorated with gold nanoparticles as composite catalyst for the reduction of 4-nitrophenol. *Reactive and Functional Polymers*. 121, 58–66. doi:org/10.1016/j.reactfunctpolym.2017.10.018.
- Aroua, M.K., Zuki, F.M., Sulaiman, N.M., 2007. Removal of chromium ions from aqueous solutions by polymer-enhanced ultrafiltration. *J. Hazard. Mater.* 147, 752–758.
- ATSDR, 1992. Toxicological profile for nitrophenols: 2- and 4-nitrophenol. Atlanta, GA, US Department of Health and Human Services, Public Health Service, Agency for Toxic Substances and Disease Registry (Report No. TP-91/23).

B

- Benaglia, M., Bonsignore, M., 2016. Process for the reduction of nitro derivatives to amines.
- Bibi, S., Price, G.J., Yasin, T., Nawaz, M., 2016. Eco-friendly synthesis and catalytic application of chitosan/gold/carbon nanotube nanocomposite films. *RSC Adv.* 6, 60180–60186.
- Bilici, A., Ayten, B., Kaya, I., 2015. Facile preparation of gold nanoparticles on the polyquinoline matrix: Catalytic performance toward 4-nitrophenol reduction. *Synth. Met.* doi:10.1016/j.synthmet.2015.01.009.
- Bingwa, N., Meijboom, R., 2014. Kinetic evaluation of dendrimer-encapsulated palladium nanoparticles in the 4-nitrophenol reduction reaction. *J. Phys. Chem. C* 118, 19849–19858.
- Borah, B. J., Dutta, D., Dutta, D.K., 2010. Controlled nanopore formation and stabilization of gold nanocrystals in acid-activated montmorillonite. *Applied Clay Science*. 49, 317–323. doi:10.1016/j.clay.2010.06.016.

C

- Chen, S., Wang, T., Yao, Y., Wei, A., 2018. Facile synthesis of novel fibrous silica@apatite@ Au composites with superior photo-catalytic activity. *Mater. Des.* 147, 106–113.

Chenouf, M., Megías-Sayago, C., Ammari, F., Ivanova, S., Centeno, M. Á., Odriozola, J.A., 2019. Montmorillonite-stabilized gold nanoparticles for nitrophenol reduction. *Comptes Rendus Chimie*. doi:10.1016/j.crci.2019.07.005.

Corma, A., Garcia, H., 2008. Supported gold nanoparticles as catalysts for organic reactions. *Chem. Soc. Rev.* 37, 2096–2126.

D

de Lima, R.O.A., Bazo, A.P., Salvadori, D.M.F., Rech, C.M., de Palma Oliveira, D., de Aragão Umbuzeiro, G., 2007. Mutagenic and carcinogenic potential of a textile azo dye processing plant effluent that impacts a drinking water source. *Mutat. Res. Toxicol. Environ. Mutagen.* 626, 53–60.

De Roos, A.J., Ray, R.M., Gao, D.L., Wernli, K.J., Fitzgibbons, E.D., Ziding, F., Astrakianakis, G., Thomas, D.B., Checkoway, H., 2005. Colorectal cancer incidence among female textile workers in Shanghai, China: a case-cohort analysis of occupational exposures. *Cancer Causes Control.* 16, 1177–1188.

E

Esumi, K., Isono, R., Yoshimura, T., 2004. Preparation of PAMAM- and PPI-Metal (Silver, Platinum, and Palladium) Nanocomposites and Their Catalytic Activities for Reduction of 4-Nitrophenol. *Langmuir.* 20, 237–243. doi:10.1021/la035440t.

F

Fazzini, S., Nanni, D., Ballarin, B., Cassani, M.C., Giorgetti, M., Maccato, C., Trapananti, A., Aquilanti, G., Ahmed, S.I., 2012. Straightforward synthesis of gold nanoparticles supported on commercial silica-polyethyleneimine beads. *J. Phys. Chem. C* 116, 25434–25443.

Fedorczyk, A., Ratajczak, J., Kuzmych, O., Skompska, M., 2015. Kinetic studies of catalytic reduction of 4-nitrophenol with NaBH₄ by means of Au nanoparticles dispersed in a conducting polymer matrix. *Journal of Solid State Electrochemistry.* 19, 2849–2858. 2849–2858. doi:10.1007/s10008-015-2933-5.

G

Gao, B., Wang, X., Shen, Y., 2006. Studies on characters of immobilizing penicillin G acylase on a novel composite support PEI/SiO₂. *Biochem. Eng. J.* 28, 140–147.

Gu, S., Wunder, S., Lu, Y., Ballauff, M., Fenger, R., Rademann, K., Jaquet, B., Zaccone, A., 2014. Kinetic Analysis of the Catalytic Reduction of 4-Nitrophenol by Metallic Nanoparticles. *The Journal of Physical Chemistry C*. 118, 18618–18625. doi:[10.1021/jp5060606](https://doi.org/10.1021/jp5060606).

I

Islam, M.T., Padilla, J.E., Dominguez, N., Alvarado, D.C., Alam, M.S., Cooke, P., Tecklenburg, M.M.J., Noveron, J.C., 2016. Green synthesis of gold nanoparticles reduced and stabilized by squaric acid and supported on cellulose fibers for the catalytic reduction of 4-nitrophenol in water. *RSC Adv.* 6, 91185–91191.

K

Kawahashi, N., Shiho, H., 2000. Copper and copper compounds as coatings on polystyrene particles and as hollow spheres. *J. Mater. Chem.* 10, 2294–2297.

Keith, L., Telliard, W., 1979. ES&T special report: priority pollutants: Ia perspective view. *Environ. Sci. Technol.* 13, 416–423.

Kohantorabi, M., & Gholami, M.R., 2017. Kinetic Analysis of the Reduction of 4-Nitrophenol Catalyzed by CeO₂ Nanorods-Supported CuNi Nanoparticles. *Industrial & Engineering Chemistry Research*. 56, 1159–1167. doi:[10.1021/acs.iecr.6b04208](https://doi.org/10.1021/acs.iecr.6b04208).

L

Liu, Y., Wu, D., Zhang, W., Jiang, X., He, C., Chung, T.S., Goh, S.H., Leong, K.W., 2005. Polyethylenimine-grafted multiwalled carbon nanotubes for secure noncovalent immobilization and efficient delivery of DNA. *Angew. Chemie Int. Ed.* 44, 4782–4785.

Luo, J., Zhang, N., Liu, R., Liu, X., 2014. In situ green synthesis of Au nanoparticles onto polydopamine-functionalized graphene for catalytic reduction of nitrophenol. *RSC Adv.* 4, 64816–64824.

M

Mao, K., Chen, Y., Wu, Z., Zhou, X., Shen, A., Hu, J., 2014. Catalytic Strategy for Efficient Degradation of Nitroaromatic Pesticides by Using Gold Nanoflower. *Journal of Agricultural and Food Chemistry*. 62, 10638–10645. doi:[10.1021/jf5034015](https://doi.org/10.1021/jf5034015).

Mirafzal, G.A., Summer, J.M., 2000. Microwave irradiation reactions: synthesis of analgesic drugs. *J. Chem. Educ.* 77, 356.

N

Nasrollahzadeh, M., Sajadi, S.M., Rostami-Vartooni, A., Bagherzadeh, M., Safari, R., 2015. Immobilization of copper nanoparticles on perlite: Green synthesis, characterization and catalytic activity on aqueous reduction of 4-nitrophenol. *J. Mol. Catal. A Chem.* 400, 22–30.

P

Pang, Y., Zeng, G., Tang, L., Zhang, Y., Liu, Y., Lei, X., Li, Z., Zhang, J., Xie, G., 2011. PEI-grafted magnetic porous powder for highly effective adsorption of heavy metal ions. *Desalination*. 281, 278–284.

Ponnusamy, V.K., Mani, V., Chen, S.-M., Huang, W.-T., Jen, J.-F., 2014. Rapid microwave assisted synthesis of graphene nanosheets/polyethyleneimine/gold nanoparticle composite and its application to the selective electrochemical determination of dopamine. *Talanta*. 120, 148–157.

R

Rocha, M., Costa, P., Sousa, C.A.D., Pereira, C., Rodríguez-Borges, J.E., Freire, C., 2018. 1-serine-functionalized montmorillonite decorated with Au nanoparticles: A new highly efficient catalyst for the reduction of 4-nitrophenol. *Journal of Catalysis*. 361, 143–155. doi:10.1016/j.jcat.2018.02.027.

S

Seo, Y.S., Ahn, E.-Y., Park, J., Kim, T.Y., Hong, J.E., Kim, K., Park, Yohan, Park, Youmie, 2017. Catalytic reduction of 4-nitrophenol with gold nanoparticles synthesized by caffeic acid. *Nanoscale Res. Lett.* 12, 7.

Shivhare, A., Ambrose, S.J., Zhang, H., Purves, R.W., Scott, R.W.J., 2013. Stable and recyclable Au 25 clusters for the reduction of 4-nitrophenol. *Chem. Commun.* 49, 276–278.

T

Tafesh, A.M., Weiguny, J., 1996. A review of the selective catalytic reduction of aromatic nitro compounds into aromatic amines, isocyanates, carbamates, and ureas using CO. *Chem. Rev.* 96, 2035–2052.

Tang, J., Alam, S., Abbass, H., Lokan, C., 2009. Carbon spheres with controllable silver nanoparticle doping. *The Journal of Physical Chemistry C*. 114, 977–982. doi:10.1021/jp9102492.

Tremp, J., Mattrel, P., Fingler, S., Giger, W., 1993. Phenols and nitrophenols as tropospheric pollutants: emissions from automobile exhausts and phase transfer in the atmosphere. *Water, Air, Soil Pollut.* 68, 113–123.

V

Veerakumar, P., Velayudham, M., Lu, K.-L., Rajagopal, S., 2013. Silica-supported PEI capped nanopalladium as potential catalyst in Suzuki, Heck and Sonogashira coupling reactions. *Appl. Catal. A Gen.* 455, 247–260.

Vineis, P., Pirastu, R., 1997. Aromatic amines and cancer. *Cancer Causes Control* 8, 346–355.

Vo, V.S., Mahouche-Chergui, S., Nguyen, V.-H., Naili, S., Carbonnier, B., 2019. Crucial role of covalent surface functionalization of clay nanofillers on improvement of the mechanical properties of bio-epoxy resin. *ACS Sustainable Chemistry & Engineering*. doi:10.1021/acssuschemeng.9b02088.

W

Wang, S., Yan, J., Chen, L., 2005. Formation of gold nanoparticles and self-assembly into dimer and trimer aggregates. *Mater. Lett.* 59, 1383–1386.

Woo, Y.-T., Lai, D.Y., 2001. Aromatic amino and nitro–amino compounds and their halogenated derivatives. *Patty's Toxicol.*

Wu, Q., Chen, S., Liu, H., 2014. Effect of surface chemistry of polyethyleneimine-grafted polypropylene fiber on its CO₂ adsorption. *RSC Adv.* 4, 27176–27183.

Wunder, S., Lu, Y., Albrecht, M., Ballauff, M., 2011. Catalytic Activity of Faceted Gold Nanoparticles Studied by a Model Reaction: Evidence for Substrate-Induced Surface Restructuring. *ACS Catalysis*. 1, 908–916. doi:10.1021/cs200208a.

X

Xiao, F., Qin, Y., Wang, N., Pan, D., 2018. Towards mass production of Au nanoparticles supported on montmorillonite microspheres for catalytic reduction of 4-nitrophenol. *Applied Clay Science*, 166, 74–79. doi:10.1016/j.clay.2018.09.016.

Xiong, C., Zheng, Y., Feng, Y., Yao, C., Ma, C., Zheng, X., Jiang, J., 2014. Preparation of a novel chloromethylated polystyrene-2-amino-1,3,4-thiadiazole chelating resin and its

adsorption properties and mechanism for separation and recovery of Pt (IV) from aqueous solutions. *J. Mater. Chem. A* 2, 5379–5386.

Y

Yu, R., Zhang, S., Luo, Y., Bai, R., Zhou, J., Song, H., 2015. Synthetic possibility of polystyrene functionalization based on hydroxyl groups of graphene oxide as nucleophiles. *New J. Chem.* 39, 5096–5099.

Yuan, Z., Cai, N., Du, Y., He, Y., Yeung, E.S., 2013. Sensitive and selective detection of copper ions with highly stable polyethyleneimine-protected silver nanoclusters. *Anal. Chem.* 86, 419–426.

Z

Zhang, F., Yang, P., Matras-Postolek, K., 2016. Au Catalyst Decorated Silica Spheres: Synthesis and High-Performance in 4-Nitrophenol Reduction. *J. Nanosci. Nanotechnol.* doi:10.1166/jnn.2016.10858.

Zhang, J., Chen, G., Chaker, M., Rosei, F., Ma, D., 2013. Gold nanoparticle decorated ceria nanotubes with significantly high catalytic activity for the reduction of nitrophenol and mechanism study. *Appl. Catal. B Environ.* Doi:10.1016/j.apcatb.2012.11.030.

Zhang, M., Lu, X., Wang, H.-Y., Liu, X., Qin, Y., Zhang, P., Guo, Z.-X., 2016. Porous gold nanoparticle/graphene oxide composite as efficient catalysts for reduction of 4-nitrophenol. *RSC Adv.* 6, 35945–35951.

Zhang, P., Shao, C., Zhang, Z., Zhang, M., Mu, J., Guo, Z., Liu, Y., 2011. In situ assembly of well-dispersed Ag nanoparticles (AgNPs) on electrospun carbon nanofibers (CNFs) for catalytic reduction of 4-nitrophenol. *Nanoscale.* 3, 3357–3363.

Zhao, P., Feng, X., Huang, D., Yang, G., Astruc, D., 2015. Basic concepts and recent advances in nitrophenol reduction by gold-and other transition metal nanoparticles. *Coord. Chem. Rev.* 287, 114–136.

Zhou, B., Zheng, L., Peng, C., Li, D., Li, J., Wen, S., Shen, M., Zhang, G., Shi, X., 2014. Synthesis and characterization of PEGylated polyethylenimine-entrapped gold nanoparticles for blood pool and tumor CT imaging. *ACS Appl. Mater. Interfaces.* 6, 17190–17199.

Zhu, W., Wu, Y., Yan, C., Wang, C., Zhang, M., Wu, Z., 2013. Facile synthesis of mono-dispersed polystyrene (PS)/Ag composite microspheres via modified chemical reduction. *Materials (Basel).* 6, 5625–5638.

Section 2

Palladium nanoparticles decorated dually functionalized green synthesized graphene/clay nanohybrid: A promising heterogeneous catalyst for water remediation

1. Introduction

Decoration of solid supports with nano-sized metallic nanoparticles is of great interest in tuning materials properties for the fabrication of advanced hybrid materials for applications from electronic (Bashir et al., 2019), biomedical (Zhang et al., 2012), energy storage (Rosaiah et al., 2017), and sensing (Zhao et al., 2019), to heterogeneous catalysis (Luo et al., 2019).

Nano-sized metallic particles possess unique optic and electronic properties (Shipilova et al., 2020). In addition to these properties, they have a remarkable surface-to-volume ratio, resulting in a high number of available active sites per unit area in comparison with their bulk analogs, making them excellent candidates for catalysis (Singla et al., 2016). However, this feature is often strongly altered, when the metallic nanoparticles (MNPs) are used alone, they tend to agglomerate because of their high surface free energy. This induces a strong decrease in their thermodynamic dispersion stability and hence the loss of their surface area, that resulted in drastic decrease MNPs properties such as catalytic activity. Indeed, it is known that the catalytic performances of MNPs is intimately related to their size and stability (Dong et al., 2015). To improve the MNPs dispersion and to take full advantage of the benefits of nanosized effect, it is necessary to support the metallic nanoparticles by a solid platform such as polymers (Liang et al., 2013), clay nanoparticles (Dutta et al., 2018), mesoporous silica (Chen et al., 2010), cellulose nanoparticles (Kaushik and Moores 2016), carbon nanotubes (Fang et al., 2017) and graphene nanoplatelets (Su et al., 2017a), to name but a few. In particular, graphene, as a 2D monolayer of graphite, has been emerging as promising supporting material for MNPs due to its several unique properties, such as ultrasmall dimension, extraordinary specific surface area, unique mechanical, thermal, chemical, optical and electrical properties, as well as excellent electron transport property at room temperature (Liu et al., 2019). The graphene-based nanostructures have also shown great potential in heterogeneous catalysis (Dong et al., 2017).

However, despite these remarkable properties there are critical limitations to the practical applications of pristine graphene-supported MNPs in heterogeneous catalysis related to, on the one hand, the aggregation of graphene nanoparticles due to the strong π - π stacking interactions between graphene nanolayers, and on the other hand, the weak interactions between graphene and the MNPs which result in a poor control of the size and the dispersion

stability of the MNPs, thereby making the catalytic active sites inaccessible (Guo et al., 2019). Chemical surface modification of graphene with suitable functional entities exhibiting high binding affinity to metal ions can be used for the direct generation of metal nanoparticles having fine controlled size, morphology, size distribution, and density on the surface of the support. This is powerful strategy for designing highly stabilized and homogeneously dispersed MNPs (Si and Samulski 2008). The functionalization is very versatile as it enables the introduction of various desired functional moieties including amine, thiol, phosphonic, sulphonic and carboxylic acid, and so on, providing an opportunity for in-situ designing a wide variety of catalytic systems by using reducing agents like hydrazine, ascorbic acid, sodium citrate, sodium borohydride (De Silva et al., 2017 ; Şenol et al., 2019). Furthermore, graphene surface functionalization has a dual role, namely, improving ability to anchor and stabilizing MNPs, and enhancing the dispersion of graphene, because the functional surface modifiers act also as surface passivation agents. Although functionalized graphene/MNPs systems exhibit interesting catalytic properties, their stability is compromised by the stability of the interface between graphene support and the functional groups (Kou et al., 2011). To date, strategies including non-covalent and covalent chemical modification methods have been developed to design MNPs-decorated graphene nanohybrids (Silva and Cesarino 2019). The covalent surface functionalization strategy is expected to be more appropriate as it provides much stronger interfacial adhesion compared to that obtained with the non-covalent one. This leads to more stable and higher resistant hybrid nanocatalysts which would result in preventing metal leaching. Furthermore, the stability of nanocatalysts plays a key role not only because it preserves a desirable catalytic activity during recyclability/reusability tests but also for its preventing toxic effect of leached metal nanoparticles difficult to recover from solution (Sinha et al., 2019). Palladium nanoparticles (PdNPs) are one of the most commonly used transition metal nanoparticles as green catalysts for the efficient synthesis of chemical intermediates utilized in the design of pharmaceutical, agricultural, antioxidants, pigments advanced materials using, for example, cross-coupling (Mahouche Chergui et al., 2010) or annulation reactions (Sharma et al., 2017). In addition, PdNPs in the presence of hydrogen donors have been applied as efficient catalysts in the selective conversion of toxic compounds such as dyes into environmentally benign ones through the cost-effective and environment-friendly hydrogenation reactions (Jin et al., 2010; Su et al., 2017b).

Indeed, the high aqueous solubility of dyes and their wide use in several fields such as pharmaceutical (Wainwright 2008), food (Nollet 2004), paint (Pawlak et al., 2006), paper

(Hunger 2003) and textile (Muthu 2018), leads to an inevitable presence in wastewater which can have significant impact in environment and human health because of their acute toxicity. With the same aim of respecting the environment, nowadays, development of new generation of renewable and cost-effective value-added chemicals such as catalysts from sustainable, widely available, and low-cost precursors through environmentally friendly procedures is crucial. For this, and for the first time, graphene synthesized from sucrose, a natural disaccharide, as carbon resource, using bentonite, a natural inorganic multilayered nanomaterial, as a nanostructured template and pyrolysis green process as a scalable approach for producing carbonaceous materials, was used for the supporting of metal nanoparticles. The as-synthesized graphene-like nanomaterial (GHN) was then largely functionalized by epoxy reactive moieties (Chen et al., 2012; Tang et al., 2016). Owing to enhanced epoxy reactive groups density at the surface of GHN and stability/durability of functionalized GHN nanohybrid, two epoxy-based surface modifiers have been used to covalently functionalize GHN. First, (3-glycidyloxypropyl) trimethoxysilane (GPTMS) was grafted on both clay and graphene sheets of GHN with the double advantage of decoration of surface with epoxy moieties and delamination of the clay and graphene sheets. Then, due to their improved dispersion quality, the surface of GHN becomes more accessible which enable it to be used for further grafting of tris(4-hydroxyphenyl)methane triglycidyl ether (TGE). TGE trifunctional epoxy was used here as a surface modifier for covalent functionalization of graphene sheets in GHN, following method previously reported by Martinez-Rubi for producing a soft covalently bonded interface around the SWCNT (Martinez-Rubi et al., 2011).

The ring-opening of the grafted reactive epoxy groups using $\text{KMnO}_4/\text{H}_2\text{SO}_4$ led to their readily convert to chelating carboxylic acid group (Sui et al., 2013). The deprotonated COOH grafted to GHN surface has been exploited to anchor large number of Pd^{2+} metallic ions viacomplexation reaction. The complexed Pd^{2+} were subsequently in-situ reduced for the generation of uniformly dispersed nano-scale palladium particles on GHN surface. Finally, the novel designed GHN- $\text{COOH}@$ PdNPs nanohybrid material was used as efficient and recyclable heterogeneous nanocatalyst in reduction of different types of dyes.

2. Experimental section

2.1. Chemicals

The sodium bentonite clay (BT) was purchased from Canadian Clay Products, Inc (65-85 meq/100g ion-exchange capacity, 2.6 g/cm^3 density) and used without further treatment. All

the following chemicals were purchased from Sigma-Aldrich and used as received: saccharose ($C_{12}H_{22}O_{11}$, 99.5 %), (3-glycidyloxypropyl) trimethoxysilane (GPTMS, $C_9H_{20}O_5Si$), tris(4-hydroxyphenyl)methane triglycidyl ether (TGE, $C_{28}H_{28}O_6$), sodium cubes, contains mineral oil, 99.9% trace metals basis), naphthalene (99%), palladium chloride ($\geq 99.9\%$), anhydrous toluene (99.8%), anhydrous tetrahydrofuran (99.8%) and sodium borohydride ($NaBH_4$, 99%). The 0.1N sodium hydroxide (NaOH) was purchased from VWR Chemicals BDH Prolabo. The aqueous solutions used in this work were prepared with Millipore water (DI water).

2.2. Preparation of GHN

Graphene-like hybrid nanomaterial was prepared according to the previously described eco-friendly method where natural clay and saccharose were used as precursor materials. Firstly, homogenized BT particles ($< 2\mu m$) were vigorously dispersed in DI water at 83.3 % by weight. After 24 h of swelling at room temperature, the resulting suspension was mixed for 20 min with an aqueous solution of saccharose (2 g/mL by weight) in 1:5 weight ratio (BT: saccharose) using a Velp mixer with a stirring speed of 400 rpm. Subsequently, the mixture was dried in an oven for 48 h at $50^\circ C$, followed by an activation in a furnace at $800^\circ C$ for 1 h at a heating rate of $5^\circ C/min$ under nitrogen flow. Finally, the obtained dark monolith was ground using a mortar and pestle (Pulvirisette 6, Laval Lab Inc.) until the particle size is less than $20\mu m$.

2.3. GPTMS surface functionalization of GHN (GHN-GPTMS)

Initially, 100 mg of GHN powder was homogeneously dispersed in 50 ml of 0.1M HCl under stirring for 15 min. The mixture was then ultrasonicated for 30 min to separate the sheets between them and facilitate the clay surface protonation. The suspension was filtered and rinsed with distilled water for several times to remove Cl^- and any impurities, followed by dried at $60^\circ C$ under vacuum. The obtaining activated graphene/clay GHN-OH was recovered for further use. GHN-GPTMS was prepared by dispersing 100 mg of GHN-OH in 50 ml of anhydrous toluene followed by adding of 2 ml of GPTMS under magnetic stirring. The reaction mixture was heated at $50^\circ C$ and the suspension was continued stirring for 16 h under an inert atmosphere. The silanized product was collected by centrifugation after vigorous washing with water and ethanol and later dried at $60^\circ C$ overnight.

2.4. TGE surface functionalization of GHN (GHN-TGE)

Prior to TGE grafting on the surface of GHN and in order to improve its dispersion, GHN was treated with an alkali metal (Na) in the presence of naphthalene which play the role of electron transfer mediator (Pénicaud et al., 2005). Then, 100 mg of GHN was dispersed in 50 ml of anhydrous toluene by stirring for 15 min and sonication for 30 min. Separately 550 mg of naphthalene and 100 mg of sodium were mixed in 100 mL of anhydrous toluene with constant stirring at room temperature for few minutes. The colloid solutions were mixed under an inert atmosphere for 16h of stirring. Afterwards, the reaction mixture was washed by ethanol drop wise adding up to disappearance of the observed gas release, indicating the total unreacted sodium removal. Followed by purification of reaction mixture using rinsing with ethanol, water and then with acetone. Then it was dispersed in 100 mL of anhydrous THF by magnetic stirring and ultrasonication for 15 min, 2.3 g of TGE (10^{-1} M) was added to the suspension and the mixture was stirred at room temperature overnight under an inert atmosphere. The GHN-TGE functionalized powder was filtered and washed several times with THF, with water and then with ethanol. The product was dried in vacuum at 60 °C.

2.5. Post functionalization of GHN (GHN-GPTMS-TGE / GHN-TGE-GPTMS)

A dual surface functionalization of GHN was carried out with GPTMS and TGE going step by step. For this, GHN-GPTMS was post-functionalized by TGE and vice versa GHN-TGE by GPTMS in the same conditions as in the case of mono functionalization.

2.6. Ring opening of the epoxide modified GHN (GHN-COOH)

G/MMT-GPTMS-TEG was dispersed in sulfuric acid (1M) with constant stirring then filtered after vigorous washing with water. After, an aqueous solution of potassium permanganate (20 mg) was added and the mixed solution was stirred for few hours at room temperature. The obtained nanostructure (GHN-COOH) was filtered and washed with water to remove residuals, followed by dried in a vacuum oven.

2.7. Immobilization of palladium nanoparticles (GHN-COOH@PdNPs)

GHN-COOH@PdNPs nanohybrids were prepared by rapid and easy process. Initially, GHN-COOH was alkaline treated by sodium hydroxide solution (0.1M) to deprotonate the carboxylic acid functions. Subsequently, the product (GHN-COO⁻) was collected without washing and added to a PdCl₂ solution of 10^{-2} M. The mixed solution was stirred for an

overnight at room temperature. To the resulting suspension 10 ml of NaBH₄ solution 0.1 M was added drop wise and stirred for 1h. The obtaining product was filtered and washed several times with water then dried at 60 °C in a vacuum oven.

2.8. Evaluation of catalytic activity of GHN-COOH@PdNPs

The reduction study of alizarin (Alz), methylene blue (MB) and Eosin Y (Eo-Y) was carried out using GHN-COOH@PdNPs nanohybrids catalyst in the presence of aqueous NaBH₄ as a reductant at room temperature. In a typical procedure, nanohybrids catalyst (1 mg) was dispersed in deionized H₂O (1 mL). Then, 0.1 mM of dye solution (Alz or MB or Eo-Y) and NaBH₄ (25 mM) were added. At once, the reaction mixture was placed under continuous stirring into the spectrophotometry to control the reduction progress. The absorption spectra were recorded in the range of 200–800 nm by automatic measuring of dye concentration at regular time intervals. For the evaluation of the catalytic performance of synthesized nanohybridss, reference tests were studied in the reduction of Alz, MB and Eo-Y. In the first hand, to identify the adsorption capacity of nanohybrids, the UV-vis spectra were recorded for the dye solutions without addition of NaBH₄. On the other hand, the UV-vis spectra of the dye concentrations were recorded in the absence of nanohybrids in order to evaluate the contribution of NaBH₄ in the total reduction reaction. The reusability experiments were achieved by reuse of the nanohybrids catalyst several times in the same reaction conditions. After completion of each reaction cycle, the GHN-COOH@PdNPs nanohybridss catalyst was separated out by centrifuge then washed with deionized water and dried at 80°C for the following runs. The reusability efficiency evaluation was achieved by comparison of the reaction kinetics of the different cycles.

2.9. Characterization

The graphitic structure of GHN sample was studied by alpha 300R confocal Raman microscope with a wavelength of 532 nm. The spectra were recorded using Vitec software.

The microstructure and the elemental mapping of GHN were recorded by a SU8230 model scanning electron microscope (SEM, Hitachi) operated at 10 kV equipped with an Oxford energy dispersive X-ray spectrometer detector (EDS).

Thermal characterization was performed on a Pyris Diamond TGA Perkin Elmer instrument by heating the samples from 25 °C to 800 °C at 10 °C.min⁻¹ under pure N₂ atmosphere.

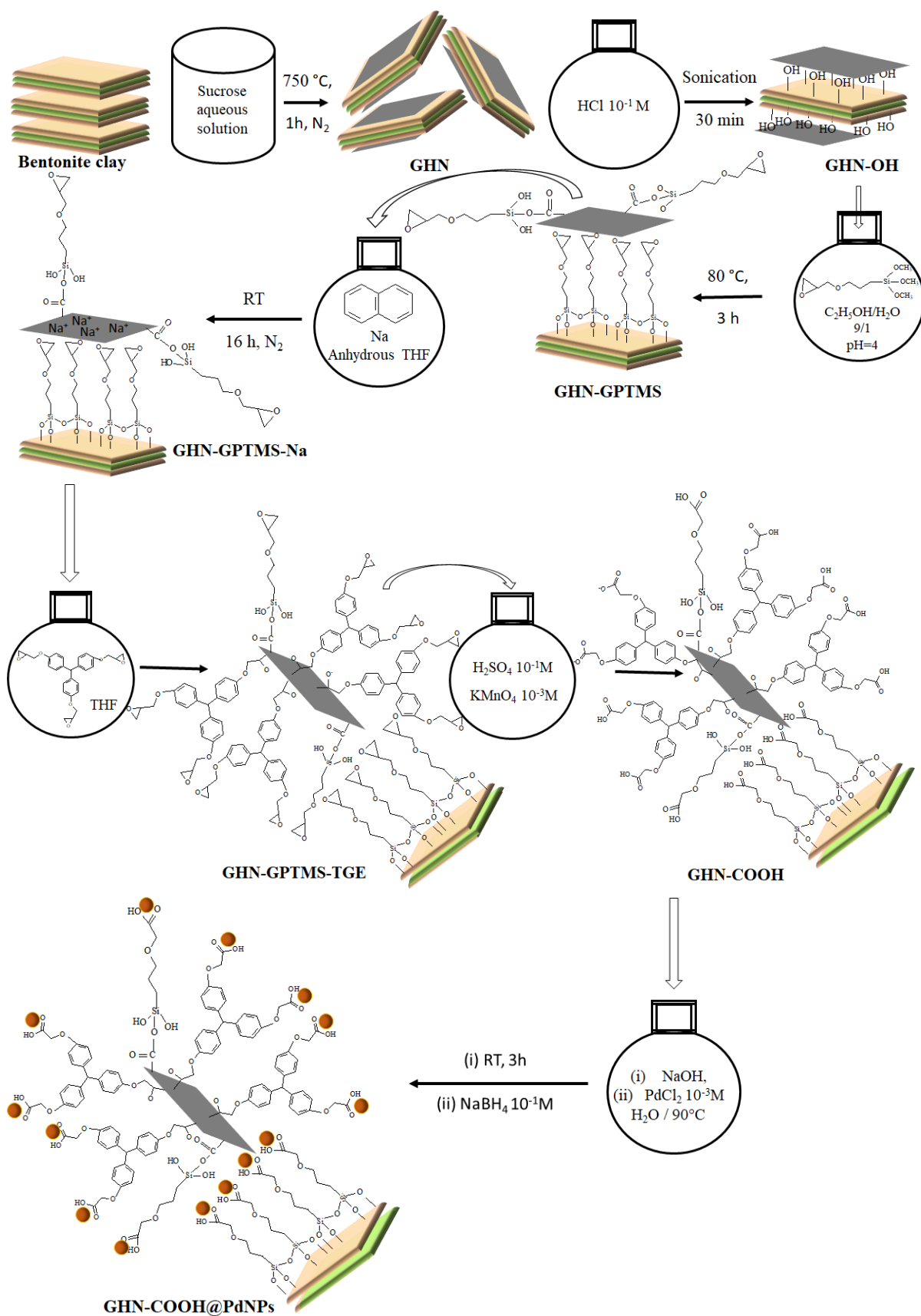
To characterize the synthesized nanohybrids, structural analyses were accomplished through X-ray diffraction measurements (XRD) and X-ray photoelectron spectroscopy (XPS)

technics. XRD analysis of the GHN-COOH@PdNPs hybrid catalyst was carried out on a Bruker D8 advance diffractometer. The XRD spectra of the powdered sample was recorded between a scan angles 10° and 90° using Cu $K\alpha$ ($\lambda = 1.54 \text{ \AA}$) radiation.

The XPS characterization was conducted for elucidating surface composition/elemental chemical states of the prepared nanohybrid materials. The spectra were recorded using Thermo Scientific K-Alpha spectrometer equipped with a monochromatic Al- $K\alpha$ X-ray source ($h\nu = 1486 \text{ eV}$, spot size = $400 \text{ }\mu\text{m}$, pass energy of surveys = 200 eV and of narrow regions = 50 eV), and magnetic lens enables analysis of small areas with increased sensitivity. The charge compensation was provided by a combination of an electron flood gun with an argon ion gun. The collected spectra were analysed by using Advantage software. C1s/O1s atomic ratios were calculated from the intensity of C1s and O1s peaks in survey spectra, multiplied by sensitivity factors (C1s = 1 and s O1s = 2.75).

Morphology and chemical composition of GHN-COOH@PdNPs nanohybrids were investigated with SEM. The analyses were performed with a MERLIN microscope integrated with an energy Energy-dispersive X-ray spectroscopy (EDX) from Zeiss equipped with InLens and SE2 detectors using an accelerating tension 20 kV with a diaphragm aperture of $30 \text{ }\mu\text{m}$. Prior to analyses, the samples were coated with sputtered layer of platinum using a Cressington 208 HR sputter-coater.

UV-vis spectral analysis (Cary 60 spectrophotometer) was performed in the scanning range of $200\text{-}800 \text{ nm}$ to monitor the catalytic performance of GHN-COOH@PdNPs nanohybrids towards the conversion ratio of the dye molecules.



Scheme 3. Schematic representation of the steps for the preparation of supported palladium nanoparticles using graphene like nanomaterial synthesized by a green method via natural precursors.

3. Results and discussion

3.1. Preparation and structural characterization of GHN

The pyrolysis technique is recognized as a green and low-cost synthesis method, which has increased significantly its use in practical applications especially for the generation of carbonaceous materials from biomass (De Silva et al., 2017; Kong et al., 2020). Indeed, using this technique, graphene-like materials were successfully prepared on sand (Gupta et al., 2012) and clays (Azizi et al., 2019; Ruiz-García et al., 2013), using sucrose as source of carbon (Das et al., 2017). Such graphene originated from natural resources has been shown to be promising in various applications such as adsorption of pollutants, energy storage, and reinforcing of polymers. Here, with the aim of using graphene-like nanomaterial (GHN) derived from sucrose through pyrolysis using bentonite clay as a template, to stabilize catalytic palladium nanoparticles, its required functionalization with chelating surface modifiers. Thus, GHN was first functionalized with (3-glycidyloxypropyl) trimethoxysilane (GPTMS) and in a second step with tris(4-hydroxyphenyl)methane triglycidyl ether (TGE). The as-obtained epoxy-rich GHN nanomaterial was then subjected to treatment with $\text{KMnO}_4/\text{H}_2\text{SO}_4$ in order to convert the surface grafted epoxy groups to carboxylic acid used finally to in-situ generate PdNPs from palladium aqueous solution using NaBH_4 as reducing agent. The experimental procedure is presented in detail in *Scheme 3*.

The graphitic nature of the synthesized GHN is confirmed by the Raman analysis in *Figure 23a*. An intense peak at around 1350 cm^{-1} (D band) corresponds to the sp^3 carbon atoms of disordered graphene sheets and a second less intense peak near 1570 cm^{-1} (G band) is attributed to the in-plane vibration of sp^2 carbon atoms. A smaller peak appears at higher frequency ($\sim 2750\text{ cm}^{-1}$) and is also a sp^2 Raman signature. Both G band and 2D band reflect the crystalline structure of graphitic carbon (Jorio et al., 2011). It is observed that the amorphous carbon reflected by the D band is prominent which means a high defect level. This is probably due to the formation of bonds with carbon atoms having sp^3 hybridization and the functionalization of graphene (Hoepfner and Pezzin 2016). To evaluate the disorder of GHN, the ratio of the D to G peak intensities ($I_{\text{D}}/I_{\text{G}}$) is calculated (~ 1.09) suggesting a partial amorphous nature of GHN resulting from the extensive oxidation (Ganguly et al., 2011; Stankovich et al., 2007; Zhuo et al., 2013). It was reported that during the oxidation reaction, disordered sp^3 -oxidized domains with various oxygen functional groups (such as epoxides, ketones, hydroxyls, carbonyls) could surround the sp^2 graphitic domains (Hansora et al., 2017).

The XPS survey and high-resolution of the C1s region of GHN are shown in **Figure 23b and c**. For the survey spectrum, the peaks centered at around 74.4, 102.7, 119.5, 152.8, 533.4, and 1072 eV are attributed to Al2p, Si2p, Al2s, Si2s, O1s, and Na1s clay constituting atoms, respectively. The spectrum also exhibits strong peak at 284.4 eV assigned to C1s, evidencing the presence of graphene sheets (a carbonaceous nanomaterial) on the surface of bentonite layers.

The C1s spectrum of GHN is fitted with five peak components attributed to the sp² graphite component (C=C) at 284.2 eV, the sp³ bonded carbon (C-C /C-H) at 285.6 eV, the epoxide group and alcohol groups (C-O-C/C-OH) at 286.7 eV, the carboxyl groups (HO-C=O) at 288.5 eV and π - π^* transition satellites at 290.5 eV; which is in full accordance with the Raman results.

The microstructure and the elemental mapping of GHN are shown in **Figure 23-d** and clearly substantiate the formation of a graphene/clay composite material. The surface morphology of GHN shows the aggregated arrangement of graphene nanosheets and the clay layers. This result is in line with previous study (Narayanan et al., 2020). The elemental mapping indicates the presence and the good distribution of C, O, Na, Mg, Al, Si and Fe in the composite. Both carbon and oxygen are originated from graphene while other elements are originated from clay minerals with a predominant amount of Si (19.61 % of total mass) compared to the other elements of clay. The graphitic nature of GHN and the presence of exogenous groups are also confirmed by the high proportion of carbon, which represents 50.51 % of total mass, and oxygen (22.49 % of total mass).

Thermal stability of nanomaterial (clay/graphene) is investigated and compared to each precursor (clay and sucrose) by TGA analysis. An important variation in weight loss is observed as shown in **Figure 23-e**. The bentonite curve presents 3 stages corresponding to the dehydration (under low temperature), the elimination of the water coordinated to the interlayer cations (at higher temperature) and the dehydroxylation (above 500 °C) (Donoso et al., 2010). The thermal profile of sucrose exhibits three phases corresponding to the evaporation of the surface adsorbed moisture (~ 100 °C), the decomposition of -OH groups and liberation of CO, CO₂ and H₂ (from 209 °C to 340 °C) and the 100% weight loss (322-558°C) (Eggleston et al., 2012). Thermal decomposition of clay/graphene composite has occurred in four stages: desorption of the interlayer water (< 150 °C), liberation of oxygen functional groups (150-400 °C) the oxidation of the carbon skeleton of graphene (400-700 °C), and dehydroxylation of the structural O-H (700 to 800 °C) (Gong et al., 2014; Ouellet-Plamondon et al., 2014). It is observed that the total mass loss of composite is 60 % which is

located between that of clay and sucrose. This suggests the existence of a strong attachment between these two components which is due to interaction between hydroxyl groups presenting in sucrose and the bentonite clay by hydrogen bonding.

In addition, the above statements were supported by the BET surface area measurements based on nitrogen adsorption. Indeed, the specific surface area of GHN (S_{BET} of 266.94 m^2/g) was found to be three times higher than that of BT (87.42 m^2/g). This can be explained by the nano-sandwich structure of GHN formed from graphene and bentonite layers.

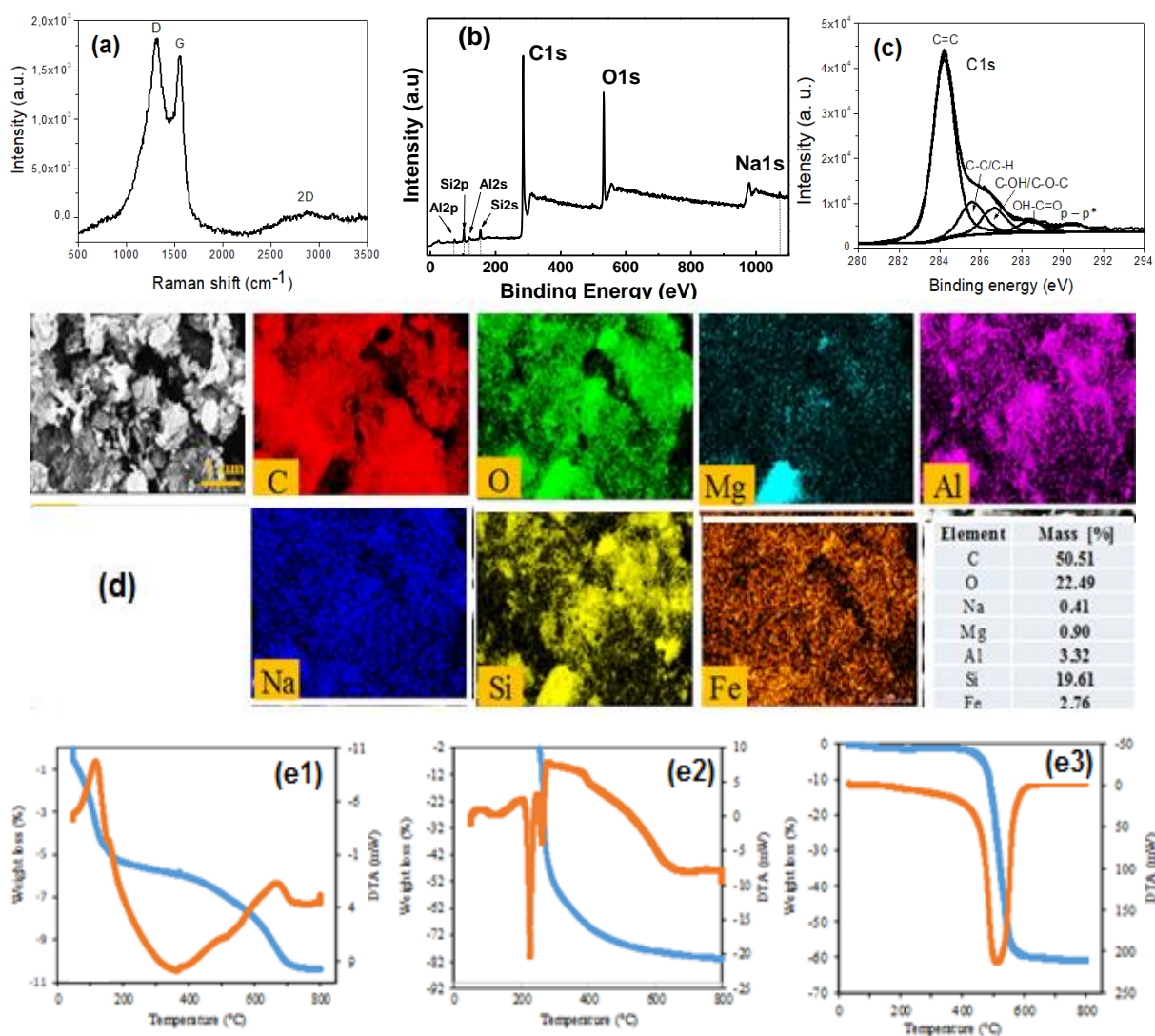


Figure 23. (a) Raman spectrum, (b) XPS survey scan, and (c) XPS C1s high-resolution region, (d) SEM images of GHN, and TGA curves of (e1) bentonite, (e2) sucrose, and (e3) GHN.

3.2. Surface functionalization of GHN

The surface modification of GHN plays a dual role as it facilitates the separation of the clay and graphene layers from each other's preventing their aggregation and imparts appropriate functional groups to the GHN to enable stabilization and well-dispersion of metallic nanoparticles. These properties can easily be tuned by varying both the surface modifiers nature and their grafted density. In this work, two surface modifiers were used for functionalization of GHN. The GHN samples were functionalized by GPTMS and TGE separately and then the samples were post functionalized with the same epoxy-containing surface modifiers; TGE for GHN-GPTMS and GPTMS for GHN-TGE. To testify their grafting on the surface of clay and graphene layers of GHN, details information about the surface composition and the functional groups present on the different samples were obtained by XPS analysis.

Figure 24 shows a comparison of the survey spectra of pristine and functionalized GHN. All spectra show the presence of both clay and graphene related elements the same as those detected in pristine GHN, confirming that the structure of GHN was preserved upon functionalization. In addition, both C1s (~284 eV) and O1s (~532 eV) peaks intensities in all functionalized GHN samples are much higher comparing to the C1s and O1s in pristine GHN, providing strong evidence for the grafting of molecule rich in carbon and oxygen on the surface of GHN; GPTMS ($C_9H_{20}O_5Si$) and TGE ($C_{15}H_{19}NO_4$). The detail of surface composition calculated from the survey spectra is given in the **Figure24**. The differences between the values of O1s/C1s atomic ratios of each functionalized GHN reveal that the degree of surface functionalization was varied as a function of surface modifier nature as well as their order of grafting when two epoxy-containing molecules were used. From these results, one can notice that the degree of functionalization varied in the following order: GHN-TGE < GHN-TGE < GHN-TGE-GPTMS < GHN-GPTMS-TGE. For better understanding of chemical changes occurred upon GPTMS and TGE grafting, C1s high-resolution spectra depicted in **Figures 25 b-e** were investigated and as it can be seen evident differences are exhibited between spectra profiles. The deconvolution of the C1s spectrum of GHN-GPTMS is fitted with four peak components centered at 284.2, 285, 286.2, and 288.5 eV attributed to C_{sp2} , C_{sp3} , C-O-C (ether/epoxy), and C-O-Si in agreement with the chemical structure of GPTMS at the surface of the GHN nanomaterial, respectively. For GHN treated with TGE, the C1s spectrum could be deconvoluted into four peaks centered at 284.2, 285, 286,4 and 288 eV assigned to C_{sp2} , C_{sp3} , C-O-C (ether/epoxy), C=O (aldehyde), respectively. It is worthy to note that the C=O of aliphatic aldehyde component may be originated from the

isomerization of epoxy groups (Martinez-Rubi et al., 2011). All these results confirmed the presence of GPTMS and TGE on the surface of GHN samples. However, one can notice that the contribution of C-O-C component of GHN-GPTMS is larger than that of GHN-TGE. This can probably be explained by the fact that the GPTMS silane coupling agent can bind to both edges and internal surface of clay and graphene layers while TGE can only be grafted onto graphene.

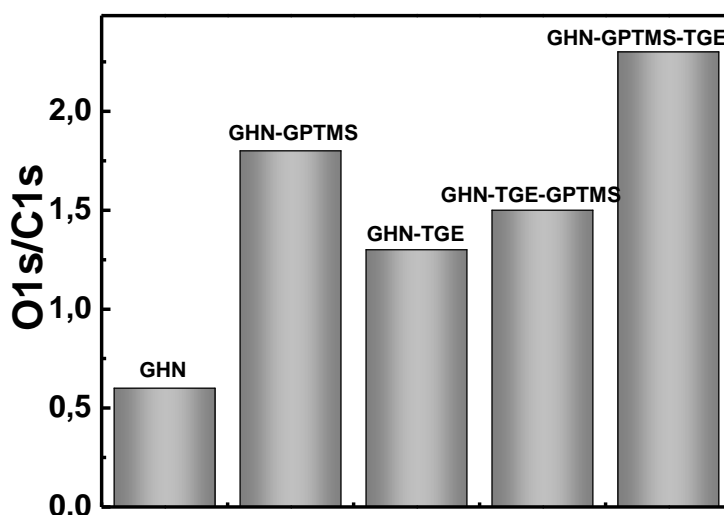


Figure24. Atomic fraction and values of O1s/C1s ratios of pristine and all functionalized GHN samples.

By comparing between C1s spectra of GHN-GPTMS-TGE with GHN-TGE-GPTMS, the degree of grafting is largely higher in the case where GHN was first treated with GPTMS then followed by TGE, indicating an enhanced C-O-C epoxy component at 286 eV in accordance with the higher O1s/C1S ratio of GHN-GPTMS-TGE than GHN-TGE-GPTMS (**Figure24**).

This marked difference can be explained by the delamination of the graphene and the clay layers after grafting of GPTMS which facilitates the penetration of TGE molecules in between the layers and thus their grafting. In contrast, when TGE was used first, the grafting density is low as shown above, which results in poor dispersion of GHN and thus limiting the accessibility of GPTMS molecules to the internal surface of graphene and clay.

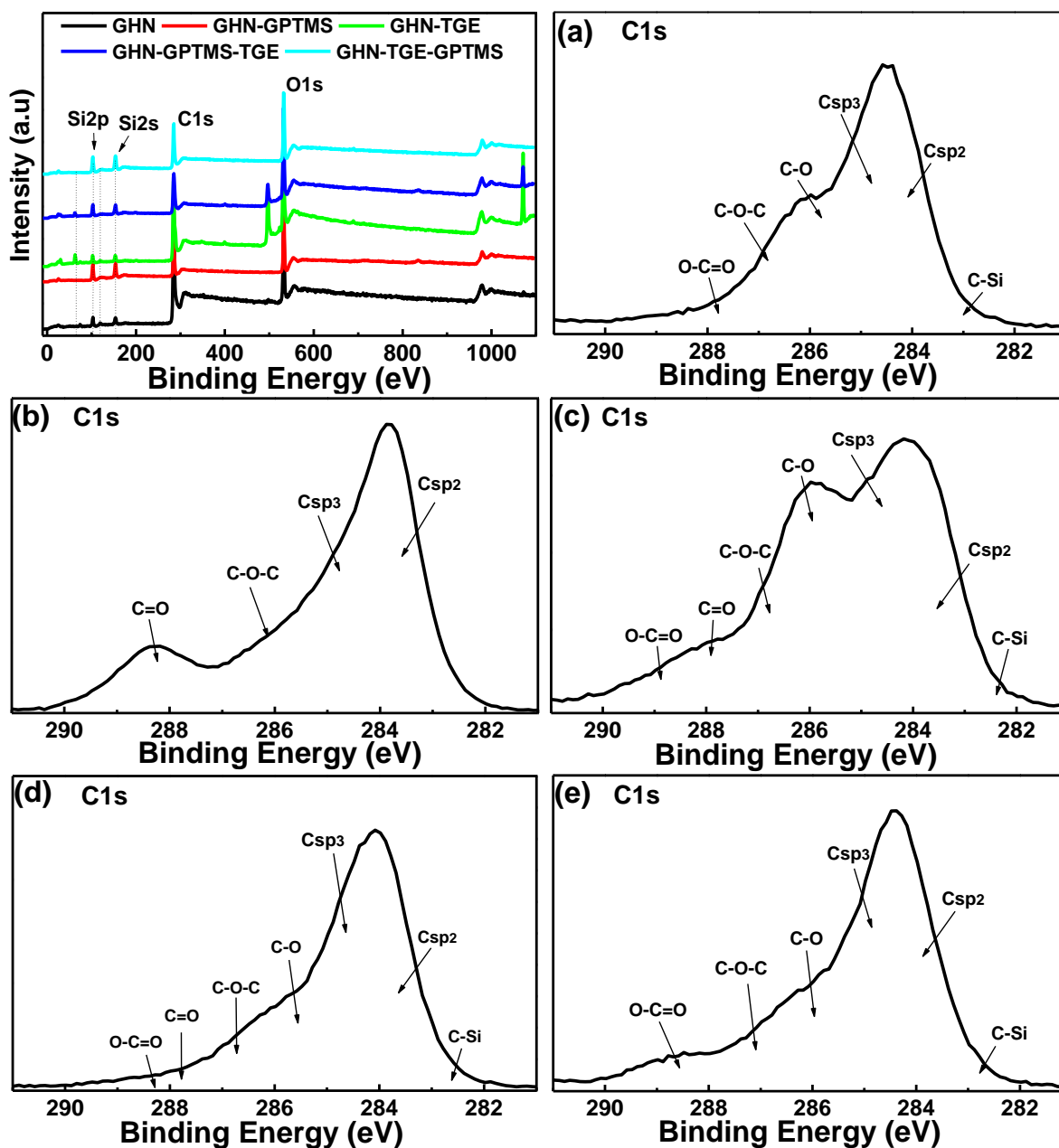


Figure 25. XPS survey and C1s high-resolution spectra of (a) GHN-GPTMS, (b) GHN-TGE, (c) GHN-GPTMS-TGE, (d) GHN-TGE-GPTMS, (e) GHN-COOH prepared by conversion of epoxy groups of GHN-GPTMS-TGE to carboxylic acid ones.

3.3. Palladium nanoparticles decorated GHN

The functionalized GHN nanohybrid contains large density of carboxylic acid moieties at the surface, allowing palladium nanoparticles to growth and bind to the GHN layers since COOH functional group is an effective complexing agent for divalent cations, such as Pd²⁺ (Mahouche Chergui et al., 2010).

SEM analysis is carried out to evaluate the distribution and dispersion state of palladium nanoparticles generated on the surface of the carboxylate-rich GHN nanohybrid. **Figure 26a** clearly shows that the surface of the layered nanohybrid material was fully covered with homogeneously and uniformly distributed PdNPs. Energy dispersive X-ray analysis (EDX) was used to identify the elemental composition of the nanohybrid. The EDX spectrum shown in **Figure 26b** revealed a signal of palladium centered at 2.85 eV with an estimated amount around 14 wt.%. The dense covering of the surface of GHN with PdNPs was indicative of the effectiveness of surface functionalization.

To provide information about the nature of the palladium generated on the GHN-COOH nanohybrid, XPS was performed and the result is shown in **Figure 26c**. It can be obviously seen from the Pd 3d XPS high-resolution spectrum intense doublet peaks at 335.6 and 340.7 eV binding energies assigned to 3d_{5/2} and 3d_{3/2} electronic state of zero valent palladium, respectively, confirming the successful formation of PdNPs on the surface of GHN. In addition to Pd (0), shoulders of the main peaks are also detected at higher binding energies values of 337 and 343 eV, characteristic of the Pd (II) ions, which can be explained by the oxidation of a small amount of PdNPs to form PdONPs. These results are close to those reported in the literature for supported palladium nanoparticles (Zeng et al., 2016).

The XPS results were supported by XRD characterization, as shown in **Figure 26d**. The typical pattern of GHN@PdNPs presents different planes of this nanomaterial (Qiu et al., 2019). While, the peaks at about $2\theta = 39.95, 46.16, 68$ and 81.5° are related to the (111), (200), (220) and (311) diffraction peaks for face-centered-cubic structure palladium crystals (Saikia et al., 2016), demonstrating that the palladium nanoparticles were successfully in-situ generated on the surface of GHN nanohybrid. It is noteworthy that the narrow and intense peak observed at $2\theta = 26,5^\circ$ corresponding to the diffraction from (002) plane, confirms that the highly ordered structure of GHN was preserved.

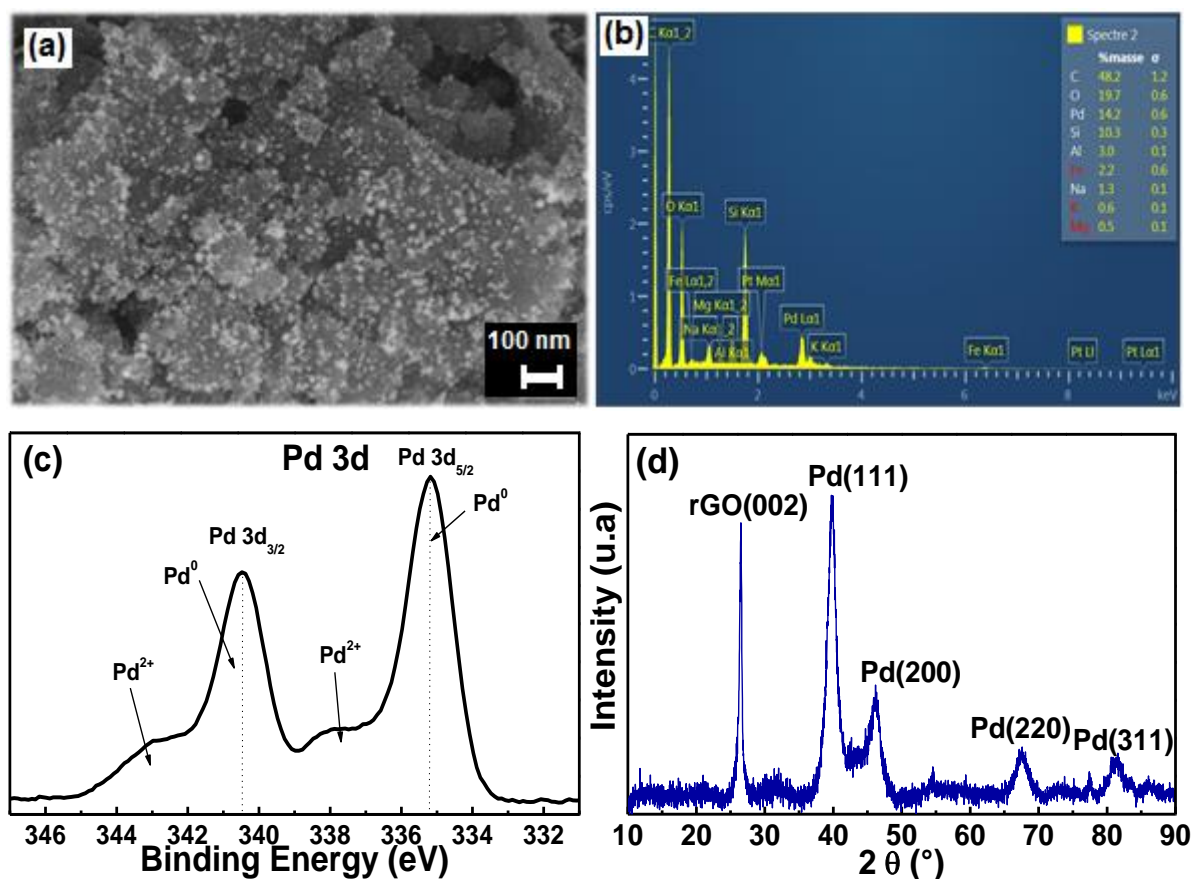


Figure 26. (a) SEM image, (b) EDS spectrum, (c) Pd 3d high-resolution XPS spectrum, (d) XRD pattern of GHN-COOH@PdNPs.

3.4. Catalytic properties of GHN-COOH@PdNPs

In order to evaluate the catalytic activity of the palladium nanoparticles-decorated hybrid nanomaterials, the reduction of dyes, namely Alz, MB and Eo-Y was chosen as a model reaction under the action of NaBH₄ as reducing agent. Firstly, the adsorption properties of synthesized nanohybrid as well as the reduction capacity of NaBH₄ in the absence of catalysts were checked and presented in **Figure 27**. For this, an amount of 1 mg of catalyst was dispersed in 1 mL of water and sonicated for 4 min before mixed with dye solutions. Thus, the adsorption of the dyes by the nanohybrids was studied without introducing of NaBH₄ and the absorbance variation was monitored by time dependent UV-vis spectrophotometry. The experimental results show that no obvious decrease of the intensities of adsorption peaks of Alz, MB and Eo-Y was detected as well as no visible change on the initial dye solution colour was observed after 24h of contact time. The slight decrease of the characteristic adsorption peaks may be due to the adsorption effects by the complexation of dye molecules into the modified GHN structure (Bhawani et al., 2019; Fu et al., 2016).

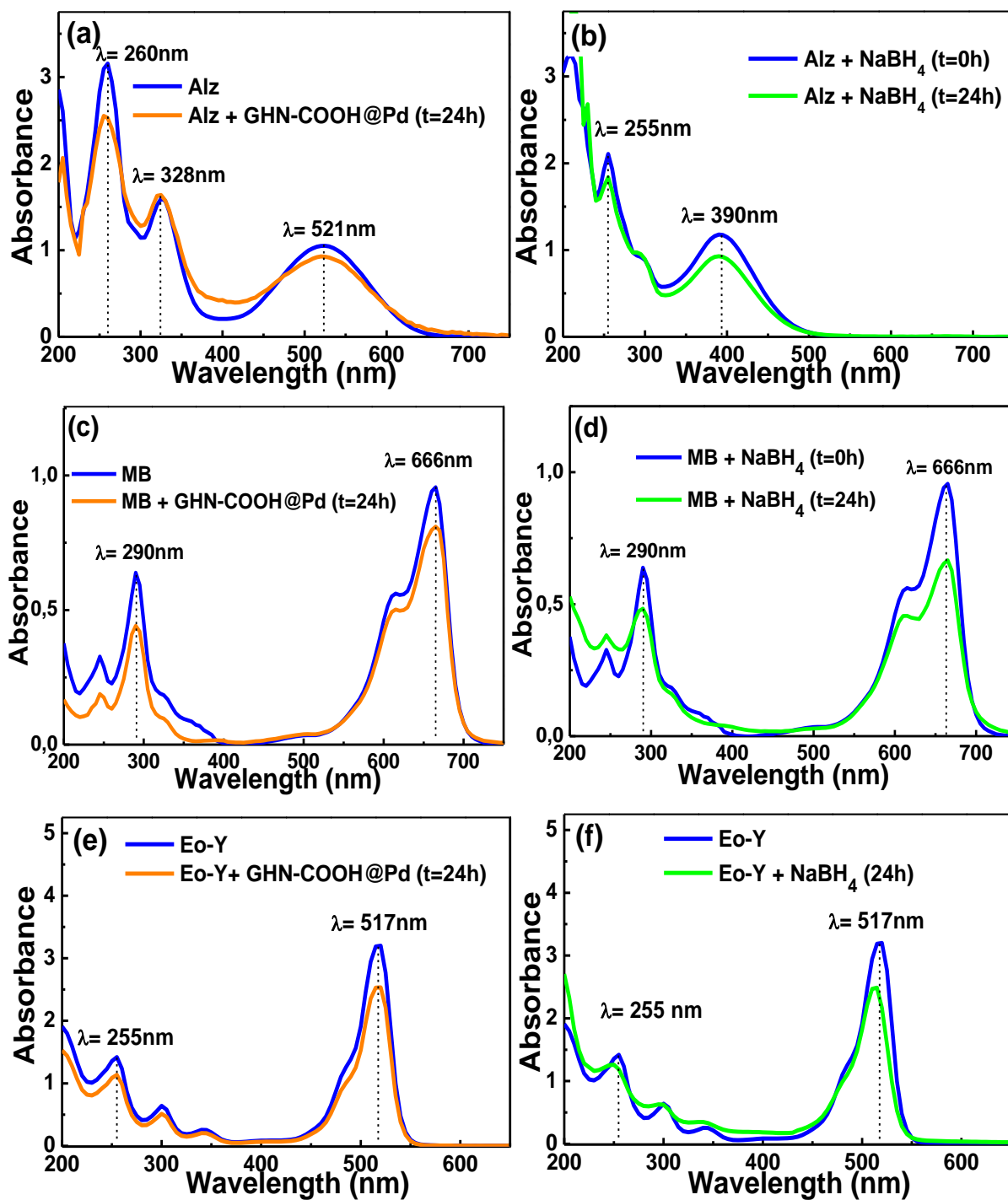


Figure 27. (a, b, c) UV-vis absorption spectra of pure (blue) ALZ, MB, and Eo-Y, and (red) 24h after addition of GHN-COOH@PdNPs nanocatalyst without NaBH₄, respectively. (b, d, f) UV-vis absorption spectra of pure (blue) ALZ, MB, and Eo-Y, and (green) 24h after addition of an excess NaBH₄ without catalyst, respectively. Reaction conditions: [Dyes] = 0.1 mM, [NaBH₄] = 25 mM, [GHN-COOH@PdNPs] = 0.25 g/L.

Furthermore, when the dye solutions were mixed with freshly prepared aqueous solution of NaBH_4 in the absence of the Pd nanocatalyst, a partial reduction of the characteristic adsorption peak at 390 nm, 666 nm and 517 nm corresponding to Alz, MB and Eo-Y occurred respectively. These investigations showed that in the absence of PdNPs, very slow and slight decrease of the intensity of the characteristic peak of each dye was occurred even after a long time (24h).

To investigate the catalytic activity of the GHN-COOH@PdNPs nanohybrid, a higher NaBH_4 concentration of 25 mM was used as compared to that of dyes ($[\text{Alz}] = [\text{MB}] = [\text{Eo-Y}] = 0.1 \text{ mM}$). The catalytic reduction, at room temperature, of dye solutions was carried out by introducing 1 mg of nanohybrids catalyst in the “dyes/ NaBH_4 ” solution.

The recorded UV-Vis spectra (**Figures 28 a-c**) showed a rapid decrease in the intensity of the maximum absorption band (λ_{max}) at 390 nm, 666 nm and 517 nm of Alz, MB and Eo-Y dye solutions respectively. The catalytic conversion was found to be complete and rapid in the presence of PdNPs. Based on these results, we can conclude that the catalyst surface is the key condition which contributes to achieve a total conversion with a fast reaction rate. However, the reduction process was achieved by the electron's transfer from the BH_4^- anions with high nucleophilicity (as electron donor species) to the dyes (as electron acceptor species) through the catalyst surface (Li et al., 2015). At the first, functionalized GHN adsorbs the dye molecules through π - π interaction which increases their concentrations into the nanohybrids and bring closer the PdNPs surface to the dye molecules (Li et al., 2015; Nejad et al., 2019). Subsequently, the diffusion of both dyes and BH_4^- anions to the surface of the metal was occurred. Then, the hydride source was rapidly transferred from BH_4^- anions to dyes mediated by the catalyst surface thereby allowing to reduce the activation energy and thus accelerate the reaction (Nejad et al., 2019). Finally, the reduced dyes products desorbed from the catalyst surface which provides a free surface where Alz, MB and Eo-Y adsorbs again to continue the following reaction (Nejad et al., 2019). **Figure 28a-c** depict the UV-Vis spectra for the reduction of Alz, MB and Eo-Y, respectively, by NaBH_4 in the presence of GHN-COOH@PdNPs nanocatalysts recorded every 30s to track the reaction progressing. It was found that the catalytic reduction the dyes happened immediately and the intensity of the characteristic UV-Vis absorption peaks of Alz (390 nm), MB (666 nm) and Eo-Y (517 nm) decrease within 210s, 240s and 420s respectively. Accordingly, a total decolorizing of dye solutions at the end of the reaction was observed. As shown in **Figure 28d**, a linear correlation between $\ln(A/A_0)$ versus reaction time (in second) was established in the degradation reaction of the three dyes. This observation suggests that the degradation reaction

can be treated as a pseudo-first-order kinetics reaction. The reaction rate constants of Alz, MB and Eo-Y dyes reduction were calculated from the plot of $\ln(A/A_0)$ versus time and were found to be $k = 1.6 \cdot 10^{-2} \text{ (s}^{-1}\text{)}$, $k = 1.65 \cdot 10^{-2} \text{ (s}^{-1}\text{)}$ and $k = 0.9310^{-2} \text{ (s}^{-1}\text{)}$, respectively.

These results proved that the NaBH_4 alone is insufficient to reduce the dyes and this requires the presence of a catalyst to accelerate the kinetic reaction as it has been already demonstrated in other reduction reactions (Li et al., 2015; Nejad et al., 2019). Indeed, it is important to highlight the essential role of the palladium nanoparticles which act as mediator surface for electrons transfer from BH_4^- donor species to the dyes acceptor molecules (Li et al., 2015; Ncube et al., 2015), which favored the kinetic and thermodynamic reduction of dyes.

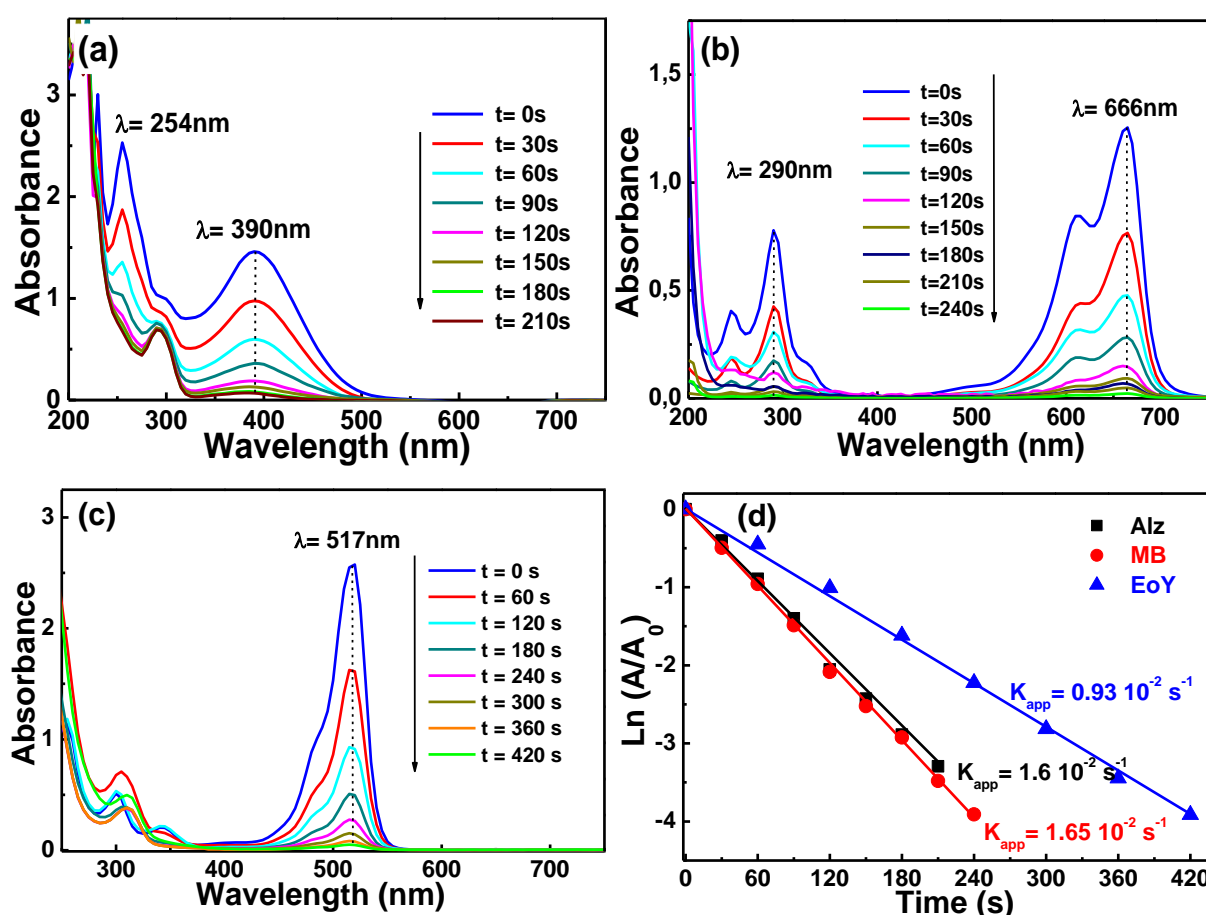


Figure 28. Time-dependent of UV–Vis absorption spectra showing the gradual of the reduction of (a) Alz, (b) MB and (c) Eo-Y. (d) Plots of $\ln(A/A_0)$ versus reaction time for pseudo-first-order reaction for the reduction of Alz, MB and Eo-Y at room temperature by using excess NaBH_4 in the presence of GHN-COOH@PdNPs as catalysts. Reaction conditions: $[\text{Dyes}] = 0.1 \text{ mM}$, $[\text{NaBH}_4] = 25 \text{ mM}$, $[\text{GHN-COOH@PdNPs}] = 0.25 \text{ g/L}$.

In order to evaluate the benefits of the synthesis method followed in our work, the catalytic performance of the PdNPs decorated carboxylate-rich graphene-like nanomaterial was compared to those reported in literature.

As seen in the **Table 4**, the nanohybrids catalyst synthesized in our work exhibits an excellent catalytic efficiency compared to other reported Pd catalysts for the reduction of organic dyes. For best knowledge, this high catalytic activity could be attributable to three main reasons.

Table 4. Comparison of literature results obtained with Pd PNs catalysts for the reduction of various dyes.

Catalyst	Dye molecule	k_{app} ($10^{-2} s^{-1}$)	Time (min)	Reference
Pd ₇₅ Au ₂₅ /Dens-OH	MO	0.587	3.5	Ilunga et al., 2017
GO/Pd nanocomposite			5	Omidvar et al., 2017
Natrolite zeolite/Pd nanocomposite			5	Hatamifard et al., 2015
Pd-PEI-RGO	MB	0.74	6	Li et al., 2015
Pd-TNPs/RGO nanohybrid		0.66	7	Fu et al., 2013
PDA-RGO/Pd		0.4	13	Fu et al., 2016
Pd NPs/Fe ₃ O ₄ -PEI-RGO nanohybrids	MO R6G RB	-	10	Su et al., 2017b
Si/Pd catalyst	Eo-Y	0.11	20	Wang et al., 2009
GO/Pd NCs	CV	0.48	-	Sivaranjan et al., 2017
GO/Ru-Pd NCs		0.55	-	
GO/Pd NCs	MG	0.47	-	
GO/Ru-Pd NCs		0.54	-	
GHN/Pd nanocomposite	MB	1.65	4	<i>This work</i>
	ALZ	1.6	3.5	
	Eo-Y	0.93	7	

Firstly, the homogeneous Pd NPs loading on the two-dimensional graphene oxide surface allows to a high surface area for complexing the dye molecules (Bhawani et al., 2019; Nejad et al., 2019). Secondly, the organic functionalization process of the graphene-like nanomaterial surface lead to a greater stabilizing of Pd NPs and inhibits the aggregation of the small-sized nanoparticles (Wu et al., 2013; Xu et al., 2008). Thirdly, the good dispersion of the nanohybrids catalysts in water provides a high efficient contact between the catalytic sites (Pd NPs) and the exposed dye molecules (Hemmati et al., 2018; Li et al., 2015).

Furthermore, these three factors cause a very high reduction rate with respect to the previously reported ones. Interestingly, this work demonstrates a facile and efficient approach for preparing supported Pd nanocomposites as well as its great benefices in the catalytic reduction of hazardous dyes solutions. Finally, the synergistic effects between the Pd NPs and the silane modified graphene oxide structure makes of our nanohybrid catalyst a promising candidate for more wide catalysis applications (Navalon et al., 2016; Zhuo et al., 2013).

3.5. GHN-COOH@PdNPs Catalyst regeneration

Although GHN-COOH@PdNPs promoted a great catalytic efficiency, it is typically vital to assess the nanocatalyst stability as an influencing factor in the practical application. Therefore, recyclability of GHN-COOH@PdNPs in the catalytic reduction of MB (10^{-4} M) in presence of NaBH₄ was investigated for 8 consecutive cycles. At the end of each reduction cycle, the nanohybrid catalyst was readily separated from the reaction mixture by centrifugation, washed with water and ethanol, dried under vacuum, and then reused in the same reaction conditions for the next catalysis cycle. By comparing the degradation rates of eight reduction cycles, it is found that not considerably change in the reduction activity and the catalyst exhibited a similar catalytic efficiency, as shown in **Figure 29**. Therefore, the high catalytic performance, the great stability and the easy recycling make the GHN-COOH@PdNPs catalyst a promising nanohybrid material for environmental remediation.

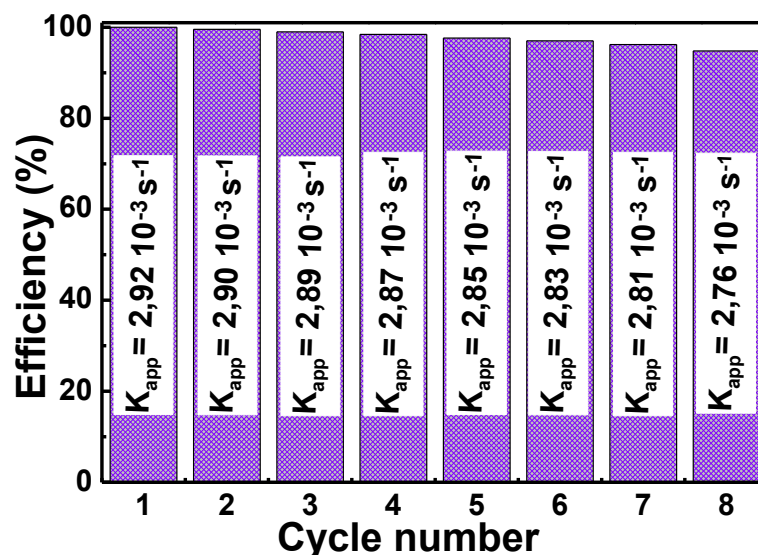


Figure 29. Reusability of GHN- GHN-COOH@PdNPs catalyst for the reduction of MB with NaBH₄ for eight cycles.

4. Conclusion

In summary, a dual surface functionalization of graphene-like nanomaterial (GHN) prepared from natural precursors was reported for the first time. GHN with a large specific surface area (S_{BET} of 266.94 m²/g) were generated from sucrose through pyrolysis green process. Subsequent functionalization of GHN by two different epoxy-containing molecules, namely GPTMS and TEG, followed by ring opening of the epoxy reactive groups *via* an oxidation reaction by H₂SO₄/K₂Cr₂O₇, allowed for the introduction of a high density of carboxylic acid functions onto the GHN surface. The as-designed GHN-COOH nanohybrid was first deprotonated using NaOH solution and then used as support for complexation of Pd²⁺ ions to finally in-situ reduce them to palladium nanocrystals using NaBH₄ as a mild reducing agent. The GHN-COOH@PdNPs nanohybrid exhibits excellent catalytic performance in the reduction of dyes in aqueous solution and can be recycled *for 8 consecutive cycles* while retaining its catalytic activity. This is as a result of the high stabilization of the Pd NPs on the GHN-COOH platform induced by the strong interaction between the Pd NPs and the grafted carboxylic acid groups. Due to the well-known versatility of epoxy groups, the sustainable strategy proposed here can straightforwardly be used to prepare various other heterogeneous catalysts by incorporating desired chelant moieties onto epoxy decorated GHN and hence use them as selective supports for high variety of catalytic metal nanoparticles.

References

A

Azizi, S., Ouellet-Plamondon, C.M., Nguyen-Tri, P., Fréchette, M., David, E., 2019. Electrical, thermal and rheological properties of low-density polyethylene/ethylene vinyl acetate/graphene-like composite. *Composites Part B: Engineering*. 177, 107288.

B

Bashir, B., Rahman, A., Sabeeh, H., Khan, M.A., Aly Aboud, M.F., Warsi, M. F., Shakir, I., Agboola, P. O., Shahid, M., 2019. Copper Substituted Nickel Ferrite Nanoparticles Anchored onto the Graphene Sheets as Electrode Materials for Supercapacitors Fabrication. *Ceramics International*. 45, 6759-6766. doi.org/10.1016/j.ceramint.2018.12.167.

Bhawani, S.A., Tariq, A., Moheman, A., Ngaini, Z., 2019. Chapter 5 - Functionalized Graphene Nanocomposites for Water Treatment, 91-107. In Jawaid, M., Bouhfid, R., Abou el Kacem, Q., (Eds.), *Functionalized Graphene Nanocomposites and their Derivatives*, 368. Elsevier. doi:10.1016/b978-0-12-814548-7.00005-2.

C

Chen, L., Chai, S., Liu, K., Ning, N., Gao, J., Liu, Q., Chen, F., Fu, Q., 2012. Enhanced epoxy/silica composites mechanical properties by introducing graphene oxide to the interface. *ACS applied materials & interfaces*. 4 (8), 4398-4404.

Chen, Z., Cui, Z.-M., Niu, F., Jiang, L., Song, W.-G., 2010. Pd nanoparticles in silica hollow spheres with mesoporous walls: a nanoreactor with extremely high activity. *Chemical communications*. 46 (35), 6524-6526.

D

Das, V.K., Shifrina, Z.B., Bronstein, L.M., 2017. Graphene and graphene-like materials in biomass conversion: paving the way to the future. *Journal of Materials Chemistry A*. 5 (48), 25131-25143.

De Silva, K., Huang, H.-H., Joshi, R., Yoshimura, M., 2017. Chemical reduction of graphene oxide using green reductants. *Carbon*. 119, 190-199.

Dong, W., Cheng, S., Feng, C., Shang, N., Gao, S., Wang, C., 2017. Fabrication of highly dispersed Pd nanoparticles supported on reduced graphene oxide for catalytic reduction of 4-nitrophenol. *Catalysis Communications*. 90, 70-74.

- Dong, Z., Le, X., Dong, C., Zhang, W., Li, X., Ma, J., 2015. Ni@Pd core-shell nanoparticles modified fibrous silica nanospheres as highly efficient and recoverable catalyst for reduction of 4-nitrophenol and hydrodechlorination of 4-chlorophenol. *Applied Catalysis B: Environmental*. 162, 372-380.
- Donoso, J.P., Tambelli, C., Magon, C.J., Mattos, R., Silva, I., Souza, J.d., Moreno, M., Benavente, E., Gonzalez, G., 2010. Nuclear magnetic resonance study of hydrated bentonite. *Molecular Crystals and Liquid Crystals*. 521 (1), 93-103.
- Dutta, D., Phukan, A., Dutta, D.K., 2018. Nanoporous montmorillonite clay stabilized copper nanoparticles: Efficient and reusable catalyst for oxidation of alcohols. *Molecular Catalysis*. 451, 178-185.

E

- Eggleston, G., Yen, J.W.T., Alexander, C., Gober, J., 2012. Measurement and analysis of the mannitol partition coefficient in sucrose crystallization under simulated industrial conditions. *Carbohydrate research*. 355, 69-78.

F

- Fang, H., Zheng, J., Luo, X., Du, J., Roldan, A., Leoni, S., Yuan, Y., 2017. Product tunable behavior of carbon nanotubes-supported Ni-Fe catalysts for guaiacol hydrodeoxygenation. *Applied Catalysis A: General*. 529, 20-31.
- Fu, G., Tao, L., Zhang, M., Chen, Y., Tang, Y., Lin, J.; Lu, T., 2013. One-pot, water-based and high-yield synthesis of tetrahedral palladium nanocrystal decorated graphene. *Nanoscale*. 5 (17), 8007-8014.
- Fu, L., Lai, G., Zhu, D., Jia, B., Malherbe, F., Yu, A., 2016. Advanced Catalytic and Electrocatalytic Performances of Polydopamine-Functionalized Reduced Graphene Oxide-Palladium Nanocomposites. *Chem. Cat. Chem*. 8 (18), 2975-2980.

G

- Ganguly, A., Sharma, S., Papakonstantinou, P., Hamilton, J., 2011. Probing the thermal deoxygenation of graphene oxide using high-resolution in situ X-ray-based spectroscopies. *The Journal of Physical Chemistry C*. 115 (34), 17009-17019.
- Gong, J., Liu, J., Wen, X., Jiang, Z., Chen, X., Mijowska, E., Tang, T., 2014. Upcycling waste polypropylene into graphene flakes on organically modified montmorillonite. *Industrial & Engineering Chemistry Research*. 53 (11), 4173-4181.

Guo, Y., Yang, X., Ruan, K., Kong, J., Dong, M., Zhang, J., Gu, J., Guo, Z., 2019. Reduced graphene oxide heterostructured silver nanoparticles significantly enhanced thermal conductivities in hot-pressed electrospun polyimide nanocomposites. *ACS applied materials & interfaces*. 11 (28), 25465-25473.

Gupta, S.S., Sreeprasad, T.S., Maliyekkal, S.M., Das, S.K., Pradeep, T., 2012. Graphene from sugar and its application in water purification. *ACS applied materials & interfaces*. 4 (8), 4156-4163.

H

Hansora, D.P., Mishra, S., 2017. *Graphene Nanomaterials: Fabrication, Properties and Applications*, 283. Singapore: Pan Stanford. doi: 10.4032/9781315364551.

Hatamifard, A., Nasrollahzadeh, M., Lipkowski, J., 2015. Green synthesis of a natrolite zeolite/palladium nanocomposite and its application as a reusable catalyst for the reduction of organic dyes in a very short time. *RSC Advances*. 5 (111), 91372-91381.

Hemmati, S., Mehrazin, L., Ghorban, H., Garakani, S.H., Mobaraki, T.H., Mohammadi, P., Veisi, H., 2018. Green synthesis of Pd nanoparticles supported on reduced graphene oxide, using the extract of *Rosa canina* fruit, and their use as recyclable and heterogeneous nanocatalysts for the degradation of dye pollutants in water. *RSC advances*. 8 (37), 21020-21028.

Hoepfner, J.C., Pezzin, S.H., 2016. Functionalization of carbon nanotubes with (3-glycidyloxypropyl)-trimethoxysilane: Effect of wrapping on epoxy matrix nanocomposites. *Journal of Applied Polymer Science*. 133 (47). doi:10.1002/app.44245.

Hunger, K., 2003. *Industrial dyes: chemistry, properties, applications*. 648. Weinheim: Wiley-VCH. doi:10.1002/3527602011.

I

Ilunga, A.K., Khoza, T., Tjabadi, E., Meijboom, R., 2017. Effective Catalytic Reduction of Methyl Orange Catalyzed by the Encapsulated Random Alloy Palladium-Gold Nanoparticles Dendrimer. *Chemistry Select*. 2 (30), 9803-9809.

J

Jin, Z., Nackashi, D., Lu, W., Kittrell, C., Tour, J.M., 2010. Decoration, migration, and aggregation of palladium nanoparticles on graphene sheets. *Chemistry of Materials*. 22 (20), 5695-5699.

Jorio, A., Dresselhaus, M.S., Saito, R., Dresselhaus, G., 2011. Raman spectroscopy in graphene related systems, 368. Weinheim: Wiley-VCH. doi: 10.1002/9783527632695.

K

Kaushik, M., Moores, A., 2016. Nanocelluloses as versatile supports for metal nanoparticles and their applications in catalysis. *Green Chemistry*. 18 (3), 622-637.

Kong, X., Zhu, Y., Lei, H., Wang, C., Zhao, Y., Huo, E., Lin, X., Zhang, Q., Qian, M., Mateo, W., 2020. Synthesis of graphene-like carbon from biomass pyrolysis and its applications. *Chemical Engineering Journal*. 125808.

Kou, R., Shao, Y., Mei, D., Nie, Z., Wang, D., Wang, C., Viswanathan, V.V., Park, S., Aksay, I.A., Lin, Y., 2011. Stabilization of electrocatalytic metal nanoparticles at metal– metal oxide– graphene triple junction points. *Journal of the American Chemical Society*. 133 (8), 2541-2547.

L

Li, S., Li, H., Liu, J., Zhang, H., Yang, Y., Yang, Z., Wang, L., Wang, B., 2015. Highly efficient degradation of organic dyes by palladium nanoparticles decorated on 2D magnetic reduced graphene oxide nanosheets. *Dalton Transactions*. 44 (19), 9193-9199.

Liang, Q., Liu, J., Wei, Y., Zhao, Z., MacLachlan, M.J., 2013. Palladium nanoparticles supported on a triptycene-based microporous polymer: highly active catalysts for CO oxidation. *Chemical Communications*. 49 (79), 8928-8930.

Liu, J., Ma, Q., Huang, Z., Liu, G., Zhang, H., 2019. Recent progress in graphene-based noble-metal nanocomposites for electrocatalytic applications. *Advanced Materials*. 31 (9), 1800696.

Luo, S., Zeng, Z., Zeng, G., Liu, Z., Xiao, R., Chen, M., Tang, L., Tang, W., Lai, C., Cheng, M., Shao, B., Liang, Q., Wang, H., Jiang, D., 2019. Metal Organic Frameworks as Robust Host of Palladium Nanoparticles in Heterogeneous Catalysis: Synthesis, Application, and Prospect. *ACS Applied Materials & Interfaces*. 11 (36), 32579-32598.

M

Mahouche Chergui, S.; Ledebt, A., Mammeri, F., Herbst, F., Carbonnier, B., Ben Romdhane, H., Delamar, M., Chehimi, M.M., 2010. Hairy carbon nanotube@ nano-pd heterostructures: design, characterization, and application in suzuki c–c coupling reaction. *Langmuir*. 26 (20), 16115-16121.

- Martinez-Rubi, Y., Ashrafi, B., Guan, J., Kingston, C., Johnston, A., Simard, B., Mirjalili, V., Hubert, P., Deng, L., Young, R.J., 2011. Toughening of epoxy matrices with reduced single-walled carbon nanotubes. *ACS applied materials & interfaces*. 3 (7), 2309-2317.
- Muthu, S.S., (Ed.), 2018. *Sustainable Innovations in Textile Chemistry and Dyes*. Textile Science and Clothing Technology, 91. Singapore: Springer. doi:10.1007/978-981-10-8600-7.

N

- Narayanan, D.P., Gopalakrishnan, A., Yaakob, Z., Sugunan, S., Narayanan, B.N., 2020. A facile synthesis of clay–graphene oxide nanocomposite catalysts for solvent free multicomponent Biginelli reaction. *Arabian Journal of Chemistry*. 13 (1), 318-334.
- Navalon, S., Dhakshinamoorthy, A., Alvaro, M., Garcia, H., 2016. Metal nanoparticles supported on two-dimensional graphenes as heterogeneous catalysts. *Coordination Chemistry Reviews*. 312, 99-148.
- Ncube, P., Bingwa, N., Baloyi, H., Meijboom, R., 2015. Catalytic activity of palladium and gold dendrimer-encapsulated nanoparticles for methylene blue reduction: a kinetic analysis. *Applied Catalysis A: General*. 495, 63-71.
- Nejad, M.S., Seyedi, N., Sheibani, H., 2019. Fabrication of functionalized two dimensional graphene oxide and promoted with phosphotungstic acid for reduction of organic dyes in water. *Materials Chemistry and Physics*. 238, 121849.
- Nollet, L.M.L., 2004. Volume 2: Residues and Other Food Component Analysis. *Handbook of Food Analysis*. 888. Boca Raton: CRC Press. doi.org/10.1201/9781482276466.

O

- Omidvar, A., Jaleh, B., Nasrollahzadeh, M., 2017. Preparation of the GO/Pd nanocomposite and its application for the degradation of organic dyes in water. *Journal of colloid and interface science*. 496, 44-50.
- Ouellet-Plamondon, C.M., Stasiak, J., Al-Tabbaa, A., 2014. The effect of cationic, non-ionic and amphiphilic surfactants on the intercalation of bentonite. *Colloids and Surfaces A: Physicochemical and Engineering Aspects*. 444, 330-337.

P

- Pawlak, K., Puchalska, M., Miszczak, A., Rosłonec, E., Jarosz, M., 2006. Blue natural organic dyestuffs—from textile dyeing to mural painting. *Separation and*

characterization of coloring matters present in elderberry, logwood and indigo. *Journal of mass spectrometry*. 41 (5), 613-622.

Pénicaud, A., Poulin, P., Derré, A., Anglaret, E., Petit, P., 2005. Spontaneous dissolution of a single-wall carbon nanotube salt. *Journal of the American Chemical Society*. 127 (1), 8-9.

Q

Qiu, T., Yang, J.-G., Bai, X.-J., Wang, Y.-L., 2019. The preparation of synthetic graphite materials with hierarchical pores from lignite by one-step impregnation and their characterization as dye absorbents. *RSC advances*. 9 (22), 12737-12746.

R

Rosaiah, P., Zhu, J., Shaik, D.P., Hussain, O., Qiu, Y., Zhao, L., 2017. Reduced graphene oxide/Mn₃O₄ nanocomposite electrodes with enhanced electrochemical performance for energy storage applications. *Journal of Electroanalytical Chemistry*. 794, 78-85.

Ruiz-García, C., Pérez-Carvajal, J., Berenguer-Murcia, A., Darder, M., Aranda, P., Cazorla-Amorós, D., Ruiz-Hitzky, E., 2013. Clay-supported graphene materials: application to hydrogen storage. *Physical Chemistry Chemical Physics*. 15 (42), 18635-18641.

S

Saikia, P.K., Bhattacharjee, R.P., Sarmah, P.P., Saikia, L., Dutta, D.K., 2016. A green synthesis of Pd nanoparticles supported on modified montmorillonite using aqueous *Ocimum sanctum* leaf extract: a sustainable catalyst for hydrodechlorination of 4-chlorophenol. *RSC advances*. 6 (111), 110011-110018.

Şenol, A.M., Metin, Ö., Onganer, Y., 2019. A facile route for the preparation of silver nanoparticles-graphene oxide nanocomposites and their interactions with pyronin Y dye molecules. *Dyes and Pigments*. 162, 926-933.

Sharma, N., Saha, R., Parveen, N., Sekar, G., 2017. Palladium-Nanoparticles-Catalyzed Oxidative Annulation of Benzamides with Alkynes for the Synthesis of Isoquinolones. *Advanced Synthesis & Catalysis*. 359 (11), 1947-1958.

Shipilova, O.I., Gorbunov, S.P., Paperny, V.L., Chernykh, A.A., Dresvyansky, V.P., Martynovich, E.F., Rakevich, A.L., 2020. Fabrication of metal-dielectric nanocomposites using a table-top ion implanter. *Surface and Coatings Technology*. 393, 125742.

- Si, Y., Samulski, E.T., 2008. Exfoliated graphene separated by platinum nanoparticles. *Chemistry of Materials*. 20 (21), 6792-6797.
- Silva M.K.L., Cesarino I., 2019. Graphene Functionalization and Nanopolymers. 157-178. In Khan A., Jawaid M., Neppolian B., Asiri A. (eds.), *Graphene Functionalization Strategies*. 398. Singapore: Springer. doi.10.1007/978-981-32-9057-0_6.
- Singla, R., Guliani, A., Kumari, A., Yadav, S.K., 2016. Metallic nanoparticles, toxicity issues and applications in medicine. 41-80. In Sudesh Kumar Yadav (eds.), *Nanoscale materials in targeted drug delivery, theragnosis and tissue regeneration*, 186. Singapore: Springer. doi.10.1007/978-981-10-0818-4.
- Sinha, A., Chen, J., Jain, R., 2019. Functionalized Graphene-Metal Nanoparticles Nanohybrids as Electrochemical Sensors. 49-62. In Khan, A., Jawaid, M., Neppolian, B., Asiri A.M., *Graphene Functionalization Strategies: From Synthesis to Applications*. 406. Singapore: Springer. doi.org/10.1007/978-981-32-9057-0_2.
- Sivaranjan, K., Vanitha, P., Sathiyaseelan, A., Kalaiichelvan, P., Sathuvan, M., Rengasamy, R., Santhanalakshmi, J., 2017. Insights into the catalytic reduction of organic dyes and antibacterial activity of graphene oxide supported mono and bimetallic nanocomposites. *New Journal of Chemistry*. 41 (11), 4348-4359.
- Stankovich, S., Dikin, D.A., Piner, R.D., Kohlhaas, K.A., Kleinhammes, A., Jia, Y., Wu, Y., Nguyen, S.T., Ruoff, R.S., 2007. Synthesis of graphene-based nanosheets via chemical reduction of exfoliated graphite oxide. *Carbon*. 45 (7), 1558-1565.
- Su, C., Zhao, S., Zhang, H., Chang, K., 2017b. Ultrafine palladium nanoparticle-bonded to polyethylenimine grafted reduced graphene oxide nanosheets: Highly active and recyclable catalyst for degradation of dyes and pigments. *Korean Journal of Chemical Engineering*. 34 (3), 609-618.
- Su, D., Zhang, Y., Wang, Z., Wan, Q., Yang, N., 2017a. Decoration of graphene nano platelets with gold nanoparticles for voltammetry of 4-nonylphenol. *Carbon*. 117, 313-321.
- Sui, Z.-Y., Cui, Y., Zhu, J.-H., Han, B.-H., 2013. Preparation of three-dimensional graphene oxide–polyethylenimine porous materials as dye and gas adsorbents. *ACS applied materials & interfaces*. 5 (18), 9172-9179.

T

Tang, X., Zhou, Y., Peng, M., 2016. Green preparation of epoxy/graphene oxide nanocomposites using a glycidylamine epoxy resin as the surface modifier and phase transfer agent of graphene oxide. *ACS applied materials & interfaces*. 8 (3), 1854-1866.

W

Wainwright, M., 2008. Dyes in the development of drugs and pharmaceuticals. *Dyes and Pigments*. 76 (3), 582-589.

Wang, F., Shao, M., Cheng, L., Chen, D., Fu, Y., Ma, D.D.D., 2009. Si/Pd nanostructure with high catalytic activity in degradation of eosin Y. *Materials Research Bulletin*. 44 (1), 126-129.

Wu, T., Ma, J., Wang, X., Liu, Y., Xu, H., Gao, J., Wang, W., Liu, Y., Yan, J., 2013. Graphene oxide supported Au–Ag alloy nanoparticles with different shapes and their high catalytic activities. *Nanotechnology*. 24 (12), 125301.

X

Xu, L., Wu, X.-C., Zhu, J.-J., 2008. Green preparation and catalytic application of Pd nanoparticles. *Nanotechnology*. 19 (30), 305603.

Z

Zhang, Y., Liu, S., Wang, L., Qin, X., Tian, J., Lu, W., Chang, G., Sun, X., 2012. One-pot green synthesis of Ag nanoparticles-graphene nanocomposites and their applications in SERS, H₂O₂, and glucose sensing. *Rsc Advances*. 2, 538-545.

Zhao, X., Li, N., Jing, M., Zhang, Y., Wang, W., Liu, L., Xu, Z., Liu, L., Li, F., Wu, N., 2019. Monodispersed and spherical silver nanoparticles/graphene nanocomposites from gamma-ray assisted in-situ synthesis for nitrite electrochemical sensing. *Electrochimica Acta*. 295, 434-443.

Zeng, M., Wang, Y., Liu, Q., Yuan, X., Zuo, S., Feng, R., Yang, J., Wang, B., Qi, C., Lin, Y., 2016. Encaging palladium nanoparticles in chitosan modified montmorillonite for efficient, recyclable catalysts. *ACS applied materials & interfaces*. 8 (48), 33157-33164.

Zhuo, Q., Ma, Y., Gao, J., Zhang, P., Xia, Y., Tian, Y., Sun, X., Zhong, J., Sun, X., 2013. Facile synthesis of graphene/metal nanoparticle composites via self-catalysis reduction at room temperature. *Inorganic chemistry*. 52 (6), 3141-3147.

Chapter 3

NANOSTRUCTURED CERAMIC MEMBRANES FOR DISCOLORATION OF WATER LOADED WITH DYES

Tubular ultrafiltration ceramic membrane based on titania nanoparticles immobilized on macroporous clay-alumina support: Elaboration, characterization and application to dye removal

1. Introduction

Membrane separation technology has become increasingly appealing to address various scientific and technological issues associated to pollutions treatment. The wide variety of ceramic membranes meant for water treatment makes this technology very promising for both purification of drinking water and treatment of industrial wastewater containing emerging organic and inorganic pollutants. The success of ceramic membranes can be rationalized by their intrinsic properties, notably in terms of thermal and chemical stability and high mechanical strength (Gestel et al., 2002; Gestel et al., 2006; Lenza et al., 2000; Romanos et al., 2001). It is well known that beside the chemical nature of membrane, its topology as well as its elaboration process influence strongly the membrane durability and resistance to harsh application conditions such as acidic and alkali media. Commercialized ceramic membranes are mainly manufactured from MOs such as alumina, silica, zirconia and titania (Gestel et al., 2006; Lenza et al., 2000; Romanos et al., 2001; Chowdhury et al., 2003). Since the pioneering research in ceramic membranes technology, α -alumina has been mostly used as raw materials in varied fabrication processes (Defriend et al., 2003).

Undoubtedly, the synergy between ceramic materials' precursors and advanced manufacture processes has led to considerable progresses providing new generations of high-performance IMs combining well-defined morphological properties (such as porosity), physicochemical stability (pH), mechanical strength and high flow resistance (pressure), separation efficiency and selectivity (Gestel et al., 2002; Lenza et al., 2000; Romanos et al., 2001; Defriend et al., 2003; Chang et al., 2014). These new generations of low cost ceramic membranes based on raw materials such as clay, starch, chamotte, apatite, and sand have been widely developed and studied on laboratory scale units working both in the microfiltration (MF) and ultrafiltration (UF) domains (Lorente-Ayza et al., 2015; Lorente-Ayza et al., 2016; Ha et al., 2015; Zhu et al., 2016; Nandi et al., 2008; Hedfi et al., 2014; Hedfi et al., 2016; Issaoui et al., 2016; Khemakhem et al., 2011; Saffaj et al., 2006; Sahoo et al., 2016). The UF process allows the removal of high molecular weight substances such as dyes (Khemakhem et al., 2011; Saffaj et al., 2006; Sahoo et al., 2016; Alventosa-deLara et al., 2012) and can be easily integrated to biological WWT (Alventosa-deLara et al., 2012; Chamam et al., 2007). Among the plethora of inorganic precursors, kaolin clay has been intensively considered as pore

forming agent raw material for the cost-effective design of stable IMs exhibiting a broad range of filtration processes (Nandi et al., 2008; Hedfi et al., 2014; Hedfi et al., 2016; Issaoui et al., 2016).

In this context, this study is intended to elaborate tubular-shape porous membranes using extrusion method followed by sintering process using a mixture of natural kaolin clay and alumina powders as ceramic materials. The so-designed tubular ceramic tube served as solid support for the preparation of defect-free UF layer via slip-casting, using TiO₂ nanoparticles suspension. The rationale for using titania nanoparticles arises from their unique characteristics among which one may cite anti-fouling character, chemical stability (Gestel et al., 2002; Bhave 1991; Song et al., 2016), suitability for separation and antimicrobial efficiency (Saffaj et al., 2005), together with high photocatalytic activity (Goei et al., 2014; Alem et al., 2009; Wang et al., 2007; Leong et al., 2014; Das et al., 2014; Sarkar et al., 2015a; Sarkar et al., 2015b). It is assumed that incorporation of titania-based active layer into porous ceramic membranes (PCMs) may lead to improved separation performances in the different fields of membrane separation processes including microfiltration (MF), ultrafiltration (UF) and nanofiltration (NF) (Song et al., 2016; Goei et al., 2014; Alem et al., 2009; Wang et al., 2007; Puhlfürß et al., 2000; Cai et al., 2015). With the final aim to meet the legal requirements for the discharge of wastewater, the ceramic titania-based UF single channel ceramic membrane was used for the removal of hazardous alizarin red, a popular indocile dye widely found in textile wastewater (Polubesova et al., 2004; Sadegh et al., 2015; De Souza et al., 2013), from alizarin red spiked aqueous solutions. As such, this paper assesses both the synthesis and characterization aspects of the hybrid membrane and discusses its separation efficiency notably in terms of permeate flux and dye retention. Finally, the impact of operating parameters, namely transmembrane pressure (TMP), pH and dye initial concentration on the permeate flux and dye rejection rate is determined.

2. Experimental

2.1. Materials

The raw starting materials used for preparing the tubular porous membrane support are clay and alumina. The kaolin clay powder of Rajmahal grade was first grinded with a ceramic mortar and then sieved to provide a granulometry of about 100 µm. α -Alumina powder (99%) with a mean particle size of 7 µm was a kind gift from Hindalco company, India. Cellulose ether (methocel), polyvinyl alcohol (PVA, MW-13000–23000 g mol⁻¹) and anionic polyelectronic

Dolapix (CE64) used as organic binder, plastisizer and dispersant agent, respectively, were purchased from Dow Chemical company. Titanium dioxide nanoparticles (TiO_2 , 98%) with a mean particle size of 10 nm were purchased from Advanced Technology Materials, India. Alizarin red dye was used as a model textile dye to prepare spiked aqueous solutions and was purchased from Sigma-Aldrich.

2.2. Characterization and instruments

The mechanical strength of the sintered ceramic supports was measured by a three-point bending flexural test using an UTM Instron 5500R (Software: Blue Hill, Universal Testing Machine of 10 tonnes capacity) to evaluate the effect of the clay-alumina composition and Methocel amount on the mechanical properties of the resulting membranes. The measurements were performed on sintered rectangular bars of 10 mm breadth, 5 mm height and 50 mm length using a span of 40 mm and a crosshead speed of 1.0 mm/min. Thermogravimetric (TGA) and differential (DTA) thermal analyses of the clay-alumina pastes were performed using a Netzsch STA 449 C apparatus (Germany) in a temperature range between 0 and 1500 °C at a heating rate of 10 °C/min under air atmosphere in order to determine the temperature–time schedule to be used for preparing the ceramic supports. Pore size of the tubular support was evaluated by means of mercury intrusion porosimetry (Micromeritics AutoPore IV 9500).

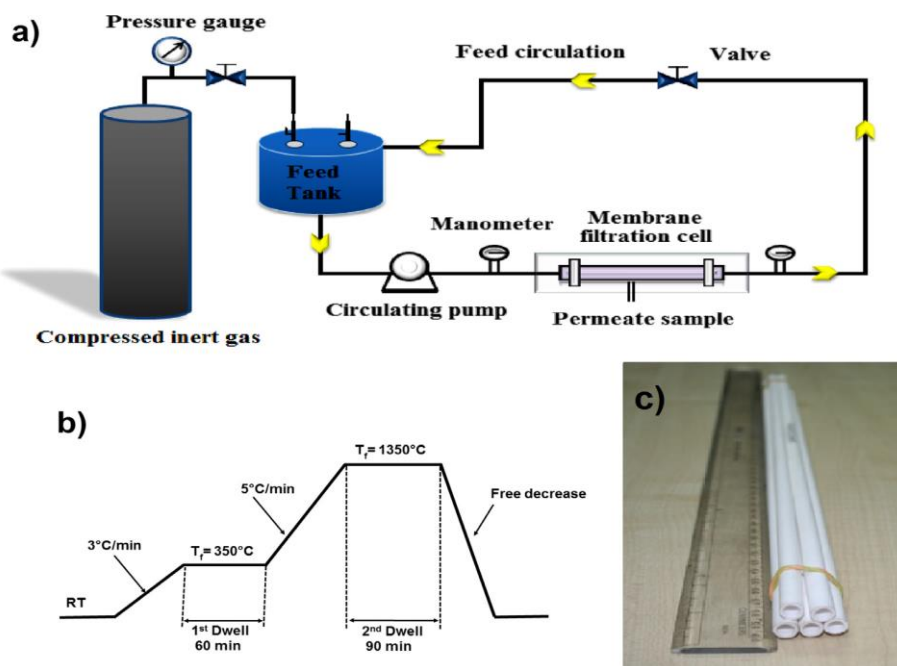


Figure 30. (a) Schematic representation of the homemade cross flow UF membrane set up. (b) Firing schedule applied for the preparation of the porous tubular ceramic supports. (c) Photograph of extruded porous tubular ceramic supports sintered at a temperature of 1350 °C for 90 min.

Field Emission Scanning Electron Microscopy (FESEM) coupled with Energy Dispersive X-ray (EDX) analysis was used to investigate the microstructure and analyze the surface morphology of both native clay-alumina support and corresponding UF membrane obtained after coating with a TiO₂ layer. The thickness of the TiO₂ layer was also determined from SEM images. To determine the transfer properties of native and TiO₂ coated supports, pure water flux and filtration tests were conducted using a home-made setup as schematically depicted in *Figure 30*.

2.3. Preparation of tubular clay-alumina supports

Ceramic precursor pastes were prepared through blending different amounts of dry kaolinite clay, alumina and Methocel powders as presented in *Table 5* (Sarkar et al., 2012).

Manufacturing of porous tubular ceramic supports was achieved via an extrusion process using a single screw type extruder (Brabender, Germany) (*Figure 30*) (Ray et al., 2015). After drying at room temperature, and sintering under a multi-step thermal treatment program for which the final temperature was set at $T_f = 1350$ °C as shown in *Figure 30b*, several tubular macroporous membrane supports with an ID = 7 mm and an OD = 10 mm were obtained (*Figure 30c*). Support with 25% clay and 75% alumina and 6 g of methocel, referred to as

C25A75M6 hereafter, has been selected for the continuation of this work due to the formation of the high aspect mullite phase even at low temperature (1150 °C) which ensure high mechanical resistance and better thermal and chemical stability (Zhu et al., 2016).

2.4. Design of TiO₂-based tubular ceramic UF membrane

The active titania UF separation layer was prepared through slip casting process involving the deposition of the casting slurry on the support for an optimal contact time of 10 min. The slurry was prepared by dispersing, under magnetic stirring, 4 g of titania powder in an aqueous solution containing well dispersed PVA (12 wt.%) and a low amount of Dolapix CE64 dispersant (0.2 wt.%). The latter improved the stability of the dispersion while the former acted as a binder and enhanced the viscosity of the solution to ensure homogenous casting of the titania nanoparticles on the inner surface of the tubular support membrane. The deposition of TiO₂ layer was ensured by mean of capillary suction inside the tubular support. Afterwards, the coated support was dried at ambient temperature for 24 h, followed by a calcination step at 800 °C for 3 h. It is important to note that in order to obtain cracks-free membrane, very low heating rate (3 °C/min) was used.

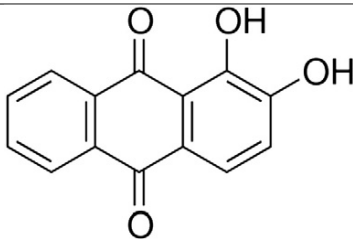
Table 5.Composition of the ceramic supports and mixing conditions.

Sample name	Composition dry mineral basis (wt.%)		Organic binder (g)	Liquid Phase (g)	Dry Mixing time (min)	Wet Mixing time (min)
	Kaolin	Alumina	Methocel	Water		
C25A75M4	25	75	4	31	15	30
C25A75M6	25	75	6	30	15	30
C25A75M10	25	75	10	28	15	45
C50A50M4	50	50	4	26	15	30
C50A50M6	50	50	6	30	15	30
C50A50M10	50	50	10	30	15	45

2.5. Cross flow ultrafiltration (UF)

The so-designed TiO₂ coated tubular porous ceramic membrane was applied to the decolorization of alizarin dye-containing solution by ultrafiltration. Major characteristics and chemical formula of alizarin dye are summarized in *Table 6*.

Table 6. Alizarin red dye characteristics.

Characteristic	Alizarin Red
Molecular formula	C ₁₄ H ₈ O ₄
Chemical name	1,2-Dihydroxy-9,10-anthraquinone
Molecular weight	240.21 g.mol ⁻¹
λ_{\max} (pH = 9)	260, 327 and 521 nm
pka	6.77
Class	Anthraquinone
Chemical structure	

Cross-filtration membrane tests were conducted using a homemade lab-scale unit. The filtration system is equipped with an adjustable outflow pump, a feed tank of 10 L capacity, and a stainless steel (316 L) module hosting a single channel membrane (length of 300 mm, outer diameter of 10 mm and inner diameter of 7 mm). The effective membrane area was 65.94 cm² and the TMP was varied in the range between 1 and 8 bar. The permeate flux value through the membrane was measured as a function of time at different transmembrane pressures. Prior to permeability measurements, the membrane was conditioned by immersion in pure deionized water for at least 24 h. Dye solutions were prepared by dissolving alizarin red in deionized water and the pH was adjusted to 9 by adding NaOH solution (1 M). All filtration tests were performed in triplicate and results are presented hereafter for the third filtration cycle.

3. Results and discussion

3.1. Design and characterization of macroporous tubular ceramic membranes

Morphological properties, chemical and mechanical stability are some of the key features to be finely controlled to design membrane materials with outstanding properties. To this aim, various ceramic-like precursor pastes were prepared based on different compositions of dry powders as summarized in *Table 5*. Alumina versus kaolin ratio as well as amount of both aqueous phase and organic binder, namely methocel, was primarily investigated together with the wet mixing time (varied between 30 and 45 min) while the dry mixing time was kept constant at 15 min. Porous tubular ceramic supports were manufactured through an extrusion process using a single screw-type extruder and a thermal treatment involving two temperature steps (noted dwell in *Figure 30b*) at 350 and 1350 °C. Temperature rates of 3 °C/min and 5 °C/min were applied for heating up the samples from RT and 350 °C, respectively.

3.1.1. Mechanical strength

To control the resistance of the tubular support sintered at a temperature of 1350 °C, mechanical resistance tests were performed on bar samples using the three-point bending flexural test. Effect of both the mass content of methocel and clay-alumina composition in the plastic paste membrane precursor on the mechanical properties of the membrane supports was investigated. It was observed for clay/alumina 50/50 tubular supports that the mechanical strength was improved from 32 to 40 MPa when the methocel binder content was increased from 4 to 6 g (*Figure 31a*). Incorporation of more than 6 g of binder to the ceramic mixture was detrimental to mechanical strength of the resulting clay alumina supports. This may be due to a considerable increase in the porosity of the support. This finding suggests that 6 g of binder are optimal for ensuring good adhesion and uniformity of the ceramic structure associated with optimal rheological properties.

Clearly, an increase in the flexural strength of the ceramic tubular supports was observed for the initial paste mixture containing 25 wt.% of clay while the binder amount was kept constant and equal to 6 g (*Figure 31b*). The increase in mechanical resistance as observed from about 12 MPa for pure alumina, to about 57 MPa for the composition 25 wt.% clay and 75 wt.% alumina may be explained by the formation of the mullite and cristobalite crystalline structures previously identified by TGA-DTA for sintered supports.

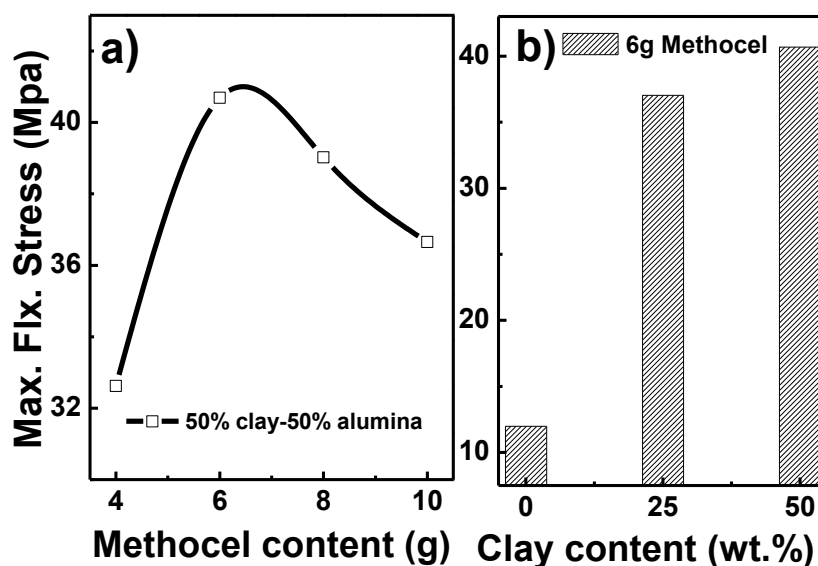
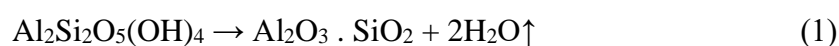


Figure 31. Effect of (a) methocel and (b) clay contents on the mechanical strength of the porous tubular ceramic supports sintered at a temperature of 1350 °C for 90 min. In (a) the clay/alumina ratio is 50/50 while in (b) the methocel content was kept constant at 6 g.

3.1.2. Thermal analysis

Both DTA and TGA thermograms were exploited to evaluate the sintering-mediated reaction between kaolin and alumina (*Figure 32*). The TGA curve for C25A75M6 support, selected in this work as support for the preparation of UF membrane, indicates weight loss of about 3 wt.% at low temperature (<100 °C). That is attributed to the evaporation of the intercalated or adsorbed water in the powder samples. The small weight loss of 4 wt.% seen in the TGA curve between 200 and 400 °C can be attributed to the removal of structural water from the ceramic materials. This is confirmed by the corresponding DTA peak at about 330 °C. The temperature range between 450 °C and 550 °C is associated to the second endothermic reaction. Regarding the TGA thermogram, such thermodynamic change corresponds to a sample mass loss of about 12 wt. %. This process arises from the burning out of the organic additives from the paste and the dehydration (structured water) of kaolin according to the reaction given in Eq. (1).



Accordingly, the structural hydroxyls are eliminated leading to the transformation of kaolin to a new metakaolin amorphous phase (Sahnoune et al., 2008; Ghorbel et al., 2008; Lecomte et al., 2007). In the high temperature regime, structural reorganization processes of the ceramic materials occur as suggested by the presence of a succession of exothermic phenomena located between 950 °C and 1300 °C. The complex nature of these reorganization phenomena

is still the subject of many studies (Sahnoune et al., 2008a; Roy et al., 1955; Castelein et al., 2001; Lee et al., 2008). Identification of the involved mechanisms and determination of the chemical composition of the eventually resulting crystalline phases are often difficult and still uncertain, especially because the thermogravimetry curve does not show weight change of the ceramic material. Roy et al. (1955) and Sahnoune et al. (2008b) showed that the exothermic peak located at about 1000 °C is due to the structural reorganization of metastable metakaolin leading to the formation of gamma-alumina ($\gamma\text{-Al}_2\text{O}_3$) with spinel structure (Al-Si) according to the following chemical reaction:



The γ -alumina transitional phase could be at the origin of mullite formation (Eq. (3)), which starts at about 1150 °C to give firstly the primary, then secondary mullites followed by the cristobalite phase formation (Castelein et al., 2001; Bergaya et al., 1996; Chen et al., 2005; Chen et al., 2001) according to:

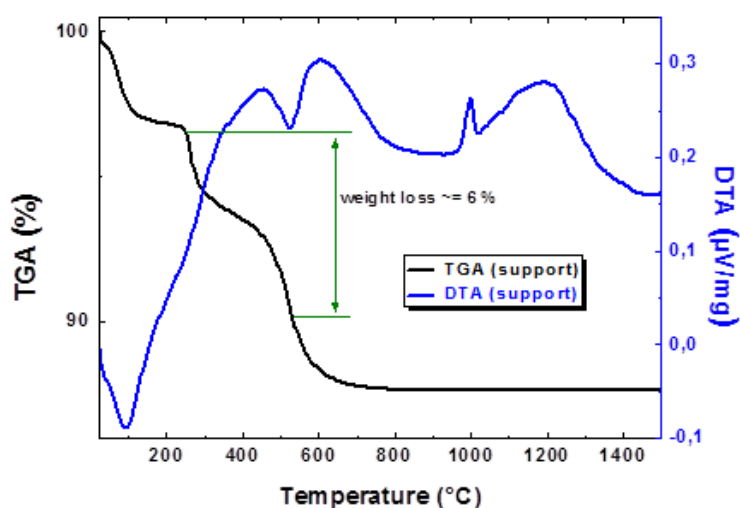
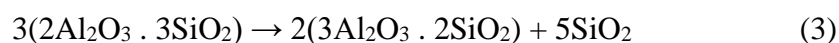


Figure 32. TGA and DTA plots recorded for the porous tubular ceramic support C25A75M6 prepared from the composition clay/alumina/methocel 25/75/6 and sintered at a temperature of 1350 °C for 90 min.

3.1.3. Porosity and pore size distribution

The pore size distribution curves of the sintered C25A75M6 support is illustrated in *Figure 33*. It can be observed a well-defined peak showing an average pores diameter ranging from 0.20 to 7 mm, and centered at 0.75 mm. This reveals a monomodal and uniform pore size

distribution which evidences the success of the extrusion process and the absence of cracks throughout the support.

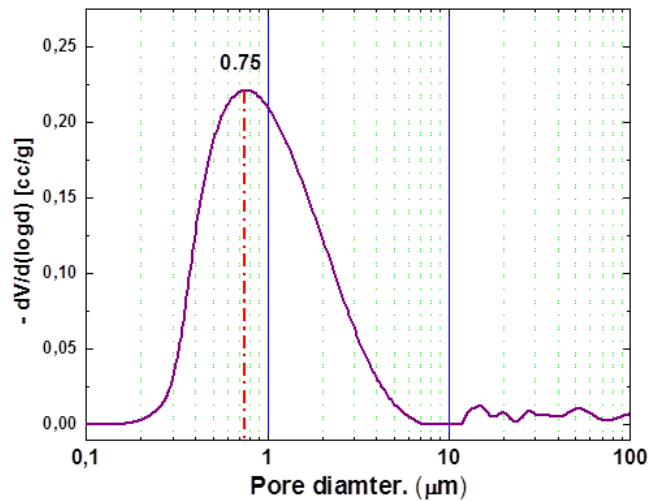


Figure 33. Pore size distribution measured for the porous tubular ceramic support C25A75M6 prepared from the composition clay/alumina/methocel 25/75/6 and sintered at a temperature of 1350 °C for 90 min.

3.1.4. Morphology

Figure 34 shows the FESEM images of the inner surface of the ceramic membrane C25A75M6 sintered at 1350 °C. The support microstructure indicates a high densification and homogeneous surface. The absence of cracks and the uniformity of the surface of the support shown both by SEM and mercury intrusion porosimetry are considered as key features for enhanced retention of the titania nanoparticles, allowing the deposition of continuous and dense coating layer.

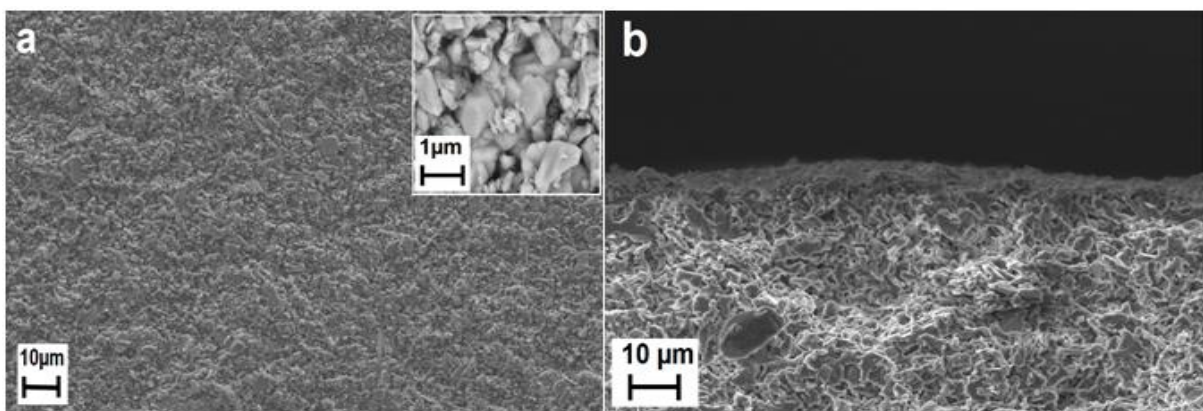


Figure 34. Field emission scanning electron microscopy images of (a) top surface and (b) cross section of the porous tubular ceramic support C25A75M6 prepared from the composition clay/alumina/methocel 25/75/6 and sintered at a temperature of 1350 °C for 90 min.

3.2. Characterization of TiO₂-coated C25A75M6 ultrafiltration membrane

3.2.1. Morphology

The titania thin layer as elaborated after calcination at 800 °C for 3 h was analyzed and imaged by FESEM. The microstructure observations of the surface and the cross-section are shown in *Figure 35*. *Figure 35a* shows that smooth and homogeneous inner surface was obtained with a mean pore diameter of about 50 nm. According to the cross-section image of the membrane, asymmetric structure was observed with TiO₂ nanoparticles tightly packed and well attached to the internal surface of the tubular support. This active filtration layer exhibits an approximate thickness of 4.2 mm (*Figure 35b*).

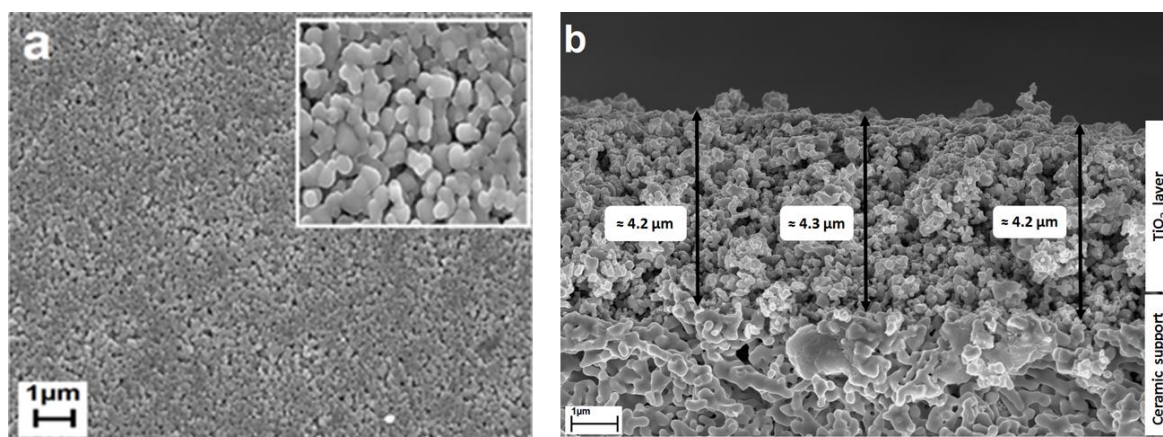


Figure 35. Field emission scanning electron microscopy images of (a) top-surface and (b) cross-section of ceramic membrane support C25A75M6 prepared from the composition clay/alumina/methocel 25/75/6 and coated with a TiO₂ layer. The inset in part (a) shows a magnified image of the TiO₂-based membrane's surface.

3.2.2. Water permeability and permeate flux

In order to assess the effect of the deposited titania layer, comparison between water permeability of the pristine tubular support and the UF membrane has been accomplished using pure water. Before starting the measurements, membrane samples were immersed in deionized water for 24 h. As shown in *Figure 36*, the water permeate flux increases linearly with the applied transmembrane pressure (TMP). The permeability of the membrane is remarkably decreased from 850 L.h⁻¹.m⁻².bar⁻¹ for the native support to 117 L.h⁻¹.m⁻².bar⁻¹ for the TiO₂ coated membrane. The permeability value determined for the TiO₂-coated membrane is typical for UF membrane. This result indicates that the TiO₂ layer is responsible for the permeability decrease that can be explained by the lower pore size of UF titania active

layer deposited on the C25A75M6 support providing further evidence of its robust embedding in the membrane support.

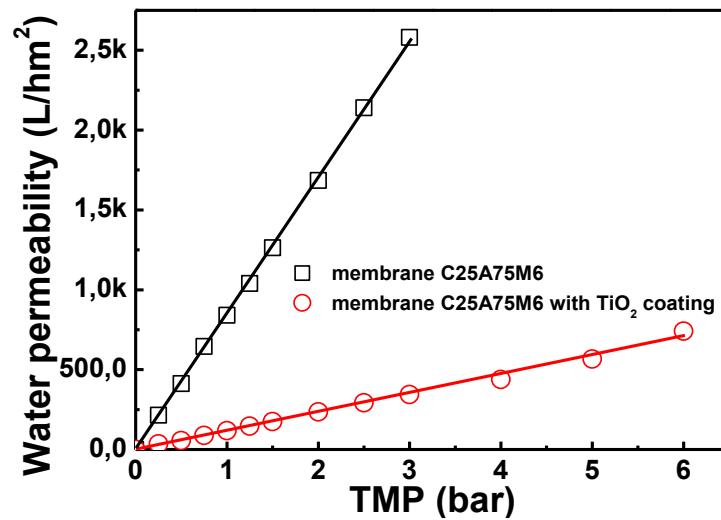


Figure 36. Variation of the water permeability as a function of the transmembrane pressure for the ceramic membrane support C25A75M6 (square) before and (circle) after coating with TiO₂ layer.

In addition, the effect of the TMP on the permeate flux (J_f) has been evaluated at room temperature and at pH 9 for three initial dye concentrations (150, 200 and 300 ppm). Similar timedependences of the permeate flux (J_f) were observed for TMP values ranging from 1 bar to 8 bar (*Figure 37*). Indeed, the permeate flux decreases continuously during the first 20 min of treatment then becomes quasi-constant. The higher stabilized flux of 140 L.h⁻¹.m⁻² is obtained at the higher applied TMP of 8 bar. The stabilized flux decreases with decrease in the TMP becoming equal to 70 L.h⁻¹.m⁻².bar⁻¹ for a TMP of 1 bar. This initial behavior showing a decline of the permeate flux is typical of UF membrane process and can be explained by the membrane fouling due to the interaction between the spiked solution and the membrane surface (Ellouze et al., 2011).

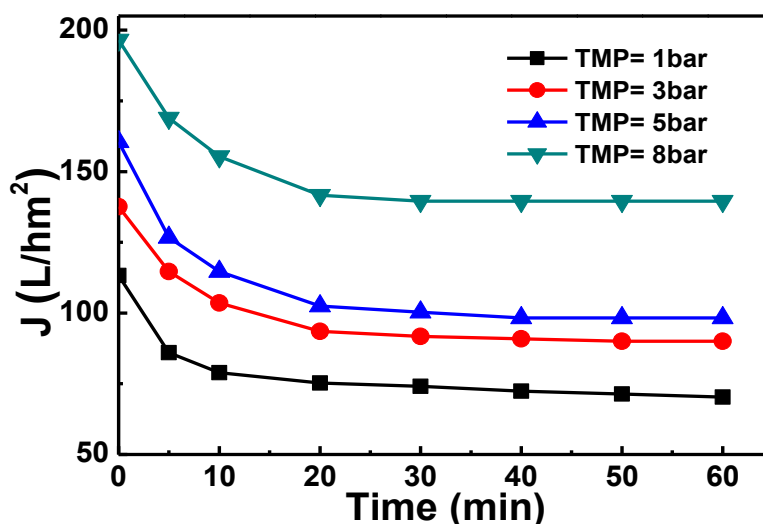


Figure 37. Time-dependences of the flux of alizarin red solutions at different transmembrane pressures for the ceramic membrane support C25A75M6 coated with a TiO₂ layer. UF conditions: [ALZ] = 150 ppm and pH = 9.

3.3. Application of TiO₂-coated C25A75M6 ultrafiltration membrane to decolorization of alizarin dye aqueous solution

In this work, the TiO₂-coated C25A75M6 membrane has been applied to color removal from aqueous solutions using alizarin red (ALZ-Red) as a model of textile dye. Efficiency of the decolorization expressed by retention percentage has been studied as a function of the initial dye concentration (150 ppm, 200 ppm and 300 ppm), pH of the dye solutions (2–12) and the TMP (1–8 bar). The retention percentage, denominated R (%), was obtained using the following equation: $R(\%) = 100 (1 - C_p/C_0)$

where C_p (ppm) is the permeate dye concentration and C_0 (ppm) the initial dye concentration.

3.3.1. Effect of pH of the feed dye solution

Efficiency of ALZ-Red removal was assessed at pH values varying from 2 to 12 for a feed concentration of 150 ppm and a separation time of 100 min (*Figure 38*). It is worthy to note that the results shown in *Figure37–39* were obtained after the third repeated test of filtration. Purification and regeneration of the membranes were performed between each filtration cycle using, first, distilled water for 15 min, sodium hydroxide solution (2 wt.%) at 80 °C for 20 min, nitric acid solution (2 wt.%) at 60 °C for 20 min, and finally water rinsing until reaching neutral pH. No significant decrease in filtration efficiency was observed in these conditions. It is clearly seen that efficiency of the UF process of alizarin depends strongly on the pH of the feed solution. Indeed, in an alkaline medium, the elimination is much more efficient than in

an acid one, and it is almost total ($R > 98\%$) at pH 9. In contrast, in acidic medium the disappearance of alizarin was about twice as low. The change is observed in a rather narrow pH range, between 6 and 8, in correspondence to both pKa (6.77) value and isoelectric point (~ 6) of alizarin and titanium dioxide, respectively. Although comprehensive discussion of the mechanism of dye removal requires further investigations, it may be assumed that efficiency of the UF process results from a delicate balance of filtration process and interaction between the membrane and the alizarin solution. Such interactions are pH-dependent and controlled by the zeta potential and charge state of the TiO_2 top layer and alizarin, respectively. At low pH (<6) titania layer may be in a protonated form that is detrimental to the separation efficiency. According to these results, pH of 9 was considered as optimum pH for the alizarin dye elimination by TiO_2 membrane and it was retained for the following study. Moreover, wastewater from the textile processing industry is often characterized by high pH (Tahri et al., 2012) and, in the case of ALZ-Red, solubility was improved in alkaline medium.

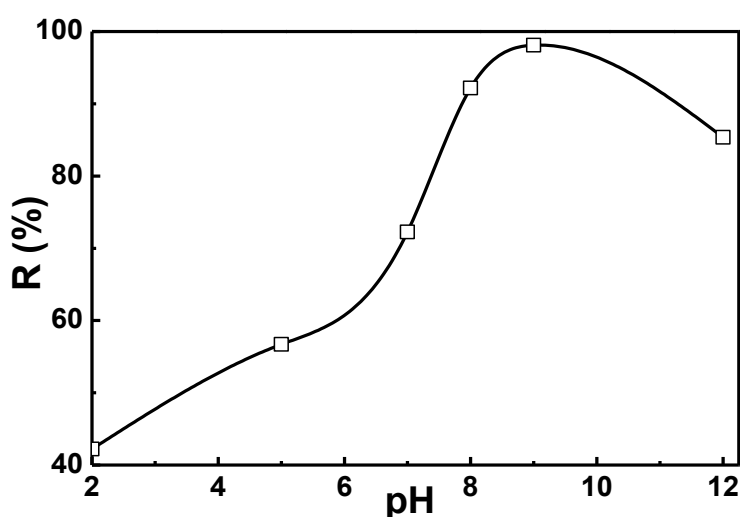


Figure 38. Variation of the color rejection rate (R , expressed in %) of Alizarin Red as a function of the pH of the dye solution as measured for the ceramic membrane support C25A75M6 coated with a TiO_2 layer. UF conditions: $[\text{ALZ}] = 150$ ppm, $\text{TMP} = 5$ bar and $t = 100$ min.

3.3.2. Effect of the concentration of the feed dye solution

This study was carried out in order to evaluate decolorization efficiency over time of the TiO_2 -coated C25A75M6 membrane towards ALZ-Red solutions with different dye concentrations. The **Figure 39** shows two different regimes. Initially (time < 20 min), the decolorization rate assumes a steep increase and the increase is steeper for low concentrations. Then, for longer time, the color rejection levels off and a plateau regime is reached faster for the lower

concentration, after about 60 min for 150 ppm to be compared to more than 120 min for 300 ppm. Nearly total decolorization is achieved faster for lower dye concentration. Indeed, in the course of the filtration process, dye molecules may adsorb onto the membrane surface driving to the formation of a cake layer. This effect is more pronounced for high dye concentration. As previously reported, accumulation of dye molecules may lead to clogging of the pores of the membrane leading to a compaction of the cake layer accompanied with a polarization phenomenon (Van der Bruggen et al., 2005). These combined effects often resulting in a decline of the permeate flux.

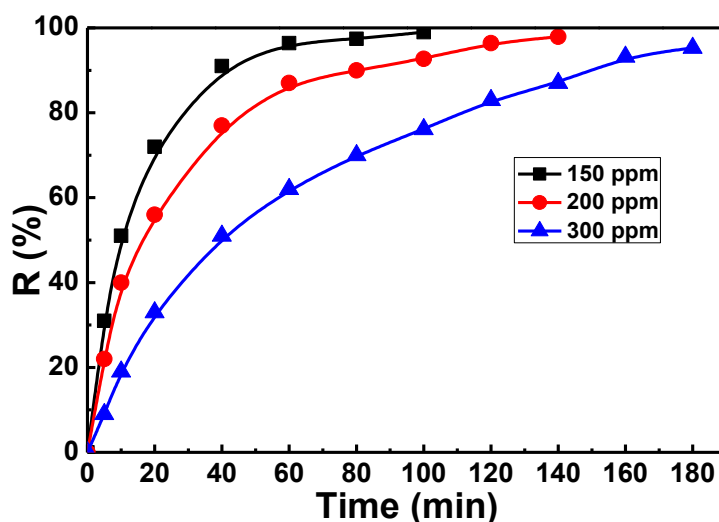


Figure 39. Time-dependences of the color rejection rate (R, expressed in %) for various initial concentrations of Alizarin Red as measured for the ceramic membrane support C25A75M6 coated with a TiO₂ layer. UF conditions: TMP = 5 bar and pH = 9.

3.3.3. Effect of transmembrane pressure

As it can be observed in *Figure 40*, the color retention, as evaluated at a concentration of 150 ppm, was strongly dependent on the applied TMP. Low TMP (1 and 3 bars) provided limited decolorization efficiency. The highest color rejection rate of about 99% was observed from a TMP of 5 bar. It is important to note that the treated water became visually very clear after treatment at 5 or 8 bars (inset in *Figure 40*). The very high permeate quality confirms the performances of the asymmetric UF titania membrane towards color removal from dye polluted water. The color rejection of dye observed is assumed to arise from a dual functionality of the titania layer, namely adsorption and filtration (Xiang et al., 2013; Zhang et al., 2012).

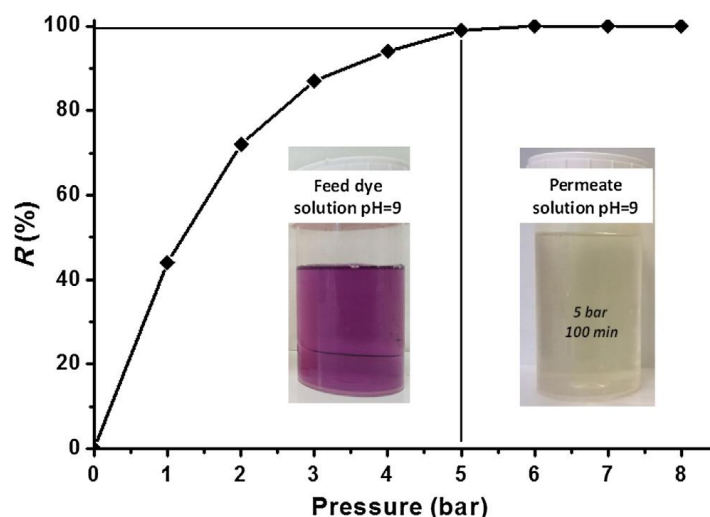


Figure 40. Variation of the color rejection rate of alizarin red dye from spiked water solution (150 ppm) as a function of the transmembrane pressure. The insets showing images of the feed dye solution (left) and the permeate solution (right) as obtained after ultrafiltration process during 100 min at 5 bar evidence the effectiveness of dye removal.

4. Conclusion

In this study, a novel ultrafiltration clay-alumina membrane coated with a titania layer was successfully elaborated via a combination of extrusion, sintering and slip casting methods. FESEM, EDX, TGA, DTA and mechanical tests were applied to investigate the effects of the content of clay, alumina and methocel binder on physical and mechanical properties of the supports. Optimal thermal stability and mechanical properties were obtained for the membrane prepared from a composition made of 25 wt.% kaolin clay, 75 wt.% alumina and 6% of methocel. The ultrafiltration layer, based on titanium oxide nano-powder deposited onto the surface of the clay-alumina membrane support (C25A75M6) has a thickness of 4.2 mm and a mean pore size of 50 nm. The asdesigned UF membrane exhibited a water permeability of $117 \text{ L.m}^{-2}.\text{h}^{-1}.\text{bar}^{-1}$, indicating that the titania layer is responsible for the decrease in permeability which was calculated to be $850 \text{ L.m}^{-2}.\text{h}^{-1}.\text{bar}^{-1}$ for the clay-alumina support with pristine surface. Finally, the ultrafiltration membrane was applied to the decolorization of dye containing aqueous solutions. Under optimal operating conditions, i.e., transmembrane pressure of 5 bars, $\text{pH} = 9$ and dye concentration of 150 ppm, the TiO_2 -coated membrane exhibited significant decolorization efficiency towards alizarin red dye as color removal of 99% was achieved. Hence, the newly designed titania-based membrane may open new avenues for the treatment of raw textile wastewater.

References

A

- Alem, A., Sarpoolaky, H., Keshmiri, M., 2009. Titania ultrafiltration membrane: preparation, characterization and photocatalytic activity. *Journal of the European Ceramic Society*. 29, 629–635.
- Alventosa-deLara, E., Barredo-Damas, S., Alcaina-Miranda, M.I., Iborra-Clar, M.I., 2012. Ultrafiltration technology with a ceramic membrane for reactive dye removal: optimization of membrane performance. *Journal of Hazardous Materials*. 209–210, 492–500.

B

- Bergaya, F., Dion, P., Alcover, J.F., Clinard, C., Tchoubar, D., 1996. TEM study of kaolinite thermal decomposition by controlled-rate thermal analysis. *Journal of Materials Science*. 31, 5069–5075.
- Bhave, R.R., 1991. *Inorganic Membranes Synthesis Characteristics and Applications*. Van Nostrand, R., Chemistry and Materials Science, 331. New York: Springer Netherlands.

C

- Cai, Y., Wang, Y., Chen, X., Qiu, M., Fan, Y., 2015. Modified colloidal sol–gel process for fabrication of titania nanofiltration membranes with organic additives. *Journal of Membrane Science*. 476, 432–441.
- Castelein, O., Soulestin, B., Bonnet, J.P., Blanchart, P., 2001. The influence of heating rate on the thermal behavior and mullite formation from a kaolin raw material. *Ceramics International*. 27, 517–522.
- Chamam, B., Heran, M., Grasmick, A., Ben, Amar, R., 2007. Comparison of textile dye treatment by biosorption and membrane bioreactor. *Environmental Technology*. 28, 1–9.
- Chang, Q., Wang, Y., Cerneaux, S., Zhou, J., Zhang, X., Wang, X., Dong, Y., 2014. Preparation of microfiltration membrane supports using coarse alumina grains coated by nano TiO₂ as raw materials. *Journal of the European Ceramic Society*. 34, 4355–4361.
- Chen, C.Y., Tuan, W.H., 2001. The processing of kaolin powder compact, *Ceramics International*. 27, 795–800.

Chen, Z., Zhang, L., 2005. Novel Method of adding seeds for preparation of mullite. *Journal of Materials Processing Technology*. 166, 183–187.

Chowdhury, S., Schmuhl, R., Keizer, K., Ten Elshof, J., Blank, D., 2003. Pore size and surface chemistry effects on the transport of hydrophobic and hydrophilic solvents through mesoporous γ -alumina and silica MCM-48. *Journal of Membrane Science*. 225, 177–186.

D

Das, R., Sarkar, S., Chakraborty, S., Choi, H., Bhattacharjee, C., 2014. Remediation of antiseptic components in wastewater by photocatalysis using TiO₂ nanoparticles. *Industrial & Engineering Chemistry Research*. 53, 3012–3020.

Defriend, K.A., Wiesner, M.R., Barron, A.R., 2003. Alumina and aluminate ultrafiltration membranes derived from alumina nanoparticles. *Journal of Membrane Science*. 224, 11–28.

De Souza, M.L., Corio, P., 2013. Effect of silver nanoparticles on TiO₂-mediated photodegradation of Alizarin Red S. *Applied Catalysis B: Environmental*. 136–137, 325–333.

E

Ellouze, E., Ellouze, D., Jrad, A., Ben Amar, R., 2011. Treatment of synthetic textile wastewater by combined chemical coagulation/membrane processes. *Desalination and Water Treatment*. 33, 118–124.

G

Gestel, T.V., Kruidhof, H., Blank, D.H.A., Bouwmeester, H.J.M., 2006. ZrO₂ and TiO₂ membranes for nanofiltration and pervaporation Part1. Preparation and characterization of a corrosion-resistant ZrO₂ nanofiltration membrane with a MWCO < 300. *Journal of Membrane Science*. 284, 128–136.

Gestel, T.V., Vandecasteele, C., Buekenhoudt, A., Dotremont, C., Luyten, J., Leysen, R., 2002. Alumina and titania multilayer membranes for nanofiltration: preparation, characterization and chemical stability. *Journal of Membrane Science*. 207, 73–89.

Ghorbel, A., Fourati, M., Bouaziz, J., 2008. Microstructural evolution and phase transformation of different sintered Kaolins powder compacts. *Materials Chemistry and Physics*. 112, 876–885.

Goei, R., Lim, T.T., 2014. Asymmetric TiO₂ hybrid photocatalytic ceramic membrane with porosity gradient: effect of structure directing agent on the resulting membranes architecture and performances. *Ceramics International*. 40, 6747–6757.

H

Ha, J.H., Lee, J., Song, I.H., Lee, S.H., 2015. The effects of diatomite addition on the pore characteristics of a pyrophyllite support layer. *Ceramics International*. 41, 9542–9548.

Hedfi, I., Hamdi, N., Rodríguez, M.A., Srasra, E., 2016. Development of a low cost microporous ceramic membrane from kaolin and Alumina, using the lignite as porogen agent. *Ceramics International*. 42, 5089–5093.

Hedfi, I., Hamdi, N., Srasra, E., Rodríguez, M.A., 2014. The preparation of micro-porous membrane from a Tunisian kaolin. *Applied Clay Science*. 101, 574–578.

I

Issaoui, M., Limousy, L., Lebeau, B., Bouaziz, J., Fourati, M., 2016. Design and characterization of flat membrane supports elaborated from kaolin and aluminum powders. *Comptes Rendus Chimie*. 19, 496–504.

K

Khemakhem, M., Khemakhem, S., Ayedi, S., Ben Amar, R., 2011. Study of ceramic ultrafiltration membrane support based on phosphate industry subproduct: application for the cuttlefish conditioning effluents treatment. *Ceramics International*. 37, 3617–3625.

L

Lecomte, G.L., Bonnet, J.P., Blanchart, P., 2007. A study of the influence of muscovite on the thermal transformations of kaolinite from room temperature up to 1100 °C. *Journal of Materials Science*. 42, 8745–8752.

Lee, W.E., Souza, G.P., McConville, C.J., Tarvornpanich, T., Iqbal, Y., 2008. Mullite formation in clays and clay-derived vitreous ceramics. *Journal of the European Ceramic Society*. 28, 465–471.

Lenza, R.F.S., Vasconcelos, W.L., 2000. Synthesis and properties of microporous sol–gel silica membranes. *Journal of Non-Crystalline Solids*. 273, 164–169.

Leong, S., Razmjou, A., Wang, K., Hapgood, K., Zhang, X., Wang, H., 2014. TiO₂ based photocatalytic membranes: a review. *Journal of Membrane Science*. 472, 167–184.

Lorente-Ayza, M.M., Mestre, S., Sanz, V., Sánchez, E., 2016. On the underestimated effect of the starch ash on the characteristics of low cost ceramic membranes. *Ceramics International*. 42, 18944–18954.

Lorente-Ayza, M.M., Sánchez, E., Sanz, V., Mestre, S., 2015. Influence of starch content on the properties of low-cost microfiltration ceramic membranes. *Ceramics International*. 41, 13064–13073.

N

Nandi, B.K., Uppaaluri, R., Purkait, M.K., 2008. Preparation and characterization of low cost ceramic membranes for microfiltration applications. *Applied Clay Science*. 42, 102–10.

P

Polubesova, T., Epstein, M., Yariv, S., Lapides, I., Nir, S., 2004. Adsorption of alizarinate–micelle complexes on Na-montmorillonite. *Applied Clay Science*. 24, 177–183.

Puhlfürß, P., Voigt, A., Weber, R., Morbé, M., 2000. Microporous TiO₂ membranes with a cut off <500 Da. *Journal of Membrane Science*. 174, 123–133.

Ray, M., Bhattacharya, P., Das, R., Sondhi, K., Ghosh, S., Sarkar, S., 2015. Preparation and characterization of macroporous pure alumina capillary membrane using boehmite as binder for filtration application. *Journal of Porous Materials*. 22, 1043–1052.

R

Romanos, G.E. Steriotis, T.A., Kikkinides, E.S., Kanellopoulos, N.K., Kasselouri, V., Ramsay, J.D.F., Langlois, P., Kallus, S., 2001. Innovative methods for preparation and testing of Al₂O₃ supported silicalite-I membranes. *Journal of the European Ceramic Society*. 21, 119–126.

Roy, R., Roy, D.M., Francis, E.E., 1955. New Data on thermal decomposition of Kaolinite and Halloysite. *The American Ceramic Society*. 38, 198–205.

S

Sadegh, H., Shahryari-ghoshekandi, R., Tyagi, I., Agarwal, S., Gupta, V.K., 2015. Kinetic and thermodynamic studies for alizarin removal from liquid phase using poly-2-hydroxyethyl methacrylate (PHEMA). *Journal of Molecular Liquids*. 207, 21–27.

Saffaj, N., Persin, M., Younsi, S.A., Albizane, A., Bouhria, M., Loukili, H., Dach, H., Larbot, A., 2005. Removal of salts and dyes by low ZnAl₂O₄–TiO₂ ultrafiltration

membrane deposited on support made from raw clay. *Separation and Purification Technology*. 47, 36–42.

Saffaj, N., Persin, M., Younsi, S.A., Albizane, A., Cretin, M., Larbot, A., 2006. Elaboration and characterization of microfiltration and ultrafiltration membranes deposited on raw support prepared from natural Moroccan clay: application to filtration of solution containing dyes and salts. *Applied Clay Science*. 31, 110–119.

Sahnoune, F., Chegaar, M., Saheb, N., Goeuriot, P., Valdivieso, F., 2008a. Algerian kaolinite used for mullite formation. *Applied Clay Science*. 38, 304–310.

Sahnoune, F., Chegaar, M., Saheb, N., Goeuriot, P., Valdivieso, F., 2008b. Differential thermal analysis of mullite from Algerian kaolin. *Advances in Applied Ceramics*. 107, 9–13.

Sahoo, G., Halder, R., Jedidi, I., Oun, A., Nasri, H., Roychoudhury, P., Majumdar, S., Bandyopadhyay, S., Ben Amar, R., 2016. Preparation and characterization of microfiltration apatite membrane over low cost clay-alumina support for decolorization of dye solution. *Desalination and Water Treatment*. 57, 27700–27709.

Sarkar, S., Bandyopadhyay, S., Larbot, A., Cerneaux, S., 2012. New clay–alumina porous capillary supports for filtration application. *Journal of Membrane Science*. 392–393, 130–136.

Sarkar, S., Chakraborty, S., Bhattacharjee, C., 2015b. Photocatalytic degradation of pharmaceutical wastes by alginate supported TiO₂ nanoparticles in packed bed photo reactor (PBPR). *Ecotoxicology and Environmental Safety*. 121, 263–270.

Sarkar, S., Sondhi, K., Das, R., Chakraborty, S., Choi, H., Bhattacharjee, C., 2015a. Development of a mathematical model to predict different parameters during pharmaceutical wastewater treatment using TiO₂ coated membrane. *Ecotoxicology and Environmental Safety*. 121, 193–198.

Song, Z., Fathizadeh, M., Huang, Y., Chu, K.H., Yoon, Y., Wang, L., Xu, W.L., Yu, M., 2016. TiO₂ nanofiltration membranes prepared by molecular layer deposition for water purification. *Journal of Membrane Science*. 510, 72–78.

T

Tahri, N., Masmoudi, G., Ellouze, E., Jrad, A., Drogui, P., Ben Amar, R., 2012. Coupling microfiltration and nanofiltration processes for the treatment at source of dyeing-containing effluent. *Journal of Cleaner Production*. 33, 226–235.

V

Van der Bruggen, B., Cornelis, G., Vandecasteele, C., Devrees, I., 2005. Fouling of nanofiltration and ultrafiltration membranes applied for wastewater regeneration in the textile industry. *Desalination*. 175, 111–119.

W

Wang, Y.H., Liu, X.Q., Meng, G.Y., 2007. Preparation of asymmetric pure titania ceramic membranes with dual functions. *Materials Science and Engineering: A*. 445–446, 611–619.

Xiang, Z., Di, C., Zhiwei, W., Yang, L., Rong, C., 2013. Nano-TiO₂ membrane adsorption reactor (MAR) for virus removal in drinking water. *Chemical Engineering Journal*. 230, 180–187.

Z

Zhang, X., Wang, Y., You, Y., Meng, H., Zhang, J., Xu, X., 2012. Preparation, performance and adsorption activity of TiO₂ nanoparticles entrapped PVDF hybrid membranes. *Applied Surface Science*. 263, 660–665.

Zhu, Z., Wei, Z., Sun, W., Hou, J., He, B., Dong, Y., 2016. Cost-effective utilization of mineral-based raw materials for preparation of porous mullite ceramic membranes via in-situ reaction method. *Applied Clay Science*. 120, 135–141.

Chapter 4

HYBRID CERAMIC MEMBRANE REACTOR SYSTEM **FOR WATER AND WASTEWATER TREATMENT** **INTENSIFICATION**

Introduction

Since their disclosure, membranes separation and heterogeneous catalysis have been widely investigated as efficient approach for water purification and wastewater remediation (Ahmad et al. 2006; Aloulou et al., 2018; Jlassi et al., 2013). However, very few scientific reviews have examined the literature on combination of membrane filtration and catalysis into single hybrid system. Nowadays, catalytic membrane reactor (CtMR) present an innovative methodology for water and wastewater treatment, including removal of suspended particles, inorganic ions and organic pollutants (Jiang al., 2013; Liu et al., 2020; Xu et al., 2019; Zhang et al., 2018; Zhong et al., 2011). CtMR constitutes an association, in which membrane and catalyst interact, in a single system, for both catalytic reaction through catalytically active nanomaterials and a physical separation by permselective membranes (Jiang al., 2013). The coupling system allows the implementation of a continuous process with simultaneous separation and catalytic reduction of organic pollutants, recovery of free powder catalysts from the reaction mixture and makes it possible to limit membrane fouling (Chen al., 2015; Jiang al., 2013; Liu et al., 2017; Zhong et al., 2011).

Until now, ceramic membrane is one of the most popular membrane used in a membrane reactor due to their mechanical, thermal and chemical stability. Moreover, ultrafiltration (UF) constitute the most appropriate process for effluent and wastewater treatment. Dittmeyer and Caro (2008) and Liu et al. (2017) have developed various ceramic UF membrane (α -Al₂O₃: 60 nm, 100 nm and 200 nm; ZrO₂: 65 nm; TiO₂: 5 nm and γ -Al₂O₃: 5 nm) for the efficient removal of nitrated pollutants from water in presence of supported monometallic Pd and bimetallic Pd-Cu and Pd-Sn catalysts. In other research works, *Zhong and colleagues* were successfully employed asymmetric tubular UF ZrO₂/Al₂O₃ membrane to recover nano-sized nickel catalysts from the reaction slurry after 4-nitrophenol reduction (Zhong et al., 2011).

Furthermore, widely range of materials including polymers, graphene, clay and others can be used as rigid substrates of different shape and composition for the fabrication of nanostructured catalytic materials. Monolithic composites and ternary nanocomposites through are considered as the most suitable catalyst supports for the fabrication of nanostructured hybrid catalytic materials interfacial polymerization incorporating Nanoscale zero-valentmetallic NPs (Jlassi et al., 2013; Khalil et al., 2015; Mahouche-Chergui et al., 2013). Nanostructuring by using layer-by-layer coating methods for fabricating improved separation layer have been also reviewed to control selectivity and permeation flux of the ceramic membrane (Aloulou et al., 2018).

The scope of the present work is the development of novel membrane reactors by employing selective tubular UF ceramic membrane and polymeric nanostructured catalyst suitable for simultaneously separation and catalytic reduction of harshly water polluted.

Section 1

Hybrid Treatment System Combining Heterogeneous Catalysis with Membrane Separation for Improved removal of 4-Nitrophenol and Textile Wastewater

1. Experimental

1.1. Chemicals and materials

Titanium dioxide nanoparticles (TiO_2 , 98%, $\Phi=10\text{nm}$), polyvinyl alcohol (PVA, MW-13000–23000 g mol^{-1}), methocel, Nitric acid (HNO_3 , $\geq 99.999\%$), Sodium hydroxide (NaOH, $\geq 97.0\%$, pellets) for membrane cleaning, 4-nitrophenol (4NP) and sodium borohydride (NaBH_4 , 98%) were purchased from Sigma–Aldrich Chemical Company, France. Raw wastewater was provided by SITEX textile industry, Tunisia. Raw mud, used for membrane support shaping, was provided by the hydro cyclone laundries of phosphate from Gafsa Phosphate Company, Tunisia. Gold-decorated polymeric nanocomposites were used in this study as suspended catalysts to insure chemical reduction reaction.

1.2. Material design and membrane nanostructuring

The green tubular supports were prepared using homemade apparatus for shaping a plastic mud paste by extrusion method. The followed procedures for making ceramic support from the micronized mud powder ($60\mu\text{m}$) were similar to that reported by Khemakhem et al. (2015). The active UF layer based on nano- TiO_2 powder was performed by dip-coating process for a dipping time of 60s. The preparation method of colloidal titania suspension and the heating treatment program of deposited membrane are described in the previously work of Oun et al. (2017).

The ternary gold decorated clay/polymer nanocomposites were prepared by chemical grafting, in-situ photopolymerization, impregnation and chemical reduction method as described in *Section 1 of Chapter 2*.

1.3. Membrane characterization

As reported by *Khemakhem and co-workers* raw mud powder was sufficiently characterized by several techniques (Khemakhem et al., 2011; Khemakhem et al., 2015). In this work, the microstructure morphology and the surface uniformity of the asymmetric nano- TiO_2 membrane as well as the adherence quality between the UF deposited layer and the membrane support were investigated by scanning electron microscopy (SEM) using a MERLIN scanning

electron microscope from Carl Zeiss. The pore size distribution and total pore volume of the fabricated UF membrane were measured by mercury porosimetry analysis.

1.4. Experimental procedure (CMR)

The cross-flow filtration tests were performed using a homemade apparatus (Khemakhem et al., 2009) equipped with a feed tank having a working volume of 2 L and asymmetric tubular UF membranes having 7 mm inner diameter (i.d.), 10 mm outer diameter (o.d.), 150 mm length and effective area of 75.4 cm²).

The experiments were performed by circulating feed solution into ceramic membrane reactor (CMR) system in the presence of monometallic gold supported catalysts suspensions. The permeate flux and filtration process were run at room temperature and under applied transmembrane pressure (TMP) range between 0.25 and 4 bar. The TMP was controlled by using two adjustable pressure valves located in both sides of membrane. Regularly collection of the permeate samples were performed for measuring permeate flux and rejection ratio while the retentate was returned back into the feed tank.

Hydraulic permeability (L/hm² bar) of the prepared UF nano-TiO₂ membrane was carried out by measuring the water flux (J_w) as a function of time at different TMP values according to Darcy's law equation: $J_w = L_p * TMP$ (Bouazizi et al., 2016).

Individual UF process was operated as reference to evaluate the performance intensification accorded by catalysis/separation coupling system. Moreover, the efficiency of the hybrid CMR process was evaluated for treating of aqueous 4NP solutions in the optimal conditions previously optimized by single UF membrane separation. Then, synergetic potential of suspended nanocomposite catalyst effect and the cross flow UF were carried out on a textile wastewater, to exhibit the advancement in engineered hybrid CMR system.

1.5. Analytical methods

The purification efficiency was monitored by measuring the following parameters (COD, dye content, pH and turbidity) according to standardized protocols. HACH RATIO 2100A turbidimeter was used to measure the turbidity of feed solution and permeate. The pH is obviously one of the basic characteristics of water. It indicates possible corrosion problems and the possibility of the presence of toxic metals. In the present work, the pH was measured using a digital pH- meter (NeoMet pH-220 L). Electrical conductivity measurement was performed by a NeoMet EC Meter EC-400 L conductimeter. The COD corresponds to the determination of the amount of oxygen required to oxidize the organic and inorganic matter

suspected to be oxidized. This parameter gives an estimate of the dose of organic and inorganic pollutants present in the wastewater.

2. Results and discussion

2.1. Permeation experiments and rejection performance

The preliminary experiments were performed in membrane module without catalyst loading in order to evaluate the performance of ceramic UF membrane during treatment of 4NP before coupling with catalysis in a hybrid system.

During single UF process, the permeation properties and the membrane rejection performances were examined. The results in term of Normalized flux (J_N), cumulative permeate volume (CPV), J_C and 4NP rejection are shown in *Figure 41*. The time dependent variation in J_N of 4NP feed solution (250 ppm) through the pristine membrane was calculated under different values of TMP ranging from 0.5 to 4 bar.

The results displayed in *Figure 41a* show a permeate flux decline with time. This behavior was observed for all experiments with 4NP. Moreover, a significant permeate flux decline of around 36.6% took place in the case of 4NP filtration at high pressure of 4bar. While, a decrease of only 6% of the initial flux was recorded at low pressure of 0.5 bar during the same operated time of 180min.

Figure 41c shows that the permeation flux increased with TMP until 2 bar and then become independent of pressure for a values beyond 2 bars. This behavior is due to the polarization of the concentration phenomena, which corresponds to the formation of a layer on the membrane surface by the retained substances during filtration. Then 2 bar will be considered as the optimal working TMP and then retained for the further experiments.

It can be also observed that the decrease of the permeate flux with time was more important within the first 60 min, and beyond that, the decline kinetic was slow and the UF membrane reached a steady state flux. The same trend was widely mentioned in the literature (Bouazizi et al. 2017a; Chougui et al. 2019; Ma'ruf et al. 2019; Malik et al. 2020; Ouaddari et al. 2019; Xu et al. 2010).

Further analysis of the data show that the flow rate of cumulative permeate reduced with the filtration time. This was observed whether at low or high pressure. Thus, the flow rate at the beginning of the experiment is always more important than that at a more advanced treatment time even without considering the TMP. Consequently, this can be an indication for the deterioration of membrane permeation properties. More precisely, for a TMP of 2bar a CPV of more than 260 mL was recorded within operation time of 15min.

The permeate flux and retention of organic pollutants is very dependent to the pressure change (Chhaya et al. 2012; Oun et al. 2017; Xu et al. 2010). In this context, **Figure 41c** illustrates the filtration flux were studied under the effect of working pressure at a fixed 4NP concentration. Compared to pure water flux, a linear improvement of 4NP permeate flux was observed only for TMP range of 0.5-2 bar. Beyond 2 bar, the permeate flux increase very weakly. This behavior is described in the literature by critical flux concept. It can be identified as the limitation of linear relationship in the experimental plot of permeate flux change with TMP.

It should be mentioned that Davis and workers were the first to use the term of critical flux (Davis et al. 1987). After that, relatively few studies have studied the relation between working pressure, flux and membrane fouling which is caused by stagnant cake layer on the membrane surface during the filtration process and intensifies with pressure (Chen et al 1995; Chen et al. 1997; Kim et al.1993).

However, as in earlier research works, the critical flux was defined as “the flux below which no fouling occur” (Bacchin 1994; Bacchin et al. 1995; Benkahla et al. 1995; Blatt et al. 1970; Field et al. 1995; Howell 1995; Reihanian et al. 1983). The critical flux, as mentioned by the literature corresponds to the required flux to overcome repulsion due to osmotic pressure in the cross flow filtration (Bacchin et al. 2006; Tahri et al. 2012). As it can be clearly seen from the empirical results shown in **Figure 41c** the critical flux was 165 L/hm² and the associated "critical pressure" was 2 bar.

On the other hand, the pollutant concentration is a significant factor in all water treatment process and particularly in the ultrafiltration membrane separation (Damodar et al. 2010). In this case, the membrane performance was explored in single UF process, in terms of 4NP removal by studying the variation of the 4NP retention with feed concentration (50–2000 ppm) at fixed TMP of 2bar and during 180 minutes of operating time.

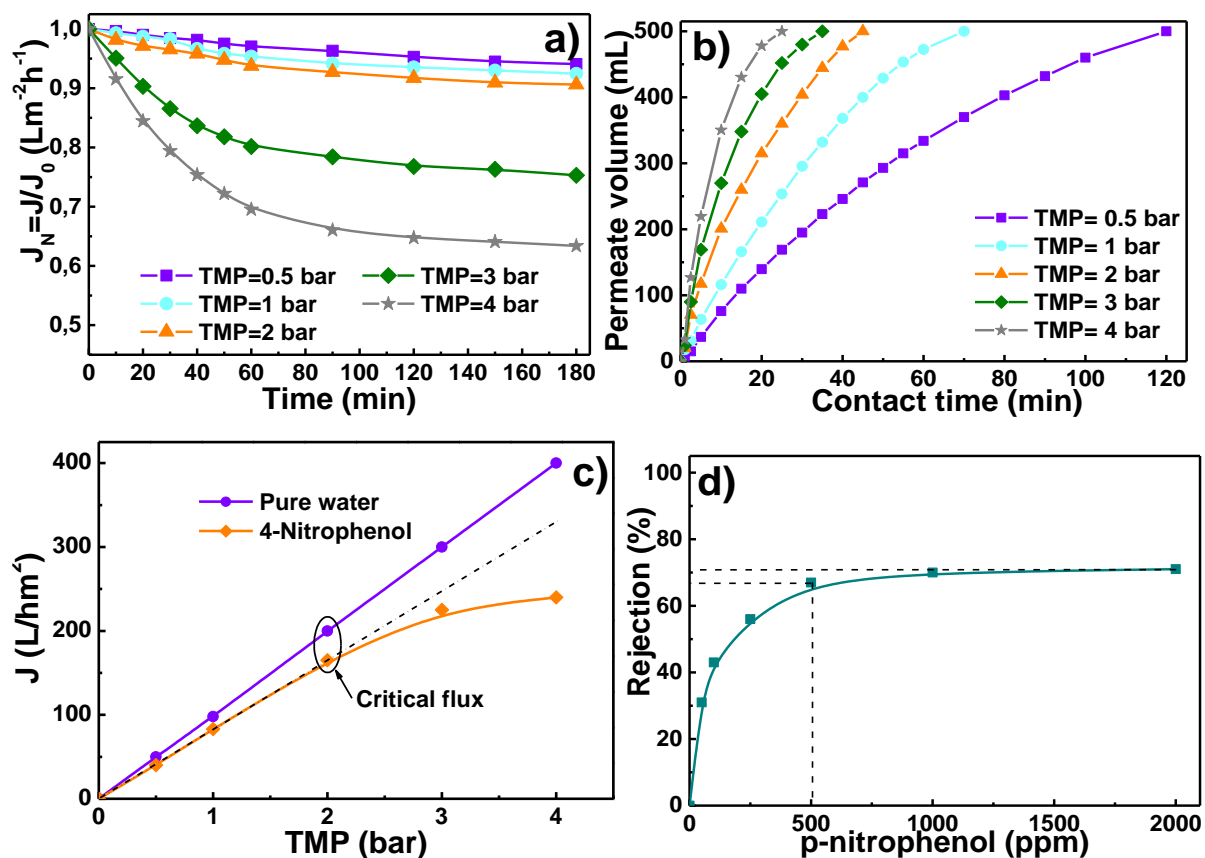


Figure 41. (a) Normalized flux ($J_N = J/J_0$), (b) CPV of 250ppm 4NP solution as function of UF operation time at different TMP, (c) critical permeation flux and (d) effect of 4NP concentration on the membrane rejection rate at 2 bar.

As it can be seen in **Figure 41d**, the 4NP retention increases sharply with the increase of the initial concentration from 0 to 70% -75% at a concentration between 5000 and 1000 ppm and then become almost independent of concentration reaching an equilibrium. The 4NP retention seems follow a logarithmic relation with the pollutant concentration. From **Figure 41d**, the rejection was improved from 31% to 67% by increasing initial concentration from 50 to 500ppm. Then, at higher feed concentrations (>500ppm) the removal rate increases very slowly. This may probably due to the accumulation and aggregation of pollutant molecules during filtration, resulting, with various other mechanisms, in membrane fouling (Fersi, et al. 2009; Hairom et al. 2014; Howe et al. 2002; Jiang et al. 2018; Wiesner et al. 1996). Interestingly, increasing of feed concentration promotes foulants particles accumulation on the membrane surface and 4NP removal becomes more significant than at lower concentration (Saffaj et al. 2004). A possible explanation could be the additional concentration promotes the resistance to permeation of the pollutants by contributing to the molecules aggregation (Lin et al., 2016; Hamada et al., 1991; Bouazizi et al., 2017b). The aggregation seems more effective

as concentration of molecules increases. According to various research works, higher feed concentration leads to the enhancement of osmotic pressure and then the permeate flux should to be decreased (Antón et al. 2015; Banerjee et al. 2010; Choudhury et al. 2019; Hamada et al. 1991; Hilal et al. 2007; Yu et al. 2012). Moreover, the best rejection, observed when increasing the feed concentration, was explained by the membrane fouling which reduces the apparent membrane pore size (Howe et al. 2002; Ripperger et al. 2002; Saffaj et al. 2004; Waite et al. 1999). On the other hand, Zahrim and workers indicated that the plateau observed at high feed concentration was related to the fouling establishment on the membrane surface (Zahrim et al. 2011). Based on these experimental results, it seems that the best operating conditions favorable for an optimal 4NP removal by UF membrane were for TMP of 2 bar and initial feed concentration of 500 ppm.

2.2. Hybrid water treatment system in CMR

2.2.1. Nanocatalyst integration for 4NP removal

In order to evaluate the nanocomposite contribution into the continuous catalysis/UF process, the approach consisting in single UF with and without MMT-PGMA-NH₃⁺@Au nanocomposite catalyst integration was followed. The effect of variation of catalyst loading on the process performances in term of permeation flux and 4NP removal were investigated.

Figure 42 shows an evaluation of the influence of the catalyst dose on the permeate flux and permeate quality and then on the performances of the hybrid system during the treatment of 4NP aqueous solution. **Figure 42a**, shows the evolution of the permeate flux with time at different catalyst dose varying from 100 to 500 mg/L under the hybrid continuous catalysis/UF system and a single UF. It is very clear that the addition of the catalyst allows the limitation of membrane fouling observed under a single UF where a decrease of over 35% in permeate flux was observed after 3 h of UF. Moreover, the results show that the presence of catalytic NP in the CMR configuration allows a rapid stabilization of the permeate flux. The highest flux value was observed with the highest dose of catalyst, i.e., 500 mg/L. The stabilized flux increased from 143 L.m⁻².h⁻¹ to 165 L.m⁻².h⁻¹ when the catalyst dose increased from 100 to 500 mg/L respectively. It is worthy to notice that, when 100 mg/L of catalyst was added, the permeate flux decreases slightly during the first minutes of filtration and then quickly stabilized. It is suggested that suspended catalyst particles in the feed accumulate on the membrane surface forming an additional filter layer, which allowed to a drop of the permeation flux (Xia et al., 2007).

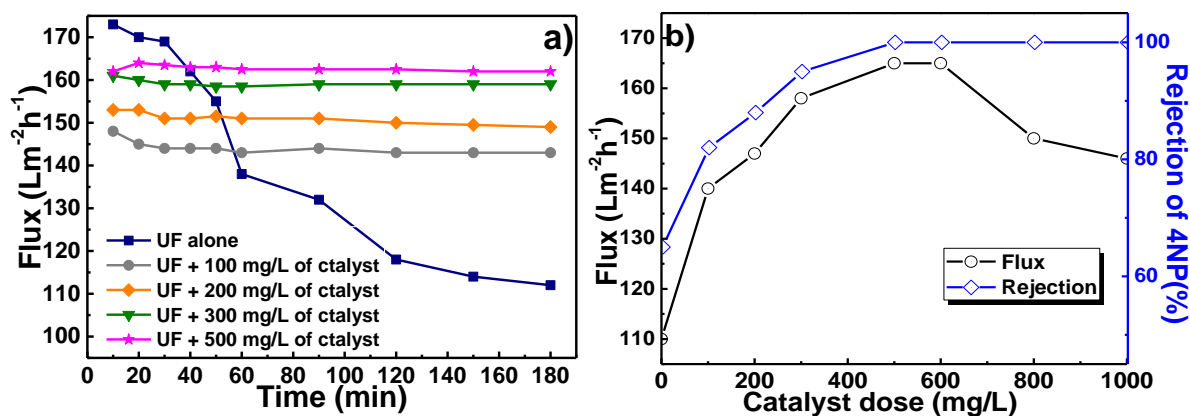


Figure 42. Effect of the catalyst dose on (a) Permeate flux stability with filtration time (b) Permeate flux and 4NP retention; (TMP = 2, initial 4NP concentration = 500ppm, working time= 3h).

In this study, the results demonstrate that the catalyst particles are completely retained by the membrane. Therefore, by further increasing of integrated amount of nanocomposite from 100mg/L to 500mg/L, the formed nanocomposite filter layer become thicker. This led to a first barrier occurred to retain the pollutant molecules, adsorbed on the membrane surface. Thus, membrane fouling is inhibited and a high and stable permeability was established (Zhong et al. 2011).

In agreement with these results, Tansakul et al. (2011) and Hammami et al. (2017) revealed that powdered activated carbon (PAC) integration in hybrid water treatment process (Adsorption/UF) enhanced permeate flux. Moreover, ultrafiltration flux should to improve with the enhancement of PAC loading by crushing surface and detach the cake layer deposited on the membrane surface. Contrary, the smaller fouling rate was exhibited at the higher PAC dose.

Prior research works suggest that control of cake permeability through monitoring the aggregate size could allow to a better fouling reduction and then a strong increase in the flux was observed (Ripperger et al. 2002; Waite et al. 1999).

In this context, it was suggested by *Zhong and co-workers* that the accumulation of the nanosized nickel nanocatalyst on the MF and UF ceramic membranes surface during the hydrogenation of 4NP to 4-aminophenol (4AP) permit the nickel particle aggregation. Consequently, the enlargement of the aggregate caused by further particles number leads porous cakes formation and high flux is often obtained (Zhong et al. 2011).

More recently, *Mozia et al. (2015)* have proven that introducing of catalytic particles into the feed tank using tubular ceramic membrane in the hybrid system coupling catalysis with ultrafiltration, allows a permeate flux stabilization. The authors explained the limitation of the

decrease of the permeate flux by the abrasion of the deposited cake layer by the suspended catalytic TiO₂ particles.

To identify the optimal dose of catalyst to be added, the influence of wider catalyst loading (100 - 1000 mg/L) were tested under constant working pressure of 2bar and initial feed concentration of 500 ppm. As expected, the UF permeation flux and membrane retention of 4NP were increased with the enhancement of catalyst loading.

As shown in **Figure 42**, the heterogeneous catalysis assisted UF process achieves the maximum yield (total 4NP removal and a high permeate flux of 167 L.m⁻².h⁻¹) for a catalyst dose of 500mg/L. However, once the slurry concentration of catalyst exceeds this optimum value, the influence of the addition of catalyst on the process performances is no longer the same. In this study, an increase of nanocomposite concentration beyond 500 mg/L still has any influence on the rejection performance, which was remained constant (100%). While, it was accompanied by a clear decrease in flux. This mainly attributed to the increase of the deposited layer thickness on the membrane surface, resulting from the interaction between the pollutants and the nanocomposite. Therefore, after reaching an equilibrium, a further catalysts dose leads to the layer grows which improve the layer resistance. Consequently, the filtration flux decline (Zhong et al. 2011).

2.2.2. CMR for textile wastewater removal

The next stage of this investigation was devoted to the study of the performance of the coupling the heterogeneous catalysis with UF in CMR system for application in the treatment of textile effluent.

The aim in this approach is mainly based on its ability to remove contaminants, in particular dyes via the catalytic membrane offering simultaneously catalytic reaction which allows the reduction of organics by MMT-PGMA-NH₃⁺@Au and physical separation by UF membrane.

The effluent used in this case is a mixture of different effluents coming from the dyeing cycle (SITEX company). The characteristics of this effluent are illustrated in **Table 7**. This effluent has a harsh alkaline pH, high salinity and a relatively intense coloration.

The comparison between performances of both single UF and hybrid system was achieved in terms of permeate flux and of permeate quality (pollution retention). It is worthy to highlight that, due to its high loading charge, the raw effluent has underwent a pretreatment by MF using a pristine ceramic mud support (mud = sub-product from phosphate industry). The MF pretreatment allows the minimization of the load content, lower energy consumption and the limitation of UF membrane fouling.

Table 7. Characterization of the raw effluent of SITEX textile industry.

pH	Conductivity ($\mu\text{S/cm}$)	Turbidity (NTU)	Color	TDS	COD	SS	Cl ⁻	Na ⁺	SO ₄ ⁼
11 \pm 1	2600 \pm 50	200	350	14000	3020	509	960	1980	960
			\pm 100	\pm 2000	\pm 400	\pm 60	\pm 100	\pm 120	\pm 100

2.2.2.1. Permeation study: influence of VCF on permeate flux

The permeate flux variation can be monitored as a function of time or also using the volume concentration factor (VCF) defined as follows:

$\text{FCV} = V_0/V$, where V_0 is the volume of the feed and V is the volume of concentrate.

The variation of permeate flux with and without integration of composite nanocatalyst as a function of the VCF is shown in **Figure 43**. It can be observed that a maximum VCF of 3.5 was obtained with the application of a single UF, while with the hybrid system the maximum value was of 6. This result indicates that the hybridization of the system provides a permeate flux significantly higher than that produced by a single UF which can be explained by the different changes that can bring by the adding of catalyst, mainly on the intrinsic properties of UF membrane (fouling resistance, selectivity and permeability of the membrane). **Figure 43** shows also a rapidly drop of the J_N with VCF to reach a value of 3 and then became independent of VCF when UF was applied alone. Indeed, the flux decreased by about 60% during the first minutes of filtration process. However, the flux decline was less important in the presence of slurred nanocatalyst resulting in permeate flux decrease not exceeding 15% and 13% at VCF of 6, respectively by introducing MMT-PGMA-Au in the membrane reactor.

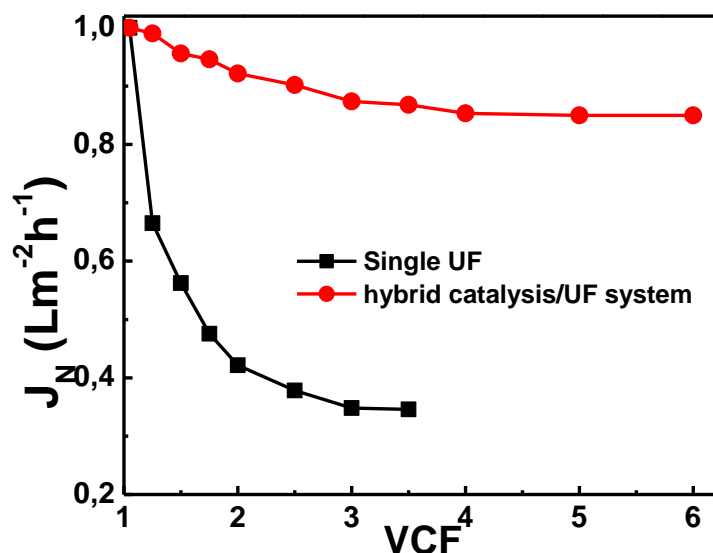


Figure 43. Variation of the permeate flux with VCF for textile wastewater treatment (Conditions: $W_{\text{catalyst}} = 0.5 \text{ g/L}$; $\text{TMP} = 2\text{bar}$).

Therefore, for simple UF, the solute concentration and suspended solids (SS) in the feed solution strongly affected the membrane permeate flux, which can be explained by the increase in the rate of saturation of the membrane surface with the foulant particles due to the nature and physical properties of the effluents (Bouazizi et al., 2016). The high permeate flux stability, as a result of the nanocomposite catalyst integration, was enhanced by the continuous synergy of separation and catalytic reaction in membrane surface.

In addition to their catalytic properties toward organics removal, the nanocomposite integration avoids the adhesion of fine particles onto the membrane surface by the formation of a dynamic nanocomposite separation layer, avoiding membrane surface fouling. These results are in agreement with that reported in the literature (Bouazizi et al., 2016; Hammami et al., 2017).

2.2.2.2. Enhancement of permeate flux quality

The elaborated titania UF membrane was applied to the treatment of textile effluent. As can be seen, the raw effluent is characterized by a high conductivity ($2600 \mu\text{s/cm}$) which is due to the excess of salts and by a significant turbidity (200 NTU), due to the high amount of the suspended material (5.1 g/L) which is responsible for the dark coloration of the effluent. The performance of the simple UF and the hybrid process in terms of COD reduction, turbidity and color (Abs) were studied. The filtration experiments were carried out at working pressure of 2 bar and at VCF of 2.5 for UF process and of 6 bars for the hybrid system.

Table 8. Performance of the hybrid catalysis/UF process.

Parameter	Raw effluent	Biologically treated effluent	UF permeate	NF permeate	Catalysis/UF In CMR
pH	11	≈ 8.5	≈ 8.2	7.4 - 6.8	7.8 - 7.2
Conductivity (μS/cm)	2600	789	784	320	780
Turbidity (NTU)	200	34	0.8	0.1	0.2
COD (mg/L)	3020	192	170	<30	<15
TDS (mg/L)	14000	4800	4780 ± 20	<1850	4700 ± 50
Color (mg/L)	350	110	30 ± 5	0	0
SS (mg/L)	509	40	2	0	0

The experimental results obtained in this study are presented in the *Table 8*, the retention of the different pollutants are very important for both UF and catalysis/UF processes. Almost total color and turbidity removal were achieved in both cases respectively (99.9% and 100% for color and 99.9% and 99.9% for turbidity). It can be mentioned that color and turbidity removal were practically independent of VCF and almost completely achieved for both VCF of 2.5 and 6 because of the excellent performance of the prepared UF membrane. On the other hand, the best COD removal was achieved for hybrid process giving COD values lower than 170 mgL⁻¹ and 15 mgL⁻¹ at VCF of 3 and 6 for UF and hybrid processes respectively.

In general, COD rejection increases by increasing VCF. *Bes-Piá and co-workers* suggested that this behavior is related to the difference between organic molecule sizes and pore's diameters of the membrane, besides of the fouling layer (Bes-Piá et al., 2010). In the case of simple UF, the increasing of VCF promotes the membrane fouling by solutes and fine particles that were not removed in the microfiltration pretreatment of the feed solution.

In contrast, the excellent COD removal by the hybrid system is not attributed to membrane fouling as much as it is due to the additional porous layer dynamically formed by hybrid catalyst. The comparison of performances for simple UF and considered hybrid system with others treatment processes is shown in *Table 8*.

2.3. Membrane regeneration

During the long-term use of ceramic membrane for wastewater remediation, an expected fouling of UF membrane may be occurred. Therefore, effective membrane cleaning strategies are required for flux recovery, in view of its practical applications in the industrial scale. Therefore, at the end of each filtration cycle, for the simple or hybrid system, the membrane has systematically undergone cleaning steps, according to the nature of fouling by rinsing with water, use of acidic and alkaline solutions at low and high TMP. It is to highlight that in the case of chemical cleaning a water rinsing until neutralization is necessary after each operation.

Figure 44 shows the flux recovery of the UF membrane and separation efficiency for color removal after applying UF membrane for consecutive ten running cycles in simple and hybrid treatment. As indicated in **Figure 44a**, the titania UF membrane has a high flux recovery after cleaning process, indicating the presence of irreversible membrane fouling in the case of simple UF caused by the complexity of the raw effluent. Integrating polymer based catalytic nanocomposite for the hybrid system allowed the recovery of the initial flux values (**Figure 44a**) and significant color removal (**Figure 44b**).

However, although the modest salts rejection rate was obtained, the reuse of the permeate remains possible in the dyeing cycle after adjustment of the salt quantity according to the dyeing formulation.

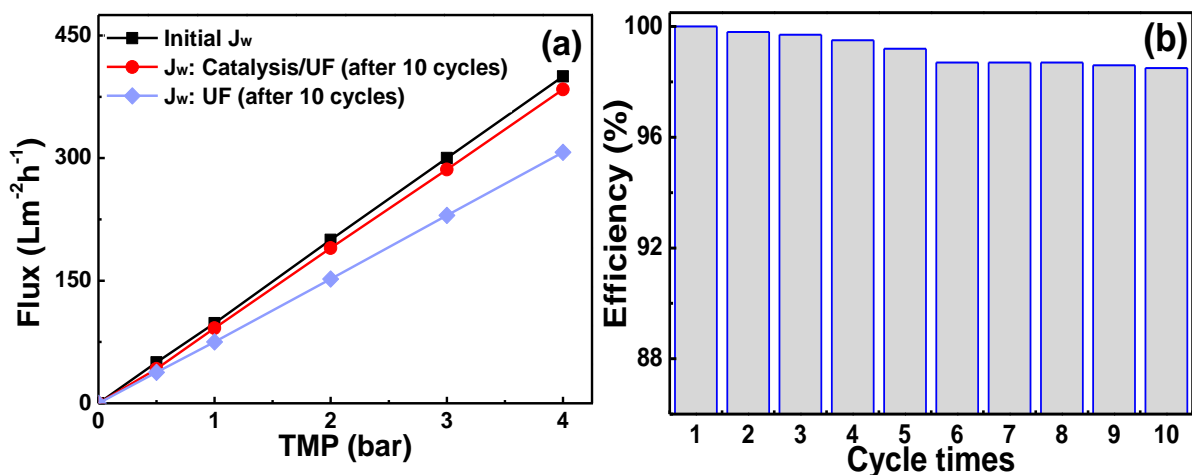


Figure 44. Regeneration of UF membrane operating in hybrid system in the case of the use of 500mg/L of catalyst (case of textile effluent treatment).

3. Conclusion

In summary, tubular ceramic membrane was exhibited remarkable performances toward 4NP removal (67%). Then, higher performance in terms of permeate flux behavior and 4NP retention was observed by powdered nanocomposite catalysts integration in the filtration system. Stabilized permeate flux with almost no flux reduction with filtration time and a total retention of 4NP at a pressure of 2 bars and catalyst dose of 500 mg/L were observed.

Furthermore, hybrid treatment system containing low cost ceramic UF membrane and catalytic gold nanoparticles mediated nanocomposite was successfully developed and applied for wastewater degradation. In addition, the experimental results revealed that loading CMR with catalyst nanoparticles provide strong benefits in continuous catalysis-UF textile wastewater treatment. Continuous circulated nanocatalyst leads to creation of a dynamic layer on the membrane surface. Hence, that intensify the treatment performances by providing additional separation barrier and enhance permeation by crushing fouling layer.

Excellent COD, color, turbidity removal and permeate flux value quite near to that of water permeability with highly purified water were observed. Good performance was also supported by the stability of both membrane and catalyst.

In this study, it can be concluded that nanocomposite catalysts provide to the membrane UF excellent performances and make contribution to the industrial application of coupling systems of heterogeneous catalysis with membrane separation.

References

A

- Ahmad, A.L., Puasa, S.W., Abiding, S., 2006. Crossflow ultrafiltration for removing direct-15 dye from wastewater of textile industry. *Asean Journal on Science and Technology for Development*. 23, 207-216.
- Aloulou, W., Hamza, W., Aloulou, H., Oun, A., Khemakhem, S., Jada, A., Chakraborty, S., Curcio, S., Amar, R.B., 2018. Developing of titania-smectite nanocomposites UF membrane over zeolite based ceramic support. *Applied Clay Science*. 155, 20–29. doi:10.1016/j.clay.2017.12.035.
- Antón, E., Álvarez, J.R., Palacio, L., Prádanos, P., Hernández, A., Pihlajamäki, A., Luque, S., 2015. Ageing of polyethersulfone ultrafiltration membranes under long-term exposures to alkaline and acidic cleaning solutions. *Chem. Eng. Sci.* 134, 178–195.

B

- Bacchin, P., 1994. Formation et résistance au transfert d'un dépôt de colloïdes sur une membrane d'ultrafiltration. Doctorale thesis. p181.
- Bacchin, P., Aimar, P., Field, R.W., 2006. Critical and sustainable fluxes: theory, experiments and applications. *Journal of Membrane Science*. 281, 42-69.
- Bacchin, P., Aimar, P., Sanchez, V., 1995. Model for colloidal fouling of membranes. *Aiche Journal*. 41, 368-377.
- Banerjee, P., De, S., 2010. Steady state modeling of concentration polarization including adsorption during nanofiltration of dye solution. *Sep. Purif. Technol.* 71, 128–135.
- Benkahla, Y.K., Ould-Dris, A., Jaffrin, M.Y., Si-Hassen, D., 1995. Cake growth mechanism in cross-flow microfiltration of mineral suspensions. *Journal of Membrane Science*. 98, 107-117.
- Bes-Piá, A., Cuartas-Urbe, B., Mendoza-Roca, J.-A., Alcaina-Miranda, M.I., 2010. Study of the behaviour of different NF membranes for the reclamation of a secondary textile effluent in rinsing processes. *Journal of Hazardous Materials*. 178, 341–348. doi:10.1016/j.jhazmat.2010.01.085.
- Blatt, W.F., Dravid, A., Michaels, A.S., Nelsen, L., 1970. Solute polarization and cake formation in membrane ultrafiltration: causes, consequences, and control techniques (pp 47–91). In J.E. Flinn (Ed.), *Membrane Science and Technology*. 234. New York: Springer US. doi:10.1007/978-1-4684-1851-4_4.

- Bouazizi, A., Breida, M., Achiou, B., Ouammou, M., Calvo, J.I., Aaddane, A., Younssi, S.A., 2017a. Removal of dyes by a new nano-TiO₂ ultrafiltration membrane deposited on low-cost support prepared from natural Moroccan bentonite. *Applied Clay Science*. 149, 127-135.
- Bouazizi, A., Breida, M., Karim, A., Achiou, B., Ouammou, M., Calvo, J.I., Aaddane, A., Khiat, K., Younssi, S.A., 2017b. Development of a new TiO₂ ultrafiltration membrane on flat ceramic support made from natural bentonite and micronized phosphate and applied for dye removal. *Ceram. Int.* 43, 1479–1487.
- Bouazizi, A., Saja, S., Achiou, B., Ouammou, M., Calvo, J.I., Aaddane, A., Younssi, S.A., 2016. Elaboration and characterization of a new flat ceramic MF membrane made from natural Moroccan bentonite. Application to treatment of industrial wastewater. *Applied Clay Science*. 132-133, 33–40. doi:10.1016/j.clay.2016.05.009.

C

- Chen, S., Yu, J., Wang, H., Yu, H., Quan, X., 2015. A pilot-scale coupling catalytic ozonation–membrane filtration system for recirculating aquaculture wastewater treatment. *Desalination*. 363, 37–43. doi:10.1016/j.desal.2014.09.006.
- Chen, V., Fane, A.G., Madaeni, S., Wenten, I.G., 1997. Particle deposition during membrane filtration of colloids: transition between concentration polarization and cake formation. *Journal of Membrane Science*. 125, 109–122.
- Chen, V., Kim, K.J. Fane, A.G., 1995. Effect of membrane morphology and operation on protein deposition in ultrafiltration membranes. *Biotechnology and Bioengineering*. 47, 174-180.
- Chhaya, Mondal, S., Majumdar, G.C., De, S., 2012. Clarifications of stevia extract using cross flow ultrafiltration and concentration by nanofiltration. *Separation and Purification Technology*. 89, 125–134.
- Choudhury, P.R., Majumdar, S., Sarkar, S., Kundu, B., Sahoo, G.C., 2019. Performance investigation of Pb(II) removal by synthesized hydroxyapatite based ceramic ultrafiltration membrane: Bench scale study. *Chemical Engineering Journal*. 355, 510-519.
- Chougui, A., Belouatek, A., Rabiller-Baudry, M., 2019. Synthesis and characterization of new ultrafiltration ceramic membranes for water treatment. *Journal of Water Process Engineering*. 30, 100620. doi:10.1016/j.jwpe.2018.04.017.

D

- Damodar, R.A., You, S.J., Ou, S.H., 2010. Coupling of membrane separation with photocatalytic slurry reactor for advanced dye wastewater treatment. *Separation and Purification Technology*. 76, 64–71.
- Davis, R.H., Leighton, D.T., 1987. Shear-induced transport of a particle layer along a porous wall. *Chemical Engineering Science*. 42, 275-281.
- Dittmeyer, R., Caro, J., 2008. Catalytic Membrane Reactors. In Ertl, G., Knoezinger, H., Schueth, F., Weitkamp, J., (Eds.), *Handbook of Heterogeneous Catalysis*, 3865. Weinheim, Germany: Wiley-VCH. doi.10.1002/9783527610044.hetcat0117.

F

- Fersi, C., Gzara, L., Dhahbi, M., 2009. Flux Decline Study for Textile Wastewater Treatment by Membrane Processes. *Desalination*. 244, 321-332.
- Field, R.W., Wu, D., Howell, J.A., Gupta, B.B., 1995. Critical flux concept for microfiltration fouling. *Journal of Membrane Science*. 100, 259-272.

H

- Hairom, N.H.H., Mohammad, A.W., Kadhum, A.A., 2014. Nanofiltration of Hazardous Congo Red Dye: Performance and Flux Decline Analysis. *Journal of Water Process Engineering*. 4, 99-106.
- Hamada, J.K., Nonogaki, H., Fukushima, Y., Munkhbat, B., Mitsuishi, M., 1991. Effects of hydrating water molecules on the aggregation behavior of azo dyes in aqueous solutions. *Dyes Pigment*. 16, 111–118.
- Hammami, A., Charcosset, C., Ben Amar, R.R., 2017. Performances of Continuous Adsorption-Ultrafiltration Hybrid Process for AO7 Dye Removal from Aqueous Solution and Real Textile Wastewater Treatment. *Journal of Membrane Science & Technology*. 07, 1-8. doi:10.4172/2155-9589.1000171.
- Hilal, N., Al-Abri, M., Al-Hinai, H., 2007. Characterization and retention of UF membranes using PEG, HS and polyelectrolytes. *Desalination*. 206, 568–578.
- Howe, K.J., Clark, M.M, 2002. Fouling of Microfiltration and Ultrafiltration Membranes by Natural Waters. *Environmental Science and Technology*. 36, 3571–3576.
- Howell, J.A., 1995 Sub-critical flux operation of microfiltration. *Journal of Membrane Science*. 107, 165-171.

J

- Jiang, H., Meng, L., Chen, R., Jin, W., Xing, W., Xu, N., 2013. Progress on Porous Ceramic Membrane Reactors for Heterogeneous Catalysis over Ultrafine and Nano-sized Catalysts. *Chinese Journal of Chemical Engineering*. 21, 205-215. doi: 10.1016/S1004-9541(13)60460-7.
- Jiang, M., Ye, K., Lin, J., Zhang, X., Ye, W., Zhao, S., Van der Bruggen, B., 2018. Effective dye purification using tight ceramic ultrafiltration membrane. *Journal of Membrane Science*. 566, 151–160.
- Jlassi, K., Singh, A., Aswal, D.K., Losno, R., Benna-Zayani, M., Chehimi, M.M., 2013. Novel, ternary clay/polypyrrole/silver hybrid materials through in situ photopolymerization. *Colloids and Surfaces A: Physicochemical and Engineering Aspects*. 439, 193–199. doi:10.1016/j.colsurfa.2013.04.005.

K

- Khalil, A. M., Georgiadou, V., Guerrouache, M., Mahouche-Chergui, S., Dendrinou-Samara, C., Chehimi, M.M., Carbonnier, B., 2015. Gold-decorated polymeric monoliths: In-situ vs ex-situ immobilization strategies and flow through catalytic applications towards nitrophenols reduction. *Polymer*. 77, 218–226. doi:10.1016/j.polymer.2015.09.040.
- Khemakhem, M., Khemakhem, S., Ayedi, S., Ben Amar, R., 2011. Study of ceramic ultrafiltration membrane support based on phosphate industry subproduct: Application for the cuttlefish conditioning effluents treatment. *Ceramics International*. 37, 3617–3625.
- Khemakhem, M., Khemakhem, S., Ayedi, S., Cretin, M., Ben Amar, R., 2015. Development of an asymmetric ultrafiltration membrane based on phosphates industry sub-products. *Ceramics International*. 41, 10343–10348.
- Khemakhem, S., Larbot, A., Ben Amar, R., 2009. New ceramic microfiltration membranes from Tunisian natural materials: Application for the cuttlefish effluents treatment. *Ceramics International*. 35, 55–61.
- Kim, K.J., Chen, V., Fane, A.G., 1993. Some factors determining protein aggregation during ultrafiltration. *Biotechnology and Bioengineering*. 42, 260-265.

L

- Lin, J., Ye, W., Baltaru, M.C., Tang, Y.P., Bernstein, N.J., Gao, P., Balta, S., Vlad, M., Volodin, A., Sotto, A., Luis, P., Zydney, A.L., Van der Bruggen, B., 2016. Tight

ultrafiltration membranes for enhanced separation of dyes and Na₂SO₄ during textile wastewater treatment. *Journal of Membrane Science*. 514, 217–228.

Liu, H., Zhang, J., Lu, M., Liang, L., Zhang, H., Wei, J., 2020. Biosynthesis Based Membrane Filtration Coupled with Iron Nanoparticles Reduction Process in Removal of Dyes. *Chemical Engineering Journal*. 387, 124202. doi:10.1016/j.cej.2020.124202.

Liu, Y., Peng, M., Jiang, H., Xing, W., Wang, Y., Chen, R., 2017. Fabrication of ceramic membrane supported palladium catalyst and its catalytic performance in liquid-phase hydrogenation reaction. *Chemical Engineering Journal*. 313, 1556–1566. doi.org/10.1016/j.cej.2016.11.037.

M

Mahouche-Chergui, S., Guerrouache, M., Carbonnier, B., Chehimi, M.M., 2013. Polymer-immobilized nanoparticles. *Colloids and Surfaces A: Physicochemical and Engineering Aspects*. 439, 43–68. doi:10.1016/j.colsurfa.2013.04.013.

Ma'ruf, A., AgusSalim Al Fatoni, M., MulyadiPurnawanto, A., &Meilani, I., 2019. Utilization of Natural Zeolite for Development of Ceramic/Polymer Composite Membrane for Ultrafiltration. *Materials Today: Proceedings*. 19, 1547–1551.

Malik, N., Bulasara, V.K., Basu, S., 2020. Preparation of novel porous ceramic microfiltration membranes from fly ash, kaolin and dolomite mixtures. *Ceramics International*. 46, 6889-6898.

Mohammad, A.W., Teow, Y.H., Ang, W.L., Chung, Y.T., Oatley-Radcliffe, D.L., Hilal, N., 2015. Nanofiltration membranes review: Recent advances and future prospects. *Desalination*. 356, 226–254. doi:10.1016/j.desal.2014.10.043.

Mozia S., Szymanski K., Michalkiewicz B., Tryba B., Toyoda M., Morawski A.W., 2015. Effect of process parameters on fouling and stability of MF/UF TiO₂ membranes in a photocatalytic membrane reactor. *Separation and Purification Technology*. 142, 137–148.

O

Ouaddari, H., Karim, A., Achiou, B., Saja, S., Aaddane, A., Bennazha, J., El Amrani El Hassan, I., Ouammou, M., Albizane, A., 2019. New low-cost ultrafiltration membrane made from purified natural clays for Direct Red 80 dye removal. *Journal of Environmental Chemical Engineering*, 7, 103268. doi:10.1016/j.jece.2019.103268.

Oun, A., Tahri, N., Mahouche-Chergui, S., Carbonnier, B., Majumdar, S., Sarkar, S., Sahoo, G.C., Ben Amar, R., 2017. Tubular ultrafiltration ceramic membrane based on titania nanoparticles immobilized on macroporous clay-alumina support: Elaboration, characterization and application to dye removal. *Separation and Purification Technology*. 188, 126–133.

R

Reihanian, H., Robertson, C.R., Michaels, A.S., 1983. Mechanisms of polarization and fouling of ultrafiltration membranes by proteins. *Journal of Membrane Science*. 16, 237-258.

Ripperger, S., Altmann, J., 2002. Cross flow microfiltration-state of the art. *Separation and Purification Technology*. 26,19–31.

S

Saffaj, N. Loukili, H., AlamiYounssi, S., Albizane, A., Bouhria, M., Persin, M., Larbot, A., 2004. Filtration of solution containing heavy metals and dyes by means of ultrafiltration membranes deposited on support made of Moroccan clay. *Desalination*. 168, 301-306.

T

Tahri, N., Masmoudi, G., Ellouze, E., Jrad, A., Drogui, P., Ben Amar, R., 2012. Coupling microfiltration and nanofiltration processes for the treatment at source of dyeing-containing effluent. *Journal of Cleaner Production*. 33, 226-235.

Tansakul, C., Laborie, S., Cabassud, C., 2011. Adsorption combined with ultrafiltration to remove organic matter from seawater. *Water Research*. 45, 6362-6370.

W

Waite, T.D., Schafer, A.I., Fane, A.G., Heuer, A., 1999. Colloidal fouling of ultrafiltration membranes: impact of aggregate structure and size. *J. Colloid Interface Sci*. 212, 264–274.

Wiesner, M.R., Aptel, P., 1996. Mass Transport and Permeate Flux and Fouling in Pressure-driven Process. *Water Treatment Membrane Handbook*. McGraw-Hill, New York.

X

Xia, S.J., Liu, Y.N., Li, X., Yao, J.J., 2007. Drinking water production by ultrafiltration of Songhuajiangriver with PAC adsorption. *J. Environ. Sci*. 19, 536-539.

Xu, C., Pan, X., Fang, L., Li, J., Li, F., 2019. Enhanced reduction of organic pollutants by Fe/Cu@Pd ternary metallic nanoparticles under aerobic conditions: Batch and membrane reactor studies. *Chemical Engineering Journal*. 360, 180–189. doi:10.1016/j.cej.2018.11.212.

Xu, J., Chang, C.Y., Gao, C., 2010. Performance of a ceramic ultrafiltration membrane system in pretreatment to seawater desalination. *Separation and Purification Technology*. 75, 165–173.

Y

Yu, S., Chen, Z., Cheng, Q., Lü, Z., Liu, M., Gao, C., 2012. Application of thin-film composite hollow fiber membrane to submerged nanofiltration of anionic dye aqueous solutions. *Separation and Purification Technology*. 88, 121–129.

Z

Zhang, Y., Wei, S., Hu, Y., Sun, S., 2018. Membrane technology in wastewater treatment enhanced by functional nanomaterials. *Journal of Cleaner Production*, 197, 339–348. doi:10.1016/j.jclepro.2018.06.211.

Zahrim, A.Y., Tizaoui, C., Hilal, N., 2011. Coagulation with polymers for nanofiltration pre-treatment of highly concentrated dyes: a review. *Desalination*. 266, 1–16.

Zhong, Z., Li, W., Xing, W., Xu, N., 2011. Crossflow filtration of nanosized catalysts suspension using ceramic membranes. *Separation and Purification Technology*. 76, 223–230. doi:10.1016/j.seppur.2010.08.005.

Section 2

Novel Ceramic Membrane for Removal of Explosives and Pesticides Contaminants from Water: Combination of Monolithic Catalyst with Co-Sintered Tight UF Membrane

1. Experimental

1.1. Materials

In this study, mud powder from sub-product of phosphates transformation industry (Tunisia) was used as starting materials for the fabrication of ceramic membranes. Titanium oxide (99.5%) and polyvinyl alcohol (99%, M.W. 89000-98000), purchased from Sigma Aldrich were selected as the precursors to achieve the layer-by-layer coating. According to the information provided by the manufacturer, the particles size of the titanium oxide powders is ~21 nm on average. Glycidyl methacrylate (GMA, $\geq 97\%$), ethylene glycol dimethacrylate (EGDMA), 2,2'-azobisisobutyronitrile (AIBN, 98%), 1-dodecanol (1-Dod, 98%), cyclohexanol (99%), iminodiacetic acid (IDA, $\geq 98.0\%$), Ethylenediamine (EDA, $\geq 99.5\%$), trimethylamine ($\text{Et}_3\text{-N}$), anhydrous tetrahydrofuran (THF, $\geq 99.9\%$), acetone ($\geq 99.5\%$), Sodium borohydride (NaBH_4 , $> 99\%$), Nickel(II) chloride (NiCl_2 , 98%), Chloroauric acid (HAuCl_4 , $> 99\%$), 4-Nitrophenol (4NP, $> 99\%$), chloramphenicol (CAP, $\geq 98\%$) and 2,6-dinitroaniline (2,6-DNA, 97%) were purchased from Sigma-Aldrich, France. Deionized water was used in the all experiments.

1.2. Synthesis of P1-IDA@NiNPs and P1-EDA@AuNPs monolithic catalysts

1.2.1. Preparation of poly(EGDMA-co-GMA) monoliths "P1"

The organic p(EGDMA-co-GMA) abbreviated P1 monolith was prepared through photo-induced radical polymerization. 5.2 mL GMA, as a reactive monomer, was copolymerized with 3.4 mL of the cross-linker EGDMA in solvent mixture consisting of 10.8 mL 1-decanol and 1 mL cyclohexanol as porogenic solvents. Reaction mixture was stirred for 15 min under continuous flow of nitrogen gas in the presence of AIBN (1% w/w of the total amount of monomers) as an initiator. To trigger the photo-induced free-radical copolymerization (FRCP), the mixture was placed in a Spectrolinker XL-1500 UV oven (Spectronics, Westbury, NY, USA) equipped with six lamps (6×15 W) and the reaction was proceeded under irradiation at 365 nm with continuously stirring for 1 h. Subsequently, the synthesized monolith was collected by centrifugation and purified through soxhlet extraction overnight in THF, as extracting solvent, to remove the porogenic solvent and eventually non-reacted

monomers. Finally, the white EGDMA-co-GMA sample was dried at 60 °C under vacuum for 24h.

1.2.2. Nickel NPs decorated IDA functionalized polymeric monolith

1 g of monolith P1 was dispersed in a mixture of 25 mL of methanol and 25 mL of deionized water. Then, a few drops of 1M sodium hydroxide aqueous solution were added to adjust pH of the reaction medium, followed by the addition of iminodiacetic acid (IDA, 1M) sequentially. The reaction system was heated to 80 °C and maintained under magnetic stirring overnight. Afterwards, the product was collected by centrifugation then rinsed several times with methanol, ethanol and deionized water successively. Finally, the obtained P1-IDA powder was dried under vacuum at 60 °C for 24 hours.

The synthesis of P1-IDA@Ni was carried out as following. Firstly, 1g of the monolith containing -COOH chelating groups (P1-IDA) was dispersed in 0.1 M sodium hydroxide solution for 1 h and the deprotonated P1-IDA was filtered and then dispersed in 20 mL of NiCl₂ (1M) and allowed to react at room temperature for 2h. After suspension filtration and water washing of the obtained P1-IDA@Ni²⁺, it was dispersed in 10 mL of milli-Q water and then 5mL of freshly prepared NaBH₄ solution (0,1M) were added dropwise to the suspension under nitrogen atmosphere to conduct the in-situ generation of NiNPs on the monolith surface. The resulting P1-IDA@Nimonolith was purified by acetone and water and then collected powders were dried under nitrogen atmosphere.

1.2.3. Gold NPs decorated EDA functionalized polymeric monolith

The Chemical functionalization of the prepared monolith was performed in situ. 1g of the P1 previously prepared was immersed into 100 mL isopropanol in presence of 2mL of triethylamine useful as catalyst for amination reaction.

While stirring, 7mL of ethylene diamine (EDA) was added and the reaction mixture was heated up to 85 °C for 24 h. After that, the resulting solute was washed abundantly by isopropanol and ethanol. Finally, the obtained powder was dried in vacuum oven at 60°C for 2h.

After treatment of EDA-functionalized monolith with 0.1 M hydrochloric acid solution, 500 mg of the resulting chelant P1-EDA monolith was dispersed in 10 mM gold (III) chloride hydrate solution under continuous stirring at room temperature during 2h. After suspension filtration and water washing of the obtained P1-EDA@Au³⁺, it was dispersed in 10 mL of deionized water and then 5 mL of freshly prepared NaBH₄ solution (0,1M) were added

dropwise. The reaction was maintained under stirring at room temperature for 1 h until the solution turned from white to purple, proof of AuNPs formation.

The as-obtained P1-EDA@Au monolith was finally purified through repeated centrifugation/dispersion cycles with water and absolute ethanol, and then dried under vacuum at 60°C for 3h.

1.3. Low-cost membrane design

1.3.1. Porous mud support elaboration

As phosphate sub-products, mud powder has several attractive properties including the great abundance, chemical properties and lower consolidation temperature when compared to other inorganic materials (e.g., metal oxide materials). Due to its unique properties, phosphate mud is considered as particular candidate for making low-cost membranes. The phosphate mud can give also ceramic pastes with good plasticity and an easy shaping (Khemakhem et al., 2011). Here, as robust substrate to deposit filtration layer, tubular ceramic tube was wet route prepared by using extrusion method of green paste. Thereafter, the green support was set on rollers to have a homogenous drying at ambient temperature.

1.3.2. Preparation of tight ultrafiltration titania layer

Tight ultrafiltration bilayer membranes were prepared by layer-by-layer (LbL) deposition technique on the inner surface of green ceramic support. The dry bare support was dip-coated for 60s into a stable titania slurry mainly contains a mixture of nano-TiO₂ dispersed in an aqueous solution of PVA (Oun et al., 2017). Then, the second membrane layer was carried-out in the same conditions by repeating the coating procedure twice. The wet membrane was dried overnight at room temperature then at 150 °C for 12 h, followed by co-sintering process at 800 °C for 3 h to simultaneously achieve consolidation of membrane structure and ensure the adhesion between different layers.

1.3.3. Characterization and Analytical methods

The morphology and surface chemical structure of the prepared composite materials were checked by Scanning Electron Microscopy (SEM) using a MERLIN microscope from Zeiss (Carl Zeiss, Germany), equipped with InLens, BSE and SE2 detectors using a low accelerating tension (2-3 kV) with a diaphragm aperture of 30 μm. X-ray photoelectron spectroscopy (XPS) measurements were performed on a Thermo Scientific K-Alpha XPS

instrument equipped with a monochromatic Al K α X-ray as the excitation source ($h\nu = 1486.6$ eV, spot size = 400 μm).

The metallic gold content in the monolithic materials was characterized using thermogravimetric analysis (TGA) on a SetaramSetsys Evolution 16 thermobalance., under Argon atmosphere in a temperature range of 25–800 °C, at a heating rate of 10 °C/min. Fourier Transform Infrared spectroscopy (FTIR) measurements were conducted on a Bruker Tensor 27 DTGS spectrometer in the wavenumber range of 400-4000 cm^{-1} with an average of 60 consecutive scans and a resolution of 4 cm^{-1} . Prior to analyses, the samples were dried under vacuum at 60 °C for 2h.

Several characterization methods were used to evaluate raw materials and to determine the structural and morphological properties of deposited titania layer. The chemical composition of raw mud powders was determined by X-ray fluorescence (XRF) for metals and by atomic absorption for alkaline earth metals. The particle size distribution of sieved raw powders was checked by the Dynamic Laser Beam Scattering (DLBS) technique. TGA analysis was used on raw mud to identify the mass loss vs heating temperature. Membrane morphology and surface density were examined by scanning electron microscopy (SEM). The pore size distribution of the support and titania coating layer was determinate based on BET method.

1.4. Experimental Procedures

In this work, a homemade apparatus was used to perform the hybrid treatment system. It is composed of a batch catalytic reactor coupled with a membrane module.

The treatment system (CMR) consists in a continuous catalysis/UF including the P1-IDA@Ni and P1-EDA@Au as catalysts and ceramic membrane for separation process.

Firstly, control experiments were carried out using UF membrane without catalysts addition. These experiments allowed to evaluate the individual performance of the TiO₂ membrane and quantify the contribution of membrane rejection on the total CAP and 2,6-DNA removal by the CMR system. These experiments were carried out with an initial working volume of 2 L, a tubular mono-channel membrane surface area of 24 cm^2 under a transmembrane pressure (TMP) of 4 bars throughout the filtration process. After the integration of the catalysis reaction, the membrane rejection efficiency was characterized to evaluate the created synergistic effect.

Initially, the feeding solution was injected in the CMR tank and then the required amount of catalyst was added. Thereafter, a high-pressure pump was connected to promote mixing and to deliver the feed. Once the adsorption–desorption equilibrium between membrane and the

feed solution was achieved, the system was brought to a transmembrane pressure (TMP) of 4 bar by using a pressure transducer. Feeding solution was firstly catalyzed by adding NaBH₄ to the suspended monolithic catalysts. Subsequently, the crossflow filtration was achieved.

The collected permeate was measured using a digital balance and the permeate flux was determined using the following equation:

$$J = V / (S \times \Delta t),$$

where J is the permeate flux (L.m⁻².h⁻¹), V is the volume of collected permeate (L), S is the effective surface area of the membrane (m²), and Δt is the permeation time (h).

The permeate quality was analyzed using UV–Visible spectrophotometer to evaluate the hybrid system performances.

The total removal efficiency was calculated using the following equation:

$$\text{Removal efficiency} = [(C_{\text{feed}} - C_{\text{outlet}}) / C_{\text{feed}}] \times 100,$$

where C_{feed} and C_{outlet} are the initial feed solution and sampling permeate concentration, respectively.

2. Results and discussion

2.1. Monolithic nanocomposites characterization

The FTIR spectroscopy was carried out to analyze the chemical structure of the monolith P1 and to control the functional group during the chemical modification process by IDA and EDA molecules. As shown in *Figure 45a*, the FTIR data of raw P1 presents a double weak peak at 2939 cm⁻¹ and 2996 cm⁻¹ and strong peak at 1726 cm⁻¹ corresponding, respectively, to the characteristic vibration of methylene and methyl (ν_{C-H}) and ester (ν_{C=O}) groups, presented in of GMA and EGDMA structure. In addition, three weak peaks were observed at 752 cm⁻¹, 845 cm⁻¹ and 907 cm⁻¹ assigned to the vibration band (δ_{C-H epoxy}) of epoxy ring of the GMA microspheres. Additional absorption band characteristic of C–O–C stretching vibration (ν_{C-O-C}) was detected at 1450 cm⁻¹. Indeed, after the modification reaction of the monolith using iminodiacetic acid, the disappearance of characteristic epoxy ring peaks confirms its conversion by the ring opening. Meanwhile, a new broad band assigned to hydrogen bonded alcohol O–H stretching (ν_{O-H}) centered at 3410 cm⁻¹ was appeared and hide this of carboxylic groups exist as dimers in the IDA because of to their strong hydrogen bonding. Moreover, the NiNPs immobilization onto the functionalized monolith kept busy the carboxylic groups which followed by vanishing its characteristic band.

To control the changes in surface chemical composition of the monolith P1 after the incorporation of EDA, the FTIR spectra were recorded on pristine and EDA modified

monolith as shown in **Figure 45b**. In the case of EDA modification of P1, the methylene and methyl groups vibrations were slightly shifted from 2939 cm^{-1} and 2996 cm^{-1} to 2830 cm^{-1} and 2939 cm^{-1} respectively. Further, during the EDA functionalization process, the band intensity of the epoxide groups is nearly disappeared. Additionally, in the EDA modified P1 monolith spectra, a broad and weak absorption bands were appeared at 3332 cm^{-1} and at 1558 cm^{-1} resulted from $-\text{NH}_2$ stretching ($\nu_{\text{N-H}}$) and N-H bending respectively. Thus, confirm the successful grafting of EDA onto the epoxide function of the monolith P1. Consequently, the free primary amine functions acted as ligand to immobilize the gold nanoparticles.

The thermal properties of the synthesized P1 monoliths before and after modification were determined using TGA analysis as presented in **Figure 45c and 45d**. Both P1-IDA and P1-EDA are stable up to 300. The stability of NiNPs and AuNPs supports play a vital role in their catalytic performance, as high stable support would enable the recyclability of catalysts. It's worthy to note that the monoliths stability increased after incorporating Ni and Au nanoparticles. At 700 °C, 19.5 wt.% and 16.5 wt.% residues, corresponding to the contents of metallic nanoparticles, were detected for P1-IDA@Ni and P1-EDA@Au, respectively.

The structures, phase purities and chemical nature of nickel and gold NPs decorated monoliths were examined by X-ray powder diffractometer (XRD) using Bruker D8 Advance X-ray diffractometer equipped with Cu K α ($\lambda = 1.54 \text{ \AA}$) with scan rate 2° min^{-1} and diffraction angle range 10-90°. The XRD patterns of these materials are illustrated in **Figure 45e and f**. As can be seen from **Figure 45e**, the presence of Ni was confirmed by the X-ray diffraction peaks observed at $2\theta = 17.35^\circ$, 34° , 44° and 60° attributed to (111), (200), (111) and (220) reflection planes, respectively (Castillo et al., 2015; Karthik et al., 2017; Roy et al., 2018; Yan et al., 2014). In addition, all recorded reflection peaks are indexed to the crystal face centered cubic structure of metallic (Ni^0) and nickel oxide (NiO) NPs (JCPDS card No.040850; JCPDS card No. #47-1049).

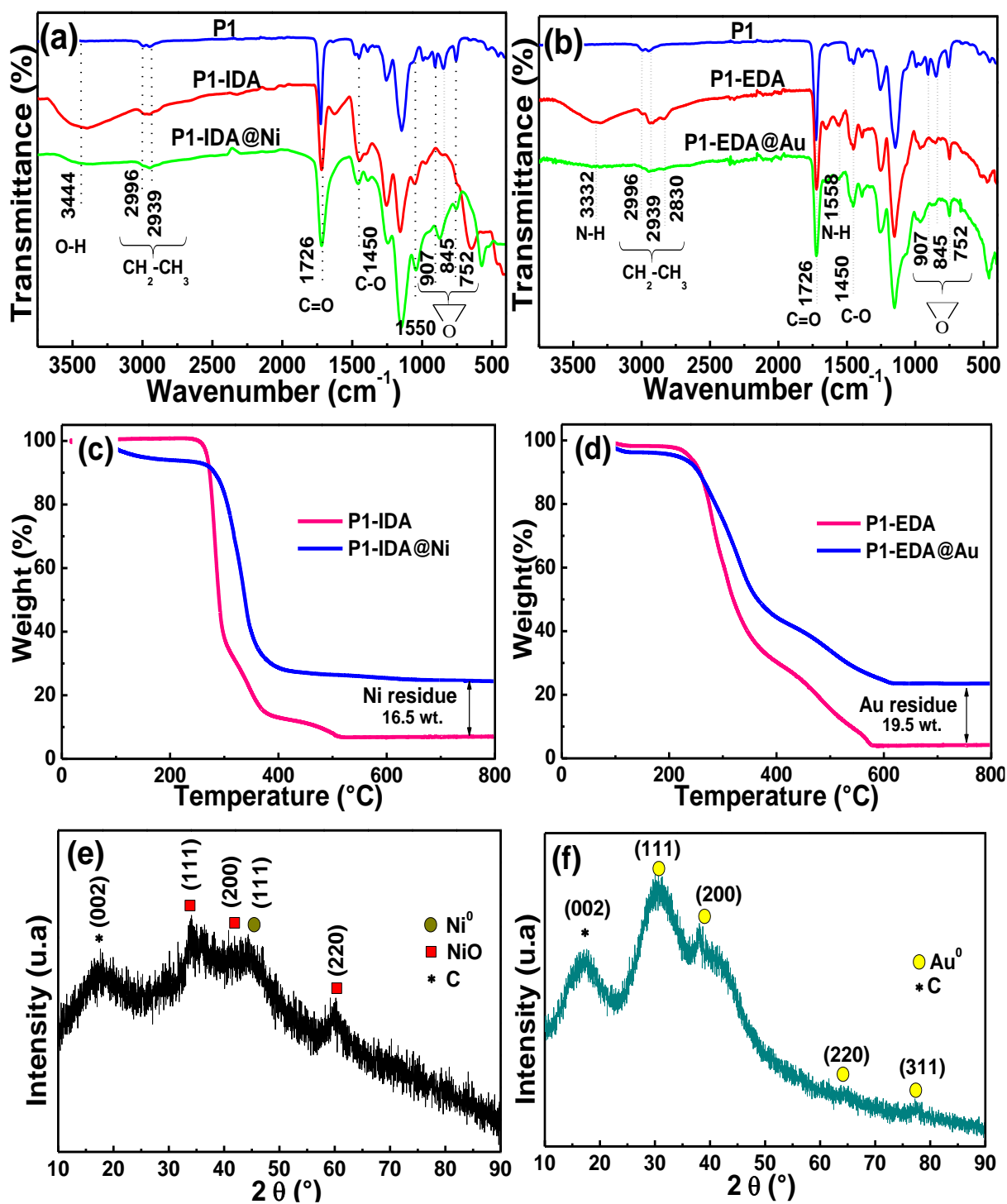


Figure 45. Physicochemical characterization of P1-IDA@Ni and P1-EDA@Au monolithic catalysts by FTIR (a and b), TGA (c and d) and XRD (e and f).

The characteristic nickel oxide peaks were due to the surface oxidation layer that covers Ni⁰ NPs by the air contact may be during the centrifugation process (Zhou et al., 2019). **Figure 45f** shows the diffraction peaks at 30.65 (111), 37.94 (200), 64.34 (220) and 77.54 (311) which indicates the formation of the crystalline face-centered cubic structure of gold

nanoparticles (Au⁰) on P1 matrix (Chen et al., 2019; JCPDS file number: 04–0784; Maity et al., 2012; Philip et al., 2009; Sen et al., 2013; Seo et al., 2017; Shankar et al., 2003; Suvith et al., 2014). The unassigned peaks indicate the crystallization of the organic matter which surround the metal nanoparticles (Philip et al., 2009; Shankar et al., 2003; Suvith et al., 2014).

2.2. 4NP removal using P1-IDA@Ni and P1-EDA@Au

To evaluate the catalytic ability of the as-prepared nickel and gold-based monoliths, the hydrogenation reaction of 4NP to 4AP was selected as catalytic model reaction in the presence of NaBH₄ as a hydrogen source at room temperature.

In this present work, the reduction of 4NP in a moderate reaction conditions of [4NP]= 0.5mM; [NaBH₄]= 12.5 mM and catalyst dose = 0.25 mg/mL was monitored by measuring absorbance intensity change during reaction time using an Agilent Cary 60 UV-Visible Spectrometer (*Figure 46*). However, *Figures 46a and b* show a quickly decrease in the intensity of the 4-nitrophenolate absorption peak at 400 nm. Meanwhile, the bright yellow color gradually fading to colorless and a new absorption peak was detected at 297 nm, which indicated the conversion of 4NP to 4AP. The completion reduction times were 100 s and 200 s when using P1-EDA@Au and P1-IDA@Ni catalysts, respectively. Accordingly, this indicates the high catalytic activity of both gold and nickel immobilized on P1 monolith with a best activity for gold NPs.

The kinetic constant (k_{app}) values determined from the slopes of the plots shown in *Figure 46c* show that the reduction 4NP in the presence of NaBH₄ using gold supported P1 was of $3.73 \times 10^{-1} \text{ s}^{-1}$, so 2.5 more higher compared to that of nickel catalyst ($1.51 \times 10^{-2} \text{ s}^{-1}$). The lower catalytic activity of NiNPs based monolith in comparison to AuNPs based monolith could be attributed to the presence of an oxide layer on the surface of NiNPs which formed when the samples are exposed to ambient air. Indeed, such a layer induces the decrease in the availability of the immobilized Ni active sites for the reduction reaction. Furthermore, it is worth to mention that in the case of P1-IDA@NiNPs, there was a slow initial decrease in the intensity of the 4NP absorption peak (see *Figure 46a*) due to the induction period clearly detected in *Figure 46c*. This time interval can be assigned to the time taken by nickel oxide layer to be reduced to nickel by NaBH₄ reducing agent present in excess in the catalytic reaction.

In order to further investigation of the contribution of NaBH₄ solution and catalysts in the total hydrogenation reaction of 4NP, the adsorption ability of the monolithic matrix and reducing effect of NaBH₄ in the absence of MNPs were carried out as reference tests.

As illustrated in *Figure 46d*, after introducing EDA-functionalized monolith (0.25 mg/mL) and an excess of NaBH₄ ([NaBH₄]/[4NP]=25), the UV–Vis absorption spectrum of 4NP at 400 nm recorded for a period of 3h shows a slight changes. The slight variation in the intensity of the absorption characteristic band at 400 nm indicated that P1-EDA (similar behavior in the case of P1-IDA) has no catalytic effects and this slight change could be explained by the adsorption of molecules on support via complexation reaction by COOH and NH₂ chelant groups present on the surface of the monoliths. Moreover, both of P1-IDA and P1-EDA and NaBH₄ contribute by 12% of the final removal rate of 4NP during 3h which correspond to 0.11% for the same conditions (reduction time of 100s) in presence of P1-EDA@Au.

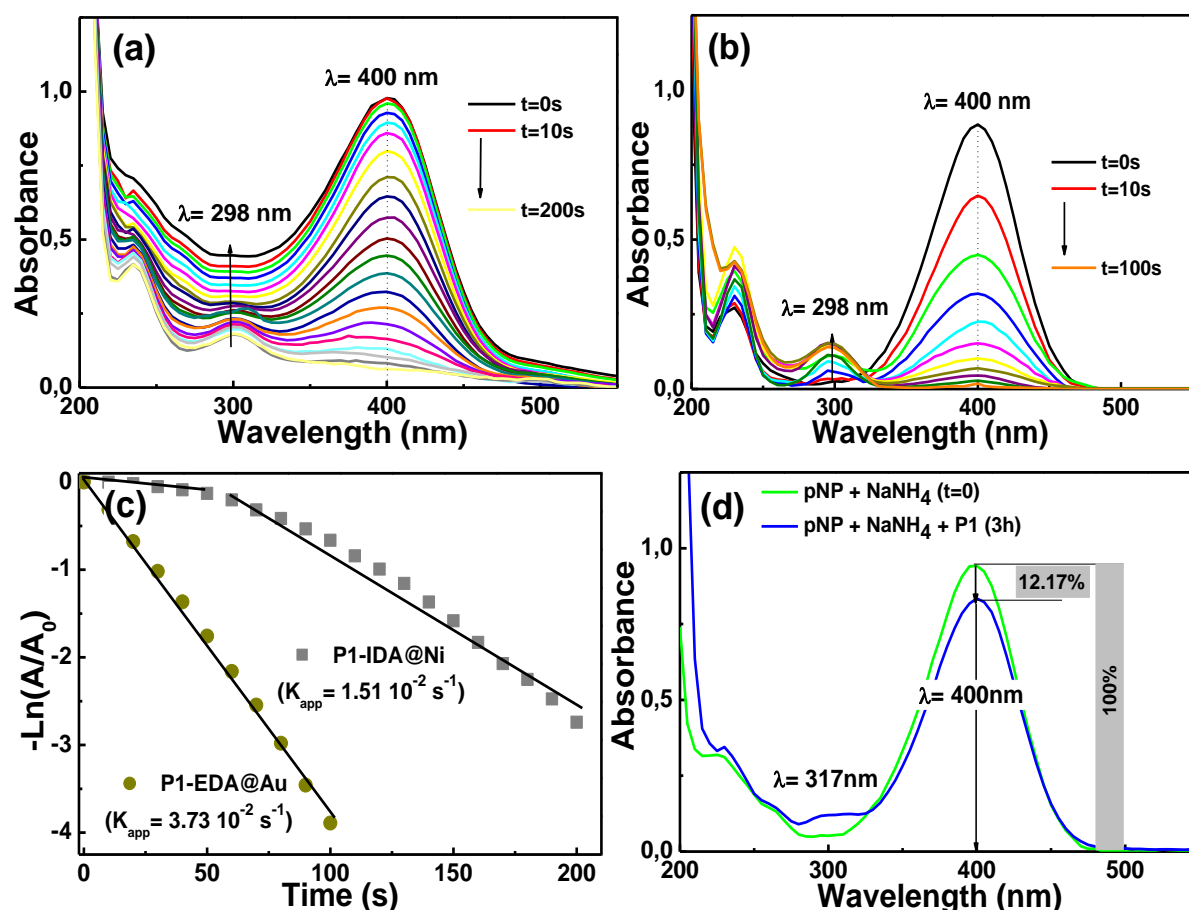


Figure 46. UV-vis spectra of 4NP during the reducing reaction using (a) P1-IDA@Ni, (b) P1-EDA@Au hybrid catalysts, (c) the corresponding pseudo-first order kinetics and (d) the reference catalytic reaction. Conditions: [4NP] = $5 \cdot 10^{-4}$ M; [NaBH₄] = 0.05 M; Dose of catalyst = 1mg/mL.

2.3. Reusability of monolithic catalysts

The reusable catalytic properties of the as-prepared catalysts were shown in **Figure 47**. The conversion of 4NP can achieve above 97% and 98% by using P1-IDA@Ni and P1-EDA@Au catalysts respectively, even after running for eight cycles (**Figure 47a and b**). This indicates the high chemical stability and the excellent catalytic performance of the synthesized nanohybrid catalysts.

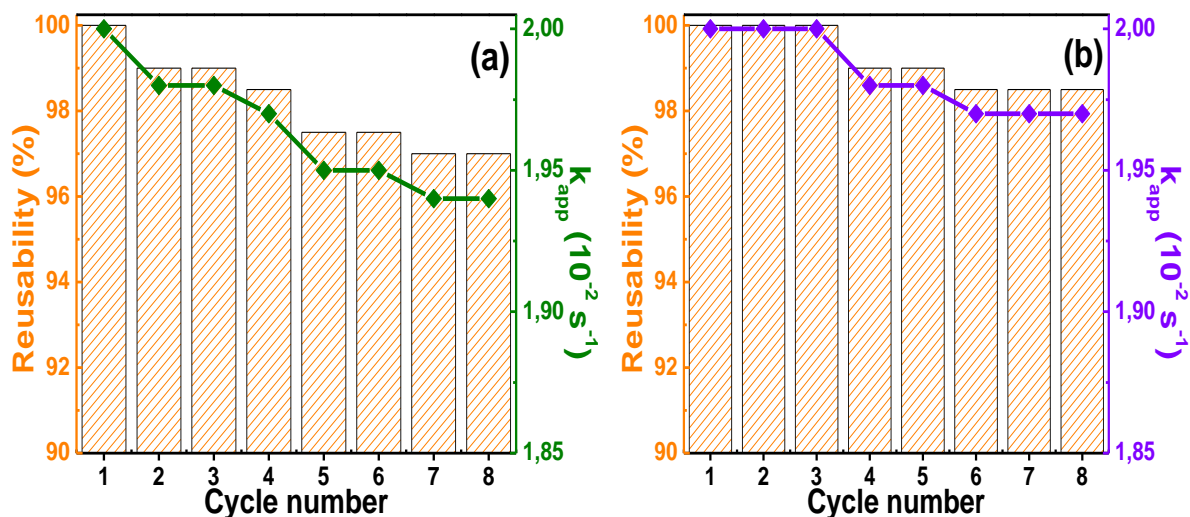


Figure 47. Cycling performance plots of (a) P1-IDA@Ni and (b) P1-EDA@Au catalysts for 4NP reduction within 200s and 100s respectively.

2.4. Ceramic membrane characterization

2.4.1. Raw mud powder characterization

The chemical composition of the raw mud reveals that the major components were calcium (CaO, 19.98%) and phosphate (P₂O₅, 8.40%) oxides as shown in **Table 9**. It can be noted that this phosphate mud is a carbonated fluor-apatite (Bouazizi et al., 2017).

Table 9. Chemical composition of phosphate mud.

Elements	P ₂ O ₅	CaO	SO ₄	SiO ₂	Fe ₂ O ₃	F ⁻	Al ₂ O ₃	MgO	CO ₂	C _{org}
(wt.%)	8.40	19.98	2.47	38.89	1.09	1.30	6.75	1.84	6.06	13.12

In addition, particle size distribution of mud powder as a function of volume distribution percentage is given in **Figure 48**. According to the statistical data, the most of particle size distribution located in the range of 8 μ m and 20 μ m with an average particle size in the order of 14 μ m. Furthermore, particle size of starting powder plays an important role in the porosity, pore size distribution and the morphological structure of the final co-sintered membrane.

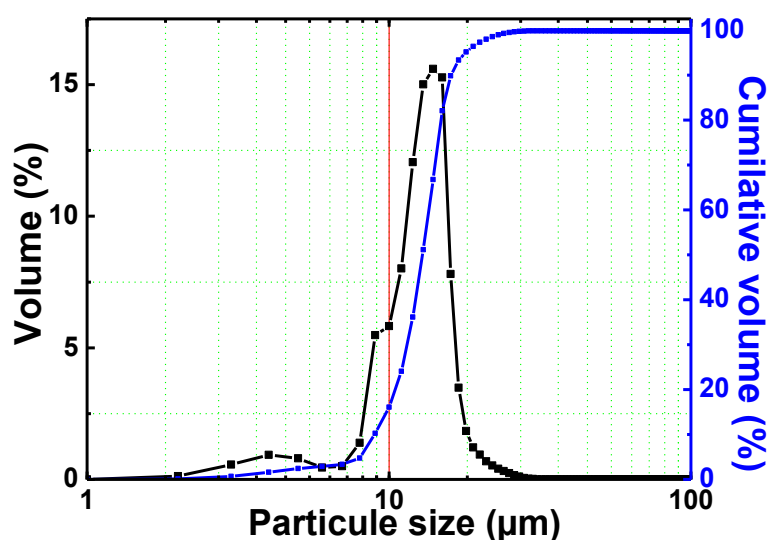


Figure 48. Particle size distribution of mud powder used for membrane elaboration.

Chen and co-workers have mentioned that the morphology and the pore structure are straightly affected by the particles mean diameter (Chen et al., 2016). As a result, they concluded that the average pore size for both the support and the membrane layers decreases with decreasing the mean diameter of the used nanoparticles. *Liu and co-workers* have explained this behavior by the good packing density provided by small particles, which could easily produce, under the heating effect, a dense membrane texture (Liu et al., 2012) confirming the low porosity of UF membrane.

2.4.2. Scanning electron microscopy (SEM)

The morphological structure, surface quality and densification of the membrane were analyzed by FESEM. **Figure 49** shows the structure of titania membrane including morphologies of the cross-section (**Figure 49a, c and e**) and surface view (**Figure 49b, d and f**) of bare support and co-sintered titania membrane layers at 800°C / 3h prepared by layer-by-layer coating.

Figure 49a shows the overall cross-section of mud support. On its symmetric structure, a first TiO₂ layer was successfully deposited. As seen, the coating penetration into surface structure of support was not readily to be quantified and the measured approximate thick value was estimated by around 18 μm (**Figure 49c**). Subsequently, the following nano-TiO₂ coating exhibit a top layer uniformly deposited on the surface of previously layer and have around 12 μm thick (**Figure 49e**).

It can be clearly deduced from FESEM images that the nano-TiO₂ coating of membrane support was reported to change both pore size and morphology of the membrane layer compared to the bare support layer. The surface of the mud support was rough and uneven (**Figure 49b**), while the membrane interlayer showed a relatively uniform and smooth surface (**Figure 49d**). These results indicate that the dip-deposition process smoothed the surface. Therefore, a good adhesion between intermediate layer/mud support was observed. Then a more dense and homogeneous texture might be formed with the second coating (**Figure 49f**). This allows performing a thin dense and defect-free ceramic membrane (Chang et al., 2006). As a result, a progressive enhancement of the surface pore density can be observed with increasing the number of coating cycles. A FESEM superficial observation of the top layer shows the consolidation of the final dense ceramic body. In other words, the co-sintering process of the asymmetric membrane intended to a similar and simultaneously consolidation of the support and the membrane layer in order to obtain a dense and crack-free membrane. According to various works, the co-sintering technique was considered as a suitable technique to fabricate asymmetric membrane having an ultra-thin filtration layer (Dong et al., 2009; Jin et al., 2001). This technique was frequently performed to prepare tubular membrane multilayers (Liu et al., 2015; Meng et al., 2014).

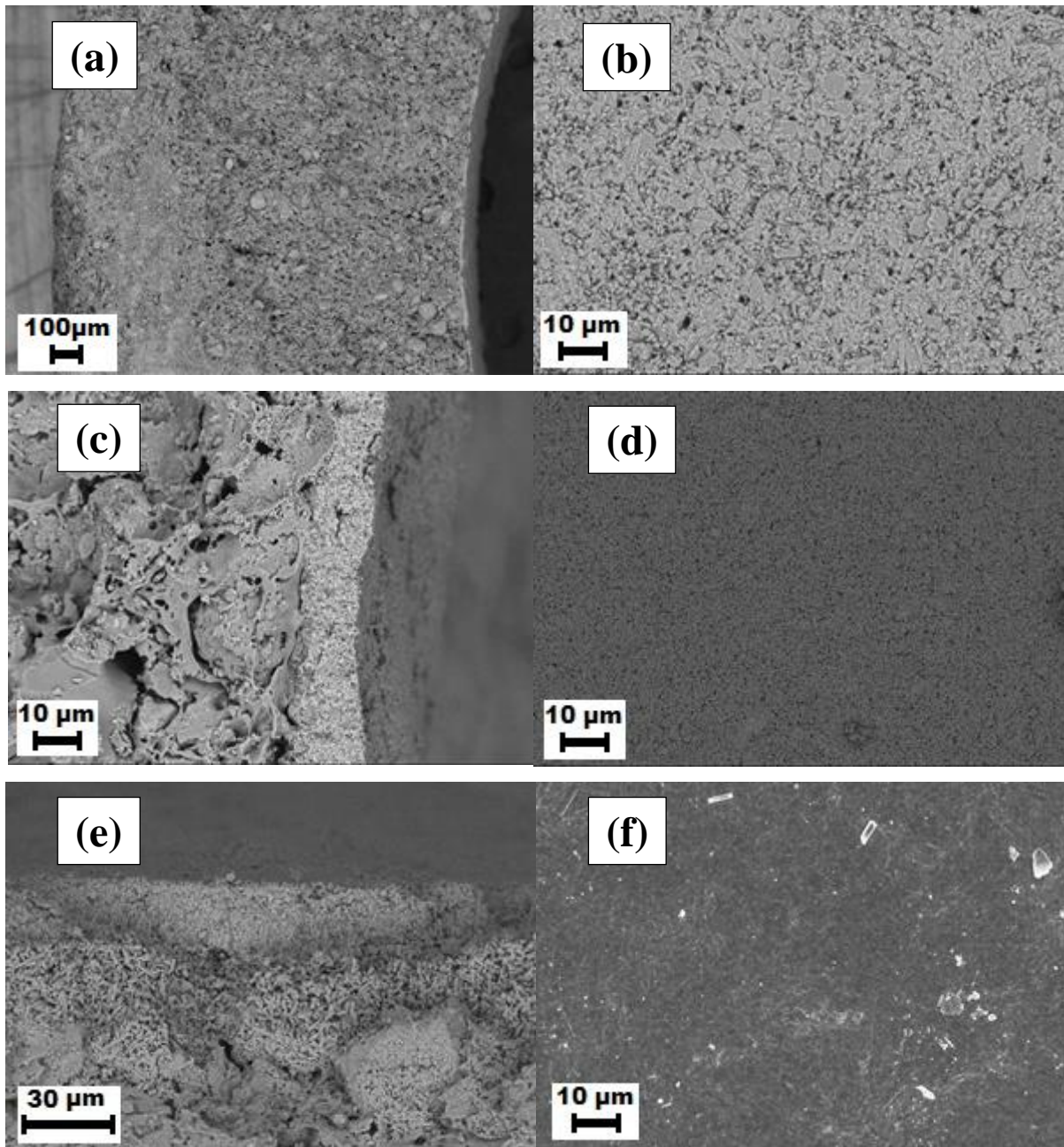


Figure 49.FESEM images of (a) overall cross-section and (b) surface view of mud support; (c) surface and (d) cross-section of intermediate layer; (e) surface and (f) cross-section of top layer membrane co-sintered at 800°C.

2.4.3. Pore size distribution and wettability properties

In this study, we investigated the pore size distribution of the bare and nano-TiO₂ coated ceramic membrane. As revealed in **Figure 50**, membrane support shows a porous structure with mean pore diameter of 0.1 μm . The deposition of titania layer on the mud surface reduced the mean pore size of the bare membrane to 18 nm for membrane interlayer and 2 nm after the deposition of the second layer.

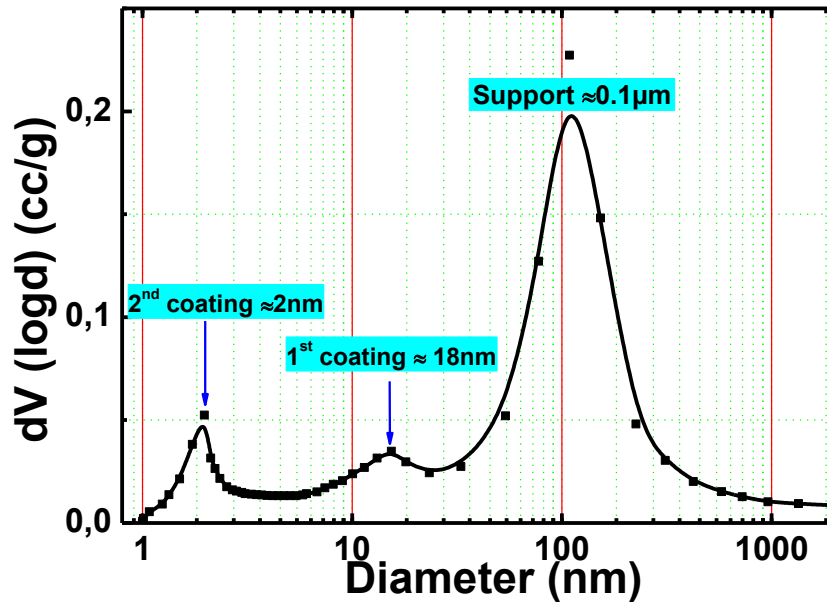


Figure 50. Pore size distribution of co-sintered bilayer membrane.

As illustrated in **Figure 50**, the top layer has a narrow and uniform pore size distribution with a mono-distribution model located at 2 nm. This membrane can work in the domain of low UF. It was found that the pore size distribution of the membrane was closely related to coating cycle number, where the mean pore diameter decreases with increasing the repeated coating cycle. Therefore, these results confirm that the layer-by-layer coating is a good technique for more controlling the membrane pore size and surface morphology of the ceramic membranes.

In order to better understand the nano-TiO₂ coating effect on the wettability properties, water contact angle was evaluated to compare the hydrophilicity of bare and LbL coated membrane surface (Nan et al., 2016). **Figure 51** shows an increase in the contact angle (CA) value with the LbL coating process, which is due to the increase of the roughness as well as the densification of the membrane surface. The water droplet laid on the support surface was

immediately absorbed for resulting to a CA of 16° which is explained by the water penetration into the porous structure of the support caused by gaps between the mud particles. Further, the first nano-TiO₂ coating of the support diminishes the wettability properties of the surface. Then, the CA increased to about 48° but still too lower than that of the hydrophobic surface.

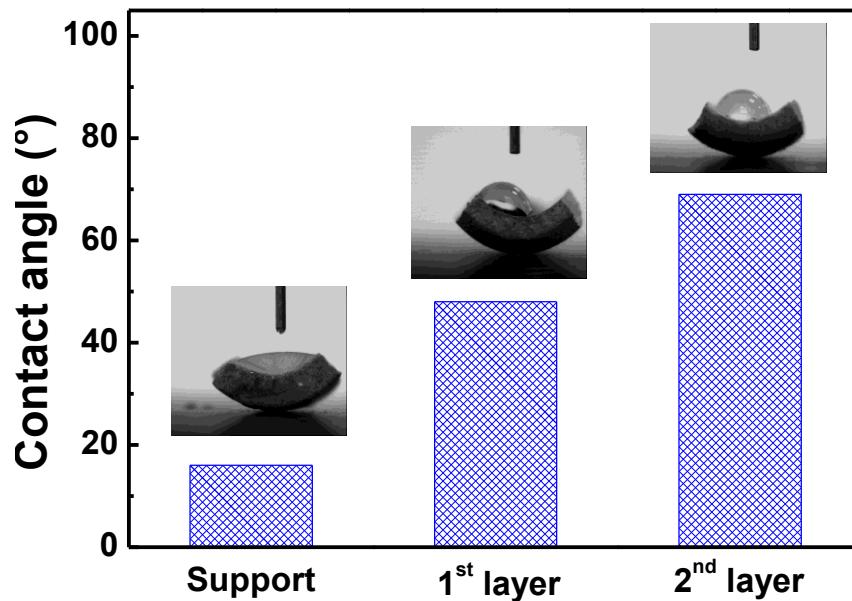


Figure 51. Water contact angle measurement for (a) bare mud support and co-sintered TiO₂ membrane surface after (b) first and (c) second LbL coating.

The deposition of the second nano-TiO₂ coating layer increased again the contact angle of bilayer membrane to a value of 69°. However, the CA remains lower than 90° and the surface still capable to absorb water. These results show a slight hydrophobic property of the UF membrane. Thus, it can be concluded that the LbL coating process could seriously affects the hydrophilicity of the ceramic membrane surface and then provides an important control of both permeation properties (Zhang et al., 2015) and fouling through the membrane (Zhu et al., 2017). Further, CA measurements are extremely sensitive to several factors such as surface roughness, surface free energy (SFE) value, surface groups (such as hydroxyl groups, which are removed in this study by the high heating temperature) and the surface physicochemical properties (Conti et al., 2018; Guo et al., 2019; Kujawa et al., 2017).

The TiO₂ coating process modifies the hydrophilicity of the membrane surface leading to a change of the interfacial interaction with solvent (water droplets, feed solutions) / membrane

surface. It can be deduced that the LbL deposition using nano-TiO₂ contributes to the mass transfer and then permeation flux, due to the antifouling properties (Chang et al., 2014).

2.5. Application to Chloramphenicol (CAP) drug and 2,6-Dinitroaniline (2,6-DNA) removal

The filtration characteristics of the T-UF titania membrane applied to the removal of CAP and 2,6-DNA from solution was performed. *Figure 52* shows the effect of the initial solution concentration at operating pressure of 4 bar.

The T-UF membrane exhibits a high rejection for both CAP and 2,6-DNA demonstrating the high potential of this novel membrane for organic pollutants removal. The rejection of the both molecules increased with increasing the initial concentration. This was also consistent with the observed decline in permeate flux at high feed concentrations, compared to that obtained with pure water flux. The high rejection of the organic molecules by the ultrafiltration membrane is surprising given the small molecular weight of both 2,6-DNA and CAP (184,1 Da to 323.1 Da) relative to the molecular weight cutoff of the T-UF membrane (approximately 2000 Da).

However, it is well known that these aromatic molecules tend to aggregate due to hydrophobic interactions between the aromatic rings of adjacent molecules during the filtration process (Hamada et al., 1991; Lin et al., 2016).

Figure 52a shows the improved of the molecule's rejection with increasing feed concentration. Due to the hydrogen bond and to the formation of molecule clusters, the pollutant molecules rejection can be highly enhanced. Indeed, Chloramphenicol and 2,6-Dinitroanilin can generate two types of molecular interactions: π - π interactions due to its aromatic ring and electrostatic interactions due to amino groups (Kastas et al., 2011). Consequently, the high rejection of these organic pollutants is due to the synergistic effects of the increase in molecules size through aggregation way and the strong electrostatic exclusion effect from the membrane surface.

On the other hand, remarkable decrease in the permeate flux with feed concentration was observed (*Figure 52b*). Here, it is interesting to point out that the decrease in permeation flux indicated that the membrane fouling behavior took place (Jana et al., 2010; Lin et al., 2016; Yu et al., 2012). The decrease of the permeate flux with the increasing of initial feed concentrations can be explained by the enhancement of the concentration polarization layer effect and the molecules adsorption onto membrane surface, (Bouazizi et al., 2017). The increasing concentration of these organic species would enhance the membrane surface

resistance effect, which allowed more retention and thus the increasing of rejection efficiency (Karim et al., 2018).

Based on the literature, the experiments developed by Lin et al, (2016) on tight ceramic UF membrane (with mean pore size of 0.91 nm) for dye removal shows under the similar experimental conditions (working pressure of 4 bar, dye concentration of 50-2000 ppm) a close permeate flux of 105-95L.m⁻².h⁻¹ compared to that found in our work for pesticide (118-85 L.m⁻².h⁻¹) and drug (115-75 L.m⁻².h⁻¹) (Lin et al., 2016). Furthermore, the permeate flux values obtained in the present study remained acceptable (Jiang et al., 2018; Lin et al., 2016).

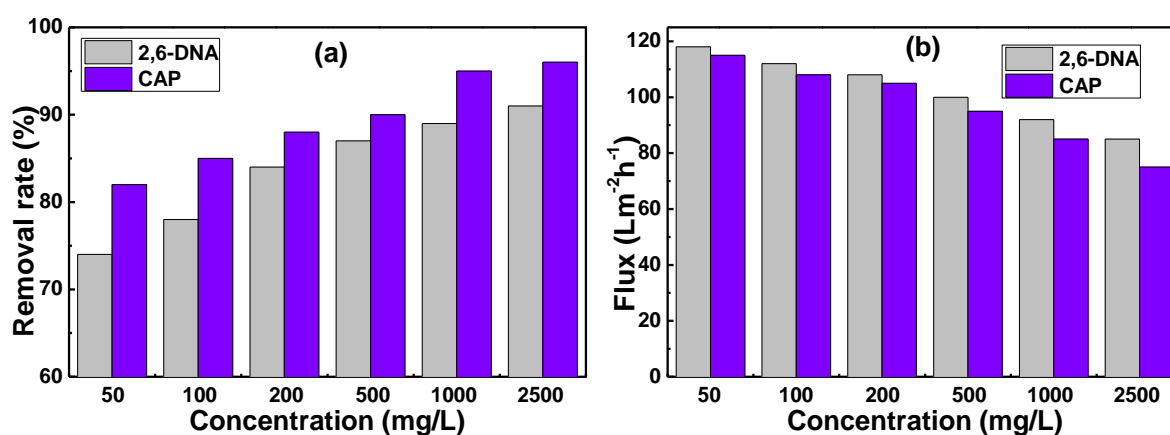


Figure 52. Variation of the (a) rejection rate and (b) permeation flux with CAP and 2,6-DNA concentrations at 4 bar using nanostructured titania membrane.

Wang and workers were demonstrated that to overcome the fouling problem and increase the membrane separation efficiency of the commercial dense NF membranes, the LbL deposition was a perfect method to synthesize preferment ceramic multilayer membranes with a rejection rate of over 96.0% (Wang et al., 2013). Further analysis reported in the literature revealed the strong advantage of T-UF membrane compared to NF membranes during membrane separation experiments (Lin et al., 2015; Vander et al., 2001).

2.6. Synergistic effect of catalysis reaction and membrane filtration in CMR system

In this investigation, the performance of the bilayer membrane was evaluated during the treatment of CAP and 2,6-DNA solutions in the T-UF-CMR under catalyst dosage effect. Hybrid process efficiency in term of permeate flux and rejection (of the organic pollutants)

was studied in the presence of catalysts by P1-IDA@Ni and P1-EDA@Au loadings from 50 to 250 mg/L.

In the case of the use of P1-IDA@Ni catalyst (**Figure 53a**), the rejection of 2,6-DNA and CAP was enhanced with enhancing monolithic catalyst amount in comparison to the T-UF only. A high rejection of the organic compounds was observed even at a low catalyst concentration. In addition, a total rejection rate was achieved by using catalyst dose of 200 mg/L for both explosive (2,6-DNA) and drag (CAP) molecules.

However, under the same conditions of TMP (4bar) and feed concentration (200ppm), a lower dose of 150 mg of the P1-EDA@Au hybrid monolith was sufficient for total organics removal during the treatment of both 2,6-DNA and CAP (**Figure 53b**). The high performance in retention rate of the hybrid system is attributable to the interaction associated with the physicochemical properties of the membrane, the hydrodynamic effect of the solution circulation and catalytic contribution of the powdered monolith catalyst.

On another hand, similar results were achieved in term of permeate flux enhancement by integration of monolith catalysts after 2h of running time. The experimental results of the occurred changes on permeate flux during hybrid UF/catalysis, indicated that the water flux was found to progressively increase with monolithic catalyst loading in T-UF-CMR compared to the case of reference membrane (Mozia et al., 2014). Hence, the permeate flux increased for 2,6-DNA and CAP, respectively, from 106 L.m⁻².h⁻¹ and 100 L.m⁻².h⁻¹ to 122 L.m⁻².h⁻¹ and 132 L.m⁻².h⁻¹ by adding 250 mgL⁻¹ of P1-IDA@Ni and from 108 Lm⁻² h⁻¹ and 105 Lm⁻² h⁻¹ to 132 L.m⁻².h⁻¹ and 135 L.m⁻².h⁻¹ by adding the same dose of P1-EDA@Au. It can be concluded that the continuous increase of catalyst amount may improve again the permeation by decreasing membrane fouling. Furthermore, the contribution of P1-EDA@Au to the permeation flux was higher under all experimental conditions compared to the P1-IDA@Ni. This is presumably because P1-EDA@Au has a better catalytic efficiency to destroy organic compounds due to the higher surface reactivity of Au NPs, resulting in the decrease of the membrane surface fouling.

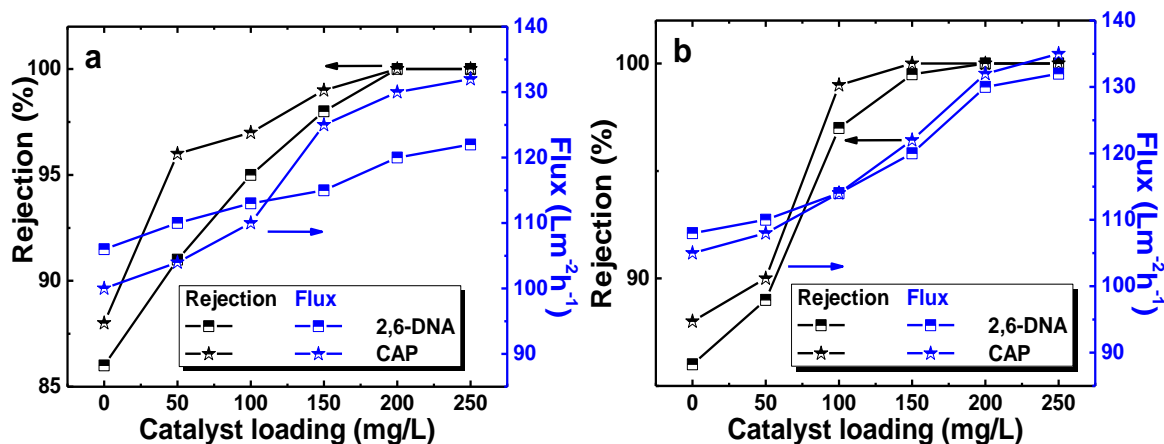


Figure 53. Effect of catalyst loading on the permeate flux during CAP and 2,6-DNA treatment by hybrid catalysis / T-UF process. Catalyst: (a) P1-IDA@Ni; (b) P1-EDA@Au. ([2,6-DNA] = [CAP] = 200ppm, TMP =4bar, t=2h).

These results show the great influence of the catalytic monoliths introduction in the conventional membrane separation system. The continuous circulation of the feed solution under the effect of pumping force provides a dynamic layer of the catalyst particles on the membrane surface. It was observed that the porous surface of the supplementary separation layer created by the circulated catalyst slurry improves the hydrophilicity of the membrane covered with the catalytic particles (Mozia et al., 2014). On the other hand, the increase of catalyst loading in the system may promote the degradation of the organic matter by improving the catalyst active sites and decreasing of reaction activation energy, which allowed the acceleration of the degradation rate (Li et al., 2019; Sert et al., 2017). Therefore, the flux improvement as well as the enhancement of the separation of dissolved matters took place.

2.7. Reusability evaluation of the T-UF CMR

The reusability potential of the T-UF membrane, catalyst stability and the synergistic control of the heterogeneous catalysis-assisted physical separation performance were evaluated in the CMR system. *Figure 54* illustrates the treatment efficiency in terms of TOC removal and fouling-control property (maintained flux) of the CMR used during four successive cycles to treat over a running cycle of 2h each.

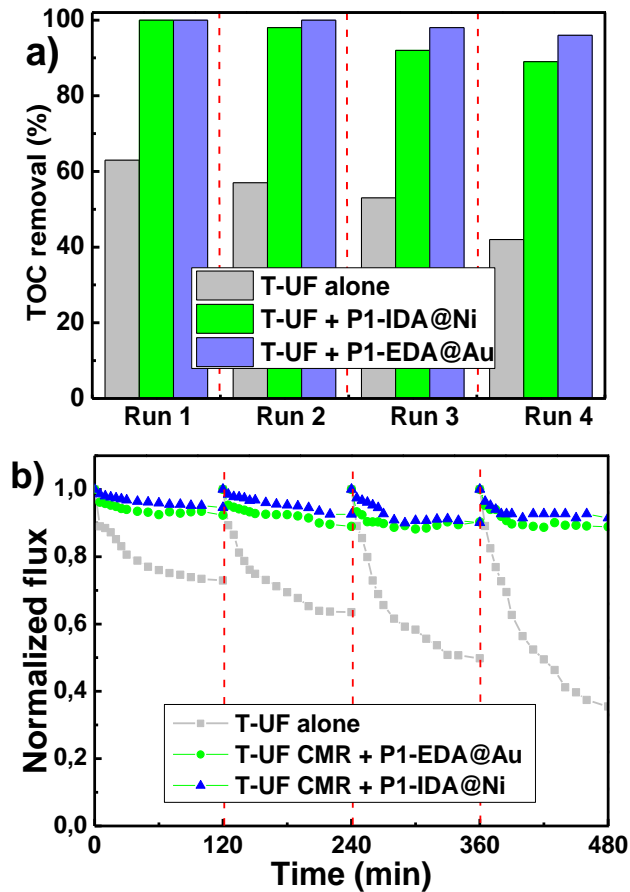


Figure 54. Reusability potential of the bilayer titania membrane in terms of (a) permeate flux and (b) rejection performances in the CMR system after each inter-cycle cleaning.

After each experiment, hot water (60 °C) was put under circulation through the membrane during 1 h for membrane cleaning step. Thus, a fresh feed solution was introduced for the subsequent running cycle. *Figure 54a* illustrates the TOC removal efficiency by T-UF membrane with and without the catalyst integration. Regarding the first run, the results indicated a complete TOC removal by using the hybrid separation/catalysis treatment in comparison to the single UF separation by the T-UF membrane, which allows to TOC decrease by only 60%. In addition, hybrid system maintains a high TOC removal (>96% and 89% with P1-EDA@Au and P1-IDA@Ni successively) after the fourth treatment run. Contritely, single UF process illustrates a poor TOC rejection that does not exceed 42%.

Figure 54b shows the permeation change during the four treatment cycles and the recovered flux after each cleaning step. A significant permeation flux decrease was observed with single UF process. Moreover, 75.2 % of the initial flux was maintained after the first cleaning step and significant loss of permeation properties was recorded during four UF cycles. This result suggests that the catalyst still preserve a high removal capability due to its high stability.

On the other hand, the hybrid system showed a large contribution of catalytic activity of suspended P1-EDA@Au and P1-IDA@Ni monoliths against the TOC removal. Interestingly, the hybrid system could keep almost constant the initial flux. However, a slightly change on the initial permeation flux was observed after each treatment cycle. Furthermore, over than 97% of the initial flux has been recovered after the 4th cycle. This suggests the reusability potential of T-UF CMR due to the recycling efficiency of the catalysts and the fouling control ability assisted by the dynamic layer deposition of the used catalyst slurry.

2.8. Membrane filtration resistance

Among of the main objective of this work is to explain the most distribution of fouling resistance and identify each contributing resistance on the overall flux decline. The resistance-in-series model (He et al., 2018; Tahri et al., 2012, Cheng et al., 2017) was described in order to reveal the fouling mechanisms of the membrane. Permeate flux was calculated after each filtration step at fixed TMP using Eq. (1) in order to determine the membrane resistance through the Eq. (2):

$$J = \text{TMP}/\mu.R_T \quad \text{Eq. (1)}$$

where, TMP (bar) is the transmembrane pressure, μ (Pa.s) is the permeate viscosity and R_T (m^{-1}) is the total resistance

$$R_T = R_m + R_r + R_{ir} \quad \text{Eq. (2)}$$

where, R_m is the self-membrane resistance or intrinsic membrane resistance, R_r present reversible resistance and R_{ir} is the irreversible resistance

R_m was determined by measuring the initial pure water flux of virgin membrane (J_0):

$$R_m = \text{TMP}/\mu J_0 \quad \text{Eq. (3)}$$

where, J_0 ($\text{L.m}^{-2}.\text{h}^{-1}$) is the initial pure water flux of virgin membrane

R_T was measured according to the final permeate flux (J_2), as shown in Eq. (4):

$$R_T = \text{TMP}/\mu J_2 \quad \text{Eq. (4)}$$

where, J_2 ($\text{L.m}^{-2}.\text{h}^{-1}$) is the final permeation flux of used membrane

R_r was calculated through the ultrapure water flux after membrane rinsing (J_1)

$$R_r = R_T - \text{TMP}/\mu J_1 = \text{TMP}/\mu J_2 - \text{TMP}/\mu J_1 \quad \text{Eq. (5)}$$

where, J_1 ($\text{L.m}^{-2}.\text{h}^{-1}$) is the ultrapure water flux of cleaned membrane

Hence, R_{ir} was deduced according to Eq. (6):

$$R_{ir} = R_T - R_m - R_r = \text{TMP}/\mu J_1 - \text{TMP}/\mu J_0 \quad \text{Eq. (6)}$$

2.9. Antifouling properties

The experimental results developed in this study allows to profoundly understanding the membrane-fouling phenomenon. According to the membrane resistance in-series model, the effect of membrane pore size and the suspended catalysts integration on the fouling control capability of the CMR system were especially studied.

Table 10 reveals the experimental values of different fouling profile calculated after 10 running cycles.

Table 10. Membrane resistance analysis during the different treatment processes.

Process	Monolayer UF	Bilayer T-UF	Hybrid T-UF CMR	
	membrane	membrane	P1-IDA@Ni	P1-EDA@Au
R_m	1.11	2.22	2.22	2.22
R_T	5.17	7.54	2.61	2.46
R_r	3.25	4.7	0.32	0.19
R_{ir}	0.81	0.62	0.07	0.05

Initially, the single UF process was carried out by examining the effect of LbL deposited layer number (pore size) on the fouling resistances during the treatment process. **Figure 55** shows that R_r has the main contribution towards the R_T for the both co-sintered mono and bilayer membrane. In respect of co-sintered monolayer UF membrane, the R_r was calculated to be $3.25 \cdot 10^9 \text{m}^{-1}$ accounting for 63 % of the R_T .

A similar trend was observed for the co-sintered bilayer T-UF, where the R_r contribution was increased by 7%. It can be seen from **Figure 55** that the difference in contribution of the R_{ir} to the R_T , before and after the second layer deposition, was very low (1%). In fact, the deposition of the second membrane layer allows the decrease of membrane pore size, which improve the deposition of organic species onto the membrane surface and consequently the reversible resistance over the filtration time (Bugge et al., 2012; Jørgensen et al., 2012). Then, the decrease of R_{ir} value as the membrane size decreased highlights the T-UF versus conventional UF process and confirm the LbL deposition performance.

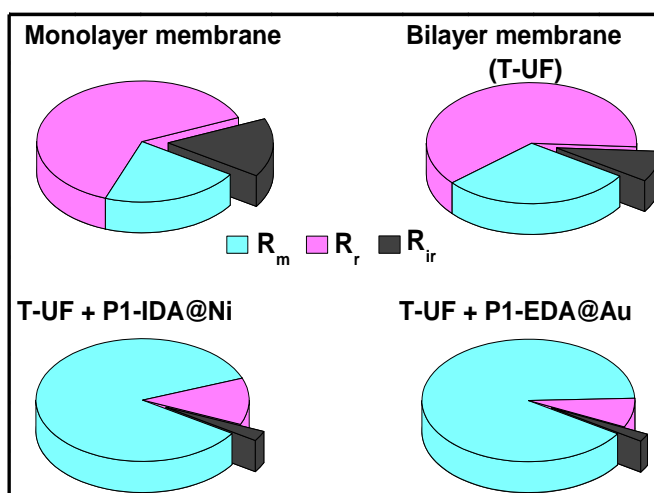


Figure 55. Membrane resistance distribution in the single filtration process and the hybrid treatment system.

On the other hand, the T-UF in CMR process illustrates the different fouling profiles with the initial feed TOC in order to identify the process intensification brought by suspended catalyst integration in the hybrid system. The total membrane fouling resistance calculated for the hybrid system was very low compared to that calculated for single UF. Then, the R_r and R_{ir} contributions of the individual membrane resistances was generally negligible.

Firstly, the contribution of R_m increased significantly from 21% and 29% to 85 % and 90% as the P1-IDA@Ni and P1-EDA@Au catalyst were integrated to the T-UF membrane separation respectively. This explain that the permeate flux improved with the integration of suspended catalysts in the T-UF CMR system. Besides, R_{ir} would highly decrease by the continuous filtration/catalysis hybrid process, owing to the degradation of the organic matter in the reactor tank by catalytic effect of the catalyst and then physically separated onto the membrane surface. However, as the hybrid catalyst amount enhanced, the tendency of R_{ir} was much highest in the T-UF CMR system due to the cake layer degradation by the circulated catalyst slurry.

Finally, it is worthy to note that the cumulate volume by T-UF CMR process also increased with catalytic intensity of the used P1-EDA@Au due to the difference catalytic activity of Au NPs towards Ni NPs. It can be concluded that the integration of the catalytic hybrid monoliths in the UF separation system enhanced the permeate flux by degradation of the organic pollution. T-UF CMR system can combine some merits such as the easy recycle of both P1-

IDA@Ni and P1-EDA@Au catalysts and relatively high catalytic efficiency through the fouling control and the degradation of pollutants.

3. Conclusion

Gold and Nickel nanoparticles can be uniformly decorated onto porous monolithic (P1) materials to form hybrid catalysts by using Ethylenediamine (EDA) and iminodiacetic acid (IDA) as a connecting molecule respectively. The resulting P1-immobilized MNPs were successfully used as robust catalysts for the batch reduction of 4-nitrophenol as nitroaromatic molecule model. Besides, the development of L-b-L titania membrane for tight UF was illustrated. The membrane demonstrated excellent rejection ability for removing drug (CAP) and pesticide (2,6-DNA) in water. In addition, the best performances in permeate flux and rejection rate for nitroaromatics removal were exhibited by combining monoliths loaded MNPs catalysts with the membrane separation system. The important virtues of this hybrid catalysis/separation systems are fouling control and separation yield enhancement through the dynamic filtration layers created by suspended catalysts at the membrane surface. Thus, intensify the selective removal of feed water and then makes the system easily recyclable.

References

B

- Bouazizi, A., Breida, M., Karim, A., Achiou, B., Ouammou, M., Calvo, J.I., Aaddane, A., Khiat, K., Younssi, S.A., 2017. Development of a new TiO₂ ultrafiltration membrane on flat ceramic support made from natural bentonite and micronized phosphate and applied for dye removal. *Ceramics International*. 43, 1479–1487.
- Bugge, T.V., Jørgensen, M.K., Christensen, M.L., Keiding, K., 2012. Modeling cake buildup under TMP-step filtration in a membrane bioreactor: cake compressibility is significant. *Water Research*. 4330-4338.

C

- Castillo, C., Seguin, K., Aguirre, P., Venegas-Yazigi, D., Viegas, A. D. C., Spodine, E., Paredes-Garcia, V., 2015. Nickel nanocomposites: magnetic and catalytic properties. *RSC Advances*, 5, 63073–63079.
- Chang, Q., Zhou, J., Wang, Y., Liang, J., Zhang, X., Cerneaux, S., Wang, X., Zhu, Z., Dong, Y., 2014. Application of ceramic microfiltration membrane modified by nano-TiO₂ coating in separation of a stable oil-in- water emulsion. *Journal of Membrane Science*. 456, 128–133.
- Chang, X., Zhang, C., Jin, W., Xu, N., 2006. Match of thermal performances between the membrane and the support for supported dense mixed-conducting membranes. *Journal of Membrane Science*. 285, 232–238.
- Chen, P., Ma, X., Zhong, Z., Zhang, F., Xing, W., Fan, Y., 2017. Performance of ceramic nanofiltration membrane for desalination of dye solutions containing NaCl and Na₂SO₄. *Desalination*. 404, 102–111.
- Chen, S., Xiang, Y., Peng, C., Xu, W., Banks, M. K., Wu, R., 2019. Synthesis of a novel graphene-based gold nanocomposite using PVEIM-b-PNIPAM as a stabilizer and its thermosensitivity for the catalytic reduction of 4-nitrophenol. *Inorganic Chemistry Frontiers*. 6, 903-913.
- Chen, T., Duan, M., Fang, S., 2016. Fabrication of novel superhydrophilic and under water superoleophobic hierarchically structured ceramic membrane and its separation performance of oily wastewater. *Ceramics International*. 42, 8604-8612.
- Cheng, X., Liang, H., Ding, A., Tang, X., Liu, B., Zhu, X., Gan, Z., Wu, D., Li, G., 2017. Ferrous iron/peroxymonosulfate oxidation as a pretreatment for ceramic ultrafiltration

membrane: Control of natural organic matter fouling and degradation of atrazine. *Water Research*. 113, 32-41.

Conti, J., De Coninck, J., Ghazzal, M.N., 2018. Design of water-repellant coating using dual scale size of hybrid silica nanoparticles on polymer surface. *Applied Surface Science*. 436, 234–241.

D

Dong, X., Zhang, G., Liu, Z., Zhong, Z., Jin, W., Xu, N., 2009. CO₂-tolerant mixed conducting oxide for catalytic membrane reactor. *Journal of Membrane Science*. 340, 141–147.

G

Guo, J., Deka, B.J., Kim, K.J., An, A.K., 2019. Regeneration of superhydrophobic TiO₂electrospun membranes in seawater desalination by water flushing in membrane distillation. *Desalination*. 468, 114054-114063.

H

Hamada, K., Nonogaki, H., Fukushima, Y., Munkhbat, B., Mitsuishi, M., 1991. Effects of hydrating water molecules on the aggregation behavior of azo dyes in aqueous solutions, *Dyes Pigment*.16, 111-118.

He, Z., Xia, D., Huang, Y., Tan, X., He, C., Hu, L., He, H., Zeng, J., Xu, W., Shu, D., 2018. 3D MnO₂ hollow microspheres ozone-catalysis coupled with flat-plate membrane filtration for continuous removal of organic pollutants: Efficient heterogeneous catalytic system and membrane fouling control. *Journal of Hazardous Materials*. 344, 1198-1208.

J

Jana, S., Purkait, M.K., Mohanty, K., 2010. Preparation and characterization of low-cost ceramic microfiltration membranes for the removal of chromate from aqueous solutions. *Applied Clay Science*. 47, 317–324.

Jiang, M., Ye, K., Lin, J., Zhang, X., Ye, W., Zhao, S., Van der Bruggen, B., 2018. Effective dye purification using tight ceramic ultrafiltration membrane. *Journal of Membrane Science*. 566, 151–160.

Jin, W., Li, S., Huang, P., Xu, N., Shi, J., 2001. Preparation of an asymmetric perovskite-type membrane and its oxygen permeability. *Journal of Membrane Science*. 185, 237–243.

Jørgensen, M.K., Bugge, T.V., Christensen, M.L., Keiding, K., 2012. Modeling approach to determine cake buildup and compression in a high-shear membrane bioreactor. *Journal of Membrane Science*. 409-410, 335-345.

K

Karim, A., Achiou, B., Bouazizi, A., Aaddane, A., Ouammou, M., Bouziane, M., Bennazha, J., Younssi, S.A., 2018. Development of reduced graphene oxide membrane on flat Moroccan ceramic pozzolan support. Application for soluble dyes removal. *J. Environ. Chem. Eng.* 6, 1475–1485.

Karthik, M., Suresh, P., 2017. Greener Synthesis of Reduced Graphene Oxide-Nickel Nanocomposite: Rapid and Sustainable Catalyst for the Reduction of Nitroaromatics. *Chemistry Select.* 2, 6916–6928.

Khemakhem, M., Khemakhem, S., Ayedi, S., Ben Amar, R., 2011. Study of ceramic ultrafiltration membrane support based on phosphate industry subproduct: Application for the cuttlefish conditioning effluents treatment. *Ceramics International.* 37, 3617–3625.

Kujawa, J., Cerneaux, S., Kujawski, W., Knozowska, K., 2017. Hydrophobic Ceramic Membranes for Water Desalination. *Applied Sciences.* 7, 402-412.

L

Li, Q., Jia, R., Shao, J., He, Y., 2019. Photocatalytic degradation of amoxicillin via TiO₂ nanoparticle coupling with a novel submerged porous ceramic membrane reactor. *Journal of Cleaner Production.* 209, 755-761.

Lin, J., Ye, W., Baltaru, M.C., Tang, Y.P., Bernstein, N.J., Gao, P., Balta, S., Vlad, M., Volodin, A., Sotto, A., Luis, P., Zydney, A.L., Vander Bruggen, B., 2016. Tight ultrafiltration membranes for enhanced separation of dyes and Na₂SO₄ during textile wastewater treatment. *Journal of Membrane Science.* 514, 217–228.

Lin, J., Ye, W., Zeng, H., Yang, H., Shen, J., Darvishmanesh, S., Luis, P., Sotto, A., Van der Bruggen, B., 2015. Fractionation of direct dyes and salts in aqueous solution using loose nanofiltration membranes. *J. Membr. Sci.* 477, 183–193.

Liu, Z.K., Zhu, J.W., Jin, W.Q., 2015. Preparation and characterization of mixed conducting supported hollow fiber membrane. *Journal of Inorganic Mater.* 30, 621–626.

Liu, Z., Zhang, G., Dong, X., Jiang, W., Jin, W., Xu, N., 2012. Fabrication of asymmetric tubular mixed-conducting dense membranes by a combined spin-spraying and co-sintering process. *Journal of Membrane Science*. 415–416, 313–319.

M

Maity, S., Sen, I.K., Islam, S.S., 2012. Green synthesis of gold nanoparticles using gum polysaccharide of *Cochlospermum religiosum* (katira gum) and study of catalytic activity. *Physica E*. 45, 130–134.

Meng, X., Ding, W., Jin, R., Wang, H., Gai, Y., Futang, J., Ge, Y., 2014. Two-step fabrication of $\text{BaCo}_{0.7}\text{Fe}_{0.2}\text{Nb}_{0.1}\text{O}_{3-\delta}$ asymmetric oxygen permeable membrane by dip coating. *Journal of Membrane Science*. 450, 291–298.

Mozia, S., Darowna, D., Szymanski, K., Grondzewska, S., Borchert, K., Wróbel, R., Morawski, A.W., 2014. Performance of two photocatalytic membrane reactors for treatment of primary and secondary effluents. *Catalysis Today*. 236, 135-145.

N

Nan, Q., Li, P., Cao, B., 2016. Fabrication of positively charged nanofiltration membrane via the layer-by-layer assembly of graphene oxide and polyethylenimine for desalination. *Applied Surface Science*. 387, 521–528.

O

Oun, A., Nouha, T., Mahouche-Chergui, S., Carbonnier, C., Majumdar, S., Sarkar, S., Sahoo, G.C., Ben Amar, R., 2017. Tubular ultrafiltration ceramic membrane based on titaniananoparticles immobilized on macroporous clay-alumina support: Elaboration, characterization and application to dye removal. *Separation and Purification Technology*. 188, 126–133.

P

Philip, D., 2009. Biosynthesis of Au, Ag and Au–Ag nanoparticles using edible mushroom extract. *Spectrochimica Acta Part A: Molecular and Biomolecular Spectroscopy*. 73, 374–381.

R

Roy, S., Katoch, R., & Angappane, S., 2018. Large magnetoresistance in carbon-coated Ni/NiO nanoparticles. *Bulletin of Materials Science*, 41, 127-132.

S

- Sen, I.K., Maity, K., Islam, S.S., 2013. Green synthesis of gold nanoparticles using a glucan of an edible mushroom and study of catalytic activity. *Carbohydrate Polymers*. 91, 518–528.
- Seo, Y. S., Ahn, E.-Y., Park, J., Kim, T. Y., Hong, J. E., Kim, K., Park, Y., Park, Y., 2017. Catalytic reduction of 4-nitrophenol with gold nanoparticles synthesized by caffeic acid. *Nanoscale Research Letters*. 12, 7.
- Sert, E., Atalay, F.S., 2017. Enhancement of Conversion using Ceramic Membrane in Esterification of Acrylic Acid with Butanol. *Journal of Polytechnic*. 20, 437-440.
- Shankar, S. S., Ahmad, A., Sastry, M., 2003. Geranium Leaf Assisted Biosynthesis of Silver Nanoparticles. *Biotechnology Progress*. 19, 1627–1631.
- Suvith, V.S., Philip. D., 2014. Catalytic degradation of methylene blue using biosynthesized gold and silver nanoparticles. *SpectrochimicaActa Part A: Molecular and Biomolecular Spectroscopy*. 118, 526–532.

T

- Tahri, N., Masmoudi, G., Ellouze, E., Jrad, A., Drogui, P., Ben Amar, R., 2012. Coupling microfiltration and nanofiltration processes for the treatment at source of dyeing-containing effluent. *Journal of Cleaner Production*. 33, 226-235.

V

- Vander Bruggen, B., Daems, B., Wilms, D., Vandecasteele, C., 2001. Mechanisms of retention and flux decline for the nanofiltration of dye baths from the textile industry. *Sep. Purif. Technol*. 22, 519–528.

W

- Wang, L., Wang, N., Zhang, G., Ji, S., 2013. Covalent crosslinked assembly of tubular ceramic-based multilayer nanofiltration membranes for dye desalination. *AIChE J*. 59, 3834-3842.

Y

- Yan, H., Zhang, D., Xu, J., Lu, Y., Liu, Y., Qiu, K., Zhang, Y., Luo, Y., 2014. Solution growth of NiO nanosheets supported on Ni foam as high-performance electrodes for supercapacitors. *Nanoscale Research Letters*, 9, 424-430.

Yu, S., Chen, Z., Cheng, Q., Lü, Z., Liu, M., Gao, C., 2012. Application of thin-film composite hollow fiber membrane to submerged nanofiltration of anionic dye aqueous solutions. *Separation and Purification Technology*. 88, 121–129.

Z

Zhang, Y., Guo, M., Pan, G., Yan, H., Xu, J., Shi, Y., Shi, H., Liu, Y., 2015. Preparation and properties of novel pH-stable TFC membrane based on organic–inorganic hybrid composite materials for nanofiltration. *Journal of Membrane Science*. 476, 500-507.

Zhou, Y., Chen, S., Wu, D., Liu, L., Luo, H., Zhang, D., 2019. Enhanced dielectric properties of poly(vinylidene fluoride-co-hexafluoropropylene) nanocomposites using oriented nickel nanowires. *Composites Communications*. 16, 11–19.

Zhu, Z., Jiang, J., Wang, X., Huo, X., Xu, Y., Li, Q., Wang, L., 2017. Improving the hydrophilic and antifouling properties of polyvinylidene fluoride membrane by incorporation of novel nanohybrid GO@SiO₂ particles. *Chemical Engineering Journal*. 314, 266-276.

GENERAL CONCLUSION AND PERSPECTIVES

The aim of this thesis work was to develop new hybrid catalytic membrane filtration processes by coupling catalytic nanocomposites with ultrafiltration nanostructured ceramic membranes made from low-cost local materials for the treatment of wastewater containing toxic compounds such as dyes, pesticides, explosives, and drug residues.

The first part of this thesis concerned the synthesis, characterization, and application of clay and graphene-like nanocomposites decorated with metallic nanoparticles as highly performant and recyclable heterogeneous nanocatalysts for the conversion of hazardous molecules to environmentally benign ones.

First, natural clay and graphene-like prepared from natural precursors (clay & sucrose) have been surface functionalized by grafting of polyglycidyl methacrylate (PGMA) and 3-glycidyloxypropyl trimethoxysilane (GPTMS)/tris (4-hydroxyphenyl) methane triglycidyl ether (TGE), respectively. The presence of the reactive epoxy groups on clay and graphene-like surfaces allows their post-functionalization through ring-opening by using, respectively, ethylene diamine ligand and $\text{H}_2\text{SO}_4/\text{KmnO}_4$ mixture and making them promising platforms for the in-situ generation of metallic nanoparticles. Then, the resulting amine and carboxylic-acid-rich nanocomposites have been used to homogeneously immobilize gold (Au) and palladium (Pd) nanoparticles, respectively. The physicochemical characterizations of the nanocomposites including scanning and transmission electronic microscopies, X-ray photoelectronic spectroscopy, X-ray diffraction electron and thermal gravimetric analysis have shown uniformly sized Au and Pd nanoparticles dispersed at high loading on clay and graphene-like based nanocomposites, which make them particularly useful in catalysis. Finally, online UV-vis monitoring of the reduction reactions of nitroaromatics (nitrophenol, pendimethalin) and dyes using, respectively, the as-synthesized AuNPs and PdNPs decorated nanocomposites as heterogeneous catalysts in the presence of an excess of sodium borohydride have shown that they are very effective. The remarkable results obtained from the reusability tests of these nanocatalysts highlighted the crucial role of the chelant groups on the robust stabilization of the AuNPs and PdNPs ensuring a high surface-to-volume ratio and thus providing a large number of available catalytic active sites.

The second part was dedicated to the fabrication, nanostructuration and characterization of asymmetric tubular ceramic membranes consisting of a ceramic macroporous support coated with a single or several microporous TiO_2 membrane layers. The development of these membranes involves the implementation of techniques used in the ceramic industry. The shaping of membrane supports is ensured in this work by the extrusion process of a homogeneous ceramic paste to produce green tubes called supports, which ensure, after heat

treatment at high temperature (sintering), the mechanical strength of the final membranes. The nanostructuring of the membranes is carried out by two coating techniques, which are slip-casting and dip-coating. The easy realization and the speed of the deposition process as well as the controllability of the properties of the deposited layers are the basis of the choice of these two techniques. Simple drying followed by calcination made possible the moderation of the final morphological properties of the membranes (porosity, average pore diameter, support-separation layer adhesion). Two kinds of membranes were developed in this thesis work: ultrafiltration (UF) and tight ultrafiltration (T-UF) membranes elaborated by usual slip-casting, layer-by-layer (multiple-recovery dip-coating) and co-sintering processes. The coating uniformity, the thickness of the deposited membrane layers, the cohesion of the microstructure and the homogeneity of the support and the membrane surface were examined by scanning electron microscopy (SEM). The porosity and the average pore diameter of the layers as well as the membrane supports were determined by nitrogen adsorption/desorption (BET) and mercury intrusion porosimetry methods. Hydrophobicity/hydrophilicity characteristics of the membrane surfaces have been defined by the contact angle measurements. In addition, three-point bending tests were carried out to characterize the mechanical resistance of the consolidated membranes, which have been exposed to relatively high pressures when used in filtration experiments. Then, the developed membranes were used for the treatment of synthetic dyeing water of Alizarin, used as a color fixer in the textile industries (mordant dyes). The performance of these membranes was studied in terms of permeation flux and pollutant retention rate, which are, depend on the experimental parameters (initial concentration, working pressure, pH).

The last part of this manuscript was devoted to the application of hybrid separation processes combining heterogeneous catalysis based on the catalytic nanocomposites with membrane filtration using the ceramic UF and T-UF membranes described in the described in the previous parts of this work, to the treatment of water spiked with toxic and harmful nitrophenol, dyes, 2,6-dinitroaniline (2,6-DNA) et chloroamphenicol and as well as real textile wastewater derived from the textile industry of Ksar Hellal-Tunisia region. The obtained results allowed us to identify a double contribution of the catalytic nanocomposites introduced in the membrane reactor system. In addition to their catalytic performance, the synthesized nanocomposites revealed another remarkable advantage that is the creation of an additional separation layer deposited on the surface of the membranes. This dynamic layer resulted not only in an additional separation but it also allowed preventing the fouling of the membranes pores caused by the retention of the pollutants.

Thus, based on all the experimental results obtained in terms of the permeation flux, the quality of the treated water (capacity to remove effluents) and the resistance to fouling allows us to conclude a comparison between the three produced membranes.

While the development of these three membranes has been carried out from low-cost natural materials (such as clay and phosphate sub-products "mud") by using simple to implement shaping process and their applications in the purification of polluted water show very promising results, we can say that the bilayer membrane from phosphate mud was the efficientest. Moreover, it can also be noted that the synthesis by the co-sintering processes and the layer-by-layer deposition contributes to notably reducing the pores size and improves the anti-fouling properties of the membrane surface. This, would result in a higher efficiency of the active layer, this one was very favorable for the use of this membrane in tight ultrafiltration compared to other membranes.

Thus, the original combined technology presented in this study seems to be a very interesting process for a better degradation of persistent organic pollutants contained in water and which cannot be totally treated by conventional methods.

In addition to this work, during this thesis the chelatant clay-polyglycidyl methacrylate nanocomposite has been used as supports for the immobilization of in-situ generated Au and Agbimetallic nanoparticles. The formation and the well dispersion of the bimetallic ultra-small Ag@Au particles (average diameter ~4.5 nm) waere evidenced by spectroscopic and microscopic results using TEM and XPS techniques as shown in *Figure 56*. These bimetallic nanoparticles-based nanocomposites exhibited highly enhanced catalytic properties toward the reduction of nitrophenol and pendimethalin in comparison to the monometallic nanoparticles-based nanocomposites as a result of synergetic effect between Ag and Au nanoparticles (see *Figure 56*).

As perspectives for this thesis work, the idea will be to synthesize magnetic nanocomposites as heterogeneous nanocatalysts containing for example Au or Ag@Au and Fe₂O₃ nanoparticles, and this using the same synthetic strategyas that described in this manuscript. The use of such heterostructures will aim on the one hand to improve catalytic performance and on the other hand to facilitate recovery and thus recycling of the catalytic systems in simple and rapid way. Evaluation of the efficiency of these systems in Fenton hybrid process toward the complete degradation of persistent compoundscan be considered.

In addition, UF membrane system in total recycle mode of filtration have to be investigated. This requires continual recycling and return back of both permeate and concentrate streams to the feed tank. Then, the concentration of the feed solution can be considered as kept constant

during the treatment experiment. From the practical standpoint, it would be interesting to conduct the research and analysis associated with the continuous operation process to maximize the COD and color removal efficiency. Hence, these experiments will be in the aim of membrane performance evaluation in terms of permeate flux and permeate quality and to know the effect of the different operating conditions on membrane resistance in continuous treatment process by comparison to that conventional UF method.

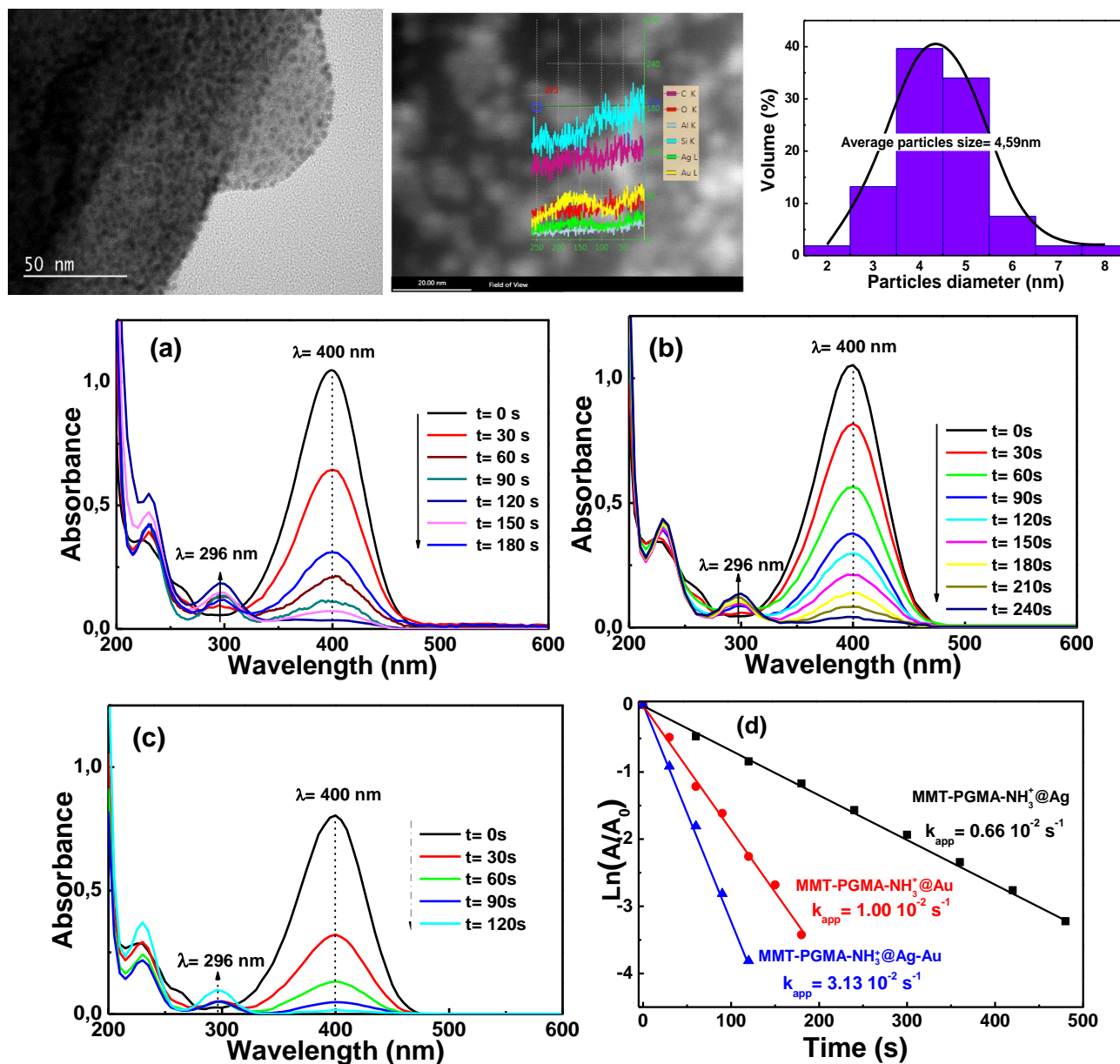


Figure 56.(a) TEM images, (b) line scan for Au, Ag, Si, Al, O and C elements and (c) pore size distribution of bimetallic MMT-PGMA-NH₃⁺@Au/Ag and UV-VIS absorption spectra of 4-NP reduction by using monometallic (d) MMT-PGMA-NH₃⁺@Ag, (e) MMT-PGMA-NH₃⁺@Au and (f) bimetallic MMT-PGMA-NH₃⁺@Au/Ag and (g) reaction kinetics.

Abstract

This PhD project aims at synthesizing innovative hybrid materials meant for (waste)water treatment applications. A special focus has been laid on establishing structure-property relationships through varying the synthesis conditions to finely tune the structural parameters of the composite materials for optimal properties. The manuscript presents three experimental chapters describing different nanostructured materials exhibiting catalytic or/and filtration abilities towards organic pollutants. These sections are preceded by an introduction and a state-of-the-art of related materials and followed by a conclusion and perspectives.

Our experimental approach was motivated by initially developing materials with unique “catalytic or filtration” property toward dual functional materials “membrane reactor for hybrid heterogeneous catalytic filtration” with the aim to develop highly competitive materials in the context of sustainability and environment protection

Keywords: Clay; Filtration; Graphene; Heterogeneous catalysis; Membrane technology; Nanocomposites; Polymer materials; Surface functionalization; Sustainable row materials; Wastewater treatment;

Résumé

Ce projet de doctorat vise à synthétiser des matériaux hybrides innovants destinés au traitement des eaux (usées). Un accent particulier a été mis sur l'établissement de relations structure-propriété rendu possible en faisant varier les conditions de synthèse des matériaux afin d'ajuster finement les paramètres structurels des matériaux composites en vue d'obtenir des propriétés optimales. Le manuscrit présente trois chapitres expérimentaux décrivant différents matériaux nanostructurés présentant des activités catalytiques ou/et de filtration vis-à-vis des polluants organiques. Ces sections sont précédées d'une introduction et d'un état de l'art des matériaux connexes et suivies d'une conclusion et de perspectives.

Notre approche expérimentale a été motivée par le développement dans un premier temps de matériaux à propriété unique «catalytique ou filtration» vers des matériaux à dualité de fonction «réacteur membranaire vers des procédés hybrides combinant filtration et catalyse hétérogène» dans le but de développer des matériaux hautement compétitifs dans un contexte de développement durable et de protection de l'environnement

Mots clés : Argile; Catalyse hétérogène; Filtration; Fonctionnalisation de surface; Graphène; Matériaux polymère; Matières premières durables; Nanocomposites; Technologie membranaire; Traitement des eaux.